Exploiting mitosis to improve anti-cancer strategies

A thesis submitted to the University of Manchester for the degree of Doctor of Philosophy in the Faculty of Biology, Medicine and Health

2016

Ailsa Bennett

School of Medical Sciences
Division of Molecular and Clinical Cancer Sciences

Table of Contents

List of Figures **5**

List Of Tables **7**

Abbreviations **8**

Abstract **10**

Declaration and Copyright notice **11**

Acknowledgements **12**

Dedication **13**

1 Chapter 1: Introduction **14**

1.1 General Introduction **14**

1.2 Mitosis **15**

1.21 The cell cycle and mitosis 15

1.22 Entry and exit into mitosis 17

1.221 Cdk1 and cyclin B1 17

1.222 Other kinases involved in mitotic entry/exit 18

1.23 Kinases 19

1.3 Spindle Assembly **20**

1.31 Microtubules 20

1.32 Motor proteins 23

1.321 Cenp-E 25

1.4 The Spindle Assembly Checkpoint (SAC) **27**

1.41 An overview of the SAC 27

1.42 Bub1 29

1.421 The roles of Bub1 and its kinase activity 29

1.422 The structure of Bub1 and inhibition 31

1.423 Bub1 in cancer 34

1.5 Mitosis and Cancer **34**

1.51 Aneuploidy, CIN and tumour evolution 34

1.52 Antimitotics 37

1.521 Second-generation antimitotics 38

1.522 Response to antimitotics and cell fate 40

1.53 Competing networks and c-myc 43

1.6 Apoptosis **44**

1.61 Overview 44

1.62 Intrinsic and extrinsic pathways 45

1.63 Inhibitors of apoptosis (IAPs) 49

1.64 Other mechanisms of cell death 50

1.65 Apoptosis and cancer 50

1.66 Targeting apoptosis with BH3 mimetics 51

1.67 Bcl-xL 53

1.671 The structure and functioning of Bcl-xL 53

1.672 Bcl-xL and its inhibitors 55

1.673 Bcl-xL in cancer 56

1.68 Apoptosis and mitosis 56

1.681 The post-mitotic response 58

1.69 Autophagy and metabolism 59

1.7 Summary and Aims **60**

2 Chapter 2: Materials and Methods **62**
2.1 Cell Biology **62**
2.2 Molecular Biology **65**
2.3 Protein Analysis **71**
2.4 Live cell imaging and microscopy **76**
2.5 Calculation of synergy scores **77**
2.6 Statistical Analysis **78**
2.7 Chemical Synthesis **78**

3 Chapter 3: Investigating 2OH-BNPP1 as a Bub1 kinase inhibitor **81**
3.1 Introduction **81**
3.2 Generation of a Bub1 *in vitro* kinase assay **82**
3.21 Optimisation of assay parameters 85
3.22 Using 2OH-BNPP1 as a Bub1 kinase inhibitor 92
3.3 Generation of a cell-based assay to detect Bub1 kinase activity **92**
3.4 Summary **97**
3.5 Discussion **100**
3.51 Is Bub1 kinase activity essential for SAC signalling? 100
3.52 Bub1 kinase activity in interphase 101
3.53 Bub1 as a therapeutic target 101

4 Chapter 4: Using a Cenp-E inhibitor GSK923295 in the development of an assay to study aneuploidy **103**
4.1 Introduction **103**
4.2 The synthesis of GSK923295 ..... **104**
4.3 Extending the utilisation of CALB **108**
4.4 Characterising GSK923295 in cell-based assays **108**
4.41 GSK923295 and its effect on chromosome alignment 108
4.42 GSK923295 and its effect on mitosis 111
4.43 The effect of GSK923295 on long-term cell fate 113
4.44 Analysing the reversibility of GSK923295 116
4.5 The establishment of an assay to study aneuploidy **118**
4.6 Summary **119**
4.7 Discussion **119**
4.71 A strategy to resolve enantiomers 119
4.72 Using GSK923295 as a mitotic tool 119
4.73 Targeting Cenp-E as a therapeutic approach 121

5 Chapter 5: Investigating the role of Bcl-xL in mitotic and post-mitotic survival **123**
5.1 Introduction **123**
5.2 Characterising a Bcl-xL inhibitor, WEHI-539 ..... **124**
5.21 Comparing siRNA and small molecule inhibition of Bcl-xL 125
5.22 The effect of WEHI-539 on Bim-induced apoptosis 127
5.23 Examining the effect of WEHI-539 on apoptosis resistance induced by Bcl-xL overexpression 127
5.24 Examining the effect of WEHI-539 on the interactions between Bcl-xL and its binding partner proteins 130
5.3 Investigating the combination of WEHI-539 and antimitotics **132**
5.31 The effect of Bcl-xL inhibition and mitotic blockers 132
5.32 Determining when cells are dying: in mitosis or post-mitosis 137
5.33 The effect of a WEHI-539 and mitotic driver combination 138

5.34 Determining synergistic combinations 144
5.4 Investigating the role of Mcl-1 in survival 147
5.41 Studying Mcl-1 levels in the presence of a mitotic blocker and driver 147
5.42 The effect of increasing or decreasing Mcl-1 expression on survival 151
5.43 Using Mcl-1 deficient DLD-1 cells to analyse the effect of ZM447439 and WEHI-539 156
5.5 Summary 156
5.6 Discussion 158
5.61 The concept of synergy and the overlapping function between Mcl-1 and Bcl-xL 158
5.62 The post-mitotic response 161
5.63 Mitosis as a stress 162
5.64 Bcl-xL inhibition in the clinic 163
5.641 Combination chemotherapy 163
5.642 Biomarkers for efficacy 164
6 Chapter 6: Discussion 167
6.1 Overview 167
6.2 Concluding remarks 169
7 References 171
8 Appendix 201
8.1 Appendix 1: Cenp-E inhibitor GSK923295: Novel synthetic route and use as a tool to generate aneuploidy 202
8.2 Appendix 2: MYC is a major determinant of mitotic cell fate 203
8.3 Appendix 3: Inhibition of Bcl-xL sensitises cells to mitotic blockers, but not mitotic drivers 204

Word count: 58726

List of Figures

Figure 1.1	Cell cycle and mitosis	16
Figure 1.2	Microtubule dynamics and the bipolar spindle	21
Figure 1.3	The motor function of Cenp-E and mode of GSK923295 inhibition	24
Figure 1.4	The spindle assembly checkpoint (SAC)	28
Figure 1.5	The structure of Bub1 kinase and its domains	32
Figure 1.6	Inhibition of Bub1	33
Figure 1.7	Analysing cellular fate following mitotic perturbation	41
Figure 1.8	Analysis of cell fate using the IncuCyte® Zoom	42
Figure 1.9	The intrinsic and extrinsic apoptosis pathways	46
Figure 1.10	Binding of inhibitors to Bcl-xL in the BH3 domain	54
Figure 3.1	Generation of tetracyline inducible HEK293 GFP-Bub1 wild-type (WT) and kinase dead (K821R) cell lines	83
Figure 3.2	The immunoprecipitation of GFP-Bub1 using a GFP-binder protein	84
Figure 3.3	Expressing wild-type (WT) and kinase-dead Bub1 and the effect on histone H2A phosphorylation	86
Figure 3.4	Optimising Bub1 enzyme concentration	87
Figure 3.5	Optimisation of histone H2A substrate concentration	88
Figure 3.6	Optimisation of ‘hot’ and ‘cold’ ATP concentration	90
Figure 3.7	Optimisation of the time of kinase reaction	91
Figure 3.8	The effect of 2OH-BNPP1 on pH2A	93
Figure 3.9	The expression of GFP-H2B-Bub1C wild-type (WT) and kinase dead (D946N) mutant	94
Figure 3.10	Expressing GFP-H2B-Bub1C WT and D964N, showing the effect on H2A phosphorylation and Sgo1 localisation	96
Figure 3.11	The expression of GFP-H2B-Bub1C WT and D946N in interphase cells and the effect on H2A phosphorylation	98
Figure 3.12	The effect of 2OH-BNPP1 on H2A-pT120	99
Figure 4.1	The resolution of a key intermediate for the synthesis of GSK923295 using *Candida antarctica* lipase B enzyme	105
Figure 4.2	The CALB- mediated enzyme resolution of racemic substrates	107
Figure 4.3	Consequence of GS923295 treatment on chromosome alignment	110
Figure 4.4	Effect of GSK923295 exposure in living cells	112
Figure 4.5	Effect of GSK923295 on the cell cycle and apoptosis	114
Figure 4.6	Analysis of the reversibility of GSK923295	117
Figure 5.1	Effect of the co-depletion of Mcl-1 and Bcl-xL	126
Figure 5.2	Effect of Bim overexpression on apoptosis	128
Figure 5.3	Effect of Bcl-xL overexpression on cell fate	129
Figure 5.4	Effect of WEHI-539 on the interaction between Bcl-xL and its binding partners	131
Figure 5.5	Effect of the combination of WEHI-539 and mitotic blockers	133

Figure 5.6	Analysing cell death in response to microtubule-targeting agents and WEHI-539	135
Figure 5.7	Analysis of cell fate with second-generation antimitotics and WEHI-539 combination	136
Figure 5.8	Analysing cellular fate with BI2536 and WEHI-539	139
Figure 5.9	Effect of the combination of WEHI-539 and mitotic drivers	141
Figure 5.10	Analysis of cell fate with mitotic drivers and WEHI-539	142
Figure 5.11	Effect of mitotic drivers on mitosis	143
Figure 5.12	Calculating Bliss Scores and Sums	145
Figure 5.13	Determining Bliss Scores for mitotic blockers	146
Figure 5.14	Effect of mitotic drivers and WEHI-539 combination on Bliss Scores	148
Figure 5.15	Bliss Sum analysis for mitotic blockers and drivers	149
Figure 5.16	Effect of mitotic arrest on Mcl-1 levels	150
Figure 5.17	Effect of overexpression of Mcl-1 on post-mitotic death	152
Figure 5.18	Effect of co-inhibition of Mcl-1 and Bcl-xL on ZM447439-treated RKO cells	154
Figure 5.19	Effect of co-treatment with A-1210477/WEHI-539 and ZM447439	155
Figure 5.20	Effect of ZM447439 and WEHI-539 exposure on cell death in DLD-1 cells	157
Figure 5.21	The balance between pro- and anti-apoptotic proteins, and the redundancy between Mcl-1 and Bcl-xL determines cell survival	160

List of Tables

Table 2.1	Cell plating density where numbers are a x 10^4 cells/ml	62
Table 2.2	Drug concentrations used	63
Table 2.3	The antibiotics used for selection in the LacZeo/TO cell lines	65
Table 2.4	siRNA sequences of the oligonucleotides used	66
Table 2.5	Cloning methods to produce the plasmids used	66
Table 2.6	Setting up the PCR reaction	67
Table 2.7	Cycling conditions used for PCR	67
Table 2.8	Primers used in cloning and sequencing	68
Table 2.9	Mutagenesis reaction set-up	68
Table 2.10	Cycling parameters for mutagenesis	68
Table 2.11	Mutagenesis primers	68
Table 2.12	Test restriction digests	69
Table 2.13	Restriction digests for cloning	69
Table 2.14	Sequencing set-up	71
Table 2.15	Cycling conditions for DNA sequencing	71
Table 2.16	Making up SDS-PAGE gels	72
Table 2.17	Antibodies used for western blotting	73
Table 2.18	Components of the kinase assay buffer	74
Table 2.19	Optimum conditions for the kinase assay	75
Table 2.20	Calculations for determination of the cold and hot ATP concentrations	75
Table 2.21	Antibodies used in immunofluorescence	77

Abbreviations

YH2AX	H2A histone, member X
APC/C	Anaphase promoting complex/ cyclosome
ATM	Ataxia telangiectasia mutated
ATP	Adenosine triphosphate
ADP	Adenosine diphosphate
Bad	Bcl-2 associated death promoter
Bak	Bcl-2 homologous antagonist killer
Bax	Bcl-2 associated X protein
Bcl-2	B-cell Lymphoma 2
Bcl-xL	B-cell Lymphoma-extra large
BH	Bcl-2 homology
Bid	BH3-interacting-domain death agonist
Bub1	Budding uninhibited by benzimidazoles 1
Bub3	Budding uninhibited by imidazoles 3
Cenp-E	Centromere-associated protein E
CIN	Chromosome instability
CPC	Chromosome passenger complex
DiM	Death in mitosis
BSA	Bovine Serum Albumin
Caspase	Cysteine-aspartic proteases
Cdc20	Cell Division Cycle 20
Cdh1	Cdc20 homolog 1
Cdk1	Cyclin-dependent kinase 1
dNTP	Deoxynucleotide triphosphates
GFP	Green fluorescent protein
GST	Glutathione S-transferase
IC_{50}	Half maximal inhibitory concentration
INCENP	Inner centromere protein
kDa	Kilodaltons
Mad1	Mitotic arrest deficient-1
Mad2	Mitotic arrest deficient-2
MCC	Mitotic checkpoint complex
Mcl-1	Myeloid cell leukemia 1

MOMP	Mitochondrial outer membrane permeabilisation
MTA	Microtubule targeting agent
MTOC	Microtubule organising centre
Noxa	Phorbol-12-myrisate-13-acetate-induced protein 1
OMM	Outer mitochondrial membrane
P53	Tumour protein 53
PBS	Phosphate buffered saline
PBST	PBS plus 0.1% Triton X-100
Plk-1	Polo-like kinase 1
PmD	Post-mitotic death
PP2A	Protein phosphatase 2A
Puma	P53 upregulated modulator of apoptosis
RNAi	RNA interference
SAC	Spindle assembly checkpoint
SDS	Sodium dodecyl sulphate
Sgo1	Shughoshin-like 1
siRNA	Small interfering RNA
TRF2	Telomeric repeat-binding factor 2
WT	Wild-type

Abstract

The University of Manchester
Ailsa Bennett
Doctor of Philosophy (PhD) in Molecular Cancer Studies
Exploiting mitosis to improve anti-cancer strategies
2016

Antimitotics are used in cancer chemotherapy for the treatment of cancers such as breast, ovarian, lung and prostate. Despite the success of agents such as Taxol, problems have emerged such as side effects, resistance and the lack of ability to predict patient responsiveness. As a result, a class of second-generation inhibitors have been developed with the aim to overcome or improve these issues. Such inhibitors target proteins and kinases involved in the control of mitosis and the cell cycle. However, these have yet to be clinically successful and therefore, this highlights the requirement for an increased understanding of the mitotic process and how antimitotics truly elicit their action. Reasons for the lack of efficacy may be due to the absence of biomarkers to stratify patients into those likely to respond to treatment. It may also be possible that other targets are required. Our understanding of the action of antimitotics is therefore paramount to improving cancer chemotherapy.

By exploiting mitosis and understanding what happens when mitosis goes wrong, this thesis aims to explore new and improved methods of targeting, but also proposes to improve our understanding of the consequences of aberrant mitoses through the use of small molecule inhibitors. In the first case the thesis investigated the targeting of the spindle checkpoint protein Bub1 with 2OH-BNPP1, where previously inhibitors against the kinase were not acknowledged. However the inhibitor used was not effective in cells and therefore further experimentation was not possible. Secondly, to explore the consequences of mitotic perturbation, an assay to explore aneuploidy was established. To do this a Cenp-E inhibitor GSK923295 was synthesised, which was subsequently used in assays with the Mps1 inhibitor AZ3146 to generate aneuploidy progeny. The Cenp-E inhibitor was then used as an antimitotic agent in the final chapter to explore the mechanism of action of mitotic blockers and drivers often used in cell biology and clinical settings. Evidence suggests that the intrinsic apoptotic pathway is activated upon exposure to these agents. With focus on this pathway, the importance of Bcl-xL on cell survival was considered, revealing particular importance in the post-mitotic response. Ultimately, this thesis should contribute to devising new and improved anti-cancer strategies.

Declaration

No portion of the work referred to in this thesis has been submitted in support of an application for another degree or qualification of this or any other university or other institute of learning.

Copyright notice

Acknowledgements

First of all I would like to thank my supervisor Professor Stephen Taylor for taking me on as his PhD student and guiding me throughout the four years. As a Chemist, I knew little about Biology, and the first year was quite a struggle. His excellent teaching, knowledge and persistence kept me on the right path to success. I would also like to thank Professor David Procter for allowing me into his Chemistry lab, and letting me practice and further my Chemistry practical skills and knowledge. I also have to mention Professor Dean Jackson, who has advised, helped and directed me throughout my PhD.

I definitely would not have survived and completed my PhD without the help of all the Taylor lab (past and present)- special thanks to Anthony, Livi and Caroline for scrutinising my thesis, helping me in the lab, and answering all my (sometimes stupid) questions. Louisa and Sam have also been great helps and also the sources of entertainment! I really couldn't have chosen a better lab to do my PhD in. I also thank Dr Beatrice Bechi for aiding me in the Chemistry synthesis.

Outside of the lab, I need to thank all of my family and friends for putting up with my moaning, worry and stress- finally the end is near! A special thanks to my dad for all his encouragement and confidence in my ability. Without my mum's support, I would not have been able to undertake and complete my PhD, she will be greatly missed.

Lastly, I would like to thank Cancer Research UK and The University of Manchester for funding.

This thesis is dedicated to my parents and is in memory of my mum

Chapter 1: Introduction

1.1 General Introduction

Mitosis is a carefully regulated process, by the end of which a cell will generate two genetically identical daughter cells. Mechanisms are present in mitosis and the cell cycle to minimise and correct any problems the cell comes across. This may include erroneous kinetochore-microtubule attachments, abnormal missegregation or inaccurate replication. Many changes occur in mitosis such as cellular architecture modifications and the halting of transcription and translation. This makes mitosis a vulnerable phase of the cell cycle, and therefore, perturbation can occur, causing downstream consequences, influencing the fate of the cell. Cancer can be characterised by a deregulated cell cycle and mitosis (Hanahan and Weinberg, 2011), and strategies to combat disease involve the induction of aberrant mitoses, with the objective of causing apoptosis (programmed cell death). Approaches to induce abnormal mitoses include the use of antimitotics and these encompass agents targeting the spindle, such as paclitaxel (Taxol) and vinca alkaloids (Jordan and Wilson, 2004), spindle assembly checkpoint (SAC) components and mitotic proteins (Jackson et al., 2007).

For the treatment of breast, ovarian, lung and prostate cancers, antimitotics such as Taxol are at the forefront of cancer chemotherapy (Dumontet and Jordan, 2010). These agents have shown great success, for example in metastatic prostate cancer, where the combination of docetaxel (an analogue of paclitaxel) and hormone therapy drastically extended survival in comparison to standard therapy alone (James et al., 2016). Taxol is now one of the highest-grossing cancer chemotherapy drugs on the market, and annual sales of $1.6 billion were achieved in 2000, with post-patent sales in 2013 of $92 million (http://www.oasmia.com/news.asp?c_id=404). Despite the successes, it is inevitable that side effects will be prevalent as a result of disrupting the peripheral nervous system (Dumontet and Jordan, 2010; Rowinsky et al., 1993). Other unfavourable aspects of antimitotic treatment include the issue of acquired resistance (Murray et al., 2012), the difficulty in predicting which patients are likely to respond, and the lack of understanding as to why paclitaxel, for example, is effective for tumours such as breast but is ineffective against solid tumours such as kidney carcinomas (Jordan and Wilson, 2004). As a result, second-generation inhibitors have been developed, where mitotic kinases and kinesins are targeted, including Plk1, Aurora A

and B, Cenp-E and Eg5 (Jackson et al., 2007; Keen and Taylor, 2009; Lens et al., 2010; Malumbres, 2011; Manchado et al., 2012; Taylor and Peters, 2008). Unfortunately, these agents have failed to deliver in the clinic (Komlodi-Pasztor et al., 2012; Mitchison, 2012). Consequently, the failure may be a result of our lack of understanding of antimitotic action in cells and tumours, and thus incorrect targets or mechanisms may have been studied.

The deregulation of mitosis can also lead to the missegregation of chromosomes, resulting in daughter cells which are genetically imbalanced. This aneuploid characteristic is a common feature of cancers, and has been implicated in tumourigenesis (Boveri, 1914; Cimini, 2008; Mitelman, 2014; Nicholson and Cimini, 2011). The presence of aneuploidy in normal somatic cells doesn't allow for survival and therefore, a major question is understanding how the cancer cells, despite the mitotic abnormalities, are able to survive and proliferate.

To understand the lack of success of second-generation inhibitors, with an appreciation of how cells respond to mitotic perturbation, I will give an overview of mitosis and apoptosis. I will firstly outline mitosis and its regulation, leading onto the mechanism of action of antimitotics, and the responses and fates often encountered upon exposure. Since evidence suggests the antitumor effect of antimitotics is via an apoptotic response, the final part of the introduction will focus on apoptosis.

1.2 Mitosis

1.21 The cell cycle and mitosis

The eukaryotic cell cycle is a highly controlled and ordered system which results in the generation of genetically identical daughter cells (Hochegger et al., 2008). It is divided into 4 defined stages, which are characterised by chromosomal properties (Figure 1.1A). This includes G1, which is an interphase state, followed by entry into S phase, involving chromosome synthesis and duplication. G2 is marked by a G2/M checkpoint. Mitosis is defined by chromosome segregation, resulting in the generation of identical daughter cells. The cell cycle is tightly regulated by the activation of cyclin-dependent kinases (Cdks) by the interaction with their cyclin binding partners.

Mitosis consists of multiple stages based on intracellular characteristics, including microtubule structures and chromosomal features and dynamics (Figure 1.1B). In 1881, Flemming first visualised and described mitosis, where microscopic changes were observed in the nucleus upon cell division (Flemming, 1881). ‘Thread-like’ structures were present in the nucleus, and these divided in a longitudinal fashion,

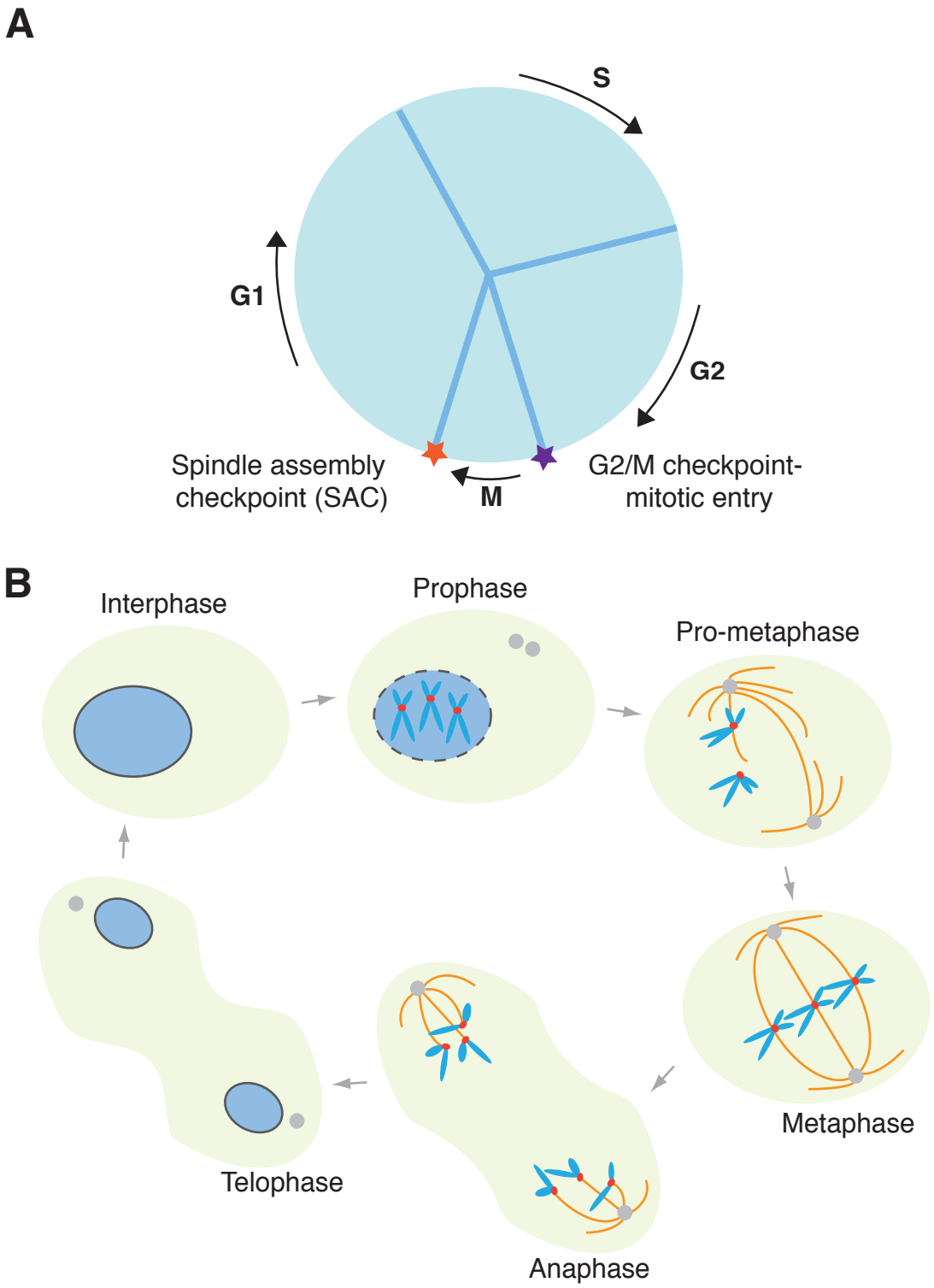

Figure 1.1 Cell cycle and mitosis.
(**A**) The mammalian cell cycle consists of G1 (interphase), S (synthesis phase) where DNA is replicated, G2, and M (mitosis) involving cell division, typically lasting 24 hours. (**B**) Mitosis consists of interphase, prophase where the nuclear envelope breaks down and chromosomes condense, prometaphase where the spindle apparatus forms, metaphase where chromosomes align along the spindle equator, anaphase involving chromosome segregation, and telophase.

moving to opposite ends of the cell upon division. These 'threads' were later defined as chromosomes.

Entry into mitosis is marked by chromosome condensation in prophase, whereby chromosome architecture becomes visible under the microscope. Here, the S-phase duplicated centrosomes move to opposite sides of the nucleus. This is followed by prometaphase where the nuclear envelope breaks down, allowing the chromosomes to move from the nucleus into the cytoplasmic region, with the mitotic spindle becoming visible. The microtubule asters nucleated at the centrosome then attach to kinetochores of the chromosomes (via 'search and capture', described in Section 1.31). Upon progression, chromosomes align at the metaphase plate, and thus this is defined as metaphase. From here, sister chromatids separate, moving towards opposite ends of the cell and the spindle elongates in anaphase. Next, chromosomes decondense, and nuclear envelopes form to give two daughter cells in telophase and cytokinesis respectively, where cytokinesis is characterised by the physical separation of the parental cytoplasm into the two daughter cells. An interphase states then follows.

1.22 Entry and exit into mitosis

1.221 Cdk1 and cyclin B1

The cell cycle and in particular mitosis, including entry and exit from this state, are regulated by the Ser/Thr Cdk's and their cyclin binding partners (Hochegger et al., 2008). With its discovery in sea urchin eggs in 1983 (Evans et al., 1983), cyclin B1 was identified as important for mitotic entry and exit when in complex with Cdk1, where levels of cyclin B1 heighten in G2 (Lindqvist et al., 2007; Nigg, 2001; Nurse, 1990; O'Farrell, 2001; Santamaría et al., 2007). The Cdk1-cyclin B1 complex was initially identified in *Xenopus* oocytes (Lohka et al., 1988), where it was indicated to be essential for early mitotic events. It has also been shown to be important for centrosomal separation and spindle formation (Blangy et al., 1995; Crasta et al., 2006; Nigg, 1995).

Prior to mitotic entry, the Cdk1-cyclin B1 complex is in an inactive state in the cytoplasm, with Myt1- and Wee1-dependent inhibitory phosphorylations at Thr14 (Liu et al., 1997) and Tyr15 (Parker et al., 1992) of Cdk1 respectively. At the end of G2, a certain threshold level of Cdk1-cyclin B1 is reached, and this autocatalyses further activation of Cdk1-cyclin B1 (Solomon et al., 1990), marking entry into mitosis. Once at the point of mitosis where Cdk1-cyclin B1 is detected at centrosomes (Jackman et al., 2003), Cdk1 activating kinase (CAK) phosphorylates Cdk1 at Thr161 within the

activation loop (Krek and Nigg, 1992; Lolli and Johnson, 2005; Solomon et al., 1992). This is accompanied by the removal of the inhibitory phosphates by Cdc25 phosphatases (Boutros et al., 2006; Strausfield et al., 1991). In late prophase, Cdk1-cyclin B1 is translocated into the nucleus (Hagting et al., 1999).

Cdk1-cyclin B1 remains activated until stable kinetochore-microtubule attachments occur. Throughout mitosis, cyclin B1 levels slowly decline causing an inactivation of Cdk1 (Pines, 2006), where at the point of anaphase, cyclin B1 levels rapidly decline and the cell exits mitosis. Ultimately, cyclin B1 is ubiquitinated (Glotzer et al., 1991) by the E3 ubiquitin ligase anaphase promoting complex/cyclosome (APC/C) (Clute and Pines, 1999; Iringer et al., 1995; King et al., 1995; Sudakin et al., 1995), targeting it for degradation by the proteasome, followed by mitotic exit.

1.222 Other kinases involved in mitotic entry/exit

Although Cdk's are the major regulators of mitotic entry and exit, other kinases also play important roles in control. Such kinases include the polo-like kinases (Plk's) (Zitouni et al., 2014) and the Aurora kinases (specifically A and B). In particular, Plk1 is expressed from G2, and is degraded at the end of mitosis (Lindon and Pines, 2004; Uchiumi et al., 1997), with maximal kinase activity at G2/M (Golsteyn et al., 1995). Prior to mitotic entry, Plk-1 is activated by the Aurora A-Bora complex (Seki et al., 2008), and this initiates Cdk-1-cyclin B1 effectors (Lindqvist et al., 2007). Plk1 regulates Cdk-1-cyclin B1 activity by direct phosphorylation and activation of the phosphatase Cdc25 (Toyoshima-Morimoto et al., 2002). Furthermore, Plk1 phosphorylates Wee1, which induces its degradation and consequently decreases Cdk1 phosphorylation (Watanabe et al., 2004).

Furthermore, the Auroras are activated, and levels peak, in mitosis (Bischoff and Al., 1998; Stewart and Fang, 2005). Specifically, Aurora B is found to complex with Survivin, Borealin and INCENP as part of the chromosomal passenger complex (CPC) (Carmena et al., 2012). In early mitosis the CPC complex is associated with the condensing chromosome arms, with re-localisation to centromeres and kinetochores in metaphase (Adams et al., 2000; Earnshaw and Bernat, 1991). The CPC localises to different locations throughout mitosis to regulate processes such as chromosome condensation, the correction of erroneous kinetochore-microtubule attachments, spindle assembly checkpoint (SAC) activation and cytokinesis (Carmena et al., 2012). Aurora B plays a role as a tension-sensor, where it detects incorrect kinetochore-microtubule attachments. This role was first reported in budding yeast (Ipl1) (Biggins

and Murray, 2001; King et al., 2007), and later reported in mammalian cells (Kaitna et al., 2002; Kallio et al., 2002). When an aberrant attachment is detected (e.g. merotelic, syntelic, see Figure 1.4A), Aurora B activates the SAC and correction occurs. The mechanism of correction involves the Aurora B-induced phosphorylation of proteins localised at the kinetochore-microtubule interface, for example, components of the KMN network (Cheeseman et al., 2006; Welburn et al., 2010), where the phosphorylation destabilises the incorrect attachment(s). Normally, when a kinetochore becomes stably attached to the microtubule, tension follows and this causes the KMN network and Aurora B to move away from one another, and so Aurora B is not able to phosphorylate the KMN network components. Aurora B also plays important roles in ensuring chromosome biorientation and regulating genome stability (Lampson and Cheeseman, 2011; Ricke et al., 2011). This includes the phosphorylation of the motor protein Cenp-E (Kim et al., 2010), aiding in the accurate congression of chromosomes to the spindle equator. Following exit from mitosis, Aurora B is subsequently degraded by the APC/C (Stewart and Fang, 2005). Aurora B also plays roles in cytokinesis, where it is essential for phosphorylation of several components of this process, including centralspindlin (Kaitna et al., 2000) and Vimentin (Goto et al., 2003).

1.23 Kinases

Kinases are central to the control of mitosis, through phosphorylation in an activation segment of the protein (Nolen et al., 2004). Kinases catalyse the transfer of the terminal γ-phosphate from the co-factor ATP to the hydroxyl moiety of the Ser/Thr/Tyr of a specific substrate. As well as being essential in mitosis, protein kinases are also important in other cellular processes, where over 30% of the cells' proteins are phosphorylated by kinases (Cohen, 2000; Pinna and Ruzzene, 1996). Protein phosphorylation is critical for metabolism, differentiation, growth, division, membrane transport and immunity (Manning, 2002).

The kinases can be divided into two families: the Ser/Thr and the Tyr kinase families (Bayliss et al., 2012; Hanks and Hunter, 1995). Protein kinase structures are highly conserved, and the core structure consists of two lobes, a small N-terminal lobe (N-lobe) and a large C-terminal lobe (C-lobe) (Figure 1.6A). These lobes are connected by a hydrophobic 'spine' and a Lys-Glu salt bridge (Kornev et al., 2006), which form a cleft where ATP binds i.e. the kinase domain. The kinase domain is composed of twelve sub-domains indicated by roman numerals (Hanks and Hunter, 1995), which are invariant throughout the kinase super-families, signifying important function (See Figure

1.5B, C as an example with Bub1 kinase). For example, sub-domain I, often referred to as the Gly-rich loop, is essential as a flexible 'flap' for the anchoring of the *α*- and *β*-phosphates of bound ATP. In sub-domain II, there is a conserved Lys residue, where the terminal $–NH_3^+$ binds the phosphates of ATP and this is essential for kinase activity ((Hanks and Hunter, 1995) and see (Figure 1.6C)). The Glu in subdomain III stabilises interactions between the Lys and ATP. Furthermore, the sub-domain VIB is so called the catalytic loop due to the Asp residue being defined as the catalytic base, where its acts as an acceptor for the proton of the –OH of the substrate. In Sub-domain VII there is a highly conserved DFG sequence (DLG in Bub1), where the Asp is crucial for the coordination of a divalent metal ion (e.g. Mg^{2+}) to stabilise the terminal phosphate of ATP and correctly orientate it for phospho-transfer. This DFG (DLG) motif is essential for activation of kinases where the Gly induces the correct orientation of the catalytic Asp (Kornev et al., 2006). This orientates the 'spine' and the Lys-Glu bridge, which defines the active conformation of the kinase.

1.3 Spindle assembly

The microtubule spindle is a structure that ensures mitotic processes proceed accurately and timely (Heald and Khodjakov, 2015). The turnover of microtubules in mitosis is 5-10 fold higher than in interphase (Saxton et al., 1984), aiding in the dynamic process of mitosis. The plus ends of microtubules are highly dynamic, and undergo periods of growth and shrinkage. Upon entry into mitosis, shrinkage occurs at a higher frequency than growth, where the long, stable cytoskeleton in interphase is modified into dynamic radial arrays, with radiation nucleated at the duplicated centrosome. The centrosome is comprised of a pair of centrioles and this is referred to as the microtubule organising centre (MTOC). When duplicated centrosomes move towards opposite ends of the cell, these mark the spindle poles. Microtubules radiate out from the centrosome (the minus end) towards the centre of the cell, the spindle midzone (plus end).

1.31 Microtubules

The spindle is composed of microtubule polymers consisting of dimers of *α*- and *β*- tubulin monomers (Figure 1.2A). These are arranged in a non-covalent fashion, forming protofilaments and microtubule structures. The minus and plus ends of the microtubule are dynamic, with exposure of *β*-tubulin defined as the plus end, and *α*-tubulin, the minus end. Due to the higher affinity of tubulin for the plus end, this end is

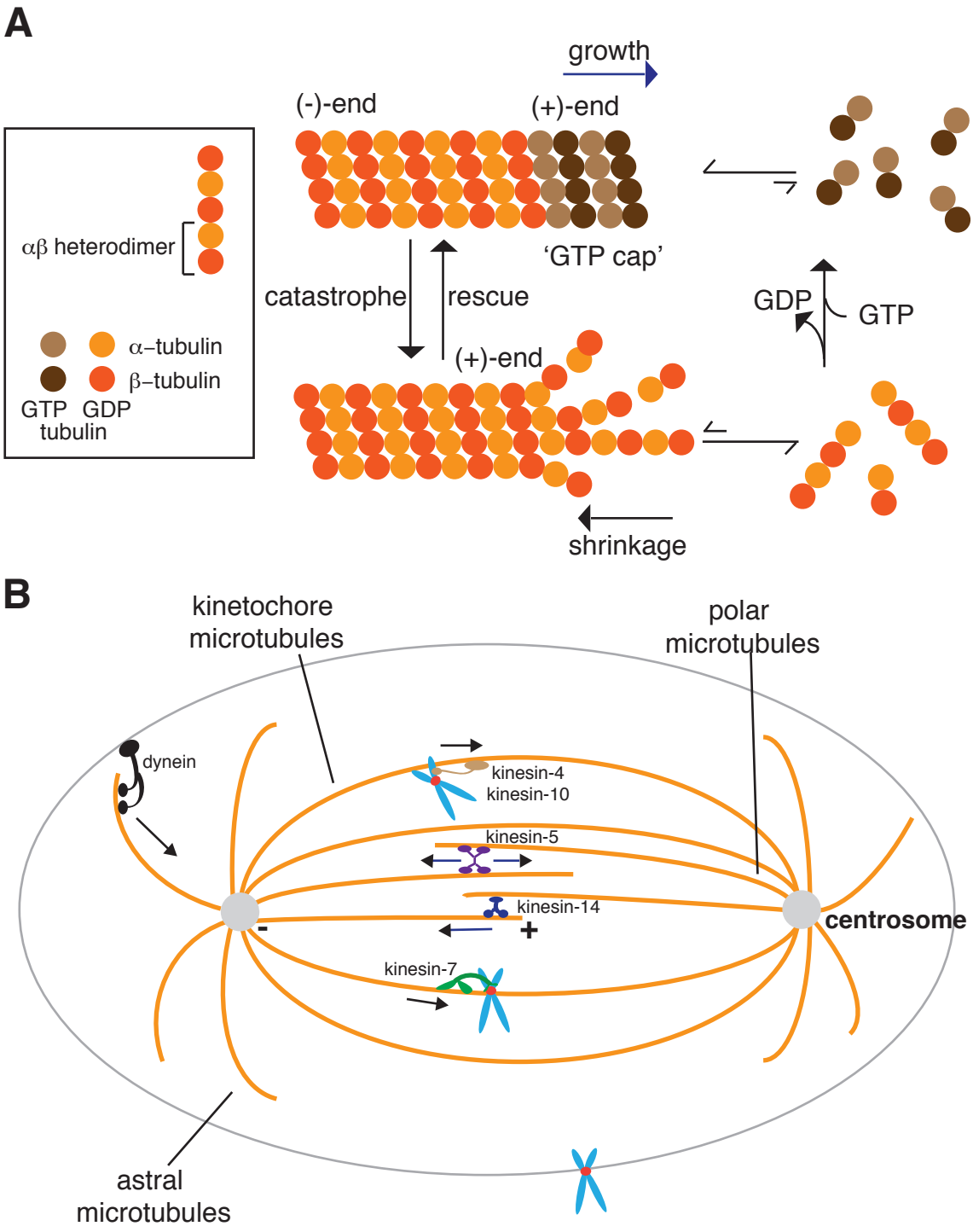

Figure 1.2 Microtubule dynamics and the bipolar spindle.
(**A**) Microtubules are composed of heterodimers of α– and β-tubulin, making up protofilaments. Growth is at the plus end of the microtubule, utilising energy from GTP hydrolysis, where a 'GTP cap' forms. When GTP hydrolysis is faster than the microtubule polymerisation, the microtubule will undergo a change from growth to shrinkage.
(**B**) Motor proteins are involved in the generation of the bipolar spindle. Kinesin-5 works to push apart the centrosomes; kinesin-4 and -10 to connect chromosomes with the spindle; kinesin-14 restricts the spindle length and kinesin-7 links kinetochores to the microtubules. Dyenin is involved in positioning the bipolar spindle within the cell.

seen as the more dynamic region and is where the majority of the growth is seen. The microtubule interchanges between growth and shrinkage where there is the addition and loss of *α*-/*β*- subunits, utilising energy from GTP hydrolysis, resulting in dynamic instability (Mitchison and Kirschner, 1984). GTP-bound tubulin binds and is subsequently hydrolysed to GDP. The ends of the microtubule mainly consist of GTP-bound tubulin and this results in a 'GTP cap'.

The 'search and capture' mechanism involves the attachment of chromatids to the spindle (Kirschner and Mitchison, 1986), and is used to define the means as to how chromosomes and microtubules initially interact. In the first instance, the microtubules effectively 'search' for a target in close range. The target 'captures' the microtubule, causing microtubule dynamics to decrease and a stable interaction follows. In this case, the target is the kinetochore, where the kinetochore is a complex comprised of multiple proteins, residing at the centromeric region of the chromosome (Tanaka et al., 2005). The proposed 'search and capture' hypothesis was later visualised in living cells (Hayden et al., 1990; Rieder and Alexander, 1990), where it was confirmed that initially, the kinetochore of a chromosome interacts with a single microtubule. Other studies have emerged indicating that the 'search and capture' mechanism is not quite this simple (Holy and Leibler, 1994; Wollman et al., 2005). It has been considered that there are mechanisms which induce the formation of microtubules when close to kinetochores. Other changes occur, for example, alterations in the conformation of the kinetochore, which aid the interaction.

The mitotic spindle is comprised of three different types of microtubules (Figure 1.2B): polar microtubules, which radiate from the poles, meeting in the midzone; kinetochore microtubules (K-fibres), that interact with the kinetochores of the sister chromatids; and astral microtubules, originating from the pole towards the cortex, functioning to position the spindle within the cell. The self-organisation properties of the spindle and the action of the motor proteins act in concert to form the bipolar spindle.

Following mitotic entry and progression through mitosis, a bipolar spindle is formed. This allows for sister chromatids to face opposite poles of the cell and biorientate, allowing for accurate segregation of chromosomes in anaphase. If in fact, the spindle is not bipolar, but is aberrantly multipolar for example, this will result in mass chromosome missegregation errors. Multipolar spindles are often associated with centrosome amplification and chromosome instability (CIN) (Chan, 2011; Lingle et al., 1998; Pihan et al., 1998). Despite this, tumour cells do not often exhibit multipolar divisions, but in fact, divide with a normal bipolar spindle (Steinbeck, 2001). This is

because a multipolar anaphase is lethal (Ganem et al., 2009; Kwon et al., 2008), and therefore cancer cells tend to cluster centrosomes to form two spindle poles (Quintyne et al., 2005), allowing for 'normal' divisions to occur.

1.32 Motor proteins

Originally, chromosome segregation was thought to be solely as a result of the forces derived from microtubule spindle assembly and disassembly (Inoué and Salmon, 1995). However, motor proteins also play an essential role in driving chromosome segregation, as well as in spindle assembly, chromosome congression and cytokinesis. Motor proteins can be divided into the minus end dyneins, and the plus end kinesins (Titus, 2012), albeit with some exceptions. In general, the motor proteins move along the microtubules transporting cargo (e.g. chromosomes), using energy from ATP hydrolysis.

Kinesins are grouped into 14 families, based on their sequence similarity (Lawrence et al., 2004). Genetic screens identified mitosis-specific kinesin motor proteins, for example in an RNAi-screen in *Drosophila*, kinesins required for processes such as chromosome alignment and spindle formation were identified (Goshima and Vale, 2003), followed by screens in mammalian cells (Zhu et al., 2005). Structurally, kinesins have a motor head, a stalk, and a cargo-binding tail ((Titus, 2012) and see (Figure 1.3A)). The motor head contains an ATP-binding site and a location for microtubule binding. The movement of kinesins along the microtubules is via a 'hand-over-hand' mechanism (Gennerich and Vale, 2009). The leading ADP-bound head exchanges ADP for ATP, and through conformational changes in the neck linker, the lagging head moves forward and binds to the microtubule. When ATP is hydrolysed, the lagging head is then 'primed' for a 'power stroke' and ATP replaces ADP on the leading head (Cochran et al., 2006). This is a continual process along the microtubule.

The initial step in the formation of the spindle is the separation of the centrosomes, moving towards opposite ends of the cell. This separation is aided by dynein motor proteins, which attach to microtubule plus ends, moving towards the minus end (Titus, 2012). Of the kinesin motor proteins, it is kinesin-4, -5, -10, -13, and -14, which play essential roles in bipolar spindle formation (Figure 1.2B). In particular, kinesin-5 (e.g. Eg5) binds separate microtubules in the spindle midzone via the two opposing motor domains, and this results in the pushing of the microtubules and poles apart. Depletion of this protein gives rise to a monopolar spindle (Ferenz et al., 2010), indicating its importance in the formation of a bipolar spindle. Kinesin-4 and -10

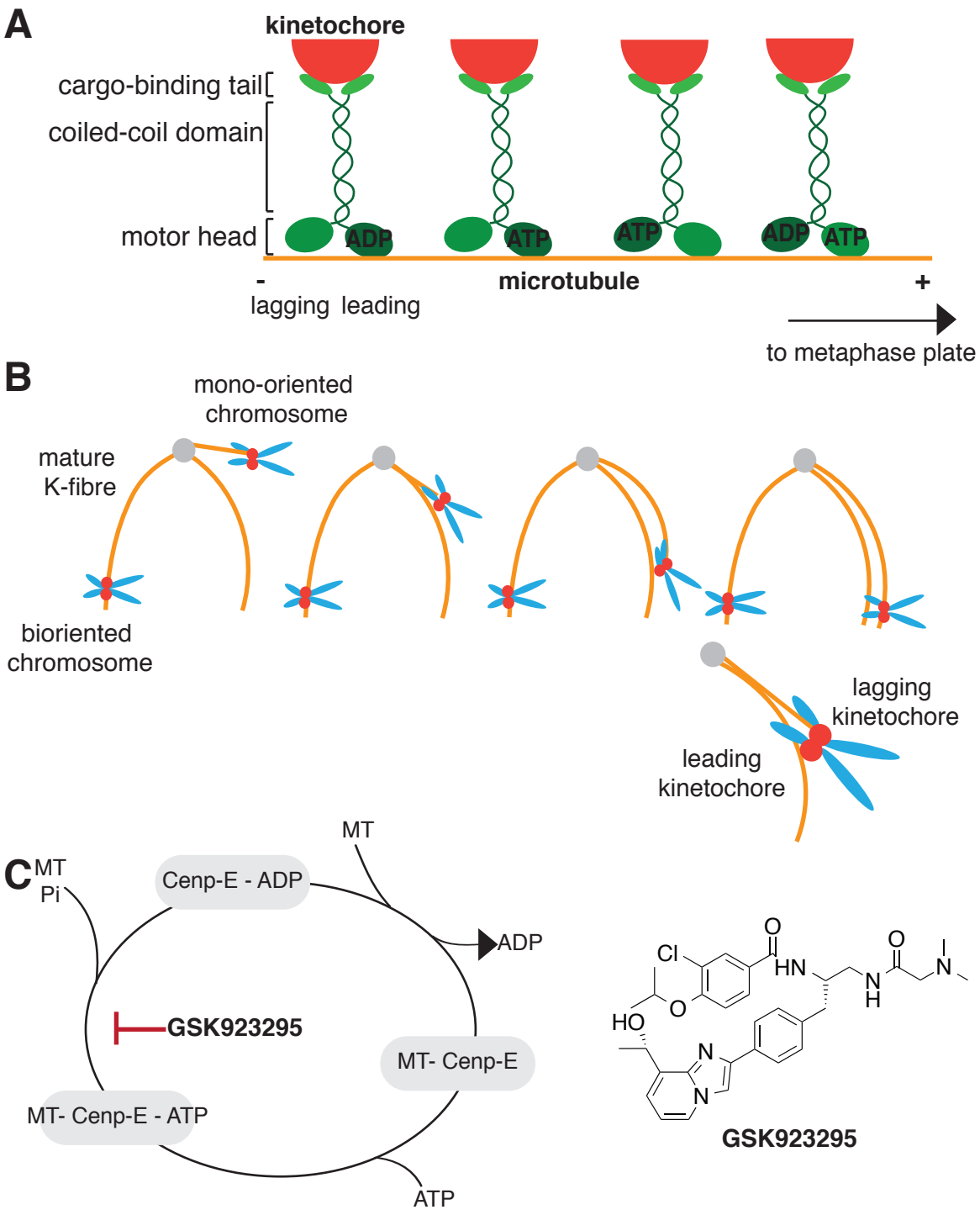

Figure 1.3 The motor function of Cenp-E and mode of GSK923295 inhibition.
(**A**) Kinesin motor proteins are made up of a cargo-binding tail, a coiled coil domain linking the tail to the motor head, where the motor head consists of an ATP binding pocket and a microtubule-binding site. Energy from ATP hydrolysis is required to transport cargo along the microtubules. Adapted from Titus and Wadsworth, 2012.
(**B**) Kinesin-7 (Cenp-E) acts to slide mono-oriented chromosomes along kinetochore fibres, ensuring eventual biorentation. Adapted from Kapoor et al., 2006.
(**C**) GSK923295 binds at an allosteric site of the motor head, distant from the ATP binding site, changing the conformation of the bound motor protein to the microtubule. This prevents further movement of Cenp-E along the microtubule. Adapted from Wood et al., 2010.

(chromokinesins) facilitate the interaction between the spindle and the chromosome arms, and also aid in the positioning of the spindle within the cell. Repression of kinesin-4 results in chromosome alignment defects (Mazumdar et al., 2004). Kinesin-13 depolymerising motors are involved in regulating microtubule dynamics, with location at the microtubule ends, the kinetochores and spindle poles. Kinesin-14 is a minus-end directed protein and enables the cross-linking of the microtubules. The inward force generated by the kinesin-14 proteins opposes that of the motor proteins involved in spindle bipolarity, therefore maintaining the stability of the spindle. Following formation of the bipolar spindle, mitosis can proceed, and subsequent phases are mediated by motor proteins, one being Cenp-E. As motor proteins are important in regulating mitosis, and because of the toxicity problems and resistance seen with traditional antimitotics, targeting the motors by small molecule inhibition is being studied (Huszar et al., 2009).

1.321 Cenp-E

Cenp-E (Centromere-associated protein E) is a kinesin-7, plus-end directed motor protein (Wood et al., 1997). With accumulation in G2 and degradation in telophase (Brown et al., 1994), it is involved in the maintenance of the stable interaction between kinetochores and microtubules (Gudimchuk et al., 2013; Putkey et al., 2002). Cenp-E is highly important in mitosis, where it is essential for the congression of chromosomes towards the metaphase plate (Kapoor et al., 2006; Kim et al., 2010, 2008; Schaar et al., 1997; Yen et al., 1991). The specific function of Cenp-E is in the 'sliding' of mono-oriented chromosomes along mature K-fibres to the metaphase plate, ensuring eventual biorientation ((Kapoor et al., 2006) and see (Figure 1.3B)).

When Cenp-E is depleted, the majority of chromosomes align along the spindle equator, with a few remaining at the poles, exemplified by antibody injection in mammalian cells (Schaar et al., 1997); protein expression depletion (Wood et al., 1997); using antisense oligonucleotides (Yao et al., 2000) and gene inactivation (Putkey et al., 2002). The resulting unaligned chromosomes are mono-oriented (Kapoor et al., 2006), and this phenotype is consistent with the ability of a single unattached kinetochore being able to prevent mitotic progression (Li and Nicklas, 1995; Rieder et al., 1995, 1994). In fact, defective Cenp-E functioning results in the activation of the spindle assembly checkpoint and a subsequent mitotic arrest (Abrieu et al., 2000; Lara-Gonzalez and Taylor, 2012; Yao et al., 2000).

With localisation at the kinetochores throughout mitosis, the activity and functioning of Cenp-E is controlled by the Aurora A and B kinases and protein phosphatase 1 (PP1), where there is a continual phosphorylation-dephosphorylation switch, imposing important regulatory control (Kim et al., 2010; Wood et al., 1997; Yen et al., 1992).

Functions of Cenp-E are not limited only to chromosome congression, since an observable concentration of Cenp-E is still present at the kinetochores of congressed chromosomes (Brown et al., 1996; Cooke et al., 1997). When Cenp-E is depleted there is a reduction in the microtubules associated with the already congressed chromosomes (McEwen et al., 2001; Putkey et al., 2002), and additionally, when Cenp-E is depleted in MEFs there is an increased incidence of lagging chromosomes in anaphase figures (Putkey et al., 2002; Weaver, 2003).

Given its role in mitosis and the fact that mice and cells with repressed Cenp-E exhibit high rates of aneuploidy (Weaver, 2003), where *in vitro* 25% of divisions resulted in aneuploid daughter cells, and *in vivo*, 95% of hepatocytes were aneuploid; the connection between Cenp-E, aneuploidy and tumourigenesis has been studied ((Weaver et al., 2007) and see (Section 1.51)). Cenp-E can act as both a tumour suppressor and as an oncogene. Analysis of patients with breast cancer revealed that those with cyclin-B1 overexpressing tumours upregulated Cenp-E and this resulted in a poor prognosis (Agarwal et al., 2009). On the other hand, low expression of Cenp-E is seen in hepatocellular carcinomas (Liu et al., 2009). Due to this observation, pharmacological inhibition of Cenp-E may be advantageous.

GSK923295 is a recently described inhibitor of Cenp-E ((Qian et al., 2010) and see (Figure 1.3C)). Discovered through a screen of 700K compounds, structures which disrupted the ATPase activity of Cenp-E were identified. From this, the lead structure was optimised to obtain GSK923295. This compound was shown to harbour a high affinity for the Cenp-E motor domain when bound to microtubules (Wood et al., 2010), inducing the formation of a stable ATP-bound/Cenp-E/MT complex (Figure 1.3C). This restricts further movement of the Cenp-E motor protein, giving rise to the typical phenotype described previously. Evidence also suggests the binding of GSK923295 at an allosteric site away from the ATP-binding site, and this inhibitor is therefore described as non-competitive towards ATP. When cells were exposed to GSK923295 cellular proliferation was inhibited (Qian et al., 2010), inducing an accumulation of cells with 4n DNA content, which is consistent with a mitotic delay (Wood et al., 2010), ultimately leading to apoptosis. In human tumour xenografts, GSK923295 exposure

resulted in reduction in tumour volume (Wood et al., 2010), and treatment has also shown efficacy in a Phase I trial (Chung et al., 2012), where partial responses and stable disease were observed.

Cenp-E is also a major component of the SAC. Cenp-E coimmunoprecipiates with BubR1 (Chan et al., 1998; Yao et al., 2000), and this interaction promotes the recruitment of BubR1 to kinetochores, which is important for its kinase activity (Mao et al., 2005, 2003; Weaver, 2003). Additionally, the evidence supporting its role in the SAC is shown in studies where there is a checkpoint override with Cenp-E depletion in the presence of microtubule-depolymerising agents (Abrieu et al., 2000).

1.4 The Spindle Assembly Checkpoint (SAC)

1.41 An overview of the SAC

To prevent premature anaphase onset, the SAC functions to maintain the cell in a mitotic state until all kinetochores are stably attached to microtubules (Lara-Gonzalez and Taylor, 2012). In order to achieve this stable attachment, all chromosomes must be biorientated in an amphitelic fashion (Figure 1.4A). Even when one chromosome fails to biorientate, this is sufficient to activate the SAC (Rieder et al., 1994).

Components of the SAC were discovered in genetic screens in budding yeast *Saccharomyces cerevisae* where Mad1, Mad2, Mad3 (BubR1), Bub1 and Bub3 mutants were shown to exit mitosis prematurely in the presence of microtubule-targeting drugs (Li and Murray, 1991; Roberts et al., 1994), and this was followed by the discovery of Mps1 (Weiss and Winey, 1996). In early prophase, Bub1 is recruited to kinetochores (Jablonski et al., 1998) via Knl1 (Kiyomitsu et al., 2007; Krenn et al., 2012), a member of the KMN network. The MELT motifs on Knl1 are phosphorylated by Mps1, which promotes Bub1 targeting to kinetochores (Yamagishi et al., 2012b). Furthermore, the autophosphorylation of Bub1 at Thr589 is important for its kinetochore docking function (Lin et al., 2014). Recruitment of Bub1 to the kinetochore is aided by the binding of Bub3 (Roberts et al., 1994; Taylor et al., 1998; Taylor and McKeon, 1997), and this site serves as a docking place for the binding of other SAC components such as BubR1, Bub3, Mad1 and Mad2. When cells enter mitosis, Mad1-C-Mad2 (C: closed) is recruited to kinetochores under Mps1 control (Hewitt et al., 2010; Lara-Gonzalez et al., 2012). From here, free cytosolic O-Mad2 (O: open) binds to the complex at the kinetochore, closing in conformation and then binds Cdc20. This forms a C-Mad2-Cdc20 complex which then interacts with BubR1-Bub3, forming the mitotic checkpoint complex (MCC) (De Antoni et al., 2005). The MCC inhibits the APC/C,

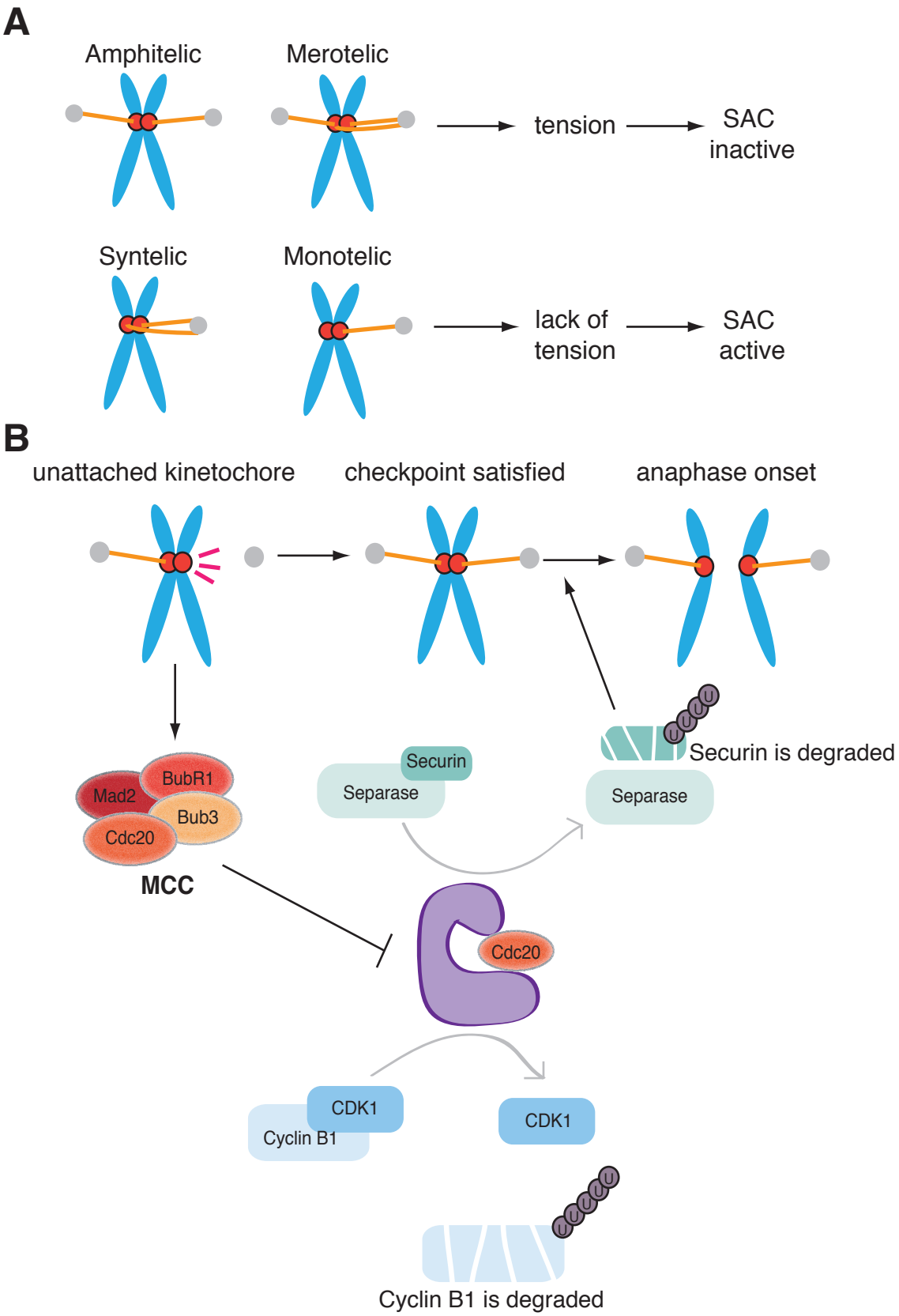

Figure 1.4 The spindle assembly checkpoint (SAC).
(**A**) Amphitelic or merotelic kinetochore attachments satisfy the checkpoint, whereas syntelic or monotelic attachments cause a lack of tension and activate the SAC.
(**B**) Upon activation, the MCC is assembled and inhibits the APC/C, preventing anaphase onset; if the checkpoint is satisfied, Cdc20 binds to the APC/C and cyclin B1 and securin are degraded. Separase is then able to cleave cohesin, and sister chromatids separate.

preventing its activating cofactor Cdc20 from binding. When the SAC is active, a protease (separase) is bound by an inhibitory securin complex, and Cdk1-cyclin B1 complexes exist. When the SAC is satisfied upon stable kinetochore attachment, the MCC is disassembled (mediated by $p31^{comet}$) (Westhorpe et al., 2011), and the APC/C is free to be bound by its cofactor: either Cdc20 or Cdh1. The Mad1-C-Mad2 core structure is then ejected from the kinetochores via 'stripping'. As the APC/C is no longer inhibited, it can function to ubiquitinate cyclin B1 and securin for degradation by the proteasome. It is the degradation of cyclin B1 which marks the exit from mitosis.

1.42 Bub1

1.421 The roles of Bub1 and its kinase activity

Bub1 (Budding uninhibited by imidazole 1) is an important player in the SAC and also exhibits kinase activity. It is significant as a scaffolding protein (Jablonski et al., 1998; Johnson et al., 2004; Sharp-Baker and Chen, 2001), where it first localises to the kinetochore in prophase, followed by other checkpoint proteins including BubR1, Cenp-E and Mad2. Furthermore, Bub1 is important for chromosome alignment and segregation, since when depleted, defects in alignment are apparent (Bernard et al., 2001; Johnson et al., 2004; Meraldi and Sorger, 2005; Perera et al., 2007; Warren et al., 2002). There is considerable evidence that Bub1 is an essential protein required for mitosis and the SAC (Johnson et al., 2004; Kitajima et al., 2005; Meraldi and Sorger, 2005; Morrow et al., 2005; Perera and Taylor, 2010; Perera et al., 2007; Tang et al., 2004), with dependence upon Aurora B for maintenance of a checkpoint arrest in response to microtubule damage (Morrow et al., 2005).

To test the significance of Bub1 depletion, a Cre-LoxP approach was used to generate a conditional null Bub1 allele (Perera et al., 2007). The knockout of Bub1 indicated its role in embryogenesis, development and the proliferation of MEFs. Further experimentation revealed that in Bub1-deficient cells, the SAC was abolished in response to monastrol, and chromosome alignment was defective.

Further studies in *Schizosaccharomyces pombe* indicated the role of Bub1 kinase in the recruitment of shugoshin Sgo1 to the centromeres (Kitajima et al., 2005), with evidence of this function also confirmed in mammalian cells (Kitajima et al., 2005; Klebig et al., 2009; Perera and Taylor, 2010; Tang et al., 2004). Shugoshin is essential for the protection of the cohesin complex localised at the chromosomal centromere (Watanabe, 2005), where the complex is comprised of the subunits Smc1, Smc3, Scc1 and SA1/2. This cohesin complex is essential to maintain sister chromatid cohesion,

preventing premature separation. Timely dissolution of the sister chromatid cohesion ensures accurate segregation. Importantly, Bub1 kinase itself is not directly required to maintain centromeric cohesion (Perera and Taylor, 2010; Perera et al., 2007).

Sgo1 is phosphorylated and activated by Cdk1 at Thr346 in early mitosis (Liu et al., 2013). Phosphorylated Sgo1 interacts with the PP2A phosphatase (Liu et al., 2013; Tang et al., 2006), and it is this complex that prevents Cdk1 and Plk1 kinases from phosphorylating cohesin components, which would render cohesin unprotected. Sgo1-PP2A counteracts the Plk1-mediated phosphorylation of SA2, a subunit of the cohesin complex. Sgo1 is then involved in the regulated recruitment of Borealin, a member of the CPC (Tsukahara et al., 2010; Yamagishi et al., 2012a). Other members of the CPC, for example, survivin, are recruited by the Haspin kinase (Wang et al., 2011), where Aurora B phosphorylates Haspin, and this permits Haspin to phosphorylate histone H3 at Thr3 (Du et al., 2012; Kelly et al., 2010; Wang et al., 2010), allowing for binding of CPC components. Following SAC satisfaction, Sgo1 is dephosphorylated and localises away from the centromere (Higgins, 2013), no longer protecting the cohesin complex. The protease separase then cleaves the centromere cohesin subunit Scc1, and the sister chromatids separate (Uhlmann et al., 2000, 1999).

The mechanism by which Bub1 is involved in the recruitment of Sgo1 to centromeres is via the direct phosphorylation of histone H2A on Thr120 (Kawashima et al., 2010), in turn, recruiting Sgo1. Bub1 kinase also phosphorylates Cdc20, and this is essential for its activity towards the APC/C (Tang et al., 2004).

However, what part the kinase activity of Bub1 plays in the SAC is relatively unknown. Studies in Bub1-null MEFs, adding back Bub1 and its kinase mutants provided evidence that the kinase activity is non-essential for functioning of the checkpoint, since timings in mitosis were unaffected (Perera and Taylor, 2010). Furthermore, studies in budding yeast *Saccharomyces cerevisiae*, with a mutant lacking the kinase domain also showed proficient SAC activity (Fernius and Hardwick, 2007). Additionally, the expression of a kinase-deficient Bub1 indicated normal checkpoint functioning (Klebig et al., 2009). On the other hand, reports in fission yeast Schizosaccharomyces pombe, showed a kinase mutant did not prevent cell division when mitosis was perturbed (Yamaguchi et al., 2003), indicating that in fact, Bub1 kinase activity is required for the SAC.

However, it was suggested that Bub1 is required for the SAC as part of a fine-tuning mechanism. *Xenopus* egg extract experiments showed that in the presence of low numbers of nuclei and a mutant lacking the entire kinase domain of Bub1, SAC

function was compromised (Chen, 2004). However, a catalytically inactive Bub1 mutant K795R was able to restore SAC function when high numbers of nuclei were present (Sharp-Baker and Chen, 2001). Therefore, Bub1 kinase activity may be important to amplify the SAC signal when there are only one or two unattached kinetochores.

Previously, efforts to study this hypothesis have utilised kinase mutants and RNAi of the Bub1 proteins, which act to completely deplete the kinase activity or the expression of the protein. However, in order to study the effect of Bub1 kinase activity on SAC functioning, a small molecule inhibitor would be required to more carefully titrate the activity and study the implications of this perturbation.

1.422 The structure of Bub1 and inhibition

Kinase active sites are structurally similar and often conserved, and therefore obtaining specific inhibitors is difficult, since it is likely that an inhibitor will target a number of kinases. However, Bub1 shows small differences in comparison to generic kinases, potentially enabling the design of specific inhibitors.

Bub1 is comprised of an N-terminal tetratricopeptide (TPR) domain and a Bub3-binding domain, both of which are important for the kinetochore localisation of Bub1 ((Kang et al., 2008; Roberts et al., 1994; Taylor et al., 1998; Taylor and McKeon, 1997) and see (Figure 1.5A)). The C-terminus comprises a Ser/Thr kinase domain. As previously mentioned in Section 1.23, kinase domains are comprised of 12 sub-domains, highlighted in Figure 1.5B,C for Bub1, showing conservation among different species (Figure 1.5D). In fact, Bub1 has been shown to have an extended P+1 loop (part of the activation segment), and this is crucial for enabling the efficient phosphorylation of substrates (Kang et al., 2008). To allow for catalysis, the C-terminal portion of the P+1 loop undergoes a slight rearrangement to facilitate the process. Two KEN boxes reside in the N-terminal portion of Bub1, with importance in ubiquitination by APC/C^{Cdh1} (Qi and Yu, 2007), and for Cdc20 binding (Kang et al., 2008).

Typically, when studying the roles of kinases, chemical genetic approaches are used and include the use of ‘analog-sensitive’ (‘as’) alleles (Alaimo et al., 2001; Bishop et al., 2000, 1999). This involves the mutation of a conserved lipophilic ‘gatekeeper’ residue in the kinase active site (Figure 1.6A), to a smaller amino acid residue, for example a glycine or alanine. The resulting mutated kinase can then be targeted by bulky ATP analogue inhibitors, which can exploit the now larger binding pocket. However, the active site of Bub1 lacks an important lipophilic gatekeeper residue commonly observed in kinases, and at this position, a small Gly amino acid residue is

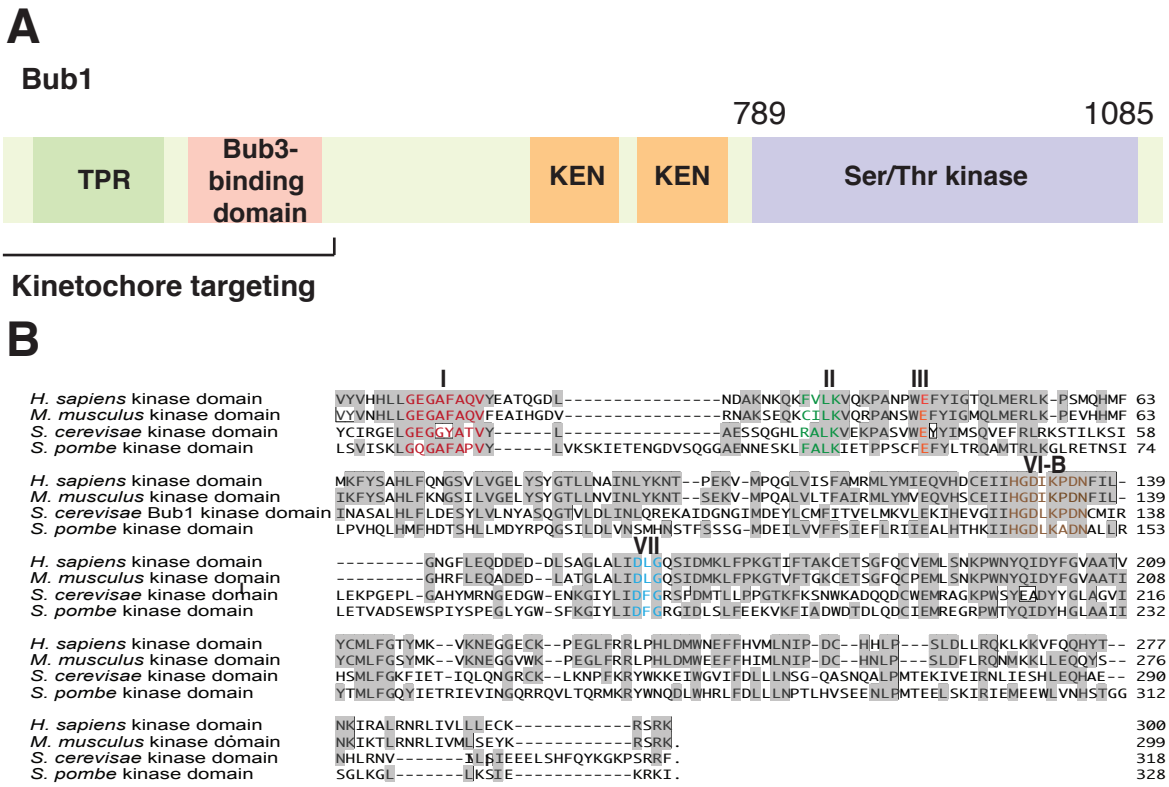

Figure 1.5 The structure of Bub1 kinase and its domains.
(**A**) The subunits of Bub1 consist of the TPR domain, the Bub3-binding domain, KEN boxes, and the kinase domain.
(**B**) Sequence alignment of the kinase domain across different species reveals homology, and the major subunits in the domain are highlighted.
(**C**) The critical motifs in the kinase domain show essential residues which are conserved across species.
(**D**) A table showing the percent identity and divergence between the kinase domains of the different species.

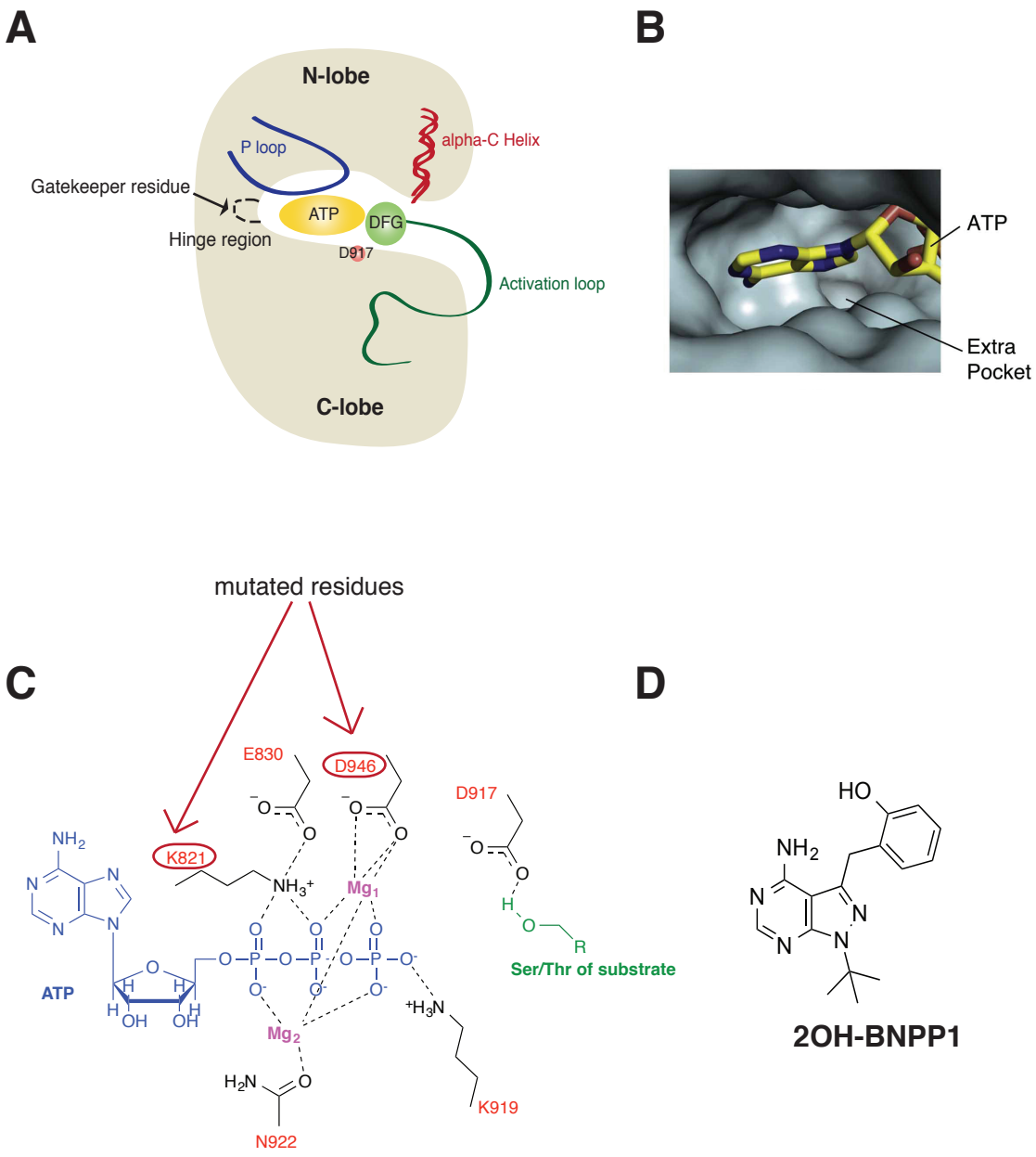

Figure 1.6 Inhibition of Bub1.
(**A**) The structure of kinases feature many different domains and include a gatekeeper residue. Often this gatekeeper is a bulky residue, but Bub1 has a glycine residue here.
(**B**) A crystal struture of the kinase domain of Bub1 with ATP bound, showing the region with an extra pocket. This can be utilised when approaching the design of Bub1-specific inhibitors. Taken from Kang et al., 2008.
(**C**) A diagram showing the binding between Bub1 residues in the ATP-binding pocket and ATP. The critical residues for kinase activity are highlighted. These are subsequently mutated in Chapter 3, giving kinase-dead mutants of Bub1.
(**D**) The structure of the Bub1 inhibitor, 2OH-BNPP1.

already present (G866 in human Bub1) (Kang et al., 2008). Therefore, an additional empty pocket is present adjacent to where ATP binds (Figure 1.6B, C). Consequently, selective inhibitors against the wild-type Bub1 kinase can be developed. Bub1 kinase was therefore screened against ATP-analogue inhibitors, which were originally designed to bind in the active site of the mutated kinases (Kang et al., 2008). From the screen, 2OH-BNPP1 was identified (Figure 1.6D), with an *in vitro* IC_{50} of 250 nM. See Chapter 3 for the analysis of 2OH-BNPP1 as a Bub1 kinase inhibitor.

1.423 Bub1 in cancer

Clinically, a low level of Bub1 expression has been indicated in a number of cancers such as lung, colon and pancreatic (Hempen et al., 2003; Shichiri et al., 2002). When Bub1 expression was reduced in mouse models, aneuploidy and tumour formation followed (Baker et al., 2009; Jeganathan et al., 2007; Schliekelman et al., 2009). Conversely, the overexpression of Bub1 has also been indicated in a number of cancers, such as breast, gastric and lymphomas (Alizadeh et al., 2009; Basso et al., 2005; Grabsch et al., 2003, 2004; van't Veer et al., 2002). Consistent with this notion, the overexpression of Bub1 was shown to contribute to aneuploidy and spontaneous tumour formation (Ricke et al., 2011), and also, the expression of Bub1 has been linked to a poor prognosis (Glinsky et al., 2005; Nakagawa et al., 2008; Sotiriou et al., 2003). Therefore, targeting Bub1 is of clinical interest in cancer chemotherapy settings.

1.5 Mitosis and Cancer

1.51 Aneuploidy, CIN and tumour evolution

Mitosis is a carefully regulated process, but mistakes can occur. If the SAC fails to detect aberrantly attached chromosomes, cells will progress through mitosis with the abnormality, potentially leading to chromosome missegregation. Daughter cells with abnormal and unequal chromosome content can be generated, with the genetic imbalances potentially manifesting at the protein level. This abnormal chromosome number is defined as aneuploidy. The aneuploid karyotype is a characteristic of cancers (Cimini, 2008; Mitelman, 2014; Nicholson and Cimini, 2011), where chromosomal gains, losses and translocations are seen. Although the effect of the aneuploid karyotype on the behaviour of cancer is not well defined, it is known that this abnormality in chromosome number does have a detrimental effect on cellular functioning (Torres et al., 2008). Abnormal chromosome karyotypes are associated with inherited disorders (Biesecker and Spinner, 2013). Interestingly, 10-30% of

fertilised human eggs are aneuploid, with >30% of miscarriages harbouring abnormal chromosome numbers (Hassold and Hunt, 2001). Of those that do survive, aneuploidy is the leading cause of genetic disorders e.g. Down Syndrome.

Aneuploidy is linked with chromosomal instability (CIN), characterised by high rates of chromosome gains and losses (Lengauer et al., 1998). High levels of aneuploidy in tumours is associated with poor prognosis, metastasis, and some level of resistance to chemotherapeutics (Heilig et al., 2010; Kuukasjärvi et al., 1997; McClelland et al., 2009; Swanton et al., 2009). The causes of whole chromosomal aneuploidy include chromosome instability (CIN) and defects in checkpoint genes (Gordon et al., 2012; Holland and Cleveland, 2009). The presence of merotelic attachments (Figure 1.3A), where one kinetochore of the chromosome is attached to both poles, may give rise to missegregation. Here, the SAC is essentially satisfied, although both kinetochores of the sister chromatids are not bound to the microtubules. Cancer cells often harbour increased frequency of merotelic attachments which can ultimately result in the generation of aneuploidy progeny (Thompson and Compton, 2010, 2008). In cases where cells have reduced levels of Cenp-E (Weaver, 2003), Bub1 (Johnson et al., 2004), or Aurora B (Ditchfield et al., 2003; Hauf et al., 2003), a mitotic arrest is followed by generation of aneuploid progeny. Aneuploidy may also arise as a result of centrosome amplification and hyperstabilised kinetochore-microtubule interactions (Ganem et al., 2009; Holland and Cleveland, 2012).

If we consider CIN, defined as an elevate rate of chromosome missegregation as a result of mitotic errors (Geigl et al., 2008; Gordon et al., 2012), this results in aneuploidy. Causes of CIN are broad, including the presence of multipolar spindles, defective spindle assembly, an aberrant SAC, and erroneous KT-MT attachments (for a review see (Thompson and Compton, 2011)).

The consequences of aneuploidy are widespread, and include changes in metabolism, cellular growth rate and the cell cycle (Gordon et al., 2012). Aneuploidy induces a stress upon the cell due to gene dosage and protein changes. In yeast strains harbouring an extra chromosome, delays in G1 were observed (Torres et al., 2007). The aneuploid strains also showed an increase in the sensitivity towards protein synthesis and folding drugs. In mammalian systems, Williams et al. observed perturbation and reduction in cellular proliferation, and aberrant metabolism when analysing trisomic MEFS, which was similarly observed across other mammalian systems (Tang et al., 2011; Torres et al., 2008; Williams et al., 2008). Furthermore, the gain or loss of chromosomes in normal diploid cells results in a G1 delay caused by

p53-dependent activation of the p21 kinase (Ganem and Pellman, 2012; Lanni and Jacks, 1998; Thompson and Compton, 2010).

As aneuploidy is detrimental to cellular growth, it is surprising that this chromosomal imbalance is a common feature of cancers. In 1914, Boveri established the link between mitosis, aneuploidy and tumourigenesis (Boveri, 2008, 1914). He observed the appearance of abnormal numbers of chromosomes in sea urchin embryos with irregular spindle poles. Already, tumours with aneuploid numbers of chromosomes had been analysed, and therefore, linking an aberrant mitosis to the formation of the aneuploid cells was suggested. Further to this, a moderate level of CIN can promote tumourigenesis (Silk et al., 2013), whilst in cases where CIN is very low or high, the detrimental impact on fitness means tumourigenesis is unlikely (Birkbak et al., 2011; Holland and Cleveland, 2012). When Cenp-E$^{+/-}$ mice were crossed with Mad2$^{+/-}$ or p19$^{ARF-/-}$ mice, increased cell death and low tumour incidence resulted, due to the high CIN. This is also supported by observations in patients, where moderate CIN indicates poor prognosis, and high CIN, a good prognosis (Birkbak et al., 2011).

Aforementioned, a weakened checkpoint gives rise to aneuploid cells; in mouse studies where one allele of the checkpoint genes Mad2, BubR1 or Bub3 were deleted, elevated rates of chromosome missegregation and incidences of tumours were apparent (Dai et al., 2004; Michel et al., 2001). Furthermore, Cenp-E$^{+/-}$ MEFs developed aneuploidy *in vitro* and *in vivo*, and mice heterozygous for Cenp-E developed spontaneous tumours resulting in lung adenomas and splenic lymphomas (Weaver et al., 2007). However, in tissues that are prone to spontaneous tumour formation, such as the liver, the presence of aneuploidy decreased tumourigenesis, where there was an increased incidence of tumours in wild-type mice in contrast to heterozygous Cenp-E$^{+/-}$ mice. Therefore, aneuploidy may promote and inhibit tumourigenesis, and this is dependent upon the level of genomic damage that is stimulated.

Since aneuploidy is anti-proliferative in non-transformed cells, the question remains: how do cancer cells tolerate aneuploidy? In human diploid cells where chromosome missegregation was induced, a reduced rate of proliferation and a p53-dependent cell cycle delay was apparent (Thompson and Compton, 2011, 2010). As cancer cells exhibit aneuploidy and often defective p53 functioning (Tomasini et al., 2008), the inability of p53 to function in the cell cycle arrest may contribute to the continued survival and proliferation of aneuploid cancer cells.

In order to examine these questions, tools to study aneuploidy are required. Common methods of aneuploidy induction include the use of antimitotics such as the Eg5 inhibitor monastrol (Cimini et al., 2001, 1999; Knowlton et al., 2006; Thompson and Compton, 2008). Following a treatment period where mono-polar spindles form, the drug is washed out and widespread merotely is detected. This gives rise to chromosome missegregation and aneuploid daughter cells. However, only one missegregation event is observed every third division (Thompson and Compton, 2008), and thus, studying the widespread effects of aneuploidy is difficult. Furthermore, in this approach, chromosomes are often stuck within the cleavage furrow or form micronuclei and this can cause DNA damage (Ganem and Pellman, 2012; Janssen et al., 2011). Therefore, methods to induce aneuploidy without the issue of DNA damage are required. Potential new methods are described in Chapter 4, with more detail given in Appendix 1 (Bennett et al., 2015).

1.52 Antimitotics

Antimitotics are used in cancer chemotherapy, although the exact mechanism of action is relatively unknown. Of the antimitotics, microtubule-targeting agents (MTA's) are the more traditional, and have shown the greatest success in the clinic (Dumontet and Jordan, 2010). Antimitotic agents perturb microtubule dynamics and this results in an abnormal spindle, which affects chromosome alignment and leads to the activation of the SAC (Weaver and Cleveland, 2005). The MTA's can be divided into microtubule-stabilising agents (e.g. paclitaxel, docetaxel), and microtubule-destabilising agents (e.g. vinca alkaloids) (Jordan and Wilson, 2004).

Paclitaxel is a microtubule-stabilising antimitotic, which binds to the *β*-tubulin subunit of the microtubule, inducing a conformational change in the tubulin. As a result, interaction with neighbouring tubulins is stabilised and this prevents depolymerisation (Rowinsky and Donehower, 1995). Taxol is the front-line chemotherapy for many cancers, and at the ASCO conference in 2015, a study in metastatic prostate cancer patients indicated that docetaxel, in combination with the traditional hormone therapy, extended the median overall survival time from 67 to 77 months (James et al., 2016). The success that Taxol has exhibited may be attributed to the fact that unlike other agents, it accumulates in cells and persists for days after loss from circulation (Mori et al., 2006; Weaver, 2014). Zasadil et al. observed the intratumoural concentration of Taxol in primary breast tumours was >100-fold higher in comparison with the plasma

concentration (Zasadil et al., 2014), consistent with previous observations in cell lines (Jordan et al., 1996, 1993; Yvon et al., 1999).

From the studies of paclitaxel in human tumours by Zasadil et al., it was indicated that the mitotic arrest induced by Taxol in cell culture experiments was not required for the tumour shrinkage observed (Zasadil et al., 2014). At clinically relevant concentrations, multipolar spindles resulted in chromosome missegregation, owing to the cytotoxic effect in the clinic (Weaver, 2014).

The efficacy of antimitotics, in particular Taxol, has been indicated in breast and ovarian cancers (Jordan and Wilson, 2004; Rowinsky and Donehower, 1995). Despite success in the clinic, antimitotics do exhibit unfavourable side effects. Paclitaxel has been indicated in peripheral neuropathy, where the microtubule structures of neuronal cells are perturbed (Dumontet and Jordan, 2010; Rowinsky et al., 1993). Additionally, some patients do not respond to antimitotics, whilst others show sensitivity. Identifying those who are likely to respond is an area which needs to be addressed. In order to establish potential biomarkers for responsiveness, Chang et al. identified a 92-gene set that was able to aid in the prediction of whether a tumour was likely to respond to neoadjuvant docetaxel therapy (Chang et al., 2003). Further to this, other gene-expression patterns have been highlighted which correlate with responsiveness to taxanes (Gianni et al., 2005). Lastly, resistance mechanisms can cause a lack of patient responsiveness, and these mechanisms can be acquired throughout treatment, or tumours may be inherently resistant (Dumontet and Jordan, 2010). Suggested mechanisms of Taxol resistance include an overexpression of the drug efflux pump, the multidrug transporter P-glycoprotein (Gottesman, 2002), changes in the metabolism of Taxol, and microtubule dynamic alterations (Drukman and Kavallaris, 2002).

In order to overcome these issues, it is important we understand the mechanism by which antimitotic exposure elicits its action. With the many problems associated with microtubule-targeting agents, much research has aimed at developing drugs which do not alter microtubule dynamics, but only halt mitotic progression.

1.521 Second-generation antimitotics

A class of second-generation inhibitors are being studied, which encompass both mitotic drivers and mitotic blockers (Keen and Taylor, 2009). Whilst causing a mitotic arrest, the microtubules are unaffected (Jackson et al., 2007). Mitotic blockers induce a mitotic arrest by activating the SAC, whereas drivers target members of the checkpoint machinery, resulting in checkpoint override and mitotic exit. Mitotic blockers

consist of inhibitors of Cenp-E, Plk1, Eg5, and the drivers include agents targeting Mps1 and the Auroras. These proteins are only expressed in dividing cells, and are often overexpressed in some cancer types, making them ideal targets. Aurora B levels are elevated in cancer (Tatsuka et al., 1998), with detrimental effects on prognosis (Lens et al., 2010). Similarly, Plk1 overexpression has also been indicated in a number of cancers (Holtrich et al., 1994; Strebhardt and Ullrich, 2006; Yuan et al., 1997), with overexpression linked to aggressiveness and poor prognosis (Takai et al., 2005). Considering the kinase inhibitors, ZM447439 is a first-generation Aurora B inhibitor used extensively in cell biology (Ditchfield et al., 2003), and also PHA-739358 has emerged as a promising clinical candidate (Kollareddy et al., 2012). BI2536 is a Plk-1 inhibitor used in cell biology (Steegmaier et al., 2007), but more recently, volazertib has shown promising preclinical results (Gjertsen and Schöffski, 2014). Furthermore, monastrol was initially developed as an Eg5 inhibitor (Mayer, 1999), causing mono-polar spindles and defective chromosome congression (Blangy et al., 1995). Other Eg5 inhibitors have since been acquired, including ispinesib and AZD4877 (Rath and Kozielski, 2015). Clinical results for the second-generation antimitotics have not been promising, where unfavourable side effects and only minor partial responses have been indicated (Chakravarty et al., 2011; Chan et al., 2012; Chung et al., 2012; Huszar et al., 2009; Komlodi-Pasztor et al., 2012; Lens et al., 2010; Mitchison, 2012; Rath and Kozielski, 2015).

Previously it was thought that tumour cells undergo mitosis at a faster rate than normal somatic cells. However, this is not always the case (Komlodi-Pasztor et al., 2012). Tumour doubling times in patients are often in the region of 300 days, in comparison to cell lines at approximately 24 hours. Consequently a low mitotic index of <1% is observed and this may be the reason for the unforeseen lack of clinical success. Furthermore, heterogeneity within cell lines and tumours has been identified (Gascoigne and Taylor, 2008), and thus, responses to a particular chemotherapeutic cannot be easily predicted. As the cytotoxic effect of Taxol is likely due to chromosome missegregation on multipolar spindles, rather than as a result of a mitotic arrest (Zasadil et al., 2014), the lack of efficacy of the second-generation antimitotics may be because a mitotic arrest is not needed to promote apoptosis and isn't required for efficacy of MTA's. This infers that perhaps other approaches of targeting need to be considered.

1.522 Response to antimitotics and cell fate

Studies have indicated that the intrinsic apoptotic pathway plays a role in the cellular response to antimitotics, through the activation of caspase-3 (Gascoigne and Taylor, 2008; Jordan et al., 1996; Marcus et al., 2005; Tao et al., 2005). Many studies have been undertaken to aid in the understanding of the cancer cell response to antimitotics (Gascoigne and Taylor, 2008; Jackson et al., 2007; Rieder and Maiato, 2004; Weaver and Cleveland, 2005). Upon exposure to antimitotic drugs, the SAC is activated, resulting in a mitotic arrest (Musacchio and Salmon, 2007), and this can be followed by different cell fates ((Gascoigne and Taylor, 2008; Rieder and Maiato, 2004) and see (Figure 1.7A)). Following a prolonged mitotic arrest cells may exit mitosis, without undergoing a division (known as 'slippage') (Rieder and Maiato, 2004; Taylor and McKeon, 1997; Weaver and Cleveland, 2005). Following slippage, the cell may survive and continually enter and exit mitosis, it may undergo post-mitotic death (PmD), or arrest in the following interphase. Additionally, a cell may undergo death in mitosis (DiM) whilst arrested, or it may divide abnormally, giving rise to daughter cells with unequal chromosome numbers.

A study in many cell lines with different drugs and concentrations concluded that cells experience intra- and inter-line heterogeneity (Gascoigne and Taylor, 2008). Aided by a single-cell based analysis it was established that cell fate can vary depending on the cell line, drug and concentration used. The single-cell analysis approach captured images of the cells (for example every 10 minutes), over a (72 hour) time period, in the presence of a given drug. Using time-lapse movies of the cells, single cells were tracked over time for their behaviour and fate. The analysis of these cells was depicted in a 'cell fate profile' (Figure 1.7B). This is a graph where typically 50 cells are analysed, and one line is one cell. The colour of the line indicates the fate of a cell (e.g. DiM), and the length of the line indicates the time period taken to undergo the particular fate. For example, red indicates DiM, and green, PmD. The representative phase-contrast images in Figures 1.8A, B show typical fates tracked and observed and the subsequent phenotypic analysis. When cells are treated with Taxol (or another mitotic blocker), cells 'round-up'. When cells undergo continual mitotic exit, large, tetraploid cells can result. In Figure 1.8B image sequences demonstrate how cells are analysed; those which divide normally, abnormally, exit or die. The observed heterogeneity *in vitro* can aid in understanding why there are unpredictable patient responses to antimitotics. Cell fate can be dictated and explained by the activity of two competing networks that are present within cells (Gascoigne and Taylor, 2009, 2008).

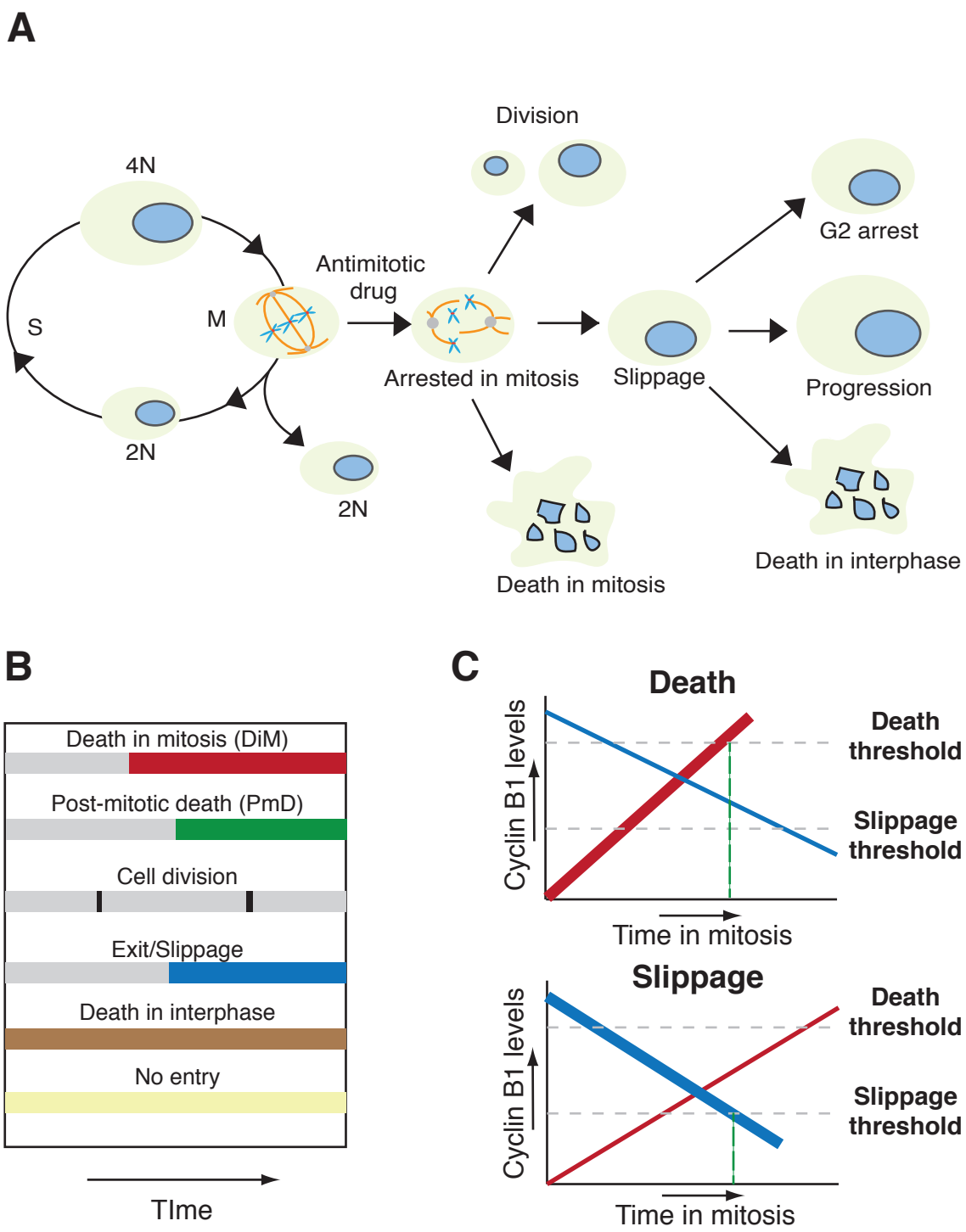

Figure 1.7 Analysing cellular fate following mitotic perturbation.
(**A**) Following mitotic arrest, cells are able to undergo different fates, including slippage, death in mitosis or an abnormal division. Adapted from Gascoigne and Taylor, 2009.
(**B**) Fate profiles are used to quantitatively describe cellular behaviour over time, where one line is one cell, and the length of the line is the time taken to undergo a particular fate, and the colour of the line depicts the behaviour.
(**C**) The competing networks model shows instances where death signals accumulate during a mitotic arrest (red), and cyclin B1 levels decline (blue). If the threshold for death is reached first, the cell will undergo DiM (such as in the RKO cell line), but if the threshold for slippage is breached first, the cell will exit mitosis (such as in the DLD-1 cell line).

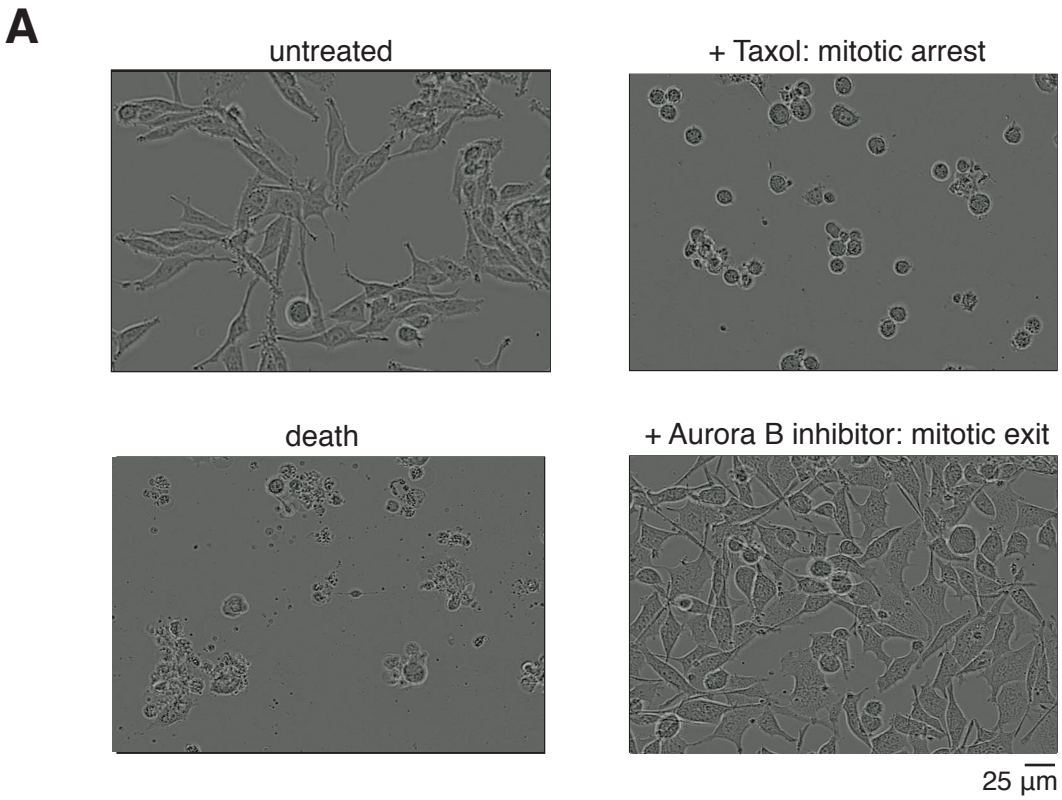

Figure 1.8 Analysis of cell fate using the IncuCyte® Zoom.
(**A**) Representative phase-contrast images of RKO cells analysed on the IncuCyte® Zoom for analysis of cell fate, where cells are shown as untreated, in mitotic arrest with Taxol, having undergone death or exited mitosis. Bar: 25 µm.
(**B**) Examples of the different cellular fates encountered upon analysis, including a normal division, an abnormal division, mitotic exit, post-mitotic death and death in mitosis. Bar: 25 µm.

1.53 Competing networks and c-myc

The competing networks model aids in the understanding of the mechanism controlling whether a cell will die in mitosis or undergo slippage (Gascoigne and Taylor, 2008). The two networks controlling cell fate are (1) the reduction in cyclin B1 levels during a prolonged mitosis, eventually resulting in slippage (Brito and Rieder, 2006) and (2) the increase in death signals accumulated over time. Both of the networks have a certain threshold, which when reached will dictate the cellular fate i.e. if the threshold for slippage is reached first, the cell will undergo this fate. While the factors controlling cyclin B1 degradation and slippage phenotype have been extensively studied, the factors controlling DiM are less known.

Cell-to-cell variation exists within a cell line or tumour and each cell will have its own competing network, where rates of cyclin B1 degradation and death signal accumulation will vary between cells. Inherently, different cell lines will have genetic differences which will give rise to differences in the rate of cyclin B1 degradation for example. This can be exemplified when the DLD-1 and the RKO cell lines are contrasted (Figure 1.7C). Upon exposure to antimitotics DLD-1 cells predominantly undergo slippage, whereas the RKO cell line mostly shows a DiM phenotype. Therefore, the death signals for the RKO cell line will accumulate faster than cyclin B1 degrades, with the inverse true for the DLD-1 cell line, where cyclin B1 will be degraded with faster kinetics.

To understand further the factors which control whether a cell will die in mitosis during a mitotic arrest, a genome-wide siRNA screen was used to identify genes which could decrease Taxol-induced DiM (Topham et al., 2015). Here, the oncogenic, transcription factor c-myc was recognised as an essential gene which controls the apoptotic machinery for DiM. It does so by down-regulating the pro-survival protein Bcl-xL and up-regulating the pro-apoptotic proteins Noxa, Bim and Bid. Previous studies have also indicated that myc suppresses Bcl-xL (Eischen et al., 2001). As c-myc was the only apoptosis-related ‘hit’, and the screen aimed to find regulators of death in mitosis, it may be surprising that more apoptotic family members didn't manifest in the screen. The reason for this may be due to the functional redundancy that exists between members of the intrinsic apoptotic network (Eichhorn et al., 2014; Eno et al., 2012; Topham et al., 2015). Considering the competing networks model, c-myc was shown to only control the death pathway but not the slippage pathway, confirming that c-myc is a master regulator of the death network (Topham et al., 2015).

1.6 Apoptosis

Cell fate following an antimitotic induced arrest can sometimes result in apoptosis, with death either in mitosis or in interphase following exit. It has been shown that the death observed is caspase-dependent and this involves the intrinsic apoptotic machinery (Doménech et al., 2015; Gascoigne and Taylor, 2008; Shi et al., 2008). In particular, Bcl-xL has been indicated to be a potent pro-survival factor during a prolonged mitosis induced by antimitotics (Bah et al., 2014; Shi et al., 2011), and therefore I will give focus to apoptosis, but also give detail on Bcl-xL.

1.61 Overview

The term 'apoptosis' was first coined in 1972 to define an observed 'programmed cell death' (Kerr et al., 1972). When a cell is destined to undergo apoptosis, morphological changes will develop, with the cell shrinking in size and showing pyknosis (chromatin condensation). The cytoplasm will become increasingly dense and the organelles progressively tightly packed, with these characteristics confirmed by light and electron microscopy in 2000 (Hacker, 2000). The plasma membrane blebs and 'budding' gives rise to apoptotic bodies. Following formation, the bodies undergo phagocytosis.

A more in-depth understanding of the cell death process arose from observations in *Caenorhabditis elegans* during development (Horvitz, 1999). Apoptosis is important for development, ageing and for homeostatic control in the maintenance of a constant population of cells within tissues (Elmore, 2007; Renehen et al., 2001). In metazoan development, the initial over-proliferation of cells requires subsequent apoptosis to establish organs and other structures (Jacobson et al., 1997). Apoptosis also acts as a defence mechanism when cells are exposed to intracellular and extracellular stimuli, to remove pathogen-infected cells from the body.

An aberrant apoptosis often leads to abnormalities and pathologies in the adult vertebrate (Elmore, 2007). This includes pathologies such as cancer, AIDS and Alzheimer's disease. Sometimes alterations to the intrinsic apoptotic machinery can occur such as overexpression of pro-survival factors (e.g. Bcl-2), or downregulation of pro-apoptotic factors (e.g. Bax). An example includes human B cell lymphoma's which overexpress Bcl-2 (Vaux et al., 1988).

1.62 Intrinsic and extrinsic pathways

Apoptosis encompasses both the intrinsic and extrinsic pathways, with overlapping mechanisms existing. The extrinsic pathway involves the binding of death ligands to trans-membrane receptors (Figure 1.9), including (death) TNF receptors (Locksley et al., 2001). When bound, Fas-Associated protein with Death Domain (FADD) is recruited, which associates with the procaspase-8 protein, inducing the formation of a death-inducing signalling complex (DISC) which then activates procaspase-8. The protease caspase-8 then acts to initiate apoptosis (Kischkel et al., 1995). This involves the cleavage of noncaspase substrates including Bid. Truncated-Bid (t-Bid) translocates to the nucleus, and downstream apoptosis then occurs.

The intrinsic pathway involves non-receptor binding stimuli such as cytokines and growth factors, and is directly involved in the response to intracellular signals, with downstream consequences involving the mitochondria (Elmore, 2007). The control of the intrinsic apoptotic network is by the Bcl-2 protein family (Adams and Cory, 2007; Topham and Taylor, 2013), and it is the balance between the pro-apoptotic and anti-apoptotic Bcl-2 proteins which dictates cell fate. The Bcl-2 family regulate commitment to apoptosis by controlling mitochondrial outer membrane permeabilisation (MOMP), where pro-apoptotic BAK and BAX (pro-apoptotic factors) are the key regulators (Certo et al., 2006; Chipuk et al., 2010). This is followed by release of mitochondrial proteins such as cytochrome c and Smac/DIABLO. Cytochrome c was discovered as a key mitochondrial protein for signalling in apoptosis (Liu et al., 1996), and activates caspase-3 via the formation of a cytochrome c/Apaf-1/caspase 9 apoptosome. Smac/DIABLO induces the activation of caspases through the inhibition of the inhibitors of apoptosis (IAPs) ((Saelens et al., 2004) and (Section 1.63)). Caspases-3 and -7 are the executioner caspases, initiating a caspase cascade which leads to apoptosis.

Classes of the pro- and anti-apoptotic proteins are categorised according to the BH (Bcl-2 homology) domains they possess and their roles in cell survival, where the conserved BH domains are BH1, BH2, BH3 and BH4. The pro-survival Bcl-2 family of proteins (Bcl-2, Bcl-xL, Bcl-w, Mcl-1) possess four BH domains, the pro-apoptotic proteins (Bax and Bak) also typically possess four, and the pro-apoptotic BH3-only proteins (Bim, Bid, Bad, Noxa, Puma) only possess one, the BH3 domain (Delbridge et al., 2016). The BH1, BH2 and BH3 domains of the pro-survival proteins characteristically form a hydrophobic groove in which a BH3 domain (an amphipathic helix of approximately 24 residues) can bind (Adams and Cory, 2007; Liu et al., 2003; Sattler et al., 1997).

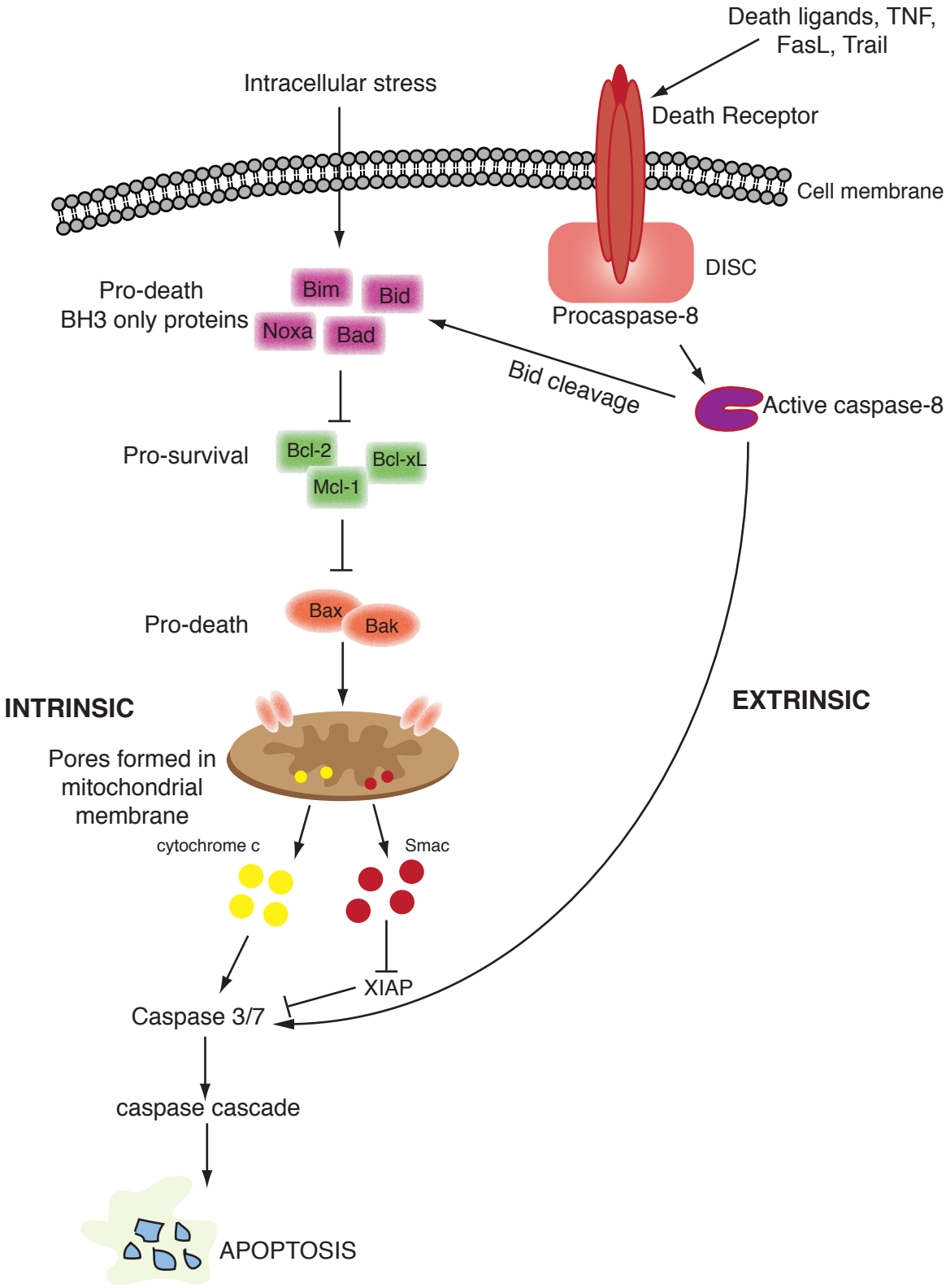

Figure 1.9 The intrinsic and extrinsic apoptosis pathways.
When exposed to intracellular or extracellular stresses, the cell may undergo intrinsic or extrinsic apoptosis. In the intrinsic pathway, the pro-survival proteins are inhibited by the BH3-only proteins, causing Bax and Bak to oligomerise at the mitochondrial outer membrane, forming pores. Cytochrome c is released, activating a caspase cascade and apoptosis ensues.

In 1978, t(14;18) chromosomal translocations in human follicular lymphoma identified the *BCL2* gene i.e. B-cell leukaemia gene (Fukahara and Rowley, 1978). Subsequent experiments in mice without IL-3 (Interleukin-3, a cytokine), but overexpressing Bcl-2 indicated Bcl-2's pro-survival role (Vaux et al., 1988). Many studies have indicated Bcl-2 as an important regulator to block apoptosis under conditions of stress (McDonnell et al., 1989; Sentman et al., 1991; Strasser et al., 1991; Tsujimoto, 1989).

Following on from this, Mcl-1 (myeloid cell leukemia 1), Bclx (also Bcl2l1) and A1 (BFL1 in humans) were identified; where *MCL1* was identified through phorbol 12-myristate 13-acetate (PMA) induction in myeloid leukaemia cells (Kozopas et al., 1993); *BCL-X* (Long and Short) was isolated in chickens (followed by humans) (Boise et al., 1993); and *A1* was induced by granulocyte-macrophage colony-stimulating factor (GM-CSF) in myeloid cells (Lin et al., 1993). Furthermore, pro-apoptotic Bax was found to co-immunoprecipitate with Bcl-2 (Oltvai et al., 1993), and further experimentation found when overexpressed, Bax stimulated apoptosis. This was the first evidence of the presence of two groups of apoptotic genes, those which promote (pro-apoptotic) and those which inhibit (anti-apoptotic) apoptosis and that these two groups interact. From here, Bak was cloned and shown to induce apoptosis following exposure to stimuli (Kiefer et al., 1995).

Following on from the discovery of the pro-survival proteins, pro-apoptotic BH3-only proteins were later uncovered. In 1995, Bad was discovered when bound to Bcl-2 in a yeast two-hybrid screen (Yang et al., 1995). Bid was identified in 1996, where upon cleavage by caspase-8, t-Bid, the truncated form, is produced and this was shown to bind both Bcl-2 and Bax (Li et al., 1998). Furthermore, Bim was recognised when screening a cDNA expression library utilising the Bcl-2 protein as a binding probe (O'Connor et al., 1998). When 293T cells were transfected with Bim_L, over 90% of the cells died following a 3-day period, indicating the pro-apoptotic activity of Bim. Noxa was observed in 2000, where expression in primary mouse cells exposed to stress was dependent upon p53 (Oda, 2000).

Differential specific interactions exist between the pro-survival and pro-apoptotic proteins (Brunelle and Letai, 2009). However, because of the structural conservation that exists between the families, interactions can occur between most of the members, ultimately resulting in functional redundancy. For example Bcl-xL interacts with Bim, Bid and Bad, and also Bak and Bax (Chen et al., 2005; Sattler et al., 1997). However, it does not show affinity for Noxa. On the other hand, Mcl-1 will bind Noxa, and shows

less affinity for Bad. It is these interactions which are imperative for the stimulation of apoptosis.

The process of MOMP can be explained by two models: the 'direct activation' model and the 'neutralisation' model (Sáez and Villunger, 2016). In the 'direct activation' model, 'activators' (BIM/BID) are bound by Bcl-2 members until a stress signal induces displacement by the 'sensitizers' (BAD/NOXA), which then allows for activation of BAX and BAK, oligomerisation and subsequent MOMP (Chipuk et al., 2010; Letai et al., 2002). On the other hand, the 'neutralisation' model suggests that the Bcl-2 proteins inhibit BAK and BAX, and upon stress, the BH3-only proteins disrupt this interaction, freeing BAK and BAX to initiate MOMP (Willis et al., 2007). Due to the redundancy that exists between the apoptotic members, establishing the minimum requirement for MOMP has been difficult (Senft et al., 2015; Villunger et al., 2011). Recently, to test this, all BH3-only proteins (and p53, Rb) were eliminated from a mammalian cell system using CRISPR/Cas9 (O'Neill et al., 2016). Whilst these cells were resistant to apoptotic stimuli, when the Bcl-2 proteins were neutralised, BAX/BAK-dependent MOMP followed. This suggests that the BH3-only proteins (or p53, Rb) are not required for the direct activation of BAK and BAX. Reconstitution assays in BCL-2 allKO HCT116 cells implied that apoptosis can occur without the presence of these members, where the only requirement for MOMP is an outer mitochondrial membrane and the C-terminus of BAX or BAK (Sáez and Villunger, 2016).

Under normal conditions, the pro-survival proteins (Bcl-2, Bcl-xL, Mcl-1) bind and sequester the pro-apoptotic proteins (Bax and Bak). The balance between the opposing families is in favour of the pro-survival proteins, maintaining survival. The pro-survival proteins normally reside on the outer mitochondrial membrane (OMM) and the pro-apoptotic proteins in the cytosol, yet there is a small amount of Bax found associated with the mitochondria (Desagher et al., 1999). There is continual retro-translocation of Bax from the membrane to the cytosol, aided by the interaction with Bcl-xL (Edlich et al., 2011). Similar patterns of behaviour are seen with Bak (Todt et al., 2015). The interaction between Bcl-2 proteins and pro-apoptotic proteins prevents the functioning of Bak and Bax in the permeabilisation of the outer mitochondrial membrane. Thus, no downstream signalling or apoptosis will occur. On the other hand, under conditions of stress, the balance tips in favour of the pro-apoptotic proteins, which ultimately leads to the initiation of apoptosis. When exposed to stress signals, the pro-survival proteins are inhibited by the BH3-only pro-apoptotic proteins, with

binding in the BH3 domain. This frees and allows Bax and Bak to oligomerise at the OMM, leading to permeabilisation and apoptosis.

Due to the overexpression of pro-survival factors in cancer, their prevalent role in the survival of tumour cells, and the evasion of apoptosis being a hallmark of cancer (Hanahan and Weinberg, 2011), targeting these proteins in chemotherapy is advantageous.

1.63 Inhibitors of apoptosis (IAPs)

Many cancers use the evasion of apoptosis in order to continue to survive and grow (Hanahan and Weinberg, 2011). Apoptosis is also essential in immune settings where it is used to prevent further viral replication (Clarke and Tyler, 2003). Despite this, viruses have acquired a mechanism to resist apoptosis, allowing for virus replication. A genetic screen revealed they do so by expressing inhibitors of apoptosis (IAPs) (Crook et al., 1993), where some, but not all, exhibit functions in apoptosis (Beug et al., 2012; Marivin et al., 2012). Mammalian examples include anti-apoptotic X-linked IAP (XIAP) and cellular IAP (cIAP), which are important in the response to endogenous and exogenous stress signalling. Under normal conditions, XIAP inhibits caspase-9, -3 and -7 activity (Deveraux et al., 1997; Eckelman et al., 2006; Shiozaki et al., 2003), inhibiting the onset of apoptosis. This may lead to the promotion of cancer cell survival.

IAPs are often overexpressed in many cancers, and therefore may be an attractive anticancer target. Small molecule inhibitors and antisense oligonucleotides have gained the most interest (Ndubaku et al., 2009; Vucic and Fairbrother, 2007), including antagonists which bind IAPs, preventing association with caspases or Smac; and also antagonists which mimic Smac and therefore bind IAPs. Importantly, some small molecule inhibitors of IAPs are in clinical trials (Fulda and Vucic, 2012), including Smac mimetics (Bai et al., 2014).

Indeed, IAPs play a key role in apoptosis, yet their role has been shown to extend beyond solely the inhibition of apoptosis. Some IAPs function in the regulation of inflammatory and innate immune signalling pathways (Estornes and Bertrand, 2015), through their E3 ubiquitin ligase activity (Estornes and Bertrand, 2015; Gyrd-Hansen and Meier, 2010), in particular cIAP-1/2 (Varfolomeev et al., 2012). This activity enables them to regulate NFκB**,** MAPK or IRF pathways, which are downstream of Pattern Recognition Receptors (PRRs) and Tumour Necrosis Factor Receptors (TNFRs) (Estornes and Bertrand, 2015). Many human diseases develop through

inflammation, and therefore targeting IAPs in this context could be promising. Due to their pivotal role in the immune response, the use of IAP antagonists in the context of cancer chemotherapy may not be appropriate. Patients with cancer are likely already immune compromised, and therefore, use of IAP antagonists will insult the immune system further.

1.64 Other mechanisms of cell death

Even though apoptosis is likely the main mechanism of cell death induced by anticancer therapies, and therefore will be the focus of my thesis, there are non-apoptotic mechanisms of cell death. These include necrosis, autophagy and mitotic catastrophe (Brown and Wilson, 2003; Brown and Attardi, 2005; Okada and Mak, 2004). The form of cell death that a cell may undergo depends on the cellular context and genetic background (Okada and Mak, 2004). Necrosis is unregulated and involves the uncontrolled release of intracellular components (Vanden Berghe et al., 2014). Autophagy occurs to direct unwanted proteins to the lysosome for degradation, and cells with increased autophagy undergo non-apoptotic death. Lastly, mitotic catastrophe is a term that was originally used to describe *Schizosaccharomyces pombe* cells that were forced into mitotic entry when Cdc2 was overexpressed (Russell and Nurse, 1984). Following on from this initial definition, it now is defined as a mechanism which detects mitotic failure and forces a cell to undergo mitosis-specific death (Castedo et al., 2004). Morphologically different from apoptosis and necrosis, it is characterised by the fragmentation of the nucleus and gives rise to micronuclei. It is observed when cells are exposed to agents which cause DNA damage or spindle disruption, and unlike apoptosis, is independent of caspase-3 and -9, and is likely to involve caspase-2 activation (Castedo et al., 2004). However, definitive explanations for the activation of mitotic catastrophe are yet to be complete. Given that the evidence for the action of antimitotics and the death in mitosis fate has been suggested to be via the caspase-dependent intrinsic apoptotic pathway, and my studies will focus on enhancing the efficacy of antimitotics, the alternative forms of death will not be considered in my thesis.

1.65 Apoptosis and cancer

The evasion of apoptosis is a hallmark of cancer (Hanahan and Weinberg, 2011). As p53 is a key tumour suppressor and plays a role in apoptosis, evasion often involves p53 loss (Lopez and Tait, 2015). Other strategies for avoiding cell death

include upregulation of pro-survival proteins (Kelly and Strasser, 2011). This upregulaton may cause resistance to anticancer agents when apoptosis is the mechanism of action (Lowe et al., 1993). Therefore, some anticancer therapies are aimed at inducing apoptosis in order to halt cancer.

Although a good approach, triggering apoptosis may not necessarily always be a good thing, and apoptosis has been indicated as being oncogenic in some settings. Evidence has suggested that perhaps the low expression of pro-apoptotic proteins results in inhibition of tumourigenesis (Labi et al., 2010; Michalak et al., 2010). On the other hand, the increased expression of pro-survival proteins showed improved prognosis (Berardo et al., 1998; Reed et al., 1996). These studies suggest that initiating apoptosis in a cancer setting is not always a beneficial approach, since the evasion of apoptosis has been indicated in the inhibition of cancer progression (Michalak et al., 2010).

The mitochondrial outer membrane permeabilisation (MOMP) is referred to as the 'point of no return'. When cells have undergone permeablisation, apoptosis will follow. Despite this view, it has been shown that MOMP is not an 'all or nothing' response, but in fact, there are graded levels of permeabilisation which will not necessarily result in cell death (Ichim et al., 2015). When a cell undergoes a sub-lethal level of stress, 'minority MOMP' occurs where some level of permeabilisation is acquired. Examples of sub-lethal stress include BH3 mimetic exposure, BH3 proteins and also slippage. As this results in a sub-apoptotic level of caspase activation, apoptosis is not triggered (Ichim et al., 2015; Orth et al., 2012). Although apoptosis is not activated, the DNase CAD induces DNA damage. In turn, high levels of DNA damage may promote genomic instability and tumourigenesis. Therefore, as eluded to previously, triggering apoptosis may have detrimental consequences. It may be that the targeting of Bcl-2 proteins in cancer chemotherapy could promote tumourigenesis. Despite this, the concept targeting Bcl-2 proteins with 'BH3 mimetics' is an active and interesting area of study.

1.66 Targeting apoptosis with BH3 mimetics

From early studies using antisense oligonucleotides to repress Bcl-2 expression (Reed et al., 1990), drugs screens followed in order to identify sequences and structures which inhibited the activity of the pro-survival proteins (Lessene et al., 2008; van Delft and Huang, 2006; Varadarajan et al., 2013). 'BH3 mimetics' were then developed which mimic the function of the BH3-only proteins by binding in the BH3

domain of the pro-survival proteins. This inhibits their function and induces apoptosis (Delbridge et al., 2016). The identification of the crystal structure of Bcl-xL in 1996 promoted structure-based design studies which was used to design and develop inhibitors against the pro-survival proteins (Muchmore et al., 1996; Sattler et al., 1997).

In the first case, ABT-737 was developed (Oltersdorf et al., 2005), followed by its orally active analogue ABT-263 (Navitoclax) (Tse et al., 2008), both of which inhibit Bcl-2, Bcl-xL and Bcl-w. These agents stimulate Bax- and Bak-dependent apoptosis (van Delft et al., 2006; Vogler et al., 2009) via the mimicking of Bad. Clinically, a 35% partial response in chronic lymphocytic leukemia (CLL) in a Phase I study was indicated with navitoclax (Roberts et al., 2012). When in combination with paclitaxel, ABT-737 and ABT-263 enhanced cell death (Bah et al., 2014; Kutuk and Letai, 2008; Oltersdorf et al., 2005; Shi et al., 2011). Although ABT-737 hits a number of pro-survival factors, it has been suggested that Bcl-xL controls the increase in cell death (Bah et al., 2014). Although effective, the inhibition of Bcl-xL is detrimental to the survival of platelets, and this induces Bax- and Bak-mediated thrombocytopenia (Mason et al., 2007; Zhang et al., 2007).

Additionally, Bcl-2 selective inhibitors such as Venetoclax ABT-199 (Souers et al., 2013) have been taken through Phase I-III trials in CLL (Davids and Letai, 2013; Roberts et al., 2015), with an overall response rate (ORR) of 84% in 56 patients with relapsed or refractory CLL. No effect was seen on platelets (Souers et al., 2013).

Mcl-1 is often overexpressed in cancer (Beroukhim et al., 2010), is a potent pro-survival factor (Glaser et al., 2012; Grabow et al., 2014; Koss et al., 2013; Xiang et al., 2010), and is a key factor in resistance shown towards ABT-263/ABT-737 (Chen et al., 2007; Konopleva et al., 2006; Tahir et al., 2007; van Delft et al., 2006). Recent attempts in the study of Mcl-1 targeting have resulted in the development of A-1210477 (Leverson et al., 2015b), shown to disrupt Mcl-1-Bim complexes and induce apoptosis in Mcl-1 dependent cell lines. It must however, be considered that Mcl-1 is involved in the maintenance of normal cell types including neuronal cells (Arbour et al., 2008), and therefore side effects may be problematic.

Lastly, inhibitors selective for Bcl-xL have been acquired. Development was difficult due to the large, shallow and hydrophobic BH3 domain (Mullard, 2012). Such inhibitors include WEHI-539 (Lessene et al., 2013), and more recently, A-1155463 and A-13311852 (Leverson et al., 2015a; Tao et al., 2014). WEHI-539 was developed utilising the crystal structure of Bcl-xL in structure-based design studies (Lessene et al., 2013), where specificity for Bcl-xL was confirmed with loss of cell viability in Mcl-1$^{-/-}$

MEFs when exposed to WEHI-539. There was no effect in wild-type MEFs, indicating the selectivity against Bcl-xL, but also confirming the redundancy between Mcl-1 and Bcl-xL in this context. Induction of platelet apoptosis also confirmed selectivity. The more recent A-13311852 shows oral bioavailability and *in vivo* studies indicated the disruption of Bcl-xL-Bim complexes, with apoptosis in Bcl-xL dependent Molt-4 cells (Leverson et al., 2015a).

The availability of the selective inhibitors will allow for the dissection of the roles of the Bcl-2 proteins in cell survival. A method which aims to study the Bcl-2 proteins and their interactions is 'BH3 profiling'. It is a method which proposes to decipher the interactions between pro-survival and pro-apoptotic proteins (Ryan et al., 2010), and it determines the dependence of tumour cell lines upon particular Bcl-2 proteins. Furthermore, this assay measures how 'primed' a cell is for death, that is, how sensitive it is to apoptosis (Deng et al., 2007), and it has also been used as a predictive method to examine the effectiveness of BH3 mimetics and chemotherapeutic drug combinations in Dynamic BH3 profiling (DBP) (Montero et al., 2015). DBP can predict response to chemotherapeutics in cancers, and it may be of use as a predictive biomarker *in vivo*. The level of 'priming' prior to therapy may be an indicator of responsiveness (Ni Chonghaile et al., 2012; Vo et al., 2013). Cancer cells are more sensitive to apoptosis than normal, 'healthy' cells, with increased 'priming' and dependence on pro-survival proteins exhibited. These 'primed' cells are more sensitive to agents which induce apoptosis (Ni Chonghaile et al., 2011), and this suggests a rationale for using BH3 mimetics.

1.67 Bcl-xL

1.671 The structure and functioning of Bcl-xL

Bcl-xL is a pro-survival Bcl-2 protein and has been shown to be a potent mitotic pro-survival factor in many contexts (Bah et al., 2014; Minn et al., 1996; Shi et al., 2011; Topham et al., 2015; Upreti et al., 2008). Structurally, Bcl-xL is composed of a globular structure, with a hydrophobic core surrounded by a helical bundle (Muchmore et al., 1996), with 4 BH domains: BH1, BH2, BH3, BH4 (Figure 1.10A). The BH1 and BH2 domains are highly conserved among Bcl-2 proteins, as these regions are important for anti-apoptotic activity and allow for heterodimerisation (e.g. with Bax/Bak). Together the BH1, BH2 and BH3 domains form a hydrophobic cleft where the pro-apoptotic proteins can bind. Mutation of the Gly138 in this cleft inhibits binding to Bax (Cheng et al., 1996; Sedlak et al., 1995), suggesting the requirement for this residue for

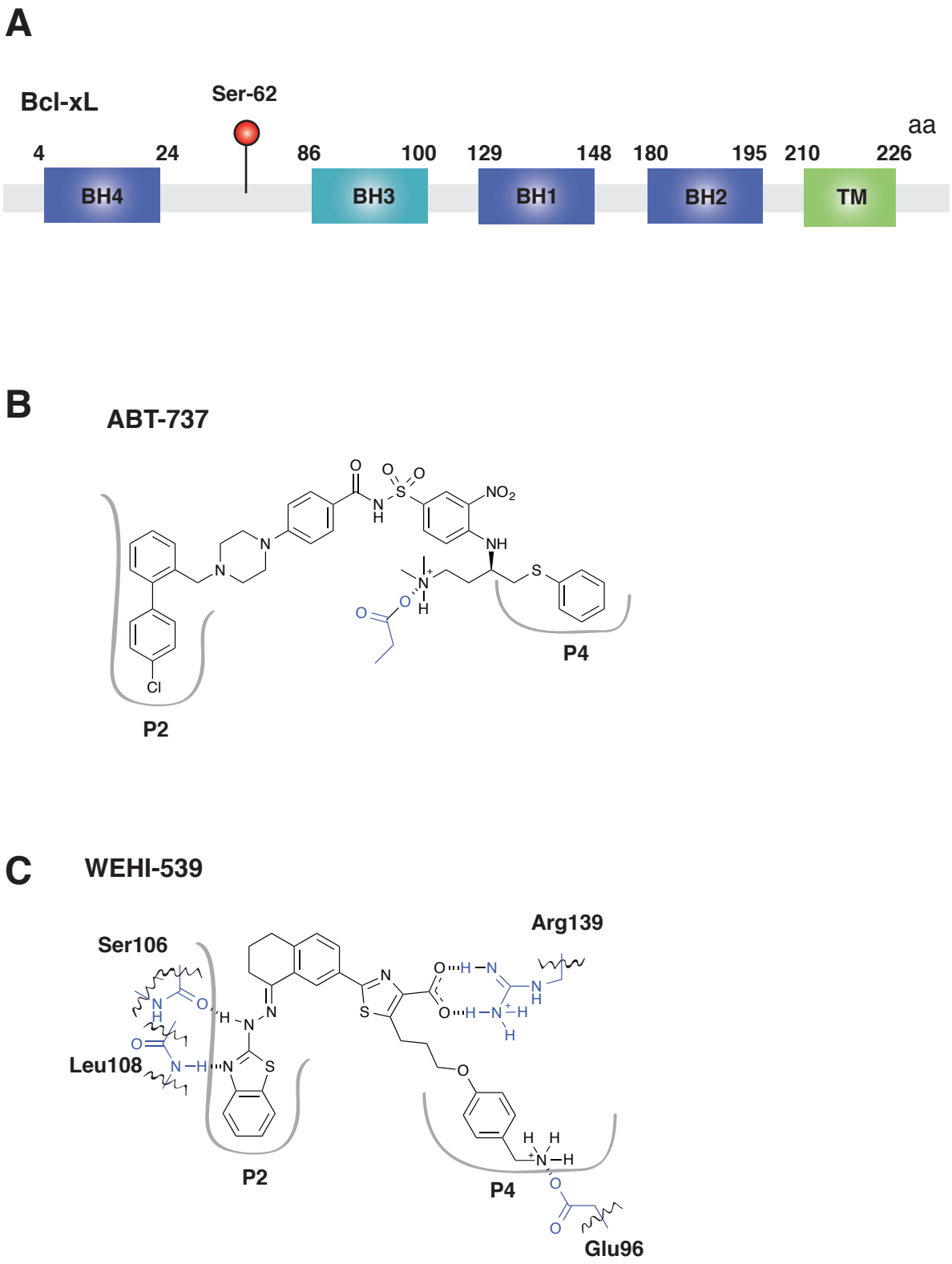

Figure 1.10 Binding of inhibitors to Bcl-xL in the BH3 domain.
(**A**) Bcl-xL contains BH1-BH4 domains and a transmembrane (TM) domain, required for binding of Bcl-xL in the mitochondrial membrane. aa= amino acids.
(**B**) ABT-737 binds in the BH3 domain of Bcl-xL (also Bcl-2 and Bcl-w), interacting with the P2 and P4 hydrophobic pockets.
(**C**) WEHI-539 binds in the BH3 domain of Bcl-xL, interacting with P2 and P4 pockets: the two hydrogen bonds to Arg139 may indicate selectivity for Bcl-xL over Bcl-2. Adapted from Czabotar et al., 2014.

the interaction. Furthermore, the C-terminal trans-membrane domain of Bcl-xL directs it to the membrane, and it is here where interactions with the binding partners occur. The analysis of a Bcl-xL-Bim crystal structure gave an insight into how interactions transpire (Liu et al., 2003), and this study also exposed the change in Bax and Bak conformation when bound to Bcl-xL and how this facilities MOMP. Although mostly found on the OMM, in normal healthy cells Bcl-xL retro-translocates between the membrane and the cytosol with transient interaction with Bax.

The mechanism by which Bcl-xL acts as a pro-survival factor was indicated in studies where Bcl-xL inhibited MOMP by binding tBid and also membrane-bound Bax (Billen et al., 2008). Bcl-xL prevents Bax from inserting in the membrane of the mitochondria, thus preventing MOMP. Bax undergoes conformational changes with an initial step involving the exposure of its N-terminus at the membrane, which is in equilibrium with other conformational changes. Bcl-xL is involved in moving the equilibrium away from Bax conformational changes and this allows it to interact with the membrane. Therefore Bax cannot bind the membrane and exert its pro-apoptotic function.

When exposed to stress signals, the BH3 amphipathic helix of a BH3-only protein will bind in the hydrophobic groove of Bcl-xL (or other pro-survival proteins), where four hydrophobic residues (h1-h4) of the BH3 protein interact with the hydrophobic groove of Bcl-xL. When these regions are in close proximity, a salt bridge is formed between an Asp of the BH3 protein and an Arg in the BH1 domain of Bcl-xL. These important interactions can be exploited when developing inhibitors of the Bcl-2 family members.

1.672 Bcl-xL and its inhibitors

As mentioned previously, developing small molecule inhibitors against the anti-apoptotic family is advantageous. For example, ABT-737 (an inhibitor of Bcl-2, Bcl-xL and Bcl-w) (Oltersdorf et al., 2005) has a number of defined interactions in the BH3 domain of Bcl-xL. When bound, ABT-737 occupies the p2 and p4 hydrophobic pockets of Bcl-xL ((Czabotar et al., 2014) and see (Figure 1.10B)). There is an electrostatic interaction between the R_2-NH^+ of the ABT-737 and the Glu96 of Bcl-xL. Furthermore, a more specific inhibitor of Bcl-xL, WEHI-539 shows differential interactions in the hydrophobic domain (Czabotar et al., 2014). WEHI-539 also occupies the p2 and p4 hydrophobic pockets of Bcl-xL. Charge interactions are seen between the Glu96 and the R-NH_3^+, and the Arg139 and the $RCOO^-$ of WEHI-539. Additionally, hydrogen-

bonding interactions are also indicated with the N of the bicyclic aromatic ring and Leu108, and also the R-NH and the Ser106. The sum of these interactions may provide affinity of WEHI-539 for Bcl-xL over Bcl-2.

1.673 Bcl-xL in cancer

Cancers often overexpress some members of the pro-survival family of proteins. Specifically, Bcl-xL is associated with mouse myeloid and T-cell leukemias (Packham et al., 1998), and also in breast cancers (Olopade et al., 1997). The over-expression of Bcl-xL is related to a poor prognosis in cancer (Cory and Adams, 2002). More precisely, a screen of the National Cancer Institute (NCI) panel of 60 cancer cell lines identified the overexpression of Bcl-xL as the key factor in determining resistance to chemotherapeutic agents (Amundson et al., 2000). Furthermore, Bcl-xL expression confers resistance to a number of drugs and is associated with tumour progression in solid tumour and haematological cancers (Amundson et al., 2000; Cleary et al., 1988; Minn et al., 1995). Consequently, initiating a more in-depth study into the role of Bcl-xL in cellular survival, and how this can be exploited in anticancer strategies, is advantageous.

1.68 Apoptosis and mitosis

Mitosis is more susceptible to apoptosis than the interphase state (Rieder and Maiato, 2004). In mitosis, proteins undergo post-translational modifications, such as ubiquitination and phosphorylation, and transcription and translation are halted (Barr et al., 2011; Nigg, 2001; Pines, 2006). Death in mitosis involves the intrinsic apoptotic network and the phosphorylation of apoptotic proteins in mitosis is important in controlling their function and interactions (Topham and Taylor, 2013).

During mitosis, phosphorylation regulates the functioning of the pro-survival proteins. In response to a mitotic arrest in the presence of microtubule inhibitors, Bcl-xL is phosphorylated at Ser62 (Haschka et al., 2015; Poruchynsky et al., 1998; Upreti et al., 2008). This phosphorylation by Cdk-1 negatively regulates the Bcl-xL/Bax interaction (Terrano et al., 2010), antagonising the anti-apoptotic function of Bcl-xL and diminishing its binding to Bax. Under normal conditions, Bcl-xL is present in the cytosol and mitochondria, and Bax in the cytosol (Du et al., 2005). When exposed to antimitotics (such as vinblastine) Bcl-xL is phosphorylated and Bax translocates to the mitochondria, carrying out its function to permeabilise the membrane (Upreti et al.,

2008). Therefore, the phosphorylation of Bcl-xL is important for the release of the sequestered Bax, in turn, inducing apoptosis.

Bcl-2 also undergoes Cdk-1-mediated phosphorylation in mitosis (Haldar et al., 1995; Terrano et al., 2010), and this antagonises its function (Yamamoto et al., 1999). A prolonged mitotic arrest increases Cdk1 activation, enhancing the extent of Bcl-2 phosphorylation and reducing its pro-survival functioning (Terrano et al., 2010). However, Haschka et al. suggested that in fact, Bcl-2 phosphorylation in mitosis causes little inhibition of its activity (Haschka et al., 2015). Furthermore, studies have indicated that Bcl-2 is not essential for survival following antimitotic exposure (Bah et al., 2014; Li et al., 2005; Shi et al., 2011), but in fact, it is Bcl-xL that plays a major role.

Mcl-1 is unique in that as well as undergoing phosphorylation during a mitotic arrest, it undergoes ubiquitin-mediated proteolytic degradation (Harley et al., 2010; Millman and Pagano, 2011; Sloss et al., 2016; Wertz et al., 2011). Phosphorylation of Mcl-1 occurs during a normal mitosis, but when exposed to microtubule inhibitors, Mcl-1 phosphorylation is increased which stimulates its degradation (Chu et al., 2012) .This is in contrast to Bcl-2 and Bcl-xL, where protein levels remain stable throughout a protracted mitosis (Terrano et al., 2010; Tunquist et al., 2010; Upreti et al., 2008). Many kinases have been implicated in the phosphorylation of Mcl-1, including Cdk-1 (Ding et al., 2008; Domina et al., 2004; Inoshita et al., 2002; Kobayashi et al., 2007; Kodama et al., 2009; Maurer et al., 2006; Morel et al., 2009). Phosphorylation of Mcl-1 at a number of sites influences its stability, for example, Thr92 and Thr163 phosphorylation by ERK prolong the half-life of Mcl-1 (Ding et al., 2008; Domina et al., 2004). Conversely, phosphorylation at Ser159 stimulates the ubiqutination and degradation of Mcl-1 (Maurer et al., 2006). In mitosis, phosphorylation at Ser64 increases the stability and pro-survival functioning of Mcl-1 (Kobayashi et al., 2007). Mcl-1 expression is important in the survival and death of cells, where degradation is an important determining factor of its functioning, for example where the degradation of Mcl-1 results in a loss of sequestered Bak (Chu et al., 2012).

The pro-apoptotic proteins also undergo post-translational modifications. The BH3-only protein Bid is regulated in mitosis, where the phosphorylation at Ser67 primes the mitochondria for apoptosis (Wang et al., 2014). At the metaphase to anaphase transition, this phosphorylation is lost. Furthermore, Bim, specifically the Bim_{EL} isoform, is regulated by phosphorylation but also undergoes proteolysis during mitosis (Haschka et al., 2015; Moustafa-Kamal et al., 2013). Unlike the other BH3-only proteins, levels of Bim are markedly decreased in mitosis, in comparison to the other

stages of the cell cycle (Wan et al., 2014). In this study, the decrease in Bim levels inversely correlated with APC/C^{Cdc20} indicating Bim as its substrate, where the suppression of Cdc20 increased sensitivity to apoptotic stimuli. With specificity towards Mcl-1, Noxa controls the degradation of Mcl-1 during mitosis when bound (Czabotar et al., 2007) and is also degraded itself (Haschka et al., 2015). Mitotic phosphorylation of both Mcl-1 and Noxa are important in inducing degradation.

The central proteases of apoptosis, the caspases, are also post-translationally modified. Caspase-9 is involved in the downstream cleavage and activation of caspase-3 (Slee et al., 1999), and it is phosphorylated at Thr125 by Cdk1-cyclin B1 (Allan and Clarke, 2007). This inhibitory phosphorylation in mitosis protects cells from apoptosis. Additionally, caspase-2 is also phosphorylated by Cdk1/cyclin B1 at Ser340, and this suppresses apoptosis (Andersen et al., 2009).

What is the stimulus that triggers the intrinsic pathway in mitosis? There is evidence that suggests it is an accumulation of DNA damage. Throughout a mitotic arrest, DNA damage accumulates (Colin et al., 2015; Hayashi et al., 2012; Orth et al., 2012), evidenced by an increase in γ-H2AX (Topham et al., 2015). Here, caspase-activated DNase (CAD) is stimulated, and cytochrome c is released from the mitochondria (Orth et al., 2012). Additionally, another mode of apoptotic trigger in mitosis may be telomere deprotection. Telomeres are protected by shelterin, with one protecting component being TRF2 (de Lange, 2009). When TRF2 is modified, it is recognised as a site of DNA damage, phosphorylating H2AX. A mitotic arrest induces Aurora B-dependent telomere deprotection, freeing TRF2, and activating ATM and the DNA damage response (Hayashi et al., 2012). When TRF2 is overexpressed in the presence of RNAi against Bcl-xL and Mcl-1, DiM was reduced, indicating a protective function for TRF2 (Topham et al., 2015).

1.681 The post-mitotic response

Although DiM is a potent phenotype following mitotic perturbations, cells may also die in interphase following mitosis (Figure 1.7A). Bcl-xL has been implicated as a player in the post-mitotic response (Minn et al., 1996; Topham et al., 2015). When cells slip from mitosis, they will exhibit tetraploidy, where DNA content is 2x that of a diploid cell. Following slippage, the cell may undergo death in the proceeding interphase. The transcription factor p53 is implicated in the control of interphase death, where in p53-null mice, apoptosis was evaded and tumour formation driven (Harvey et al., 1993). As expression of p53 is limited to only interphase, this suggests a role for p53 in post-

mitotic responses (Minn et al., 1996). If we consider p53 activation following cytokinesis failure, it is probable that p53 causes apoptosis through the Bcl-2 family members, since Bcl-xL overexpression gave rise to an increase in tetraploid cells (Minn et al., 1996). Furthermore, when Taxol-treated cells were depleted of Bcl-xL, an increase in PmD was observed (Topham et al., 2015). Also, p53 is known to regulate the pro-apoptotic BH3-only proteins Noxa and Puma (Nakano and Vousden, 2001; Oda, 2000; Yu et al., 2001), and therefore activation of p53 upon tetraploidy will likely activate the pro-apoptotic proteins and cause post-mitotic death. Further analysis of this and the role of Bcl-xL will be discussed in Chapter 5.

1.69 Autophagy and metabolism

The death in mitosis phenotype observed when cells are exposed to antimitotics can be explained by activation of the intrinsic apoptotic pathway. However, more in depth studies have revealed that metabolism and the energy requirements of the cell during this prolonged mitotic arrest may dictate whether a cell is likely to survive or die (Doménech et al., 2015). In this study, during the extended mitosis, mitophagy-dependent loss of mitochondria resulted in reduced mitochondrial mass and oxidative respiration. Glycolysis replaced oxidative respiration and the reduced ATP levels activated AMPK, and cells showed a dependence upon glycolysis for survival. The data suggested that either upregulating autophagy or inhibiting glycolysis may in fact synergise with antimitotics.

1.7 Summary and Aims

The precise mechanisms by which antimitotics kill cancer cells remain undefined. Multiple lines of evidence suggest that death occurs via the intrinsic apoptotic pathway (Allan and Clarke, 2007; Andersen et al., 2009; Gascoigne and Taylor, 2008; Shi et al., 2011). In the clinic, antimitotics such as Taxol are used in the treatment of many different cancers, however problems persist such as unfavourable side effects, resistance and the inability to predict how or whether patients will respond. To improve anti-cancer strategies we have to understand how antimitotics elicit their action. In order to do this I will use various methods of exploiting mitosis and analyse the consequences.

To understand how cells behave when mitosis is perturbed I will focus on three areas:

(i) *Establishing new methods of anticancer therapy:* this will involve testing the ability of 2OH-BNPP1 to inhibit Bub1 kinase *in vitro* and in cells;

(ii) *The establishment of an assay to induce aneuploidy*: this will involve the synthesis of a Cenp-E inhibitor GSK923295, which will be fully characterised and used in assays to generate aneuploidy;

(iii) *Understanding how antimitotics cause cell death:* this will involve understanding the role of Bcl-xL in cell death upon exposure to antimitotics.

Despite the development of second-generation inhibitors, there has been little evidence of success. It may be that incorrect targets are being studied and therefore new avenues need to be researched. One such target involves the SAC component Bub1 kinase. With no approved inhibitors, and no definitive evidence for the role of its kinase activity in the SAC, I will study Bub1 kinase and introduce and characterise an inhibitor of its activity, 2OH-BNPP1 (Kang et al., 2008). This may lead to revealing cases where Bub1 inhibition may be advantageous over other targets, leading to the development of new inhibitors.

Often, a deregulated mitosis can lead to chromosome missegregation and the onset of aneuploidy, with this being a frequent occurrence in cancers. However, the reasons why cancer cells are able to survive and proliferate, yet normal somatic cells cannot, is not well known. In order to study this phenomenon, robust cellular biology assays have to be established. I aim to aid in the generation of such an assay to study aneuploidy, with potential advantages over the traditional monastrol washout methods.

To do this I will facilitate in the synthesis of a Cenp-E inhibitor GSK923295 (Qian et al., 2010), and confirm its target in cells. This will then be used in further assays to induce chromosome misalignment, followed by SAC override and missegregation.

Furthermore, as I specified previously, the mechanism of antimitotic action may be via the intrinsic apoptotic pathway. Thus, in the final part of my thesis I will study this mechanism in more depth using a Bcl-xL inhibitor WEHI-539 (Lessene et al., 2013), where this will support the understanding of the role of the intrinsic pathway in the response of cells to antimitotics.

Chapter 2: Materials and methods

2.1 Cell Biology

Cell Culture

The cell lines used throughout include HeLa, DLD-1, RKO, and the derivatives of HEK293 LacZeo/TO, RKO LacZeo/TO, HeLa LacZeo/TO, DLD-1 LacZeo/TO (plating densities are given in Table 2.1). The LacZeo/TO cell lines contain an FRT site in the genome, and these cell lines were grown in Zeocin (Thermofisher) and Blasticidin (Melford) selection, as described previously (Girdler et al., 2006; Tighe et al., 2004; Topham et al., 2015).

Cell lines were maintained in Dulbecco's Modified Eagles Medium (DMEM) or Leibovitz (Sigma) (for caspase 3/7 measurement), supplemented with 10% fetal bovine serum (FBS)(Gibco), 2 mM glutamine (Sigma), 100 U/mL penicillin and 100 U/mL streptomycin (Sigma) at 37°C and in a humidified 5% CO_2 atmosphere. For passaging, cells were washed with Dulbecco's Phosphate Buffered Saline (PBS) (Sigma), and then incubated with 2 ml of 1x Trpysin-EDTA (Sigma) in PBS for 5 minutes. DMEM was used to neutralise before subsequent plating. For synchronisation of cells in S phase, cells were treated with 2 mM thymidine for 16 hours and then released into fresh DMEM.

Cell line	6 well	24 well	96 well	10 cm	coverslips
RKO	15	12	8	n/a	8
DLD-1	12	10	6	n/a	7
HeLa	n/a	n/a	8	n/a	8
HEK293	n/a	n/a	8	12	n/a

Table 2.1 Cell plating density where numbers are a x 10^4 cells/ml.

Drug treatments

Drugs were made up in dimethyl sulfoxide (DMSO), except for tetracycline (Sigma) in water (Table 2.2). Drugs were diluted to the appropriate concentration in DMEM. For thymidine (Sigma), the powder was dissolved in PBS and then filtered with a PES syringe filter (pore size 0.45 µm) (Whatman™), with subsequent dilution in DMEM.

Drug	Stock concentration	Final concentration	Source	Against?
2OH-BNPP1	10 mM	10 µM	Glixx labs	Bub1
GSK923295	10 mM	See legends	(Bennett et al., 2015)	Cenp-E
Taxol	10 mM	See legends	Sigma	MT
nocodazole	5 mg/ml	See legends	Sigma	MT
AZ138	10 mM	See legends	AstraZeneca (Gascoigne and Taylor, 2008)	Eg5
BI2536	10 mM	See legends	Boehringer Ingelheim (Steegmaier et al., 2007)	Plk1
ZM447439	10 mM	See legends	Tocris (Ditchfield et al., 2003)	Aurora B
MLN8054	10 mM	See legends	Millennium Pharmaceutic Inc. (Manfredi et al., 2007)	Aurora A
AZ3146	10 mM	See legends	AstraZeneca (Hewitt et al., 2010)	Mps1
WEHI-539	10 mM	See legends	Apexbio (Lessene et al., 2013)	Bcl-xL
A-12104677	10 mM	See legends	Chemietek (Leverson et al., 2015b)	Mcl-1
thymidine	200 mM	2mM	Sigma	DNA synthesis Inhibitor
tetracycline	1 mg/ml	See legends	Sigma	ribosome

Table 2.2 Drug concentrations used.

Stable cell line generation

For generation of HeLa, HEK293, and RKO cell lines expressing tetracycline-inducible exogenous protein, the Flp-In™ (Invitrogen) system was utilised. The Flp-In™ T-Rex system involves the expression of the exogenous proteins from the same genomic locus (Invitrogen, 2010). Flp recombinase catalyses the recombination

between two FRT sites. In the first case, the pFRT/LacZeo plasmid containing a Zeocin™ selection marker with a SV40 promoter was transfected into cells. After selection with Zeocin, single colonies were expanded. This approach was used for the generation of the cell lines used throughout the thesis: DLD-1, RKO, HEK293 and HeLa LacZeo/TO, which have been previously generated in the lab (Girdler et al., 2006; Tighe et al., 2004; Topham et al., 2015).

In all cases, the gene of interest was cloned into a pcDNA5/FRT vector, under the control of a CMV promoter. A hygromycin resistance gene was also contained on the plasmid. The vector was co-transfected with a pOG44 plasmid (which constitutively expresses Flp recombinase under control of the CMV promoter), into the Flp-In cell line of choice generated previously, using Lipofectamine and Lipofectamine Plus (Thermofisher). After homologous recombination between the FRT sites (in the genome and pcDNA5/FRT vector), the pcDNA5/FRT was inserted into the genome at the integrated FRT site (O 'Gorman et al., 1991). The mixture was incubated in DMEM minus FBS and Penicillin/Streptomycin (P/S) at room temperature for 15 minutes, to enable the generation of DNA-lipid complexes. Mixtures were then added carefully to the cells plated in the wells. After at least a 3 hour incubation at 37°C, transfections were stopped by the addition of DMEM with FBS and P/S and additional FBS. After 24 hours, cells were expanded into 10 cm dishes. Following an additional 24 hours, cells were put under selection with hygromycin B (Roche) and Blasticidin (Melford). Media and selection antibiotics were replaced every 4 days. After formation of visible colonies, all were pooled and expanded. For conformation of exogenous protein expression, cells were plated into a 6-well plate (Table 2.1) and tetracycline (1 µg/ml) added overnight. Cells were then processed for western blotting. This involved trypsinisation and neutralisation in PBS, followed by resuspension in 6x SDS buffer (0.35 M Tris pH 6.8, 0.1 g/ml sodium dodecyl sulphate, 93 mg/ml dithiothreitol, 30% glycerol, 50 µg/ml bromophenol blue). For generation and maintenance of stable cells lines under tetracycline control, zeocin, hygromycin and blasticidin were used at the concentrations shown in Table 2.3.

Cell line	Zeocin (100 mg/ml)*	Hygromycin (50 mg/ml)**	Blasticidin (10 mg/ml)*/**
RKO	300 µg/ml	400 µg/ml	8 µg/ml
DLD-1	60 µg/ml	400 µg/ml	8 µg/ml
HeLa	50 µg/ml	200 µg/ml	4 µg/ml
HEK293	100 µg/ml	150 µg/ml	15 µg/ml

Table 2.3 The antibiotics used for selection in the LacZeo/TO cell lines.
* for maintenance ; ** for generation

Transient transfections (RNA interference)

For transient transfections of siRNA, oligonucleotides were diluted to 2 µM in 1x siRNA buffer (Dharmacon) (Table 2.4). For 96-well transfections, 5 µl of the siRNA (or 2.5 µl of 4 µM) and 45 µl of DharmaFECT 1 transfection reagent (Dharmacon) were mixed in OPTIMEM® (Gibco) and added to the relevant wells of a 96-well plate (Greiner). After formation of the lipid-RNA complexes for 30 minutes at room temperature, cells were seeded onto the complex mixture with DMEM minus P/S. After incubation for 24 hours at 37°C, media was replaced with DMEM and drugs for further experimentation. For confirmation of repression, wells were harvested and lysed in 150 µl of 6x SDS buffer and analysed by immunoblotting.

2.2 Molecular Biology

Vectors

Stocks of the vectors generated are stored in 50% glycerol and LB/carbenicillin at -80°C for long-term storage. Table 2.5 denotes the methods of cloning used to generate the plasmids used in this thesis.

Polymerase Chain Reaction (PCR)

To amplify DNA fragments the Pfu DNA polymerase (Thermofisher) was used with a set of forward and reverse primers (Thermofisher). The reaction was set up as depicted in Table 2.6.

siRNA	Sequence
NT	UGGUUUACAUGUCGACUAA, UGGUUUACAUGUUGUGUGA, UGGUUUACAUGUUUUCUGA, UGGUUUACAUGUUUUCCUA
Bcl-xL	GGACAGCAUAUCAGAGCUU, GAAAUGACCAGACACUGAC, CCUACAAGCUUUCCCAGAA, UUAGUGAUGUGGAAGAGAA
Mcl-1	CGAAGGAAGUAUCGAAUUU, GAUUAUCUCUCGGUACCUU, GAAGGUGGCAUCAGGAAUG, GGUUUGGCAUAUCUAAUAA

Table 2.4 siRNA sequences of the oligonucleotides used.

Vector	Method of generation
Chapter 3	
pcDNA5-GFP-hBub1 WT	Restriction digest (BamHI/NotI of pcDNA3-myc-hBub1 and pcDNA5-GFP-Mps1 plasmids). Fragments already generated in-house.
pcDNA5-GFP-Bub1 K821R	Mutagenesis on above (see primers in Table 2.8).
pcDNA5-GFP-H2B-Bub1C WT	1. XhoI/NotI digest of pcDNA5-GFP-Mps1 (contains BamHI site next to XhoI). 2. Amplify H2B from pcDNA5-GFP-H2B plasmid, as a XhoI-BamHI/NotI fragment. 3. Clone into pcDNA5-GFP. 4. Digest overnight with BamHI/NotI. 5. Amplify Bub1C as a BamHI/NotI fragment from pcDNA5-GFP-hBub1. 6. Clone (5) into pcDNA5-GFP-H2B.
pcDNA5-GFP-H2B-Bub1C D946N	Mutagenesis on above (primers in Table 2.8).
Chapter 5	
pcDNA5-GFP-Bcl-xL	Restriction digest (XhoI/NotI of pcDNA5-GFP-Mps1 and pcDNA5-myc-Bcl-xL). Fragment already generated in-house.

Table 2.5 Cloning methods to produce the plasmids used.

Component	Volume / µl
dNTPs*	5 (8 mM)
10x Pfu buffer	5
Pfu enzyme (200 U)	1
Primers x 2 (forward/reverse)**	2 (0.2 mM each primer)
Template	0.2 (0.3 µg)
dH_2O	34.8

Table 2.6 Setting up the PCR reaction.
* Bioline
** of a 100 ng/ml stock

Following set up of the reaction mixture, the PCR was performed on a Geneamp® PCR System 2700 (Applied Biosystems) using the cycling conditions in Table 2.7.

Temperature / °C	Time	Cycles
94	3 mins	
94	30 secs	32
62	30 secs	
72	2 mins	
72	10 mins	
4	Hold	

Table 2.7 Cycling conditions used for PCR.

Mutagenesis

For the generation of the K821R and D946N Bub1 mutants in Chapter 3, reactions were set up as shown in Table 2.9, with the cycling conditions as shown in Table 2.10 and mutagenesis primers in Table 2.11. Following PCR amplification, 1 µl of DpnI enzyme (NewEnglandBiolabs) was added to the PCR product. After microcentrifugation for one minute, the reaction was incubated at 37°C for 2 hours. 1 µl of the reaction was the diluted in 9 µl of dH_2O. This was then added to 50 µl of XL-1 *Escherichia coli* cells. The transformation protocol was then followed.

Restriction site-gene	Sequences (5'-3')
XhoI-H2B	**F** CACCTCGAGCCAGAGCCAGCGAAGTCTCCC
BamHI-HindIII-NotI-H2B	**R** CACGCGGCCGCAAGCTTGGATCCCTTAGCGCTGGTGTACTTGGTGAC
BamHI-Bub1 (kinase domain)	**F** CACGGATCCCAGATGAGTTCACTTGGGACT
NotI-Bub1 (kinase domain)	**R** CACGCGGCCGCTTATTTTCGTGAACGCTTACATTC
Sequencing primers	
GFP	**F** CATGGTCCTGCTGGAGTTCGTG
pcDNA5 Reverse	**R** TAGAAGGCACAGTCGAGG
K821R hBub1 D946N Bub1C	**F** CACTTGGGACTGTTGATGCTC **R** GTTGCTGAGCATCTCAACACAC

Table 2.8 Primers used in cloning and sequencing.

Component	Volume / µl
10x Buffer (Pfu)	5
dNTPs	4
Primers (x2) *	1.25
Template vector	1
dH_2O	37.5
Pfu (200 U)	1
Sum	50

Table 2.9 Mutagenesis reaction set-up.
*from 100 ng/ml stock

Temperature / °C	Time	Cycles
95	3 mins	
95	20 secs	16
52	1 min	
68	18 mins	
68	10 mins	
4	Hold	

Table 2.10 Cycling parameters for mutagenesis.

Primer	Sequence (5'-3')
K821R	
Forward	GATGCTAAAAATAAACAGAAATTTGTTTTAAGGGTCCAAAAGCCTGCC
Reverse	GGCAGGCTTTTGGACCCTTAAAACAAATTTCTGTTTATTTTTAGCATC
D946N	
Forward	TCTGCTGGCTTGGCACTGATTAACCTGGGTCAG
Reverse	CTGACCCAGGTTAATCAGTGCCAAGCCAGCAGA

Table 2.11 Mutagenesis primers.

Restriction Digests

Plasmids were digested for: (i) use in validating the plasmid identity and (ii) for further use in cloning, where the reaction set-ups are given in Tables 2.12 and 2.13 respectively. For digestion of the PCR products, they were first purified using the QIAquick® PCR purification kit (Qiagen). Reactions were placed into a 37°C incubator for >60 minutes for a test digest and overnight for a cloning digest.

Component	**Volume / µl**
DNA (from PCR or miniprep) 0.3 µg for test digest	1
Enzyme 1 (20 U)	0.1
Enzyme 2 (20 U)	0.1
10x Buffer (Cutsmart®)*	1
dH_2O	7.8
Sum	10

Table 2.12 Test restriction digests.

Component	**Volume / µl**
DNA (from PCR or miniprep)- 3 µg for cloning	5
Enzyme 1 (20U)	1
Enzyme 2 (20 U)	1
10x Buffer (Cutsmart®)*	2
dH_2O	11
Sum	20

Table 2.13 Restriction digests for cloning.
***** NewEnglandBiolabs

Gel Electrophoresis

DNA fragments were then visualised using gel electrophoresis. This was used either for characterisation of digested plasmids, PCR product confirmation and also for the isolation of the vector and insert digestion products for further steps in cloning. For characterisation and product confirmation, agarose (Bioline) at the relevant concentration was dissolved in TBE buffer (88 mM Tris, 88 nM Boric acid, 2 mM EDTA, pH 8.2). For further ligation and cloning, Microsieve Clone LM agarose (Bioline) was dissolved in TBE buffer and stored at 4°C to set. All sample preparations were resuspended in a DNA dye (50% glycerol, 10% bromophenol blue, 10% xylene blue) and loaded onto the agarose gel, running at 80V for 70 minutes using a Biorad

Minisub® CELL GT (Biorad). Gels were then incubated with dH_2O and ethidium bromide (Sigma) and rocked for 20 minutes. After further washing for 20 minutes, DNA was visualised using a hand-held UV lamp (UVP). For the ligation and cloning gel, staining was performed similarly, with vector and insert bands cut from the gel using blades (Swann-Morton).

DNA ligation

Following analysis by gel electrophoresis, bands were cut and gel slices placed into eppendorfs. After heating to 55°C for 10 minutes, gel slices became molten. In separate eppendorfs, 1 µl of the vector plus 7 µl of the insert were mixed. 1 µl of 10x T4 DNA ligase reaction buffer (NewEnglandBiolabs) was also added. After solidification on ice, 1 µl T4 DNA ligase (400 U/µl) (NewEnglandBiolabs) was added on top of the gel and then incubated for at least 90 minutes at room temperature. Following this, 40 µl of dH_2O was added and the eppendorfs were heated to 55°C for 10 minutes.

Transformation and plasmid isolation

After ligation, XL1 Blue *Escherichia coli* chemically competent cells were thawed from -80°C and kept on ice. 50 µl was transferred to an ice-cold tube and 10 µl of the ligation mix was added with pipette mixing. After incubation on ice for 20 minutes, the cells were placed at 42°C for 90 seconds to allow for heat-shock enabled transformation and returned to ice. Glass beads were then used to plate out the cells onto agar and carbenicillin (100 µg/ml) plates. Plates were inverted and placed at 37°C overnight. Single colonies were then picked and placed into a Luria Broth (Invitrogen) and ampicillin (25 µg/ml) culture and left to grow at 37°C overnight in a shaking incubator. For long-term storage, bacterial cultures were then mixed with 50% glyercol (1:1) and stored at -80°C. Next, DNA plasmids were isolated and purified with the QIAprep® spin miniprep kit (Qiagen) and reconstituted in water for storage at -20°C.

DNA sequencing

Samples for sequencing were submitted to the University Core Sequencing Facility. To prepare samples for sequencing, reactions were set up using the BigDye® Terminator Sequencing Kit (Applied Biosystems) as shown in Table 2.14 (See Table 2.8 for primer sequences used), with cycling conditions for 25 cycles depicted in Table 2.15.

Component	Volume / µl
5 x BigDye® Terminator Sequencing Buffer*	3
Primer (F or R)	3.2 (6 pmol final)
BigDye® Terminator Sequencing Kit	2
Template DNA	2.7 (1 µg)
dH_2O	9
Sum	20

Table 2.14 Sequencing set-up.

Temperature / °C	Time
96	10 secs
50	5 secs
60	4 mins

Table 2.15 Cycling conditions for DNA sequencing.

Following amplification, DNA was precipitated with 8.5 mM NaAc pH 4.8, 100% EtOH, and 9 µg/ml GlycoBlue (Ambion), with an additional 80 µl dH_2O for 15 minutes on ice. Centrifugation at maximum speed for 20 minutes ensured precipitation of the pellet, which was then air-dried prior to sequencing.

2.3 Protein analysis

SDS-PAGE

Analysis for protein detection using western blotting included trypsinising cells for 2 minutes, neutralising with PBS and centrifuging for 5 minutes at 1000 rpm. Following a wash step with PBS, 6x SDS was added and proteins denatured at 100°C for 5 minutes. Depending on the molecular weight of the proteins for resolution, different percentage acrylamide gels were used (see Table 2.16). The Precision Plus Protein™ Dual Colour Standard (Bio-Rad) was used for the molecular weight ladder. After loading samples onto the gel, gels were run in either 1x running buffer (25 mM Tris, 200 mM glycine, 0.1 % (w/v SDS) or 1x MOPS buffer for the 4-12% gradient gels (Novex). Gels were run at 100V with a Hoefer™ SE260 vertical electrophoresis unit (Amersham Biosciences).

Component (for 1 gel)	Resolving gel / ml				Stacking gel / ml
	6%	8%	10%	15% (for kinase assay)	
dH_2O	3.1	4.1	6.1	8.6	5.7
1.5 M Tris pH 8.8	3.75	3.75	3.75	3.75	N/A
Tris 0.5 M pH 6.8	N/A	N/A	N/A	N/A	2.5
Acrylamide (30%)	3	4	5	7.5	1.7
10% (v/v SDS (sodium dodecyl sulfate)	0.15	0.15	0.15	0.15	0.1
10% (v/v) APS (aluminium potassum sulfate)	0.15	0.15	0.15	0.15	0.1
TEMED	0.015	0.015	0.015	0.015	0.01

Table 2.16 Making up SDS-PAGE gels (Note all reagents are from Sigma, except Acrylamide, National Diagnostics).

Immunoblotting

Upon resolution via SDS-PAGE, polyacrylamide gels were electro-blotted onto methanol-soaked Immobilon-P membranes (Millipore) with a Mini-PROTEAN® Tetra System (BioRad) in 1x transfer buffer (25 mM Tris, 190 mM glycine, 0.1 % (w/v) SDS, 20% methanol) at 50V for 70 minutes. This was followed by blocking in 5% milk (Marvel) in TBST (100 mM Tris, 150 mM NaCl, 0.1% (v/v) Tween-20, pH 7.5) for one hour. Membranes were then incubated in 5% milk and the primary antibody (Table 2.17) at 4°C overnight. After washing in 3x TBST, membranes were immersed in horseradish-peroxidase-conjugated (HRP) secondary antibodies. For visualisation EZ-ECL Chemiluminescence Reagents (Biological Industries) or Luminata™ Forte Western HRP Substrate (Millipore) were used and the Biospectrum® 500 imaging system (UVP) was used to develop. To process the images VisionWorks®LS (UVP) was utilised.

Antibody target	Host	Source	Concentration
Primary			
Anti-Bub1 (SB1.3)	Sheep	(Taylor et al., 2001)	1:1000
Anti-GFP	Rabbit	Cell signalling	1:1000
Anti-Tao1	Sheep	(Westhorpe et al., 2010)	1:3000
Anti-Bcl-xL	Rabbit	Cell Signalling	1:1000
Anti-Mcl-1	Rabbit	Santa Cruz	1:1000
Anti-Bim	Rabbit	BD BioSciences	1:500
Anti-Bad	Mouse	BD BioSciences	1:100
Anti-Myc-tag 4A6	Mouse	Millipore	1:5000
Anti-Bax	Rabbit	Santa-Cruz	1:800
Anti-Bak	Mouse	Santa-Cruz	1:800
Anti-Bid	Rabbit	Cell Signalling	1:1000
Anti-Aurora A (Thr288) / Aurora B (Thr232) / Aurora C (Thr198)	Rabbit	Cell Signalling	1:1000
Secondary			
Anti-sheep HRP	Rabbit	Zymed	1:2000
Anti-rabbit HRP	Goat	Zymed	1:2000
Anti-mouse HRP	Goat	Zymed	1:2000

Table 2.17 Antibodies used for western blotting.

Co-immunoprecipitation

For GFP-tagged proteins, the GST-GFP binder protein was used for affinity purification (Rothbauer et al., 2007; Sloss et al., 2016). In general, the open reading frame (ORF) of the GFP-binder was cloned into a pGEX-4T3 vector and then transformed into *Escherichia coli* BL21. IPTG was used to induce the GST-GFP-binder fusion protein. Glutathione sepharose beads (GST) (Amintra) were added to purify the fusion protein, with soluble glutathione used for elution, followed by dialysis. For immunoprecipitation, cells were plated into a 10 cm dish followed by overnight incubation with nocodazole (20 ng/ml) and tetracycline (see legends for details) to induce expression of the exogenous GFP-tagged proteins. After growing to near 100% confluency, cells were harvested. After centrifugation the cell pellet was resuspended in lysis buffer (0.1% Triton X-100, 100 mM NaCl, 10 mM Tris pH 7.4, 1 mM EGTA, 20 mM beta-glycerol, 10 mM NaF), cOmplete, Mini, EDTA-free Proteasome inhibitor cocktail tablet (Roche) and phosphatase inhibitor tablet (PhosSTOP EASYpack, Roche). Following incubation on ice at 4°C for 20 minutes, insoluble proteins were removed by centrifugation at maximum speed for 20 minutes at 4°C. 30 µl of the

sample was taken for analysis for an input sample. GST beads were washed twice in lysis buffer and incubated with the lysed protein sample and 30 µg of the GST-GFP-binder protein. Samples were rotated at 4°C for a minimum of 3 hours. Beads were then washed 5 times in lysis buffer, followed by addition of 6x SDS to the beads and boiling at 100°C for 5 minutes.

Kinase assay

HEK293 cells GFP-Bub1 wild-type (WT) and the K821R mutant were incubated as above (see immunopreciptation method) with the GFP-binder protein and GST beads. After incubation at 4°C and washing steps as above, the beads and bound protein were subsequently washed three times in a kinase buffer (see Table 2.18). Following washing, reactions were set up with the beads, ATP cold (Sigma), and histone H2A substrate (NewEnglandBiosciences) on ice (see Table 2.19 for details of optimum conditions). Lastly, [γ-^{32}P]ATP (hot) (PerkinElmer) was added, and the reaction incubated at 30°C for 20 minutes in a temperature controlled incubator. Following reaction completion, 6x SDS was added, and proteins denatured at 100°C for 5 minutes. After separation by SDS-PAGE (15% gel) and staining with Instant Blue (Expedeon) for one hour, the gel was dried for one hour. A phosphoimager (Typhoon FLA7000, Raytek scientific Limited Sheffield UK) was used to visualise the gel and AIDA software to process the data. ImageJ was used for quantification.

Component	**Final concentration**
Tris-HCl pH 7.4 (Fischer)	25 mM
NaCl (Fischer)	100 mM
$MgCl_2$ (Sigma)	10 mM
BSA (Sigma)	50 µg/ml
EGTA (Fischer)	0.1 mM
β -mercaptoethanol (Sigma)	0.1%

Table 2.18 Components of the kinase assay buffer

Component	Volume or concentration
Beads	10 µl
Substrate H2A	3 µl
[γ-^{32}P]ATP : 2 µCi/reaction	Stock ATP: 10 µCi/µl- 4 µl taken
Cold ATP	100 µM
Hot/cold ATP	6.5 µl
dH_2O	20.5 µl

Table 2.19 Optimum conditions for the kinase assay.
(See main text for optimum concentrations determined)

Table 2.20 shows the calculation of the ATP concentration required for each kinase reaction.

Cold ATP	**Hot ATP**
8.06 µl from 10 mM stock cold ATP: 5.5 µl of 10 mM in 90 µl = 611 µM add 6.5 µl to 40 µl: 100 µM	*Stock:* 10 µCi/µl *Specific activity:* 3000 Ci/mmol *Molarity* = (10 Ci/l)(3000Ci/mmol)= 0.0033 mmol/l= 3.33 µM *Stock hot ATP:* 3.33 µM In assay: 2.8 µl in 90 µl dH_2O Then 6.5 µl in assay: 2 µCi *per reaction* *Concentration in assay:* (3.33 µM)(2.8 µl) = c x 90 µl = 0.1036 µM (0.1036 µM)(6.5 µl) = c x 40 µl *=0.0168* µM *in assay* i.e. the concentration is very low in comparison to cold ATP Specific activity of total: 0.50 Ci/mmol 0.311 µCi x 6.5 = 2 µCi per assay 4 µl from 10 µCi stock

Table 2.20 Calculations for determination of the cold and hot ATP concentrations.

2.4 Live cell imaging and microscopy

Time Lapse microscopy

For experiments using RNAi reverse transfection, plating and transfection occurred 24 hours before drug addition and imaging began. Cells were plated (see Table 2.1 for plating density) in a microclear 96 well plate (Greiner) and maintained at 37°C and 5% CO_2. For measurement of confluency and caspase 3/7, the IncuCyte™ Zoom (EssenBioSciences) was used with a 20x objective, where the IncuCyte™ 96-well Kinetic Caspase-3/7 reagent (EssenBIoSciences) was at a final concentration of 5 µM. Processing definitions were used to train the IncuCyte to obtain a read-out of confluency and fluorescence, exploiting the built-in software. Values were normalised to 0 for time zero. For fate profiling, movies were generated from MPEG-4 image sequences. GraphPad Prism 6 was used to represent and analyse the data.

Fluorescent time lapse

Cells were plated at 8×10^4 cells/ml in a 24 well plate (Corning). After drug addition, cells were imaged using a CoolSNAP HQ camera (Photometrics) every two minutes, with a Zeiss Axiovert 200 microscope and an automated PZ-2000 stage (Applied Biosystems), with cells maintained at 37°C and a continuous flow of 5% CO_2. Images were acquired with a 60x objective. MetaMorph Software (Universal Imaging) was used to drive the shutters, filter wheels and point visiting. Images were processed using Photoshop (Adobe) and Quicktime (Apple).

Immunofluorescence

For analysis by immunofluorescence, cells were plated (see Table 2.1) onto 19 mm coverslips (VWR International) with a final volume of 500 µl. After overnight incubation, drugs and tetracycline (where required) were added. For fixation, 1% formaldehyde was added, followed by quenching with glycine (1 M glycine pH8.5 –with 1 M Tris pH 8.5) and permeabilisation with PBST (PBS and 0.1% Triton X-100). For the microtubule staining, PEM buffer was utilised, with pre-extraction using 100 mM PIPES, 1 mM $MgCl_2$, 0.1 mM $CaCl_2$, and 0.1% Triton X-100 for 90 seconds and then fixation with 4% formaldehyde in PEM buffer for 10 minutes. Cells were then incubated with the primary antibody diluted in PBST for 30 minutes, followed by washing and subsequent incubation at room temperature with the secondary antibody for 30 minutes. Hoechst 33358 (Sigma) at 1 µg/ml was then added to cells for 1 minute. Coverslips were then mounted onto slides (26 x 76 mm DeltaLab) using mounting

media consisting of 90% glycerol, 20 mM Tris-HCl pH 8.0. For imaging, the restoration microscope (DeltaVision RT; Applied Precision) using a 100x 1.40 NA Plan Apo Objective and a filter set (Sedat Quad; Chroma Technology Corp.) was used at room temperature or a Axioskop 2 microscope (Zeiss) with a 32x or 100x objective was used with a CoolSNAP HQ CCD camera (Photometrics). Analysis of images was with Metamorph® software.

FACS

For DNA content analysis, after plating, cells were trypisinised and collected. Cells were then centrifuged and washed with PBS. Samples were then fixed in 100% ethanol and stored at -20°C overnight. Following washing in PBS, cells were suspended in propidium iodide (40 µg/ml) and RNase (50 µg/ml), incubating for 30 minutes at room temperature. Flow cytometric analysis using the Cyan ADP (Beckman Coulter) analysed the DNA content of 10 000 cells. Summit 4.3 was used to analyse data.

Antibody target	**Host**	**Source**	**Concentration**
Primary			
Anti-H2A-pT120	Rabbit	Active Motif	1:1000
Anti-Sgo1	Sheep	In house	1:100
Anti-Tubulin (TAT1)	Mouse	(Woods et al., 1989)	1:300
Anti-Bub1 (SB1.3)	Sheep	(Taylor et al., 2001)	1:500
Secondary			
Anti-sheep-Cy2	Rabbit	Stratech	1:1000
Anti-mouse-Cy3	Goat	Stratech	1:1000

Table 2.21 Antibodies used in immunofluorescence.

2.5 Calculation of synergy scores

For the combinatorial studies where synergy scores were calculated, the Bliss independence model was used (Lehár et al., 2009; Wong et al., 2012). To calculate the expected response (C), the following was used, where C = (A + B) – (A x B), with A being the apoptotic response of drug A, and B, the response of drug B, expressed as percentages for a particular drug combination. From this the difference between the expected response (C) and the actual response (D), was given by (E), where E(%) = D – C x 100, and is defined as the Bliss Excess. To calculate the Bliss Sum (F) for each

concentration matrix, all values of E were summated. Positive Sum values indicated synergy, negative indicated antagonism, and zero indicated additive or no effect.

2.6 Statistical Analysis

Statistical analyses were performed with the non-parametric Mann-Whitney U Tests using GraphPad Prism 6. The box-and-whisker plots show the mean and interquartile ranges. Error bars show the standard deviation.

2.7 Chemical Synthesis

The methods were as described previously (Bellingham et al., 2010). All chemicals used throughout were obtained from Sigma. *S*-ethyl thiohexanoate (10 mmol) **3** was added to racemic 1-(2-aminophenyl)ethanol (1 mmol) *rac*–**2**, with the CALB enzyme preparation (50% w/w), all enclosed in a reaction vessel with an additional bleach trap. Maintaining the reaction at 39°C, progress was monitored using HPLC analysis (Chiralcel OD-H; Heptane: ethanol 90:10, 0.1% IPAM; Flow: 0.8 mL/min). Analysis determined the reaction was complete after a five day period. Following completion, the enzyme was removed from the reaction mixture by gravity filtration. Column chromatography was used to purify the product (ethyl acetate as the elutent), giving ester (*R)*–**4** and the unreacted alcohol (*S)*–**2**.

(*S*)-1-(2-amino-3-pyridinyl)ethanol (*(S)*–2)

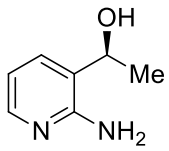

Unreacted alcohol (*S)*–**2**. Colourless oil. RT = 10.8 min. Yield: 50%. *ee*: >99%. $[\alpha]_D$ = -0.5^o (ethanol, c = 1.00).

(*R*)-1-(2-amino-3-pyridinyl)ethyl hexanoate (*(R)*–4)

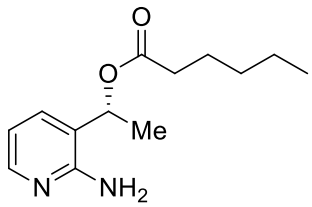

Ester (*R)*–**4** obtained from reacting alcohol *(R)*–**2**. Colourless oil. RT = 7.1 min. Yield: 50%. ^{1}H NMR (400 MHz, $CDCl_3$) δ 0.78-0.86 (m, 3H, $CO(CH_2)_4\mathit{CH_3}$), 1.18-1.30 (m, 4H, $CO(CH_2)_2\mathit{(CH_2)_2}CH_3$), 1.49-1.59 (m, 5H, $COCH_2\mathit{CH_2}(CH_2)_2CH_3$), $OCH\mathit{CH_3}$), 2.23-2.29 (m, 2H, $CO\mathit{CH_2}(CH_2)_3CH_3$), 5.15 (s, 2H, $\mathit{NH_2}$), 5.82 (q, *J* = 6.8 Hz, 1H, $O\mathit{CH}CH_3$), 6.58 (dd, J = 5.2, 7.8 Hz, 1H, H-5), 7.40-7.41 (m, 1H, H-4), 7.86-7.88 (m, 1H, H-6). ^{13}C NMR (100 MHz, $CDCl_3$) δ 13.9 ($CO(CH_2)_4\mathit{C}H_3$), 19.1 ($\mathit{CH_3}CHOH$), 22.3 ($CO(CH_2)_3\mathit{C}H_2CH_3$), 24.6 ($CO(CH_2)_2\mathit{C}H_2$), 31.1 ($COCH_2\mathit{CH_2}CH_2$), 34.3 ($CO\mathit{C}H_2CH_2$), 68.9 ($CH_3\mathit{C}HOH$), 113.6 (*C*H-5), 119.9 (*C*-3), 136.2 (*C*H-4), 146.4 (*C*H-6), 156.4 (*C*-2). 173.3 (*C*O).

1-(2-amino-3-pyridinyl)-3-(trimethylsilyl)prop-2-yn-1-ol (*rac*-8)

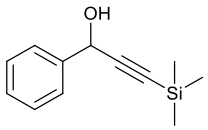

A) Formation of LDA

BuLi (8.67 ml, 1.44 M, 12.48 mmol) was added to a solution of DIPA (2.05 ml, 14.6 mmol) in THF (15 mL) at -78 °C. The solution was stirred at -78°C for 5 minutes and then allowed to cool to room temperature, upon which LDA was formed.

B) Synthesis of 1-(2-amino-3-pyridinyl)-3-(trimethylsilyl)prop-2-yn-1-ol

The LDA solution (12.48 mmol) was cooled to -78°C, and TMS acetylene (1.76 ml, 12.48 mmol) in THF (10 ml) was added dropwise, with stirring at -78°C for 30 minutes. 2-aminopyridine-3-carboxaldehyde **7** (435 mg, 3.57 mmol) in THF (8 ml) was then added dropwise. The reaction was stirred at -78°C for 15 hours. This was agitated at 0°C for 3 hours, and then at room temperature for a further three hours. Aqueous ammonium chloride (40 ml) was then added, followed by extraction with EtOAc (3 x 15 ml). The organic extracts were collected and dried over $MgSO_4$. The crude product was isolated via removal of the solvent under reduced pressure. Purification occurred with SiO_2 chromatography, with EtOAc, to yield the product as a yellow solid (300 mg, 38%). ^{1}H NMR (300MHz, $CDCl_3$) δ 7.81 (dd, *J* = 1.7, 5.1 Hz, 1H, Ar*H*), 7.43-7.45 (m, 1H, Ar*H*), 6.52 (dd, *J* = 5.1, 7.5 Hz, 1H, Ar*H*), 5.15 (s, 1H, $OH\mathit{CH}CCSi(CH_3)_3$), 0.00 (s, 9H, $\mathit{(CH_3)_3}Si$), 4.8 (br s, 2H, $\mathit{NH_2}$); ^{13}C NMR (300 MHz, $CDCl_3$) δ 157.13 (*C*COH), 148.10 (Ar*C*), 136.41 (Ar*C*), 118.71 (Ar*C*), 114.14 (*C*Si), 102.61 (CH*C*C), 63.10 (*C*HOH), 0.00 ($Si(\mathit{C}H_3)_3$). The racemic mixture was analyzed by HPLC with a Chiralpak IA column (6 x

250 mm) and an isocratic mobile phase (Heptane: EtOH 90:10, 0.1 % isopropylamine). Flow: 0.8 ml/min. Enantiomer A: 8.08 min, Enantiomer B: 8.93 min.

1-(2-amino-3-pyridinyl)prop-2-yn-1-ol (*rac*-9)

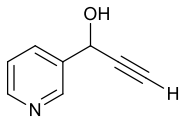

1-(2-amino-3-pyridinyl)-3-(trimethylsilyl)prop-2-yn-1-ol **12** (300 mg, 1.36 mmol) was dissolved in dry MeOH (8 ml), and K_2CO_3 (226 mg, 1.63 mmol) added. This was stirred at room temperature for 6 hours, upon which extraction occurred with EtOAc and water. The organic layers were collected and dried over $MgSO_4$. Purification occurred with SiO_2 chromatography with EtOAc. A yellow solid was isolated (50 mg, 30 %). ^{1}H NMR (400MHz, acetone-D6) δ 7.95 (dd, *J* = 1.8, 5.0 Hz, 1H, Ar*H*), 7.65 (dd, *J* = 1.5, 7.3 Hz, 1H, Ar*H*), 6.60 (dd, *J* = 4.9, 7.4 Hz, 1H, Ar*H*), 5.52 (br s, 2H, *NH*$_2$), 5.44 (s, 1H, OHC*H*CCH), 3.17 (d, *J* = 2.3 Hz, 1H, OHCHCC*H).* The racemic mixture was analyzed by HPLC with a Chiralpak IA column (6 x 250 mm) and an isocratic mobile phase (Heptane: EtOH 90:10, 0.1 % isopropylamine). Flow: 0.8 ml/min. Enantiomer A: 21.81 min, Enantiomer B: 23.61 min.

(*S*)- 1-(2-amino-3-pyridinyl)prop-2-yn-1-ol ((*S*)-9)

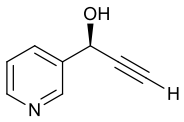

After resolution for 7 days, purification of the alcohol was via SiO_2 chromatography (EtOAc) giving a yellow oil. RT= 23.61 min. Yield: 50%. *ee*: 98%. $[\alpha]_D$ = +53^o (methanol, *c* = 0.8).

Chapter 3: Investigating 2OH-BNPP1 as a Bub1 kinase inhibitor

3.1 Introduction

Novel anticancer strategies are being developed to overcome the problems encountered using traditional taxane chemotherapy (Rowinsky et al., 1993). One such strategy involves targeting mitotic proteins such as Mps1, the Aurora's, Cenp-E, Eg5 and Plk-1 with second-generation inhibitors (Jackson et al., 2007; Keen and Taylor, 2009; Lens et al., 2010; Malumbres, 2011; Manchado et al., 2012; Taylor and Peters, 2008). On-going studies aim to study the efficacy of these agents but also it may be that targeting other mitotic proteins is necessary. At the time of the initiation of the project, there was no specific inhibitor targeting Bub1 kinase and therefore this opened up a novel field of exploration. Furthermore, aspects of the role of Bub1 activity in mitosis and the SAC are relatively controversial and so, the development of a specific inhibitor would aid in the understanding of this function. Recently, 2OH-BNPP1 was developed as a Bub1 kinase inhibitor and was shown to exploit the additional pocket in the kinase active site, present due to the lack of a bulky and hydrophobic gatekeeper residue ((Kang et al., 2008) and see (Chapter 1.422)).

The Bub1 protein is essential for SAC functioning, chromosome segregation (Johnson et al., 2004; Kitajima et al., 2005; Meraldi and Sorger, 2005; Morrow et al., 2005; Perera et al., 2007; Tang et al., 2004), and as a major scaffolding protein for the recruitment of checkpoint proteins BubR1, Cenp-E and Mad2 to the kinetochore (Jablonski et al., 1998; Johnson et al., 2004; Sharp-Baker and Chen, 2001). Although the functioning of the Bub1 protein is well studied, the role of Bub1's kinase activity is less defined, particularly its part in the SAC. Studies have indicated that the kinase activity is essential (Kang et al., 2008; Yamaguchi et al., 2003), while others have suggested it is dispensable (Fernius and Hardwick, 2007; Klebig et al., 2009; Perera and Taylor, 2010). It is known that the kinase activity of Bub1 is essential for the phosphorylation of histone H2A at Thr120, where this phosphorylation is then directly involved in the recruitment of the cohesion protector shugoshin Sgo1 to the centromeres (Kawashima et al., 2010). However, although it has been indicated that Bub1 activity is important for Sgo1 recruitment, this is not required to maintain centromeric cohesion during mitosis (Perera and Taylor, 2010; Perera et al., 2007).

Therefore, I aimed to test the effectiveness of 2OH-BNPP1 as a tool to inhibit Bub1 kinase activity, in order to confirm previous reports citing it as an inhibitor (Kang et al., 2008) and also, to understand its *in vitro* potency and then test its efficacy in cells. This would aid in the understanding of the roles of Bub1 in mitosis. In the first case I used a radioactive *in vitro* kinase assay, where the ability of Bub1 to phosphorylate its substrate histone H2A was examined (Kawashima et al., 2010), and then tested the capability of 2OH-BNPP1 to reduce this signal. Secondly, I set up a cell-based assay, analysing the H2A-pT120 signal in cells using immunofluorescence and then determined whether 2OH-BNPP1 could reduce this phosphorylation. Ultimately, I hoped to use 2OH-BNPP1 in cellular backgrounds where the checkpoint was compromised to ascertain the importance of the activity of Bub1 in the SAC.

3.2 Generation of a Bub1 *in vitro* kinase assay

In order to test whether 2OH-BNNP1 was an effective tool in the study of Bub1's kinase activity, I first established an *in vitro* kinase assay using recombinant Bub1 protein, radiolabelled ATP ([γ-^{32}P]ATP), a substrate histone H2A and autoradiography to detect radiolabelled [γ-^{32}P]-H2A (Minor, 2006).

To generate a source of recombinant protein for the assay, I produced cell lines expressing a tetracycline-inducible GFP tagged Bub1 open reading frame (ORF). To facilitate affinity purification, the ORF was N-terminally tagged with GFP. To validate that phosphorylation was due to Bub1, as opposed to a co-purifying enzyme, I also generated a cell line expressing a catalytic mutant (K821R).

Immunoblots confirmed expression of both the wild-type (WT) and K821R mutant transgenes (Figure 3.1). Next, I exposed tetracycline-induced cells (both Bub1 WT and K821R) to nocodazole for 16 hours to maximise Bub1 activity (Jablonski et al., 1998; Taylor et al., 2001). The expressed protein was then affinity purified with a GST-GFP-binder protein (Rothbauer et al., 2007; Sloss et al., 2016). Immunoblots confirmed protein input and exhibited the pull-down of Bub1 and Bub3 with the GFP-binder for both tetracycline-induced WT and kinase-dead cell lines (Figure 3.2A,B). The immunoprecipitation of Bub3 indicated the transgene was producing a functional Bub1 protein (Roberts et al., 1994; Taylor et al., 1998).

To test whether the purified GFP-tagged Bub1 was catalytically active I set up an initial kinase assay. Recombinant proteins were mixed with histone H2A, radiolabelled ATP and buffer containing 10 mM Mg^{2+}, incubated at 30°C for 20 minutes, resolved by SDS-PAGE, then subjected to phosphoimaging to detect radiolabelled

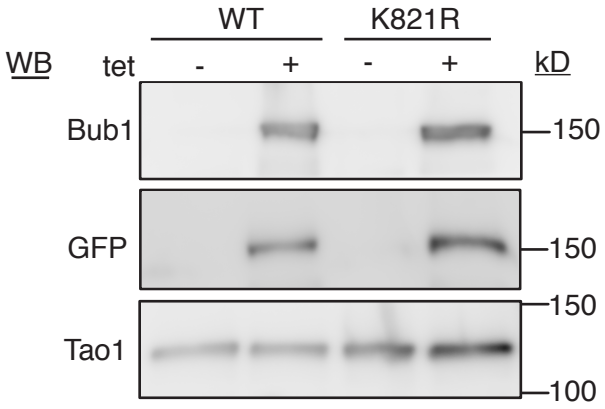

Figure 3.1 Generation of tetracyline inducible HEK293 GFP-Bub1 wild-type (WT) and kinase dead (K821R) cell lines.
Immunoblot of GFP and Bub1 following 1 µg/ml tetracycline overnight, overexpressing GFP-Bub1 wild-type (WT) and Bub1 K821R. Tao1 is used as a loading control.

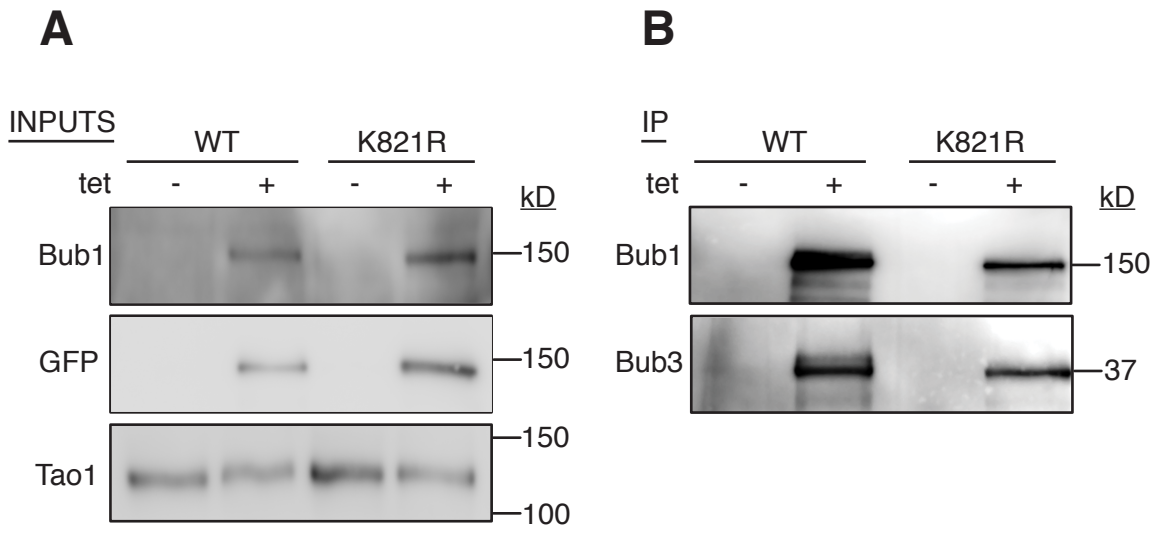

Figure 3.2 The immunoprecipitation of GFP-Bub1 using a GFP-binder protein. (**A**) Immunoblot showing the input samples prior to immunoprecipitation, with blotting for GFP and Bub1 following 1 µg/ml tetracycline overnight.Tao1 is used as a loading control. (**B**) Immunoblot of Bub1 and Bub3 following immunoprecipitation of HEK293 GFP-Bub1 WT and K821R cell line lysate with a GFP-binder protein. Expression of the transgene was induced by 1 µg/ml tetracycline overnight, with cells exposed to 20 ng/ml of nocodazole for 16 hours prior to harvesting.

phosphorylated proteins. Analysis indicated that exogenous Bub1 phosphorylated histone H2A, where a signal at 15 kDa on the kinase assay gel was observed (Figure 3.3). Note also a weaker signal at 150 kDa which is most likely autophosphorylation of Bub1 (Lin et al., 2014). Importantly, the phosphorylation of H2A appears to be directly dependent on Bub1's catalytic function because very little activity was observed with the K821R mutant. This confirms that the kinase activity of Bub1 is required for H2A phosphorylation.

3.21 Optimisation of assay parameters

Having established the basis of a Bub1 kinase assay, I next optimised various parameters. To modify enzyme concentration, different volumes of the GST beads containing GFP-Bub1 from an initial master mix were placed into the kinase reaction. When maintaining the other parameters, increasing the enzyme volume amplified the pH2A signal (Figure 3.4A). Quantification of the signal indicated a linear relationship between enzyme volume and pH2A until >10 µl where the signal then plateaued (Figure 3.4B). From 1 µl to 2 µl of the GST beads, there was a 1.3-fold increase in pH2A signal. This further increased 1.3-fold to 3 µl. From 5 µl to 10 µl there was a 1.2-fold increase, followed by non-significant increases until 30 µl. Similarly, the level of phosphorylated Bub1 (pBub1) also increased with increasing bead volume. In order to identify ATP-competitive inhibitors (like 2OH-BNPP1), it is essential to run the reaction under initial velocity conditions (i.e. the linear part of the graph), where approximately 10% of the substrate is 'used-up' by the enzyme (Bisswanger, 2014; Brooks et al., 2012). Taking these factors into account, I then highlighted 10 µl of the enzyme volume to use for further optimisation reactions.

To define the optimal H2A concentration to be used in the kinase assay, all parameters were kept constant whilst H2A mass was increased. As shown in Figure 3.5A and B, as I increased H2A concentration the signal of pH2A also grew linearly, with increases 1.6-fold from 0.5 to 1 µg, 2-fold from 1 to 2 µg, and 1.2-fold up to 3 µg. I also noted that the level of pBub1 did not show a pattern of decrease/increase when H2A concentration increased. I then determined 2 µg of H2A was required to reach a saturating substrate concentration for further assays.

Furthermore, a kinase reaction requires the use of both 'hot' and 'cold' ATP (Minor, 2006). For ease of visualisation, the assay I set up required the use of radiolabelled [γ-^{32}P]ATP, where the [γ-^{32}P] was incorporated into the threonine of H2A (Kawashima et al., 2010). Note the contribution of 'hot' ATP to the overall ATP

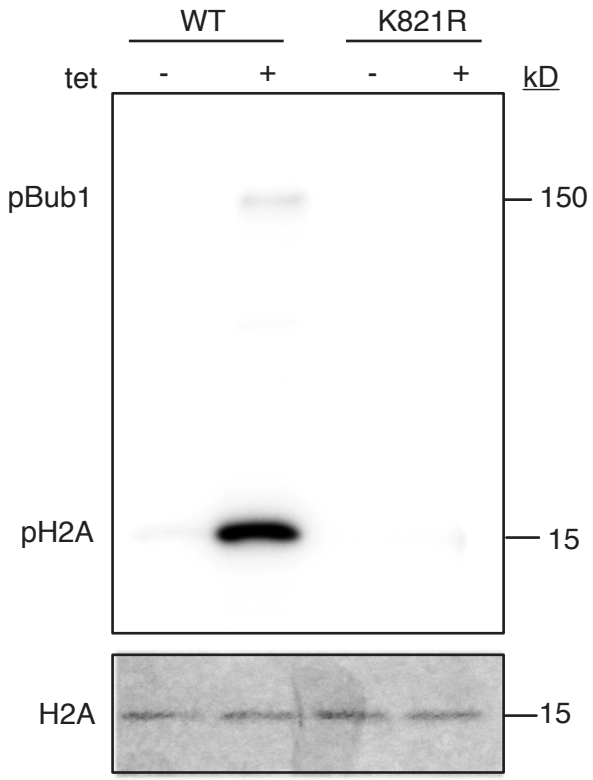

Figure 3.3 Expressing wild-type (WT) and kinase-dead Bub1 and the effect on histone H2A phosphorylation.
Kinase assay showing H2A and Bub1 phosphorylation following incubation with recombinant Bub1, histone H2A and ATP at 30°C for 20 minutes. A Coomassie blue protein blot of H2A is shown for protein loading.

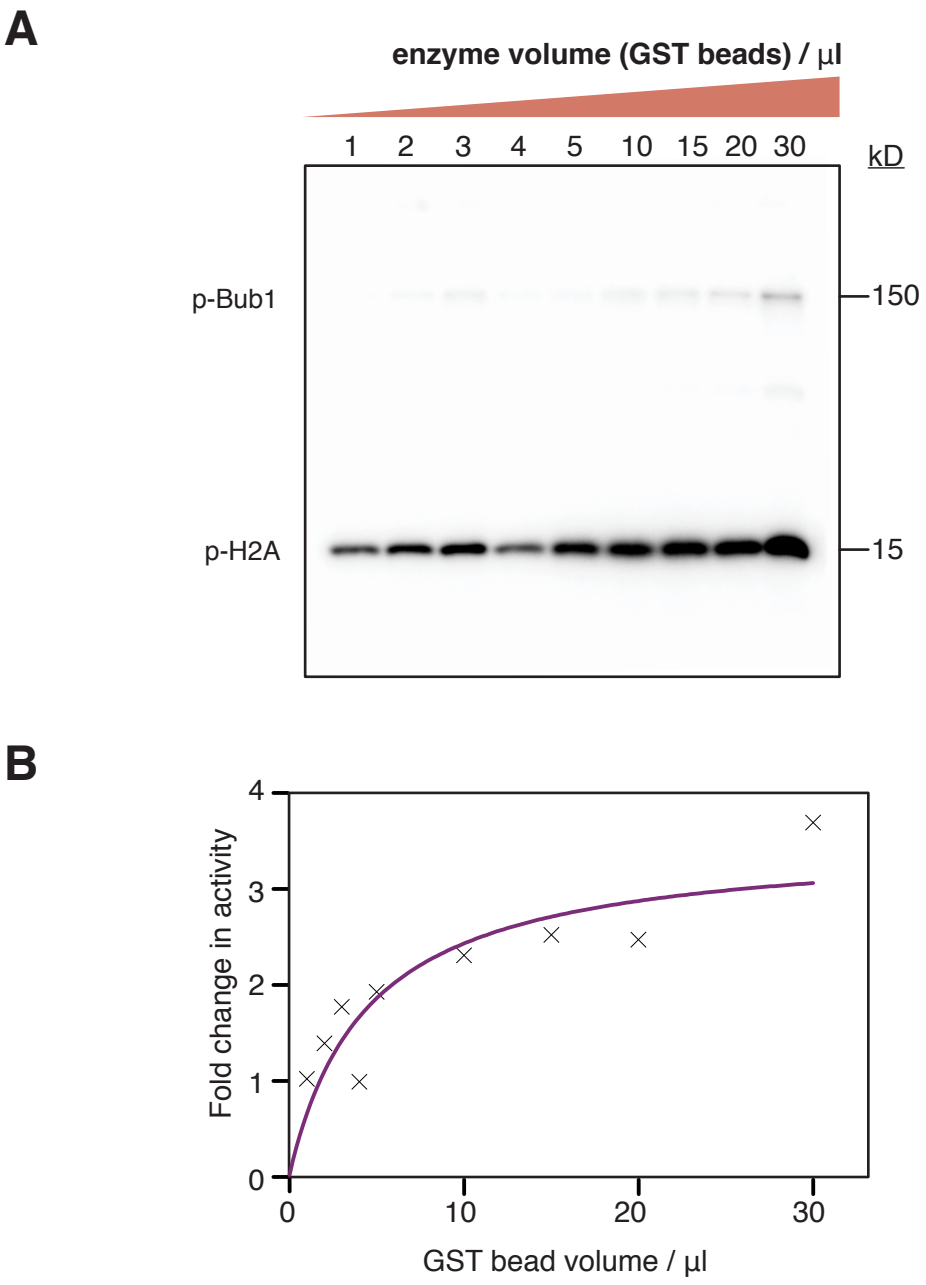

Figure 3.4 Optimising Bub1 enzyme concentration.
(**A**) Kinase assay showing the effect of increasing the volume of GST-GFP-Bub1 bead volume on the phosphorylation of histone H2A.
(**B**) Quantification of the signal in (A), where values are normalised to 1 for the minimum detected pH2A signal.

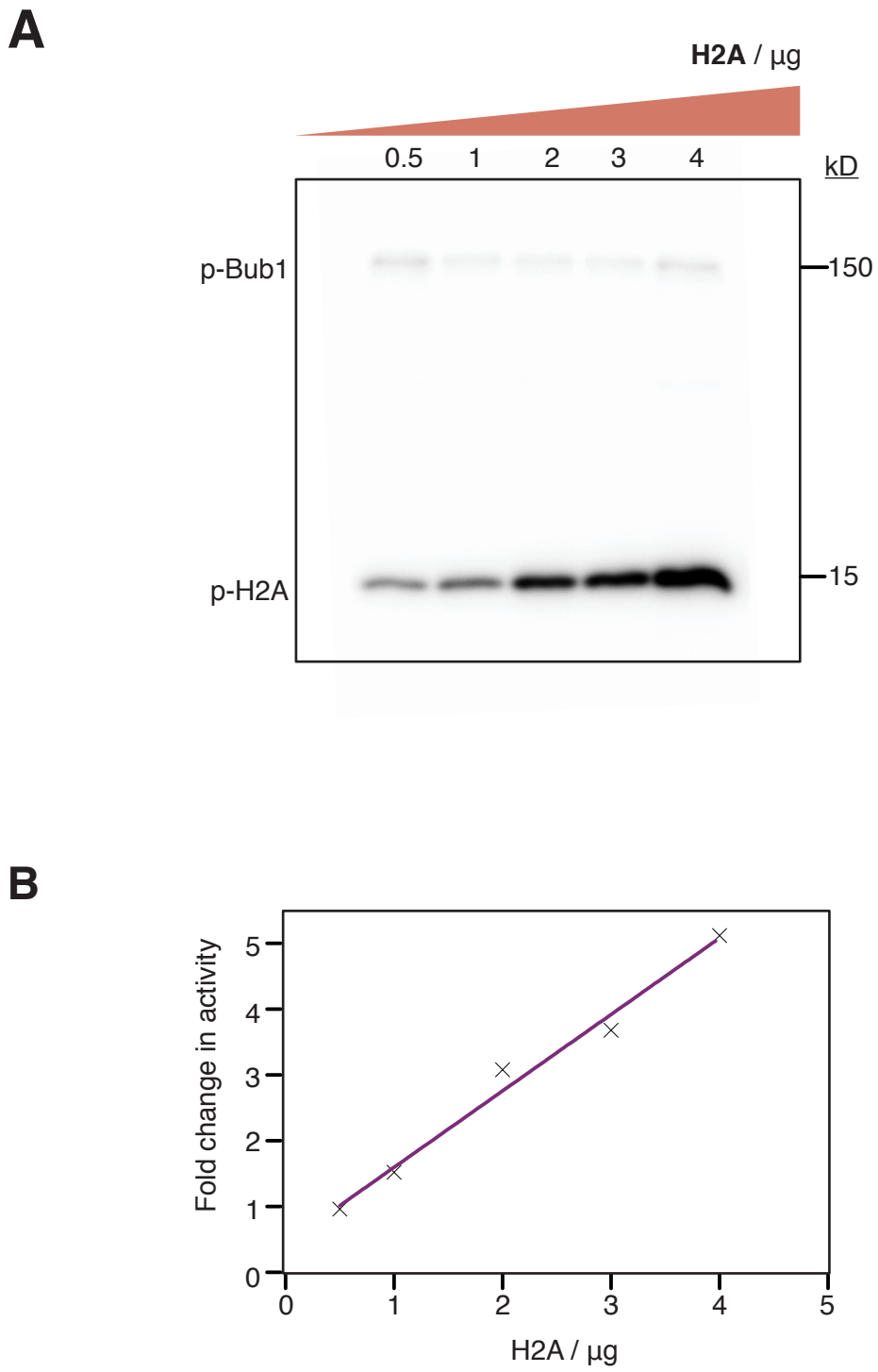

Figure 3.5 Optimisation of histone H2A substrate concentration.
(**A**) Kinase assay showing pH2A activity following incubation with increasing histone H2A substrate concentration.
(**B**) Quantification of the signal in (A) normalised to 1 for the minimum pH2A activity detected.

concentration is relatively low, since the majority of the ATP in the reaction is unlabelled. Importantly, the 'hot'/'cold' ATP was the final component added to the kinase mixture as this initiated reaction onset. In order to identify the ideal concentration of both 'hot' and 'cold' ATP, I initially titrated the amount of unlabelled 'cold' ATP from 50-400 µM, while maintaining the concentration of labelled 'hot' ATP at 2 µCi/reaction. As I increased the concentration of 'cold' ATP, the amount of pH2A signal decreased, as did pBub1 (Figure 3.6A, left panel). Maximum phosphorylation was observed at 50 µM, with the signal decreasing by 44% at 100 µM, and a further 68% decrease to 400 µM (Figure 3.6A, right panel). From my results, and previous *in vitro* kinase assays (Baron et al., 2016; Kang et al., 2008), I established that 100 µM of unlabelled ATP was a suitable concentration to use. In contrast to the result above, increasing the concentration of 'hot' ATP from 1-3 µCi/reaction resulted in an observable increase in pH2A, with similar increases for pBub1 (Figure 3.6B, left panel). With a constant concentration of 100 µM 'cold' ATP, pH2A increased by 14% from 1 to 1.5 µCi (Figure 3.6B, right panel). From 1.5 to 2 µCi, a 39% increase was observed, which further increased by 20% to 3 µCi. Importantly, I observed that 100 µM of 'cold' ATP and 2 µCi of 'hot' ATP were deemed to be ideal for observing an optimal signal. These concentrations were similar to those used in previous Bub1 kinase assays (Baron et al., 2016; Kang et al., 2008).

The final parameter analysed was the time period of the kinase reaction. As shown in Figure 3.7A, as the length of the reaction increased, as did the level of pH2A (and pBub1) signal. The onset of phosphorylation was very rapid, where a signal was detected at 15 kDa within 1 minute of labelled [γ-^{32}P]ATP addition. Furthermore, it was apparent that within 8 minutes, maximum pH2A signal was achieved. Quantifying the pH2A signal revealed the linear increase over time. Within the first 2 minutes there was a rapid (2.7-fold) increase in pH2A signal (Figure 3.7B). As the length of the kinase reaction was prolonged, the level of pH2A signal continued to increase, but at a slower rate (2-4 minutes, 1.6x; 4-8 minutes, 1.3x), reaching a plateau at about 20 minutes, indicating the consumption of resources. To maximise the signal obtained from the kinase assay, I chose 20 minutes for the remaining kinase reactions.

Lastly, the temperature at which the kinase reaction is carried out is an important factor to consider, where for most mammalian enzymes a physiological temperature of 37°C coincides with the natural condition of the enzyme (Bisswanger, 2014). Although this may be true for most enzymes, it is important to realise that some enzymes are unstable and may lose their activity at certain temperatures, with 37°C

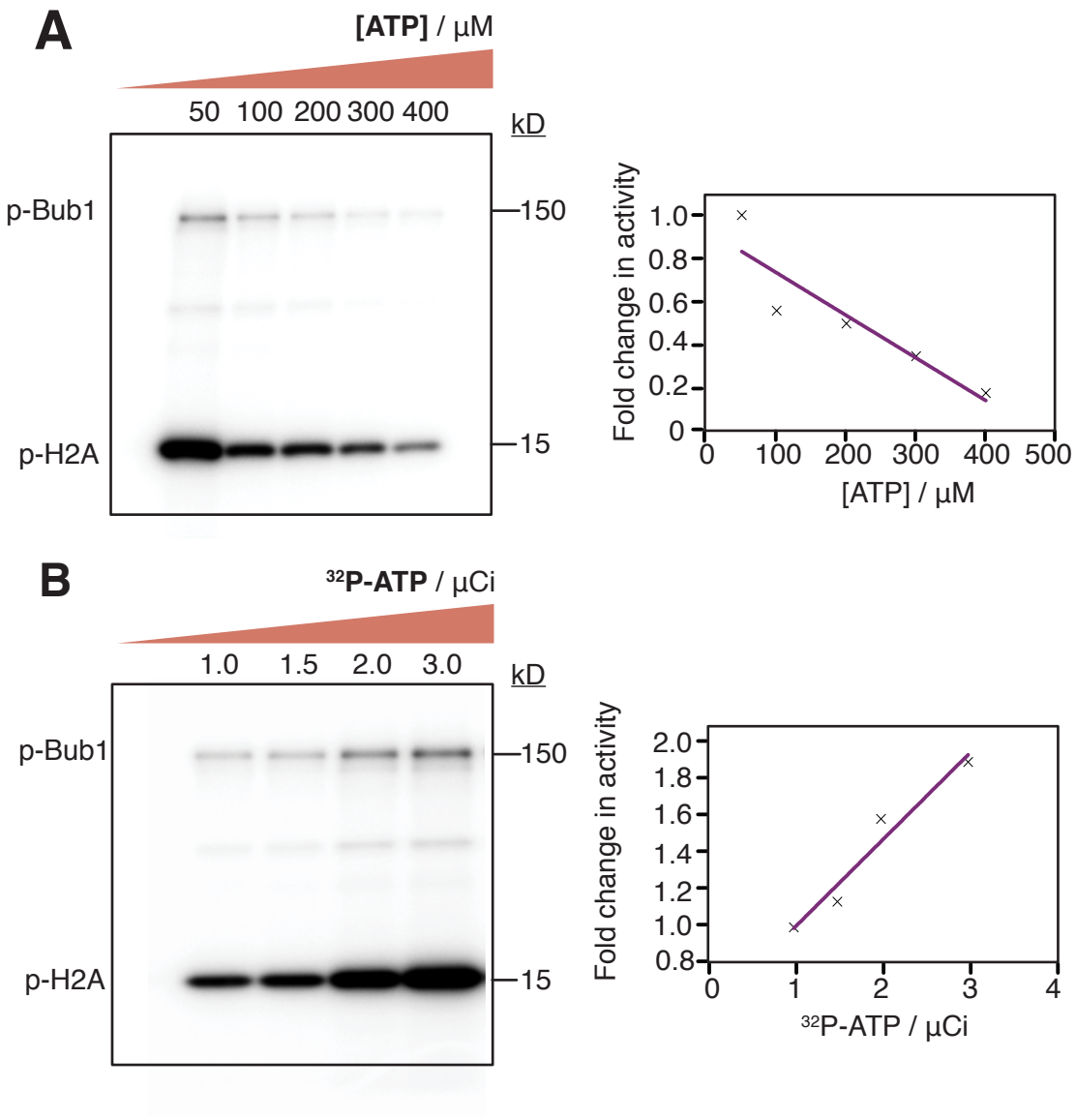

Figure 3.6 Optimisation of 'hot' and 'cold' ATP concentration.
(**A**) Kinase assay increasing cold ATP concentration and the effect on phosphorylation of histone H2A. The line graph quantifies the pH2A signal. Values are normalised to 1 for the maximum pH2A signal detected.
(**B**) Kinase assay for the effect of increasing hot ATP concentration on the phosphorylation of histone H2A. The line graph quantifies the pH2A signal. Values are normalised to 1 for the minimum pH2A activity detected.

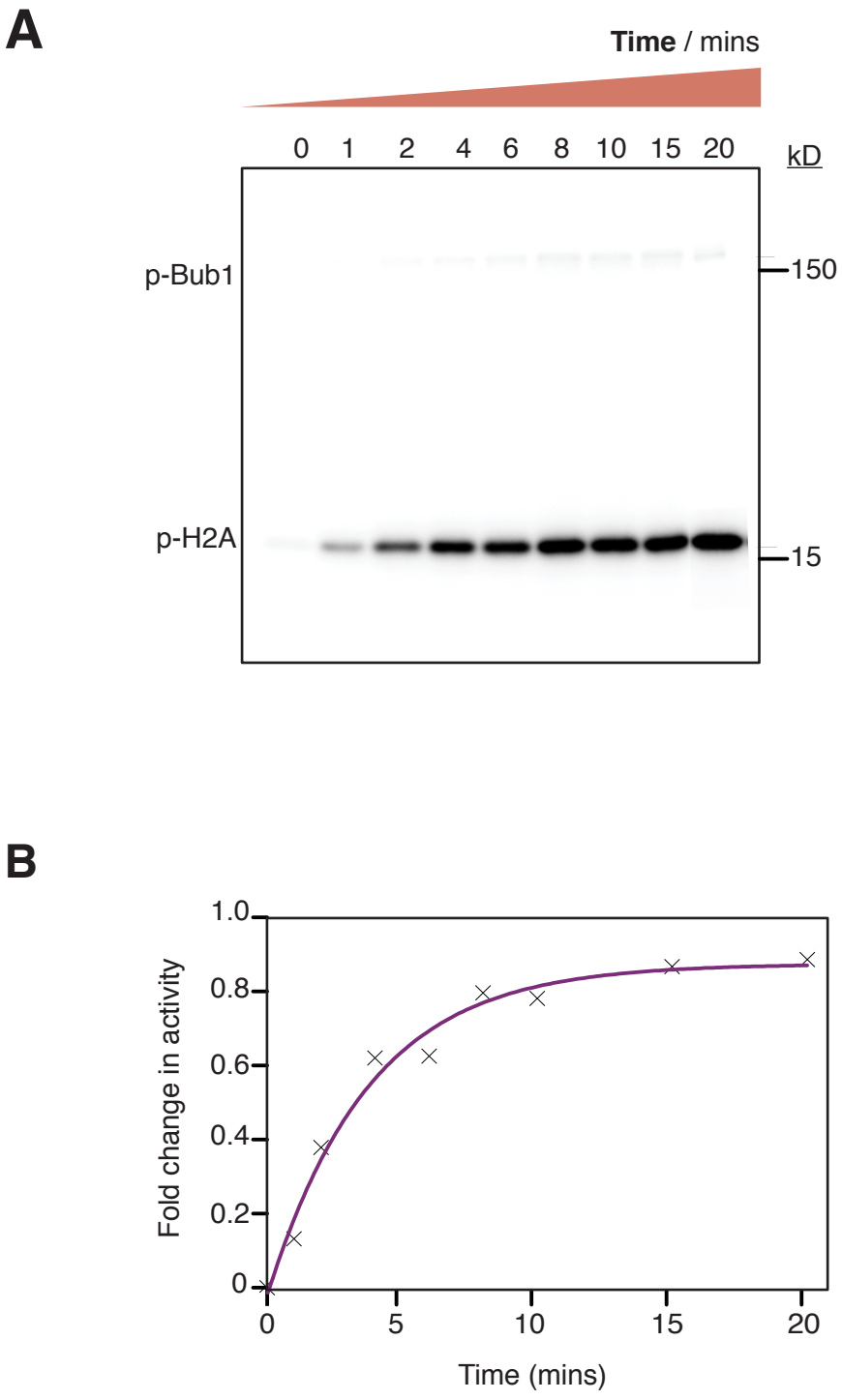

Figure 3.7 Optimisation of the time of kinase reaction.
(**A**) Immunoprecipitation kinase assay varying the time of kinase reaction, showing pH2A activity at the times indicated.
(**B**) Quantification of the signal in (A), normalised to 0 for the minimum kinase activity detected.

being the temperature at which some enzymes denature. Therefore, upon consideration of these factors and analysing previously published Bub1 kinase assays, where either 30°C (Baron et al., 2016) or room temperature (Kang et al., 2008) conditions were preferred, I chose 30°C for the kinase reactions here. This temperature allowed for near-physiological conditions to be met, with a suitable rate of reaction, but there was also a reduced probability of enzyme denaturation. Furthermore, to enable robust comparisons of results, a temperature controlled incubator was used to maintain a constant temperature of 30°C throughout the reaction.

3.22 Using 2OH-BNPP1 as a Bub1 kinase inhibitor

Having optimised the Bub1 kinase assay, I next asked whether 2OH-BNPP1 (Kang et al., 2008) was an effective *in vitro* inhibitor. Under the conditions established previously, 2OH-BNPP1 was added to the kinase reaction and the ability to inhibit H2A phosphorylation determined. As the concentration of 2OH-BNNP1 was increased, the level of pH2A decreased (Figure 3.8A). The level of auto-phosphorylated Bub1 at 150 kDa also decreased at higher inhibitor concentrations. With a relatively small decrease in pH2A up to 0.3 µM, a 54% decrease in signal was apparent when the inhibitor concentration reached 0.7 µM (Figure 3.8B). The amount of phosphorylation continued to decrease gradually from here until 10 µM, where pH2A was extremely low.

Thus, consistent with previous observations (Kang et al., 2008), 2OH-BNPP1 does indeed inhibit Bub1 kinase *in vitro*. While 10 µM is required to abolish activity of the enzyme, the IC_{50} in this *in vitro* assay is ~1.3 µM, again consistent with prior observations (Kang et al., 2008).

3.3 Generation of a cell-based assay to detect Bub1 kinase activity

Having confirmed that 2OH-BNPP1 does indeed inhibit Bub1 *in vitro*, I asked whether it was also able to do so in cells. To do this I questioned whether 2OH-BNPP1 inhibited H2A-T120 phosphorylation in a cell based assay. I initially attempted to look at endogenous histone H2A, but little effect was seen with the addition of 2OH-BNPP1 (data not shown). This was likely due to the involvement of another enzyme other than Bub1. Therefore, an assay that was absolutely dependent upon Bub1 was required. To readily visualise H2A phosphorylation, I generated a cell line expressing a tetracycline-inducible GFP-tagged histone H2B protein fused to the kinase domain of Bub1 (Figure 3.9A). Upon induction, the H2B moiety targets the Bub1 kinase domain (Bub1C) to the

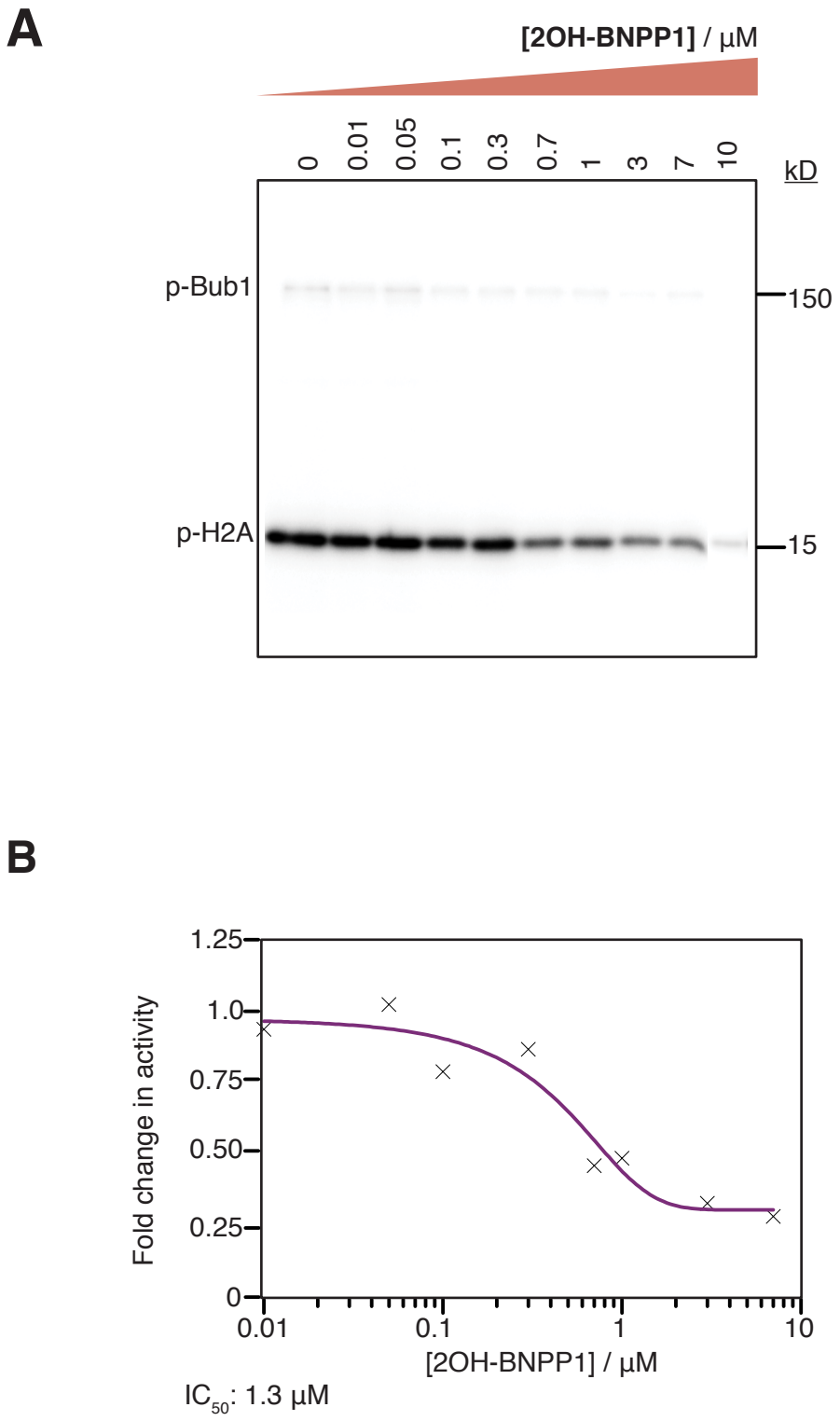

Figure 3.8 The effect of 2OH-BNPP1 on pH2A.
(**A**) Kinase assay for the incubation of varying concentrations of 2OH-BNPP1 under the optimal reaction conditions analysed previously.
(**B**) Dose response line graph determined via the data in (A), normalised to 1 for the maximum pH2A signal.

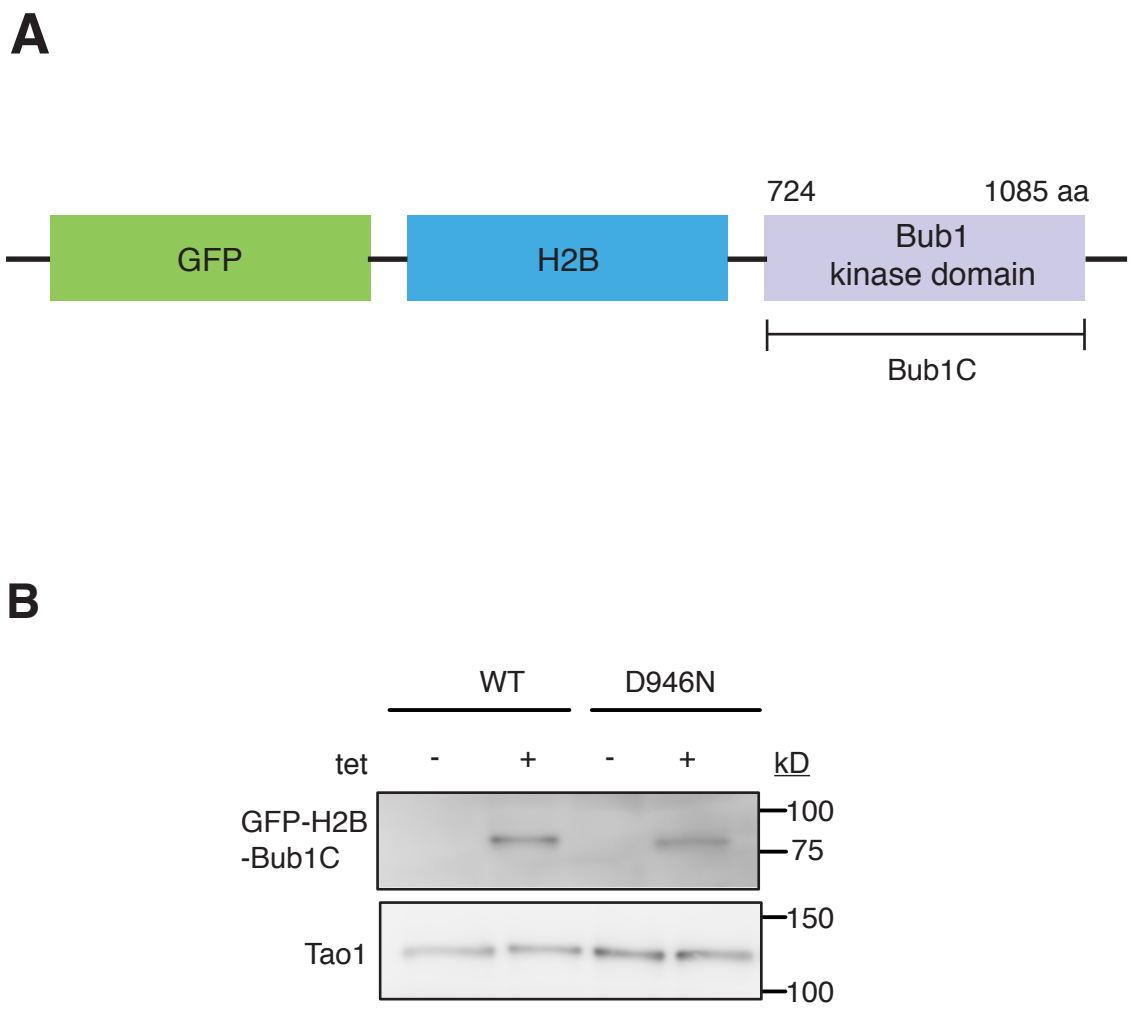

Figure 3.9 The expression of GFP-H2B-Bub1C wild-type (WT) and kinase dead (D946N) mutant.
(**A**) Schematic showing the construct used with GFP-H2B fused to the kinase domain of Bub1 (Bub1C). aa= amino acids.
(**B**) Immunoblot for GFP showing the expression of GFP-H2B Bub1C WT and D946N mutants in HeLa cells, following the addition of 1 µg/ml tetracycline overnight.

chromosome arms where it is capable of phosphorylating histone H2A (Kang et al., 2008; Kawashima et al., 2010). The advantage of this approach is that changes in the phosphorylation status of H2A can be more easily detected over the arms in comparison to the endogenous centromeric location. Similarly, as the kinetochore-associated Bub1 phosphorylates the nearby H2A on T120 at the centromeres and this is involved in the recruitment of shugoshin Sgo1 to the same location (Kawashima et al., 2010; Perera and Taylor, 2010), changes in Sgo1 localisation could also be readily detectable, as this would also be concentrated along the chromosome arms. Note Kang et al. confirmed that the Bub1C fragment was functionally similar to full-length Bub1, with *in vitro* IC_{50} values of similar magnitude (Kang et al., 2008). Following generation of the GFP-H2B-Bub1C wild-type (WT) transgene, a kinase-dead D946N mutant was further generated to confirm that the H2A phosphorylation and Sgo1 localisation observed were dependent upon Bub1 kinase activity (Hanks and Hunter, 1995; Kang et al., 2008; Perera et al., 2007).

Immunoblots confirmed that Bub1 WT and D946N transgene expression were induced by tetracycline (Figure 3.9B). Next, I used immunofluorescence to analyse mitotic cells and to establish if the transgene was functioning as expected. In control cells devoid of tetracycline, H2A-pT120 was detected using a phospho-specific antibody at the centromeres, confirming previous findings ((Kawashima et al., 2010) and see (Figure 3.10, left)). Sgo1 was also observed at a centromeric location, consistent with published studies (McGuinness et al., 2005). When tetracycline was added, GFP-H2B was observed along the chromosome arms as expected. The ectopic localisation of H2A-pT120 and Sgo1 to the arms indicated that the kinase Bub1C was also localised to the arms, demonstrating the transgene was behaving as anticipated. When analysing figures with the D946N mutant, H2A-pT120 and Sgo1 remained at the centromeres (Figure 3.10, right). This confirms the Bub1 kinase-dependent phosphorylation of H2A and recruitment of Sgo1.

Following on from analysis of mitotic figures, I next chose to study the impact of transgene expression in interphase cells. Bub1 exhibits maximal activity in mitosis, with recruitment to kinetochores in prophase (Johnson et al., 2004). There is no published evidence of Bub1 activity in interphase and therefore, I envisaged that upon transgene expression, there would be no observable affect in interphase cells. Nevertheless, it was very surprising to detect a major change in localisation of H2A-pT120 in the transgene-expressing cells. Without tetracycline, there was no nuclear H2A-pT120 staining, yet when the transgene was expressed, H2A-pT120 localisation was apparent

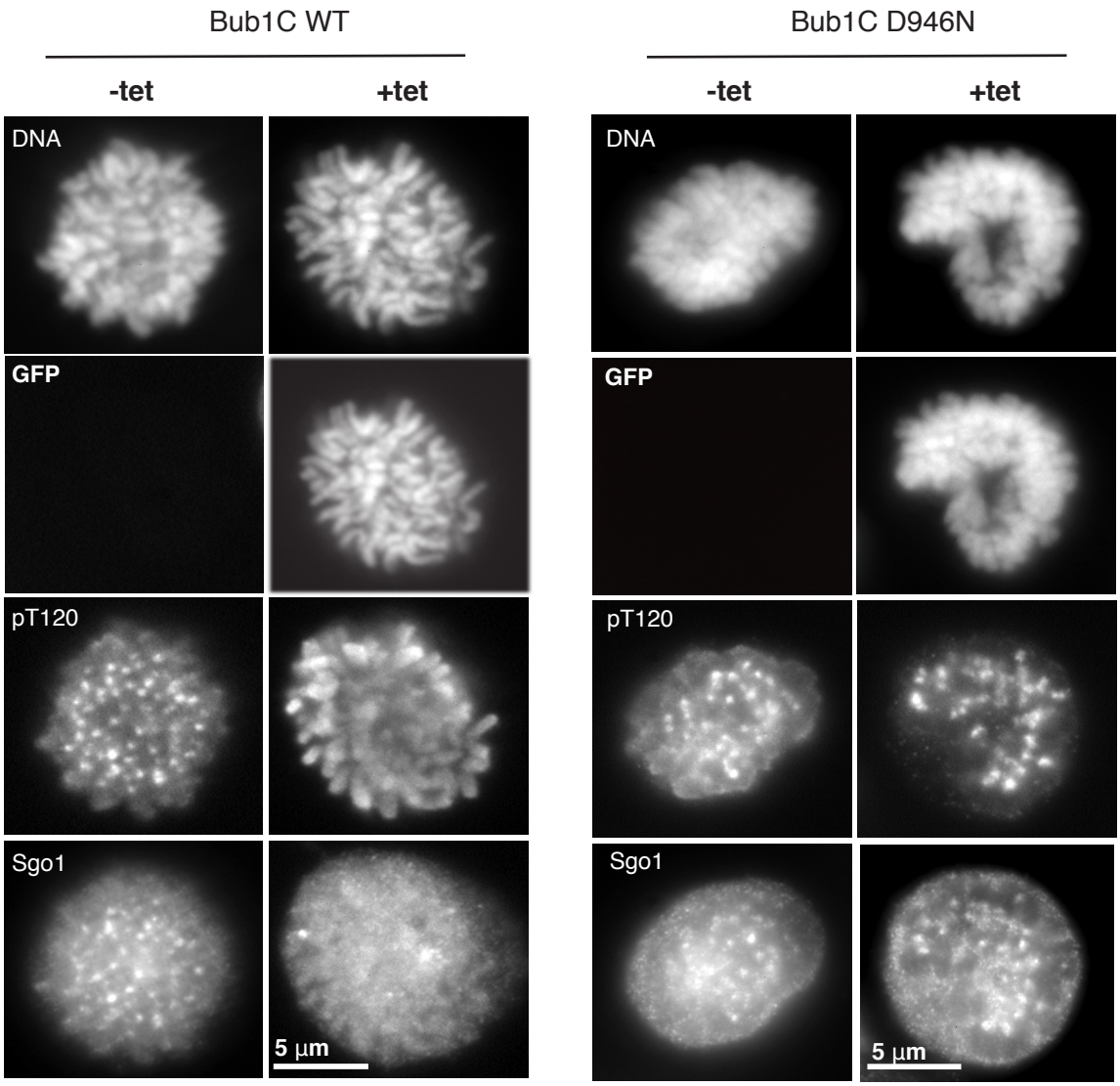

Figure 3.10 Expressing GFP-H2B-Bub1C WT and D964N, showing the effect on H2A phosphorylation and Sgo1 localisation.
Immunofluorescence images of mitotic HeLa cells expressing GFP-H2B-Bub1C WT and D946N under tetracycline (1 µg/ml) control with staining for DNA, H2A-pT120, and Sgo1. Bar: 5 µm.

throughout the cell, including within the nucleus (Figure 3.11, left). Conversely, when analysing D946N mutant cells, this phenomenon was not observed, indicating its dependency upon Bub1 kinase activity (Figure 3.11, right). Consequently, this suggests that there may be a low level of Bub1 kinase activity in interphase. It is however, important to note that this localisation pattern was only observable when the transgene was overexpressed and was not visible at the endogenous level in this assay.

After the establishment of the cell-based assay, I next used 2OH-BNPP1 in the same assay to determine its ability to target Bub1 kinase. Following overnight induction of the Bub1 transgene with tetracycline and addition of 2OH-BNPP1, cells were analysed by immunofluorescence (Figure 3.12). Visualising both mitotic and interphase figures in comparison to controls (Figure 3.10, 3.11), there was no change in H2A-pT120 and Sgo1 localisation. The chromosome arm localisation remained, even at 100 µM of 2OH-BNPP1, suggesting that 2OH-BNPP1 did not inhibit the kinase activity of Bub1 in cells. It was noted that the concentrations of the ATP-competitive 2OH-BNPP1 used were considerably higher than those in the *in vitro* assay, since ATP levels are greater within a cellular environment.

3.4 Summary

In this Chapter I performed two assays for the detection of Bub1 kinase activity. Initially, I set up an *in vitro* kinase assay using radiolabelled [γ-^{32}P]ATP, with pH2A as an indication of Bub1 activity. To establish a robust kinase assay, I completed many optimisation assays to highlight the ideal enzyme concentration, amount of substrate, total 'hot/cold' ATP and reaction time. In doing so, this enabled me to test the ability of a Bub1 inhibitor 2OH-BNPP1, to repress the activity of Bub1. Under the conditions determined, 2OH-BNPP1 was able to inhibit Bub1 kinase and reduce the phosphorylation of H2A.

In addition to the *in vitro* studies, I next created a cell-based assay with expression of a GFP-H2B-Bub1C transgene. Although this was successful whereby Bub1 was ectopically localised along chromosome arms with subsequent phosphorylation of H2A and Sgo1 recruitment to the same location, there was no evidence of 2OH-BNPP1-mediated Bub1 kinase inhibition in this assay (Figure 3.12). Of particular interest was the indication that under the conditions of my assay, Bub1 exhibited activity in interphase. However, due to the lack of evidence of 2OH-BNPP1 inhibiting Bub1 kinase in cells, I was unable to continue with this project.

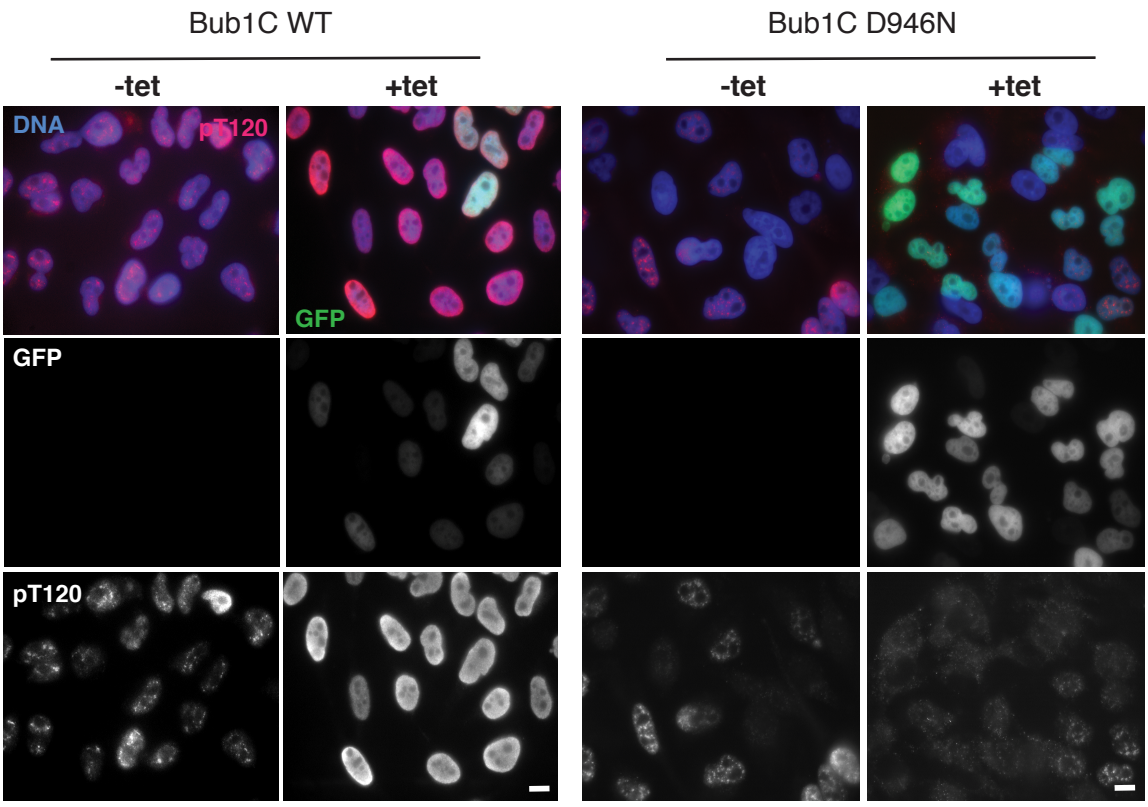

Bar: 10 µm

Figure 3.11 The expression of GFP-H2B-Bub1C WT and D946N in interphase cells and the effect on H2A phosphorylation.
Immunofluorescence images of interphase HeLa GFP-H2B Bub1C WT and D946N cells under the control of tetracycline (1 µg/ml), with staining for DNA (blue), GFP (green) and H2A-pT120 (red). Bar: 10 µm.

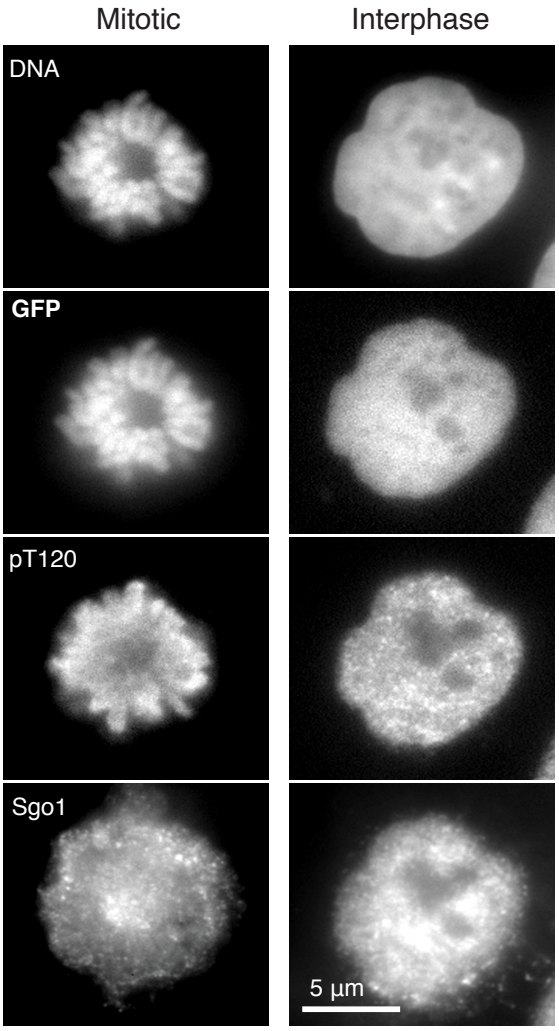

Figure 3.12 The effect of 2OH-BNPP1 on H2A-pT120.
Representative immunofluorescence images of mitotic and interphase HeLa cells expressing GFP-H2B-Bub1C WT induced by 1 µg/ml tetracycline and exposed to 2OH-BNPP1 (100 µM) overnight. Bar: 5 µm.

3.5 Discussion

3.51 Is Bub1 kinase activity essential for SAC functioning?

The role of the kinase activity of Bub1 in the SAC is controversial, with some studies showing importance (Kang et al., 2008; Yamaguchi et al., 2003) and others indicating redundant function (Fernius and Hardwick, 2007; Klebig et al., 2009; Perera and Taylor, 2010). Therefore, in my studies, I sought to test this using an inhibitor of Bub1 kinase activity 2OH-BNPP1, which would enable the fine-tuning of activity, where 2OH-BNPP1 has been described as a Bub1 inhibitor (Kang et al., 2008). I confirmed the importance of Bub1 kinase for H2A phosphorylation and Sgo1 recruitment (Kawashima et al., 2010; Perera and Taylor, 2010) but unfortunately, I saw no evidence of suppression of activity in cells (Figure 3.12). Interestingly, the initial study that cited 2OH-BNPP1 did not exhibit any evidence for the inhibition of Bub1 kinase in cells (Kang et al., 2008). Consequently, the results described by Nyati et al. are surprising where they describe 2OH-BNNP1 as a Bub1 kinase inhibitor, with suppression of TGF-β activity upon exposure (Nyati et al., 2015).

Although I have not shown the efficacy of 2OH-BNPP1 in cells, this may be due the incorrect assay used to detect kinase activity, therefore it cannot be ruled out that other assays may give contrasting results and indicate that 2OH-BNPP1 does inhibit Bub1. Furthermore, the reasons as to why 2OH-BNPP1 may not efficacious in cells may be due to the inability to penetrate the cellular membrane. However, given the molecular weight of 2OH-BNPP1 is 297 g/mol and the lipophilicity logP value is 3.02, it is unlikely that cell permeability is the issue as these values are in accordance with 'Lipinski's rule of five', for compounds which are likely to be cell permeable and easily absorbed in the body (Leeson et al., 1912; Lipinski et al., 2012). Consequently, the negative results may be due to the lack of specificity for the intended Bub1 target.

Despite the lack of success with 2OH-BNPP1 in cells, since my study, efforts have been tailored towards developing new inhibitors against Bub1 kinase activity. Recently, novel Bub1 ATP-competitive inhibitors BAY-320 and BAY-524 have been described (Baron et al., 2016; Hitchcock et al., 2013). Confirmation of Bub1 kinase activity was evident from reduced H2A-pT120 staining with immunofluorescence. Using single-cell imaging it was insinuated that perhaps Bub1 kinase activity is required for the maintenance of SAC signalling via amplification of the checkpoint signal. When HeLa cells were exposed to nocodazole followed by the addition of the kinase inhibitors, there was a 13-15% reduction in mitotically-arrested cells. Therefore, it is

likely that Bub1 kinase activity is not essential for the SAC, confirming previous reports (Perera and Taylor, 2010), but it may be required to maintain the SAC signal once it has already been activated. Evidence from *Xenopus* egg experiments also corroborates this, where Bub1 kinase activity was required to amplify a weak SAC signal generated by a few (unattached) kinetochores (Chen, 2004; Sharp-Baker and Chen, 2001).

3.52 Bub1 kinase activity in interphase

Bub1 exhibits maximal activity in mitosis, when it is localised to kinetochores (Jablonski et al., 1998). Despite this, when I analysed cells expressing the GFP-H2B-Bub1C transgene (Figure 3.11), the localisation of H2A-pT120 altered from a granular appearance to a uniform nuclear localisation throughout the cell, indicating that there may be a low-level of Bub1 active in interphase. Although there has been no previous evidence of H2A phosphorylation in interphase (Kawashima et al., 2010), Bub1 is constitutively auto-phosphorylated at the Ser969 position in the activation segment (P+1) throughout the cell cycle (Asghar et al., 2015; Lin et al., 2014). The level of Ser969 phosphorylation does not increase in mitosis but it is required for the mitosis-specific H2A phosphorylation. However, before Bub1 can be fully activated, a certain level of Bub1 concentration needs to be reached, where normally, sufficient levels are reached upon entry into mitosis. It was indicated that artificially increasing the local concentration of Bub1 in interphase does in fact initiate its activation (Asghar et al., 2015). Since Bub1 is overexpressed in my study, this may induce a sufficient level of Bub1 expression for activation in interphase. Therefore, the difference in localisation of H2A-pT120 we see in interphase cells may be a result of the 'priming' of Bub1 activity, before it is fully activated upon mitotic entry. Furthermore, this interesting observation may provide a basis for a screen for Bub1 inhibitors, where the level of H2A-pT120 would provide a measurement for the level of Bub1 kinase inhibition.

3.53 Bub1 as a therapeutic target

Since Bub1 may play a role in tumourigenesis (Ricke et al., 2011), inhibitors against Bub1 are advantageous. Bub1 kinase specific inhibitors, BAY-320 and BAY-524 have been developed (Baron et al., 2016), with the next stage being to enter these inhibitors into animal studies to determine efficacy.

Targeting SAC proteins in cancer chemotherapy is a potential therapeutic strategy (Janssen et al., 2009; Salmela and Kallio, 2013), where Mps1 targeting has

shown antitumour effects (Colombo et al., 2010; Kusakabe et al., 2015; Tannous et al., 2013; Tardif et al., 2011). Consequently, it is possible that the most promising results from Bub1 inhibition will be from combination studies with microtubule-targeting agents (MTA's) (Janssen et al., 2009).. As a single agent, it is unlikely that Bub1 kinase inhibition will show antitumour activity due to the only minor effects on mitosis observed (Baron et al., 2016), and also because the complete inhibition of the checkpoint is difficult to achieve *in vivo* (Manchado et al., 2012). However, whether targeting Bub1 will give different phenotypes and improved effects over other SAC targeting agents is not yet known. When BAY-320 and BAY-524 were combined with paclitaxel, an increase in chromosome missegregation errors and detrimental effects on cellular proliferation in aneuploid cells was evident (Baron et al., 2016). This was probably due to the elevation of erroneous KT-MT attachments which could not be corrected as a result of the partial displacement of Aurora B upon Bub1 inhibition. Similarly, combinations involving paclitaxel with Mps1 inhibitors, which also override the SAC, have shown promise. For example, partial depletion of Mps1 sensitised cells to paclitaxel (Janssen et al., 2009). In particular, combining an Mps1 inhibitor (NTRC 0066-0) with clinically relevant doses of docetaxel has proven successful, with extensions in mouse survival and tumour remission (Maia et al., 2015). Furthermore, inhibitors of Mps1 activity, BAY 1161909 and BAY 1217389 synergise with paclitaxel in taxane-resistant tumour models of triple-negative breast cancer and lung carcinoma (Wengner et al., 2016), with recent entry into Phase I clinical trials with paclitaxel. Therefore it may be likely that similar effects will be observed with Bub1 inhibition, providing a foundation for future experimentation.

In this chapter I successfully set up two independent assays for the testing of Bub1 kinase activity, but failed to determine the role of the activity in the SAC. However, recent studies established that Bub1 is non-essential for checkpoint functioning and that the inhibition of Bub1 may be clinically beneficial. Due to the lack of positive results, I next turned to study mitotic perturbation further, with the synthesis and characterisation of a Cenp-E inhibitor GSK923295.

Chapter 4: Using a Cenp-E inhibitor GSK923295 in the development of an assay to study aneuploidy

4.1 Introduction

The link between aneuploidy, mitosis and tumourigenesis has been indicated, where aneuploidy has been associated with tumour growth (Boveri, 2008, 1914, 1902). Nevertheless, the presence of aneuploidy can promote or suppress tumourigenesis (Holland and Cleveland, 2009; Silk et al., 2013; Weaver et al., 2007), where high levels of aneuploidy are thought to be toxic and intolerable for the cell (Birkbak et al., 2011; Holland and Cleveland, 2012).

Cancers exhibit high levels of aneuploidy (Cimini, 2008; Mitelman, 2014; Nicholson and Cimini, 2011), yet why cancer cells are able to survive and proliferate with the abnormal karyotype is not fully known. In contrast to cancer cells, normal somatic cells undergo death or a p53-dependent cell cycle arrest when chromosome missegregation occurs (Thompson and Compton, 2010). In fact, cancers with increased chromosome instability (CIN) are resistant to Taxol (Swanton et al., 2009, 2006), therefore it is likely they have a mechanism in place in order to resist the mitotic aberrations. Mutations in p53 are a common occurrence in several cancers (Muller and Vousden, 2014), with 75% of mutations showing loss-of-function phenotypes, with potential dominant negative effects (Petitjean et al., 2007) giving rise to defective p53 functioning (Tomasini et al., 2008). Thus, unlike diploid cells which arrest in mitosis when faced with erroneous segregation, p53-deficient cells may continue to survive and proliferate.

However, little is known about what signals to p53 and the downstream effectors, with reports suggesting proteotoxic stress due to gene dosage imbalances (Santaguida and Amon, 2015; Thompson and Compton, 2010; Torres et al., 2007; Williams et al., 2008) and therefore, future experimentation would aim to study this. As chromosome missegregation is a rare occurrence in normal somatic tissues (with a chromosome loss or gain rate of 1% (Thompson and Compton, 2008)), studying the consequences of this abnormality is difficult. This is because the examination of a small alteration in the corresponding gene dosage is not an easy task (Santaguida and Amon, 2015). Therefore, by artificially inducing elevated rates/levels of chromosome missegregation, the consequences of aneuploidy can be studied more easily. Previous efforts have used monastrol washout approaches, but with only one missegregation event every

third division (Cimini et al., 2001, 1999; Knowlton et al., 2006; Thompson and Compton, 2010), analysing the effects of aneuploidy and gene dosage changes is relatively problematic. Furthermore, the incidence of lagging chromosomes with this approach can cause DNA damage (Ganem and Pellman, 2012; Janssen et al., 2011). Therefore, methods to produce aneuploid progeny more efficiently and without the added complication of DNA damage are needed.

One approach could be to exploit the phenotype induced by Cenp-E inhibition. Cenp-E is a kinesin-7 motor protein involved in the congression of chromosomes to the metaphase plate (Schaar et al., 1997). GSK923295 is a recently described inhibitor of Cenp-E (Qian et al., 2010), and when bound at an allosteric site, ATP hydrolysis is prevented and the Cenp-E motor protein is effectively 'locked' onto the microtubule. This results in a phenotype where the majority of chromosomes align along the metaphase plate with a small number clustered at the poles (Wood et al., 2010).

Therefore, I hypothesised that by inhibiting Cenp-E and inducing chromosome misalignment, driving cells out of mitosis in the presence of these unaligned chromosomes would result in missegregation. This will result in daughter cells with unequal numbers of chromosomes. One method of overriding the checkpoint and driving cells out of mitosis is via the inhibition of the checkpoint protein Mps1 (Hewitt et al., 2010). Initially I will describe the synthesis of GSK923295 and then I will explain the characterisation of the synthesised compound using a number of assays to ensure specificity against Cenp-E. From here, I will briefly explain the set-up of the assay to generate aneuploidy using the Cenp-E/Mps1 co-inhibition approach. Details of the assay can be found in Appendix 1 (Bennett et al., 2015).

4.2 The synthesis of GSK923295

The synthesis of GSK923295 was aided by Dr Beatrice Bechi, but in this thesis I will describe the novel step which I completed. Previous methods describing the synthesis of GSK923295 focussed on a High Performance Liquid Chromatography (HPLC) based resolution of the racemic alcohol substrate *rac*-**2** ((Bellingham et al., 2010; Qian et al., 2010) and see (Figure 4.1A)). However, this step was not reproducible in the lab and therefore other methods of chiral resolution were explored.

One such method included utilising the enzyme, *Candida antarctica* Lipase B (CALB) (Anderson et al., 1998; Frykman et al., 1993; Orrenius et al., 1995; Piidkzdingrrotbtiti et al., 1994). Lipase enzymes are hydrolases often used in asymmetric synthetic approaches for the kinetic resolution of alcohols, specifically

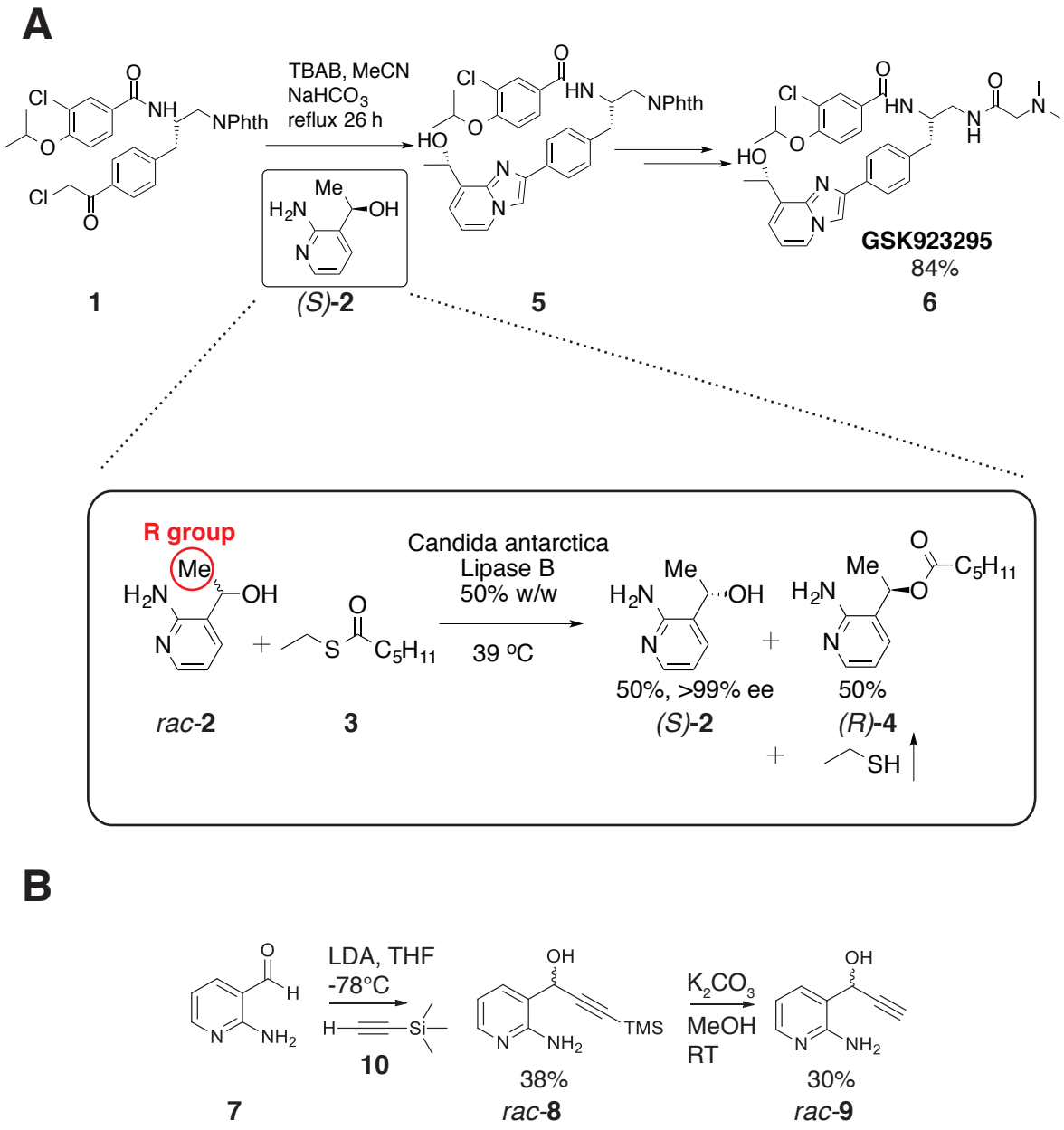

Figure 4.1 The resolution of a key intermediate for the synthesis of GSK923295 using *Candida antarctica* lipase B enzyme.
(**A**) The resolution of the racemic methyl alcohol *rac*-**2** utilised the *Candida antarctica* lipase B enzyme (50% w/w), in order to generate the enantioselective (*S*)-methyl alcohol **2**.This was used in the subsequent steps for the synthesis of GSK923295 **6**. The synthesis of **5** to **6** was performed by Dr Beatrice Bechi.
(**B**) To extend the potential scope of the CALB enzyme, two intermediates were synthesied, the trimethylsilyl **8**, and the corresponding acetylene **9**.

catalysing the enantioselective trans-esterification of secondary alcohols (Gotor-Fernández et al., 2006). Lipases give high selectivity and substrate specificity ranges are broad (Ghanem and Aboul-Enein, 2005). CALB is advantageous due to its ability to accommodate an extensive range of substrates, bringing high enantioselectivity, thermal stability and also stability in aqueous solvents (Anderson et al., 1998; Rotticci et al., 2001). Previously, aromatic secondary alcohols have been kinetically resolved with CALB (Orrenius et al., 1994; Piidkzdingrrotbtiti et al., 1994) and mutated variants of CALB have also shown success similarly (Engström et al., 2011; O'Neill et al., 2012). Since the racemic alcohol *rac*-**2** is structurally similar to other substrates successfully resolved with CALB, this approach was exploited in my studies.

In the reaction set-up, CALB was added to *rac*-**2** at 50% v/v, with excess S-ethyl thiohexanoate **3** as the acyl donor (Figure 4.1A). The reaction proceeded under solvent-free conditions at 39°C. Reaction progress was monitored using HPLC, and following a five day incubation, the enzyme specifically catalysed the acylation of the (*R*)-enantiomer, with the desired (*S*)-enantiomer left unreacted, as shown by the chromatograms (Figure 4.2A). At time zero, the (*R*)- and (*S*)- enantiomers exhibited peaks of equal intensity, whereas after five days, the (*S*)-enantiomer displayed higher intensity and the peak for the (*R*)-enantiomer was minimal. This suggested the (*R*)-specificity of CALB.

Maximum yields at 50% were obtained for the resulting ester (*R*)-**4** and the unreacted enantiomer (*S*)-**2**, where the desired enantiomer was obtained in >99% enantiomeric excess (ee). 1*S*-(2-amino-3-pyridyl)ethanol (*S*)-**2** was then obtained via purification by column chromatography. From this (through experimentation conducted by Dr Beatrice Bechi), (*S*)-**2** reacted with the phenacyl chloride **1**, resulting in the pyridyl imidazole **5**. This was then used in subsequent steps to synthesise GSK923295 **6** (Frykman et al., 1993; Orrenius et al., 1995, 1994; Rivera et al., 2001).

I have described an improved method using CALB to successfully resolve *rac*-**2** in order to obtain the desired (*S*)-enantiomer. This was then effectively used to synthesise GSK923295. Furthermore, CALB has been shown to be of use in the resolution of a wide range of substrates, and therefore, in the first case, I attempted to test the specificity range with structurally similar secondary alcohols.

A

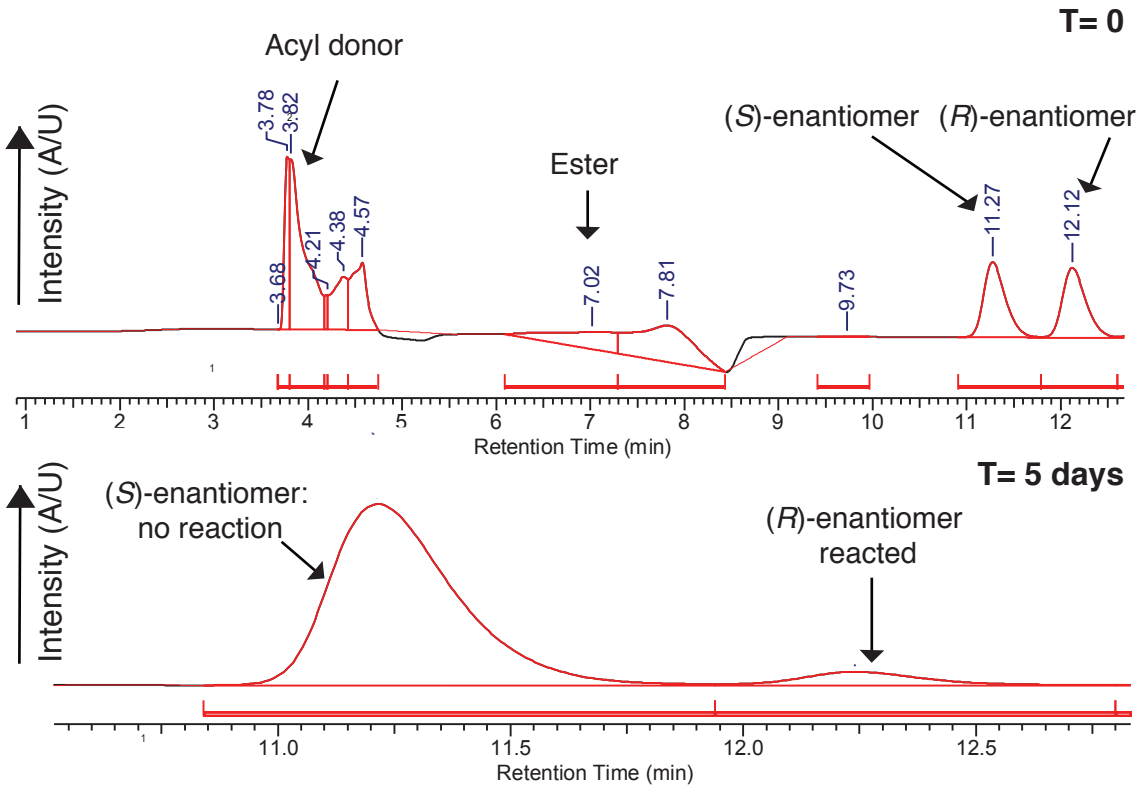

B

Substrate number	R group	Time of resolution	Products		
			Remaining alcohol		
			ee	Optical rotation	Yield
2		5 days	96	-	50
8	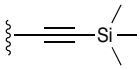	0 hr	remained racemic		
9	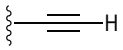	7 days	98	+	30

Figure 4.2 The CALB- mediated enzyme resolution of racemic substrates.
(**A**) Chromatograms showing the HPLC-based resolution of the reaction substrates required for the synthesis of GSK923295, with the retention times indicated. T=0 represents when the enzymatic reaction began, and T=5 days, when the enzyme reaction was complete.
(**B**) Table showing the different substrates resolved using the CALB enzyme, with the retention times, ee, optical rotation and yield determined.

4.3 Extending the utilisation of CALB

Aforementioned, CALB can be used for the resolution of a broad range of secondary alcohols and thus, I wanted to examine the scope of the substrates that could be resolved using similar methods. The substrates chosen were derivatives of *rac*-**2** (Figure 4.2B), but with extended side R-groups; a larger trimethylsilyl group and its reduced alkyne. They were chosen in order to examine the size of the R group that could be accommodated and successfully resolved using CALB. The trimethylsilyl *rac*-**8** was synthesised using lithium diisopropylamide (LDA), from the previously synthesised 2-amino-3-pyridinecarboxaldehyde **7**. At low temperatures this bulky base selectively formed a nucleophilic enolate, which then underwent alkylation forming *rac*-**8** at a 38% yield (Figure 4.1B). Upon base mediated reduction, with deprotection of the terminal alkyne group, the corresponding acetylene *rac*-**9** was generated in a 30% yield. Following on from the generation of the racemic substrates, the ability of CALB to catalyse the transesterification reaction was investigated. The intermediate substrate *rac*-**8** did not visibly undergo an enantioselective resolution, where HPLC indicated that after a seven day period the starting racemic mixture was still present. However, the reduced *rac*-**9** did undergo resolution over a seven day period, with 98% ee of the (*S*)-enantiomer over the (*R*)-enantiomer. Using this approach, derivatives of GSK923295 may be synthesised which may result in more selective or efficacious inhibitors.

4.4 Characterising GSK923295 in cell-based assays

After synthesis and purification, it was essential to ensure that GSK923295 inhibited Cenp-E with no off-target effects. Thus, I used a number of cell-based assays to confirm phenotypes and explore long-term effects of Cenp-E inhibition.

4.41 GSK923295 and its effect on chromosome alignment

Previous reports have shown that Cenp-E is essential for chromosome segregation (Schaar et al., 1997). Consequently, upon either siRNA or small molecule inhibition, chromosomes fail to congress properly (Weaver, 2003; Wood et al., 2010; Yao et al., 2000; Yen et al., 1991). While the majority of chromosomes align along the metaphase plate, a small number remain clustered around the spindle poles.

To determine whether the in-house synthesised small molecule inhibitor GSK923295 was effective at targeting Cenp-E, DLD-1 cells were incubated in the presence of 50 nM of the drug for four hours. The cells were then fixed and stained for Bub1, tubulin and DNA. Immunofluorescence images confirmed that in comparison to

control cells, where all of the chromosomes aligned along the metaphase plate, cells treated with GSK923295 exhibited a characteristic phenotype; while the majority of chromosomes aligned along the metaphase plate, a small number remained clustered at the spindle poles, with the bipolar spindle remaining intact (Figure 4.3A). Of particular note, Bub1 showed high intensity staining at the kinetochores of the unaligned chromosomes at the poles, in comparison to the kinetochores of the aligned chromosomes. This is consistent with a lack of stable kinetochore-microtubule interactions resulting in the generation of a SAC signal (Jablonski et al., 1998; Taylor and McKeon, 1997; Taylor et al., 2001). Nevertheless Bub1 still localised to kinetochores of aligned chromosomes as seen previously (Taylor and McKeon, 1997), but displayed lower intensity staining in contrast.

From this initial study, I confirmed that GSK923295 was behaving as one would expect for a Cenp-E inhibitor, where complete chromosome alignment is perturbed and although most chromosomes congress to the metaphase plate, a small number cluster at the poles.

Next, in order to identify the ideal concentration and exposure time for optimal Cenp-E inhibition with GSK923295, HeLa cells were exposed to varying concentrations of GSK923295 over a period of four hours (Figure 4.3B). For each concentration, the mitotic cells were analysed by immunofluorescence and correspondingly classified into each phase of mitosis. It is important to note that GSK923295-treated cells with the phenotype as shown in Figure 4.3A were categorised as prometaphase. In the control population, cells were in all stages of mitosis, with 12% in prophase, 21% prometaphase, 29% metaphase and 38% anaphase (Figure 4.3B). At concentrations of 1-5 nM, numbers were comparable to controls. However, at 10 nM, the number of cells in prometaphase increased to 51%, whilst the numbers in metaphase and anaphase decreased to 15% and 27% respectively. However, at 50 nM (and higher doses up to 500 nM), a complete block of metaphase and anaphase was visible, as 94% of cells were in a prometaphase-like state, where the large majority of chromosomes were aligned along the metaphase plate yet a few remained at the poles. No cells were observed in metaphase or anaphase. Therefore, in this case, 50 nM was sufficient to inhibit chromosome congression and block mitotic progression.

Furthermore, to determine the exposure time at which GSK923295 prevented chromosome congression, HeLa cells were treated with 50 nM GSK923295 for 0, 2 and 4 hours. As shown by the bar graph in Figure 4.3C, even after a two hour incubation with 50 nM GSK923295, HeLa cells were not able to progress through

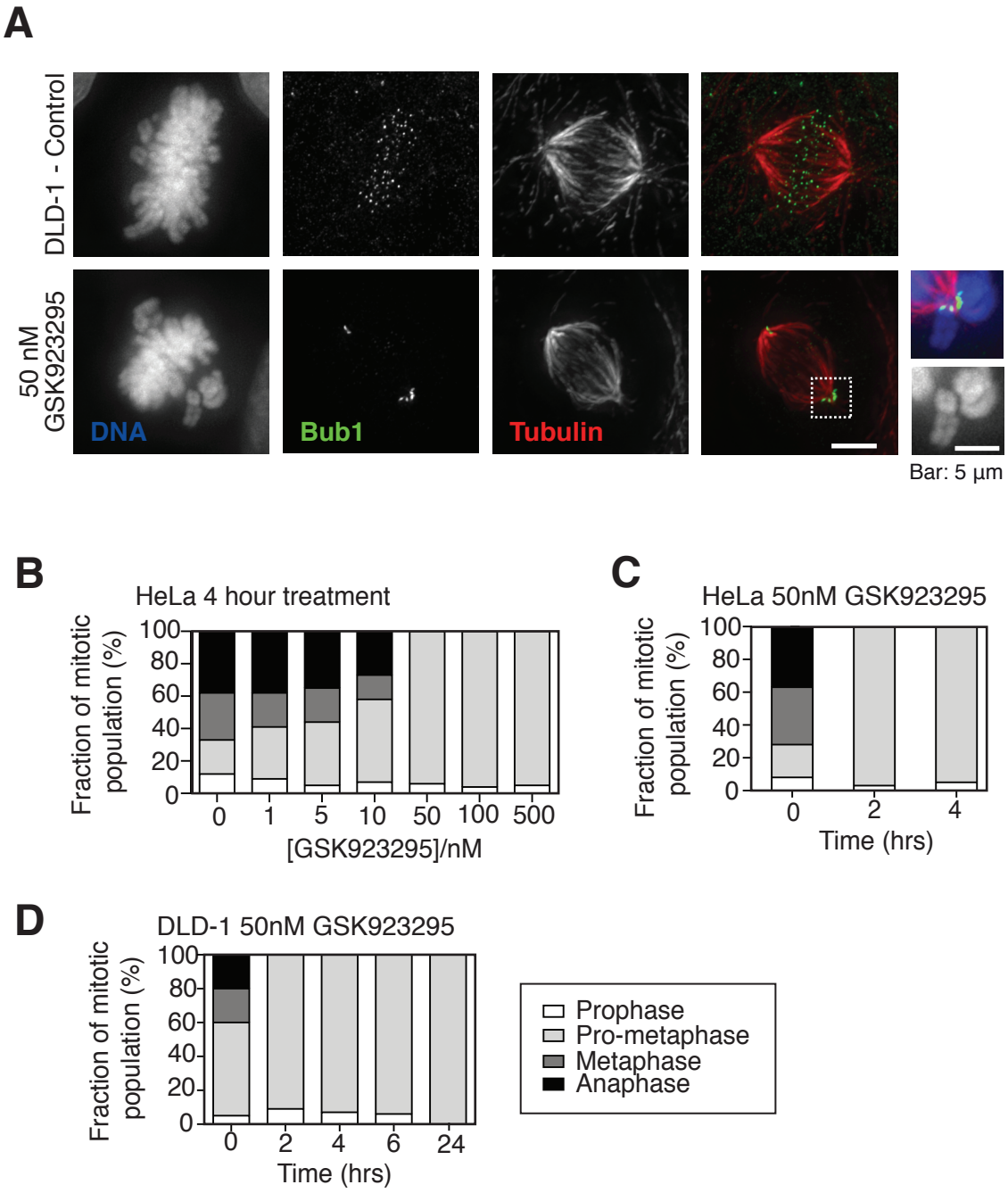

Figure 4.3 Consequence of GSK923295 treatment on chromosome alignment.
(**A**) Immunofluorescence images of control and 50 nM GSK923295 treated DLD-1 cells. Cells were fixed after four hours and stained for DNA (blue), Bub1 (green) and tubulin (red). Bar: 5 µm. Provided by Dr Anthony Tighe.
(**B**) Bar graph showing the number of HeLa cells in each phase of mitosis after a four hour treatment with increasing concentrations of GSK923295. 100 mitotic cells for each condition were counted.
(**C**) Bar graph showing the number of HeLa cells in each phase of mitosis after treatment with 50 nM GSK923295 for increasing lengths of time. 100 mitotic cells for each condition were counted.
(**D**) Bar graph showing the number of DLD-1 cells in each phase of mitosis following treatment with 50 nM GSK923295. 100 mitotic cells for each condition were counted.

metaphase or anaphase, where >95% were blocked in prometaphase. Similarly, in DLD-1 cells at the two hour time point, 91% of cells were in prometaphase (Figure 4.3D). Thus, within two hours, 50 nM GSK923295 can cause a potent prometaphase arrest.

4.42 GSK923295 and its effect on mitosis

The lack of metaphase and anaphase figures following GSK923295 treatment (Figure 4.3) suggests that the cells are mitotically arrested. It is likely that the presence of the unaligned chromosomes following GSK923295 treatment activates the SAC and therefore initiates a mitotic arrest (Schaar et al., 1997; Yao et al., 2000). However, it may be that cells with defective Cenp-E function exit mitosis without a prolonged arrest and in the presence of unaligned chromosomes, with failed chromosome segregation (Tanudji et al., 2004), thereby resulting in aneuploid daughter cells. Therefore, in order to determine if GSK923295 induces a mitotic arrest and to discriminate between different cellular fates, I analysed live cells by time-lapse microscopy. I used DLD-1 and HeLa cells expressing GFP-histone H2B to visualise the chromosomes. HeLa cells were exposed to 50 nM GSK923295 and tracked throughout mitosis (representative examples in Figure 4.4A). In the control population, all chromosomes had aligned at the metaphase plate by 36 minutes, with anaphase occurring by 48 minutes. In contrast, in the Cenp-E inhibitor treated population, 54 minutes after entry into mitosis, while the majority of chromosomes had aligned, there were still unaligned chromosomes at the poles (indicated by the white arrows). The cells remained arrested with unaligned chromosomes for a few hours, and then by 158 minutes, cells began to spin quite violently and chromosomes were seen to effectively 'fall' from the metaphase plate, giving a cohesion fatigue-like phenotype (Daum et al., 2011; Stevens et al., 2011). The chromosome scattering observed is defined by the premature separation of sister chromatids in a mitotic arrest. The pulling forces of the kinetochores attached to microtubules oppose and overcome the interactions of the cohesin complex, with reactivation of the checkpoint. Following this, the SAC is unable to be satisfied due to kinetochores not being stably attached to microtubules, and the cell may undergo slippage or apoptosis (not shown).

As the HeLa cells are prone to cohesion fatigue (Daum et al., 2011; Lara-Gonzalez and Taylor, 2012; Stevens et al., 2011) and this may hinder long-term studies of the effects of Cenp-E inhibition, I then turned to the DLD-1 cell line, with similar analysis. Control cells were shown to be at metaphase by 28 minutes, followed

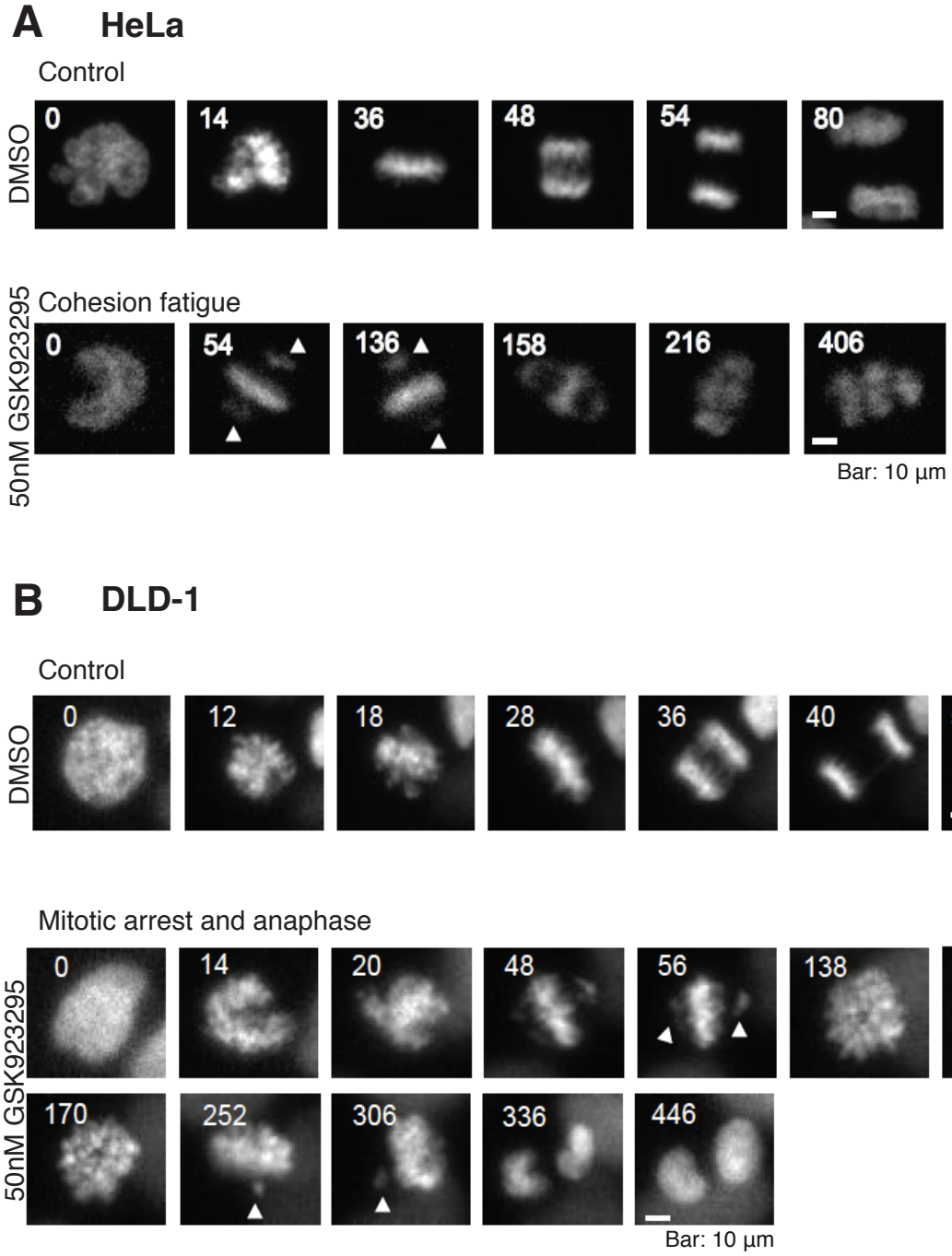

Figure 4.4 Effect of GSK923295 exposure in living cells.
(**A**) Examples of time-lapse sequences showing the fates of HeLa GFP-H2B cells under control conditions and when exposed to 50 nM GSK923295. Bar: 10 µm. The numbers indicate time in minutes, and the arrows, unaligned chromosomes.
(**B**) Examples of time-lapse sequences showing the fates of DLD-1 GFP-H2B cells under control conditions and when exposed to 50 nM GSK923295. Bar: 10 µm. The numbers indicate time in minutes, and the arrows, unaligned chromosomes.

by anaphase at 36 minutes (representative examples in Figure 4.4B). GSK933295-treated cells gave the Cenp-E inhibition phenotype (t=56 minutes), where the majority of chromosomes aligned with a few remaining at the poles (indicated by the white arrows). This state was maintained until 306 minutes, with a single unaligned chromosome still observable at this time. By 336 minutes, chromosomes separated as the cell went through anaphase, resulting in two daughter cells. This indicates that DLD-1 cells are not prone to cohesion fatigue (at least in the cells I analysed) and do eventually undergo anaphase. However, whether the resulting daughter cells are of equal chromosome number, or are in fact aneuploid, is not known.

Through live-cell imaging, I have confirmed that GSK923295 prevents alignment of chromosomes, resulting in a mitotic arrest. Prolonged mitotic arrest can result in cohesion fatigue in some cases, but in cells that are not prone to this behaviour, long-term cell fate can include slippage, division or apoptosis. These specific long-term fates will therefore be analysed in the next section.

4.43 The effect of GSK923295 on long-term cell fate

The obvious effects on mitosis and the observation that HeLa cells may undergo cohesion fatigue and DLD-1 cells, anaphase, following Cenp-E inhibition, led me to next evaluate the cellular fates that follow the prolonged mitotic arrest. Initially I analysed HeLa cells by flow cytometry using the DNA-binding dye propidium iodide, to determine the DNA content following 50 nM GSK923295 exposure over a 72 hour period (Figure 4.5A). At time zero, normal cell cycle profiles were shown with a larger proportion of cells with a 2n DNA content and a smaller proportion with a 4n DNA content. At 8 hours, a large fraction of the cells had a 4n DNA content, indicating a cell cycle arrest, resulting in an inability to progress through mitosis. After 16 hours, a sub-2n population was seen and the 4n peak decreased. The cell cycle profile then continued to disintegrate, where by 72 hours there was no separation between the 2n and 4n peaks. The disintegration of the profile and the sub-2n population indicated apoptosis onset. Therefore, in the case of the HeLa cells, the resulting cohesion fatigue causes sister chromatids to separate prematurely, activating the SAC and it is this persistent activation which results in apoptosis.

As I mentioned previously, analysing HeLa cells could be problematic due to the likelihood of cohesion fatigue occurring (Daum et al., 2011; Stevens et al., 2011). Therefore, I next turned to the colon cancer cell line RKO, to study the long-term implications of Cenp-E inhibition. The RKO cell line typically undergoes death in mitosis

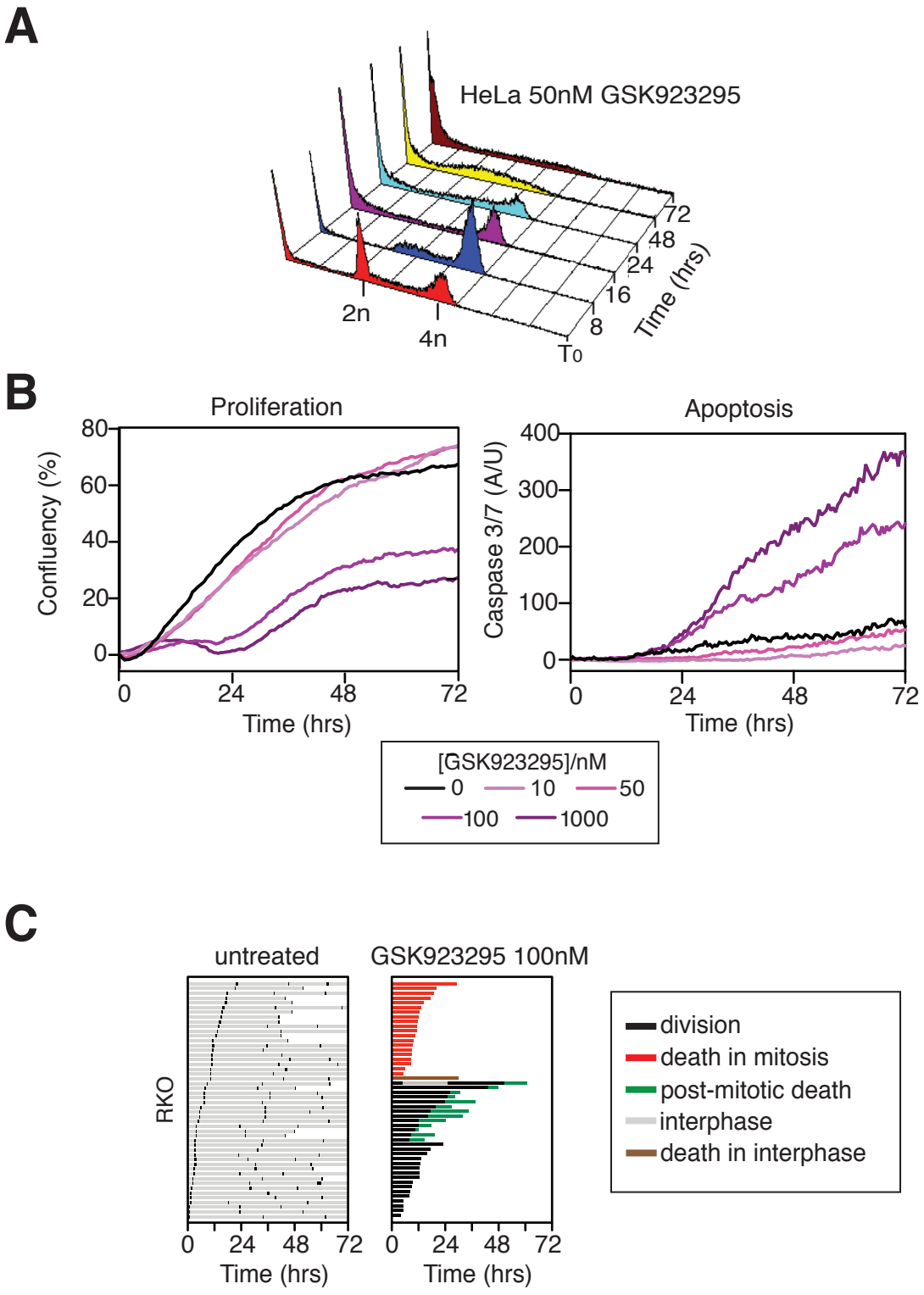

Figure 4.5 Effect of GSK923295 on the cell cycle and apoptosis.
(**A**) DNA content histograms of HeLa cells treated with 50 nM GSK923295 over a period of 72 hours.
(**B**) Line graphs indicating the normalised confluency (%) and caspase 3/7 (A/U) while RKO cells were exposed to100 nM GSK923295 over 72 hours.
(**C**) Fate profiles showing RKO cells treated with 100 nM GSK923295 and analysed for cell behaviour. Time zero in the untreated cells represents when filming started. Time zero in the treated cells represents when cells entered mitosis.

when exposed to antimitotics (Gascoigne and Taylor, 2008). To address the effects of long-term inhibition of Cenp-E on cell fate, I used the IncuCyte® Zoom for time-lapse imaging. Using this approach allowed the analysis of cellular behaviour in more detail since single cells could be tracked over a defined time period. This allowed for the generation of cell fate profiles, as described previously (Gascoigne and Taylor, 2008). RKO cells treated with varying concentrations of GSK923295 were imaged every 10 minutes over 72 hours, with cell confluency determined and apoptosis measured using a fluorescent caspase 3/7 dye. In the first case, control cells grew to near 80% confluency over three days (Figure 4.5B, left). Whilst concentrations of 10 nM and 50 nM of GSK923295 showed similar proliferative potential as the control, 100 nM and 1000 nM reduced proliferation to below 40% over the period of filming. This suggests that at the higher concentrations of GSK923295, proliferation was low due to cell death. When observing the caspase 3/7 measurements up to 50 nM, little apoptosis was seen (Figure 4.5B, right). At 100 nM and 1000 nM, high levels of apoptosis were apparent, where 24 hours marked the initial increase in apoptosis onset. These results suggest that in the RKO cell line at higher concentrations of GSK923295, cellular growth is perturbed and this is accompanied by an increase in cell death.

The caspase 3/7 measurement used depicts the total amount of apoptosis in a cell population, but it cannot distinguish between mitotic and post-mitotic death (i.e. death in mitosis (DiM) or post-mitotic death (PmD)). In order to distinguish between the DiM and PmD fates, I analysed phase-contrast movies to follow the fate of cells and data was plotted as a cell fate profile. Briefly, each cell fate profile shows the behaviour of 50 cells, where one line is one cell, the colour of the line describing the behaviour of that cell (e.g. DiM) and the length of the line defining the time taken for the cell to undergo that particular fate. In the control cells, the majority underwent three mitotic divisions over the 72 hour time period (Figure 4.5C). Upon treatment with 100 nM GSK923295, cells entered a mitotic arrest and 40% of cells remained in this state for approximately 12 hours, but subsequently died in mitosis (red bars). The profile also shows 26% of cells divided after an arrest of 15.22 hours (black bars) and then died in the subsequent interphase (green bars). Only one of these cells went into a second mitosis, and after an arrest, post-mitotic death followed. Furthermore, 32% of the population arrested in mitosis but then remained in interphase after division.

Therefore, it is apparent that cellular fate following Cenp-E inhibition- mediated mitotic arrest is heterogeneous, with cells undergoing death in mitosis, abnormal

division and post-mitotic death behaviours. Overall, the major outcome of saturating GSK923295 exposure is apoptosis.

4.44 Analysing the reversibility of GSK923295

In order to utilise GSK923295 as a small molecule tool for studying aspects of mitosis, I considered if the drug was reversible i.e. can I wash it out of cells? Are the effects of Cenp-E inhibition still visible following inhibitor removal? Are there long-term effects of Cenp-E inhibition following washout, due to residual inhibitor?

First of all, it was important to determine if cells were able to progress through mitosis following the removal of the Cenp-E inhibitor. As shown in Figure 4.3C, when I exposed cells to GSK923295, within a 2 hour period there was a >95% mitotic block in prometaphase. To test whether this block was reversible, I treated HeLa cells with 50 nM GSK923295 for a 4 hour period. This was followed by removal of the drug and replacement with fresh media. At the time periods indicated (Figure 4.6A), cells were fixed and analysed by immunofluorescence. In the untreated control population, cells were analysed with 25% in prometaphase, 29% in metaphase and 40% in anaphase. At time zero, where GSK923295 was added for four hours, removed and cells were analysed promptly, 96% of cells were in prometaphase. Even after 30 minutes following washout, cells were seen to progress through mitosis, and the number of cells in prometaphase was reduced (54%), with cells also in the latter stages of mitosis (metaphase 19%, anaphase 19%). It is important to note that there was no indication of lagging chromosomes or chromosome bridges following washout (not shown). This suggests that GSK923295 can readily be washed out of cells, and cells are able to progress normally through mitosis.

Although from fixed cell analysis, mitoses seemed ‘normal’, the long-term effects of Cenp-E inhibition needed to be considered. Therefore, I observed the fate of cells treated with the Cenp-E inhibitor over a 72 hour time period using time-lapse microscopy. Here, HeLa cells were treated with 50 nM of GSK923295 for four hours, and then following this, either the GSK923295 was washed out and replaced with fresh media or GSK923295 was washed out and then added back. It was apparent that following drug washout cells were able to overcome the previous mitotic perturbation and continue to survive and proliferate (Figure 4.6B), reaching similar levels of confluency as the untreated cells. For those cells continually exposed to GSK923295, cell growth was prevented, with no increase in confluency over the 72 hour period. Single cell fate profiling was then carried out on these cells. In the controls, 98% of

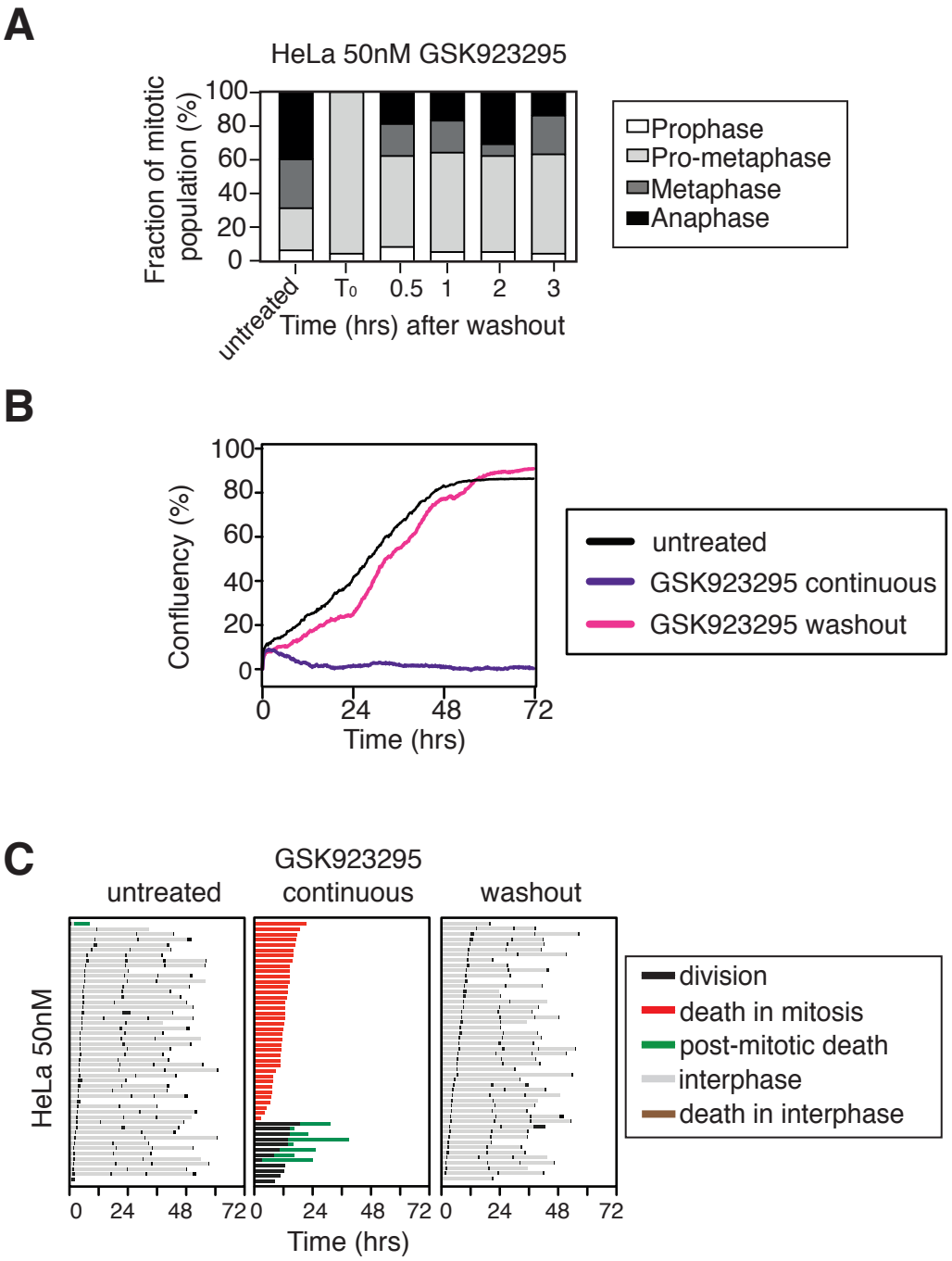

Figure 4.6 Analysis of the reversibility of GSK923295.
(**A**) Bar graph quantitating the number of cells in each phase of mitosis, following exposure of HeLa cells to 50 nM GSK923295, with washout at the time points indicated. 100 mitotic cells for each condition were counted.
(**B**) Normalised confluency (%) of HeLa cells treated with 50 nM GSK923295 either continuously or after washout following a four hour incubation.
(**C**) Cell fate profiles of the conditions in (B). Time zero in the untreated and washout cells represents when filming started. Time zero in the treated cells represents when cells entered mitosis.

cells went through multiple mitoses with 24% undergoing four divisions over the course of the experiment (Figure 4.6C). In contrast, 92% of cells exposed continuously to GSK923295 underwent death, with 9% of these post-mitotic, and 91% dying in mitosis. The 8% of cells that did not die underwent a division after a prolonged mitotic arrest and then arrested in the following interphase. When GSK923295 was washed out and cells analysed promptly, cells were seen to undergo multiple mitoses in a similar manner to controls. Timings to entry in mitosis were slightly prolonged following washout, with control cells entering after 4.2 hours and washout cells after 6.6 hours. The time between the first and second mitosis was relatively unchanged, at 17.3 hours in the controls and 16.6 hours in the washout population. Therefore, this provides evidence that GSK923295 is reversible and any residual inhibitor does not have detrimental long-term effects on cells.

4.5 The establishment of an assay to study aneuploidy

I have established that Cenp-E inhibition with GSK923295 caused the majority of chromosomes to align at the metaphase plate, with a small number clustered at the poles. Therefore, it may be that driving these cells out of mitosis would cause missegregation of the chromosomes residing at the poles. This could potentially result in the generation of cells with unequal chromosome numbers.

To test this, cells were treated with GSK923295 at 50 nM, followed by 2 μM of the Mps1 inhibitor AZ138 (Hewitt et al., 2010), used to override the SAC and drive cells out of mitosis. Details of the method are given in the Appendix 1. Note these experiments were carried out by Dr Sarah Thompson. Strikingly, of the cells analysed, 98% showed missegregation and using FISH analysis it was apparent that the resulting daughter cells were aneuploid (Bennett et al., 2015). This approach led to the missegregation of approximately 2 chromosomes per division, indicating this as a potential method to study aneuploidy. This is in contrast to the commonly used monastrol wash-out approach, where often, <50% of divisions result in missegregation and DNA damage is often a consequence (Cimini et al., 2001, 1999; Ganem and Pellman, 2012; Janssen et al., 2011; Knowlton et al., 2006; Thompson and Compton, 2010). The lack of lagging chromosomes or bridges indicates that it is unlikely that this method induces DNA damage.

4.6 Summary

This Chapter focused on the description of the robust synthesis of GSK923395, with an improved synthetic step using the CALB enzyme. The observation that the CALB enzyme is able to resolve other substrates provides potential to extend the scope of substrate resolution. This may generate improved Cenp-E inhibitor analogues. Following on from the synthesis, characterisation of the in-house GSK923295 confirmed the specificity to Cenp-E, in agreement with previous studies where chromosome congression was affected. I also discovered the reversibility of GSK923295, where following removal of the inhibitor, cells were able to progress through mitosis. Following on from characterisation, GSK923295 was used in combination with AZ3146 in assays to generate aneuploidy, with at least one chromosome missegregating every division, providing advantages over traditional methods. See Appendix 1 for the corresponding published paper (Bennett et al., 2015).

4.7 Discussion

4.71 A strategy to resolve enantiomers

An initial problem that was highlighted in the synthesis of GSK923295 was observed when resolving the (*S*)-enantiomer of the methyl alcohol 1*S*-(2-amino-3-pyridinyl)ethanol*(S)*-**2**. As the published method using chiral HPLC proved to be unsuccessful (Qian et al., 2010), a kinetic resolution-based method utilising the *Candidada antarctica* Lipase B (CALB) enzyme was exploited with efficiency to resolve the desired enantiomer. The resolution resulted in the maximum 50% yield, with >99% enantiomeric excess. Chiral intermediates are often the building blocks for natural products (Kaman et al., 2001; Rouf et al., 2011; Sekar et al., 1999) and therefore, other racemic mixtures with a chiral alcohol substrate were treated similarly, with some success. However, the lack of resolution of the larger, more bulky substrate *rac*-**8** indicates steric clashes with CALB, implying that the enzyme cannot be exploited for all secondary chiral alcohols. This method may be employed to other similar substrates, including analogues of GSK923295, which may prove to be more efficacious than the parent compound.

4.72 Using GSK923295 as a mitotic tool

I have demonstrated the potential for GSK923295 as a cell biological tool due to penetrant inhibition within a number of hours, but also, its ability to be removed from

cells, enabling reactivation of Cenp-E function. Following exposure of cells to GSK293295, and subsequent washout, the previous mitotic block observed was reversed (Figure 4.6). Cells were seen to proceed through mitosis and underwent anaphase without any delays. However, whether these mitoses proceeded without missegregation errors (e.g. lagging chromosomes) is not known. Studying the effect using high-resolution microscopy would be beneficial, but also, the longer-term effects following washout may reveal if there are any detrimental consequences of short-term Cenp-E inhibition, for example with colony formation assays. Nevertheless, in the first case, the ability of GSK923295 to be washed from cells with no obvious effects on mitosis indicates its potential use as a tool in cell biological experiments. In contrast, Taxol accumulates within cells and is retained after loss from circulation (Mori et al., 2006; Weaver, 2014), suggesting that perhaps this feature may be important for the anticancer properties of drugs.

It was interesting to note that when analysing GSK923295-treated cells by time-lapse imaging, 26% of cells arrested in mitosis and then divided after 15.22 hours (Figure 4.5C). It is not known by this analysis whether cells eventually aligned their chromosomes and satisfied the SAC before undergoing anaphase or if they underwent anaphase with unaligned chromosomes, without satisfaction of the SAC. To understand this, high-resolution microscopy would be advantageous. It was apparent that the 32% cells that did eventually divide, arrested in the subsequent interphase for the remainder of filming. If anaphase had been triggered with unaligned chromosomes then perhaps the resulting G1 arrest would have been due to DNA damage pathway stimulation involving ATM, Chk2 and p53 (Janssen et al., 2011). Furthermore, if chromosome missegregation and aneuploidy had resulted, a p53-dependent cell cycle arrest may have been the cause of the anti-proliferative effect (Thompson and Compton, 2010). On the other hand, if chromosomes had fully aligned before anaphase onset, then the prolonged arrest may have directly resulted in the G1 arrest (Uetake and Sluder, 2010). One cell imaged entered interphase following a short arrest in mitosis. Rather than residing in G1 for the remainder of the experiment, it then underwent a second mitosis. This is consistent with the concept that remaining in prometaphase for a shorter period of time does not result in a G1 arrest following exit, yet remaining in prometaphase for an increased length of time stimulates a p38-dependent G1 arrest, even with normal completion of mitosis (Uetake and Sluder, 2010)s.

Since elevated missegregation of chromosomes can result in death (Boveri 1914), there is a need to establish the link between chromosome missegregation, aneuploidy and the consequences including death. This would allow us to understand how cancers can circumvent death in order to continue to survive and proliferate with abnormal karyotypes. Furthermore, this may aid in finding ways of accelerating death in response to aneuploidy, especially as low concentrations of antimitotics such as paclitaxel induce aneuploidy (Chen and Horwitz, 2002). Elevating the level of chromosome missegregaton has also been indicated as a potential therapeutic strategy (Janssen et al., 2009). This understanding may in fact facilitate in improving second-generation inhibitors. Therefore, the generation of the assay to induce aneuploidy can aid in these issues. Advantages over monastrol washout methods were seen, with increased frequency of missegregation events and without lagging chromosomes, decreasing the likelihood of DNA damage occurring. Therefore, this approach may be used to study aneuploidy and its consequences. The use of the small molecule inhibitor combination will allow for this approach to be carried over to other cell lines and systems with ease and can be used in combination with genetic methods. Furthermore, this method may allow for RNAi screens based on the response of cells to aneuploidy.

4.73 Targeting Cenp-E as a therapeutic approach

Cenp-E is overexpressed in a number of cancers (Agarwal et al., 2009), but is also downregulated in hepatocellular carcinoma (Liu et al., 2009). Targeting may be favourable, but clinical trials with GSK923295 have yet to show success, likely due to the lack of effective predictive biomarkers (Chung et al., 2012; Qian et al., 2010; Wood et al., 2010). More recently, new Cenp-E inhibitors have been developed, such as ‘Compound A’ (Ohashi et al., 2015). Discovered by the biochemical screening of the ATPase activity of the Cenp-E motor domain, exposure resulted in chromosome missegregation and the generation of aneuploid daughter cells. Apoptosis then occurred in a p53-dependent manner. This prompted the authors to suggest that p53 could be a potential biomarker for efficacy of Cenp-E inhibition. Furthermore, the Cenp-E inhibitor PF-2771 has been indicated as having potent antitumour activity in animal models and has shown efficacy in basal-like breast cancer cell lines (Kung et al., 2014). Consequently, it is possible that targeting Cenp-E in the clinic may prove to be beneficial, but further clarification of this approach needs to be undertaken.

This chapter has described the synthesis, characterisation and use of GSK923295 in order to establish assays which can be used to follow the effects of abnormal mitosis. I did not follow up on the work carried out in the lab in the establishment of the aneuploidy assay due to the realisation that perhaps I could not be as competitive in this research area. As I wanted to study the effects of perturbing mitosis on cellular fate and in doing so, attempt to devise methods of improving existing anticancer strategies, I next turned to study the mechanisms of antimitotics used in cancer chemotherapy, with GSK923295 being among the agents analysed.

Chapter 5: Investigating the role of Bcl-xL in mitotic and post-mitotic survival

5.1 Introduction

Upon exposure to antimitotics, cells exhibit heterogenetic cellular fates (Gascoigne and Taylor, 2008). Such fates include mitotic slippage and death in mitosis (DiM). Although slippage is relatively well studied, the mechanisms that lead to DiM remain less defined. Evidence has indicated the importance of the caspase-dependent intrinsic apoptotic pathway in the DiM fate when cells are exposed to antimitotics (Allan and Clarke, 2007; Andersen et al., 2009; Gascoigne and Taylor, 2008; Shi et al., 2008). A more in-depth analysis of the factors controlling DiM and cellular fate following antimitotic exposure will enable a greater understanding of how these agents elicit their action, but also, associated problems such as side effects, resistance and predictability can also be tackled with increased knowledge.

A recent genome-wide siRNA screen identified the transcription factor c-myc as a key regulator for DiM ((Topham et al., 2015) and see (Appendix 2)). The study illustrated that when c-myc was repressed, Taxol-induced death was replaced by slippage. Further analysis revealed transcriptional repression of c-myc regulates DiM by upregulation of the pro-apoptotic factors Bim, Bid and Noxa, and downregulation of the pro-survival Bcl-xL, at the mRNA level, signifying the importance of c-myc as a master regulator of the apoptotic network. Many of the BH3-proteins including Bim, Bad, Noxa and Bid, have been implicated in DiM (Díaz-Martínez et al., 2014; Haschka et al., 2015; Wan et al., 2014; Wang et al., 2014). Furthermore, the pro-survival proteins Mcl-1 and Bcl-xL are important for survival in mitosis (Bah et al., 2014; Chu et al., 2012; Kawabata et al., 2012; Minn et al., 1996; Shi et al., 2011; Upreti et al., 2008). Therefore, it is perhaps surprising that other members of the apoptotic network did not surface from the screen; a probable explanation may be due to the functional redundancy that exists between members (Eichhorn et al., 2014; Eno et al., 2012; Topham et al., 2015). The overlapping functions remains the pivotal reason as to why studying the individual contributions of the apoptotic proteins is difficult. Furthermore, the largely population-based approaches that have been used to study the role of proteins does not allow for the roles of each individual member to be distinguished.

Myc itself drives tumourigenesis and is an attractive cancer target (McKeown and Bradner, 2014; Sodir et al., 2011). Myc functions via protein-protein interactions,

with inhibition of such interactions difficult to target (Wells and McClendon, 2007). Typically, protein globular domains are exploited in drug discovery, but since Myc lacks these domains, this suggests that Myc itself is not a particularly good drug target. Nevertheless, one strategy to overcome this is to consider targeting Bcl-xL. Bcl-xL is a potent pro-survival factor in mitosis (Bah et al., 2014; Minn et al., 1996; Shi et al., 2011; Topham et al., 2015; Upreti et al., 2008) and therefore, studying the role of Bcl-xL in the context of a perturbed mitosis upon exposure to antimitotics may aid in understanding the death phenotype. Furthermore, as mentioned above, the intrinsic apoptotic pathway has been implicated in the DiM response to antimitotics and therefore this provides a good rationale for additionally targeting the apoptotic network in this context. Furthermore, the levels of c-myc positively correlate with breast cancer patient response to taxanes (Topham et al., 2015) and c-myc negatively correlates with Bcl-xL. Therefore, the hypothesis would be that patients with low levels of Bcl-xL would also respond better to antimitotics. In the first instance, to test this hypothesis a small molecule inhibitor of Bcl-xL WEHI-539 (Lessene et al., 2013), was fully characterised in the RKO cell line. This was followed by using the inhibitor in combination with a number of antimitotics to determine if there was a synergistic response, as anticipated. This may lead to the establishment of improved anti-cancer strategies.

Previous studies have also indicated the role of Bcl-xL for the maintenance of survival following exit from mitosis (Minn et al., 1996; Topham et al., 2015). Specifically, when cells were exposed to clinically relevant (low) doses of Taxol, the inhibition of Bcl-xL with WEHI-539 increased post-mitotic death (Topham et al., 2015). Therefore I studied the role of Bcl-xL following mitotic perturbations. To do this I analysed the contribution of Bcl-xL to survival when cells were exposed to antimitotics, including blockers and drivers (Keen and Taylor, 2009; Manchado et al., 2012). Using live single-cell analysis with the IncuCyte® Zoom, the function of Bcl-xL in survival during a mitotic arrest, following mitotic slippage and after abnormal division could be tracked, with the analysis of cell behaviour and eventual fate (Gascoigne and Taylor, 2008). The availability of a small molecule inhibitor against Bcl-xL allowed for finer functional analysis, as the activity of Bcl-xL can be more finely tuned in comparison to using genetic approaches such as siRNA.

5.2 Characterising a Bcl-xL inhibitor, WEHI-539

WEHI-539 was discovered in structure-based design studies using the crystal structure of Bcl-xL (Lessene et al., 2013). Although the associated study indicated its

specificity for Bcl-xL, I wanted to confirm selectivity in the particular system used here. To do this I made comparisons with siRNA against Bcl-xL and also tested the affect on the inhibitor on interactions between Bcl-xL and the BH3-only proteins. Exposure of cells to antimitotics can lead to apoptosis or slippage (Gascoigne and Taylor, 2008), however, since the DiM phenotype is less well studied, I focused on this aspect. For this reason, I chose the RKO colon cancer cell line because the dominant phenotype in the presence of saturating concentrations of antimitotics is DiM (Gascoigne and Taylor, 2008; Topham et al., 2015). Therefore, alterations in this phenotype could be visualised with ease.

5.21 Comparing siRNA and small molecule inhibition of Bcl-xL

As previously eluded to, Bcl-xL shows redundancy with another pro-survival factor, Mcl-1 (Eichhorn et al., 2014). It was shown that HeLa cells were resistant to ABT-263 due to dependency upon Mcl-1 for survival. Overexpressing Bcl-xL and Bcl-2 in the presence of Mcl-1 suppression increased death in response to ABT-263, confirming that redundancy does exist between the pro-survival members. Previously, when both Mcl-1 and Bcl-xL were suppressed in the RKO cell line, potent apoptosis was induced (Sloss et al., 2016; Topham et al., 2015).

Therefore, in order to test the specificity of WEHI-539 in the RKO cell line, I exploited the overlapping functioning that exists with Mcl-1. Firstly, RKO cells were exposed to siRNA specific to both Mcl-1 and Bcl-xL, where immunoblotting confirmed reduced levels of both proteins (Figure 5.1B). Following transfection, cells were imaged on the IncuCyte® Zoom and the level of apoptosis measured (Figure 5.1A-C). Caspase 3/7 activation was measured as an indicator of apoptosis and then values were converted to a % apoptosis (Gascoigne and Taylor, 2008; Topham et al., 2015). For this, caspase values were normalised to the maximum fluorescence reading obtained for each individual experiment and then expressed as a percentage. Consistent with previous studies (Topham et al., 2015), while either siRNA alone resulted in little/no apoptosis, when combined, near 100% apoptosis was apparent, thus confirming that Mcl-1 and Bcl-xL are redundant in the system (Figure 5.1A, C). I next used WEHI-539 in place of siRNA against Bcl-xL, and repeated the same experiment. Results were as previous, where when WEHI-539 and Mcl-1 siRNA were combined near 100% apoptosis was observed (Figure 5.1A, D). These results with the WEHI-539 compound mirror that of the Bcl-xL siRNA, thereby suggesting that WEHI-539 specifically inhibits Bcl-xL.

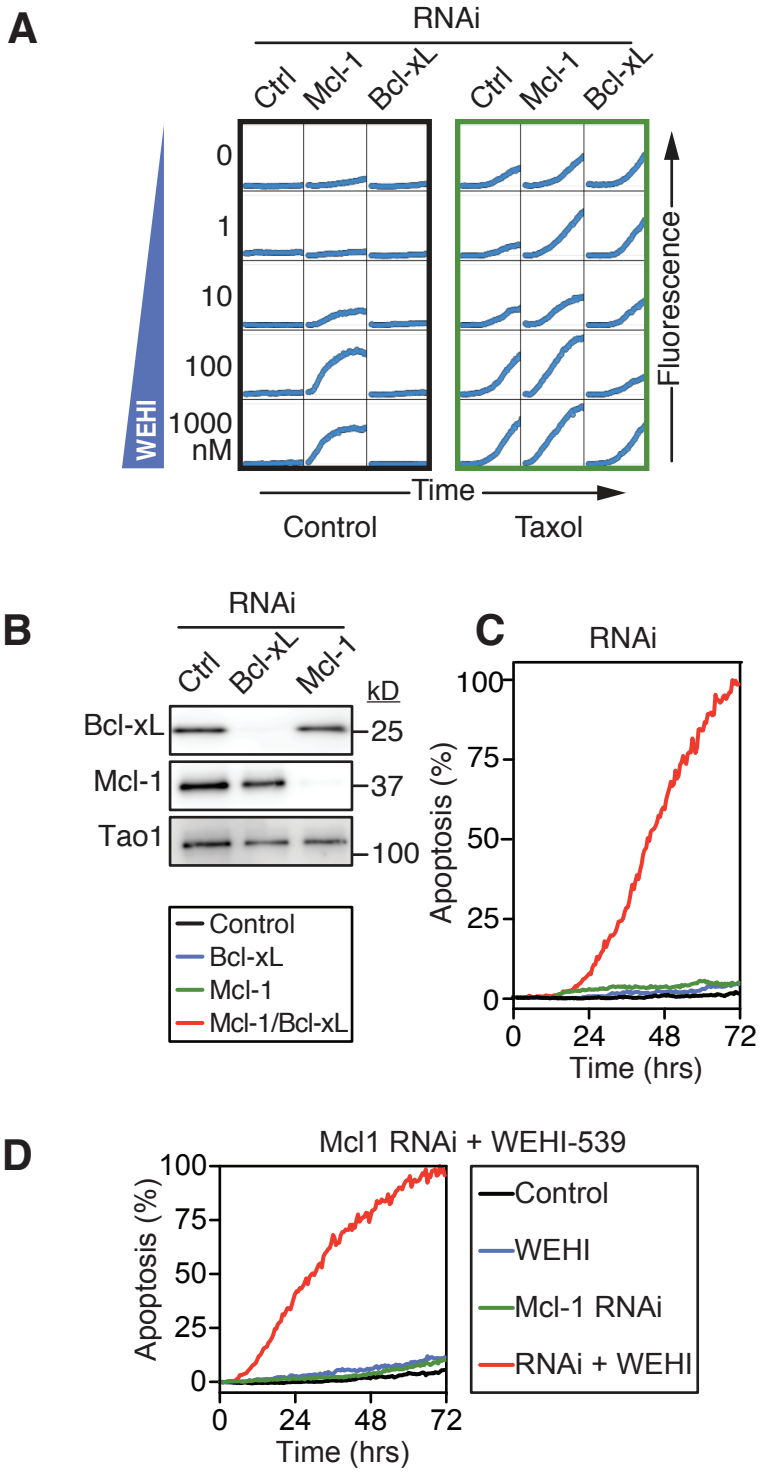

Figure 5.1 Effect of the co-depletion of Mcl-1 and Bcl-xL.
(**A**) Dose matrix plot with non-targeting (NT), Mcl-1 and Bcl-xL RNAi, and various WEHI-539 concentrations, measuring caspase 3/7 (A/U) activation (or fluorescence) as a function of time, +/- 100 nM Taxol, studied in RKO cells.
(**B**) Immunoblot showing the levels of Bcl-xL and Mcl-1 following transient transfection with RNAi for 48 hours in RKO cells.
(**C**) Line graph with the % apoptosis following Mcl-1 and Bcl-xL suppression with RNAi for a 72 hour period in RKO cells.
(**D**) Line graph where % apoptosis was measured over 72 hours after RNAi transfection for NT and Mcl-1 and 100 nM WEHI-539 treatment in RKO cells.

5.22 The effect of WEHI-539 on Bim-induced apoptosis

Bcl-xL and Bim interact, where Bim binds in the BH3 domain of Bcl-xL and is sequestered. Inhibition of this interaction sensitises cells to taxanes such as Taxol (Kutuk and Letai, 2010; Li et al., 2005; Topham et al., 2015). Therefore, I asked whether WEHI-539 was able to intensify apoptosis induced by the overexpression of Bim. RKO cells expressing untagged Bim were exposed to increasing concentrations of tetracycline to express the transgene and both confluency and apoptosis were measured over 72 hours (Figure 5.2A, B, C). As expected, increasing Bim expression increased apoptosis and decreased confluency (Figure 5.2B, C). Cells expressing varying amounts of Bim were then exposed to titrating concentrations of WEHI-539. The lowest tetracycline concentration at which Bcl-xL inhibition enhanced death following transgene expression was then highlighted. These conditions were noted in order to analyse conditions where Bcl-xL inhibition was able to enhance Bim-induced apoptosis, but also to allow for single-cell tracking of behaviour. Observing the line graph in Figure 5.2D, it was apparent that a 30 ng/ml tetracycline concentration gave a moderate level of apoptosis at 72 hours, whilst with the addition of WEHI-539, this was drastically increased. Single cell behaviour analysis revealed even without any other cytotoxic insult, the overexpression of Bim induced apoptosis (Figure 5.2E). It was evident that 26% of cells died in interphase following a mitosis within 9.3 hours, where 85% of these died following the first mitosis, and 15% following the second mitosis. When WEHI-539 was added, 78% of cells underwent apoptosis, where 82% of the total died in interphase following the first mitosis within 2.2 hours. Therefore, WEHI-539 is able to ‘mimic’ the action of a BH3-only protein.

5.23 Examining the effect of WEHI-539 on apoptosis resistance induced by Bcl-xL overexpression

In addition, another approach to test the specificity of WEHI-539 is to determine if the inhibitor reverses a cell fate phenotype induced by Bcl-xL overexpression. Bcl-xL overexpression opposes Taxol-induced apoptosis (Topham et al., 2015). Thus in order to confirm WEHI-539 specifically inhibits Bcl-xL, I reasoned that this resistance to apoptosis should be reversed upon addition of the Bcl-xL inhibitor. RKO myc-Bcl-xL cells were exposed to increasing concentrations of tetracycline and WEHI-539 (Figure 5.3A, B) and apoptosis was measured, with data expressed as a concentration matrix. Following transgene expression (with 100 ng/ml tetracycline) in the presence of 100 nM Taxol, apoptosis was greatly suppressed, confirming previous observations ((Topham

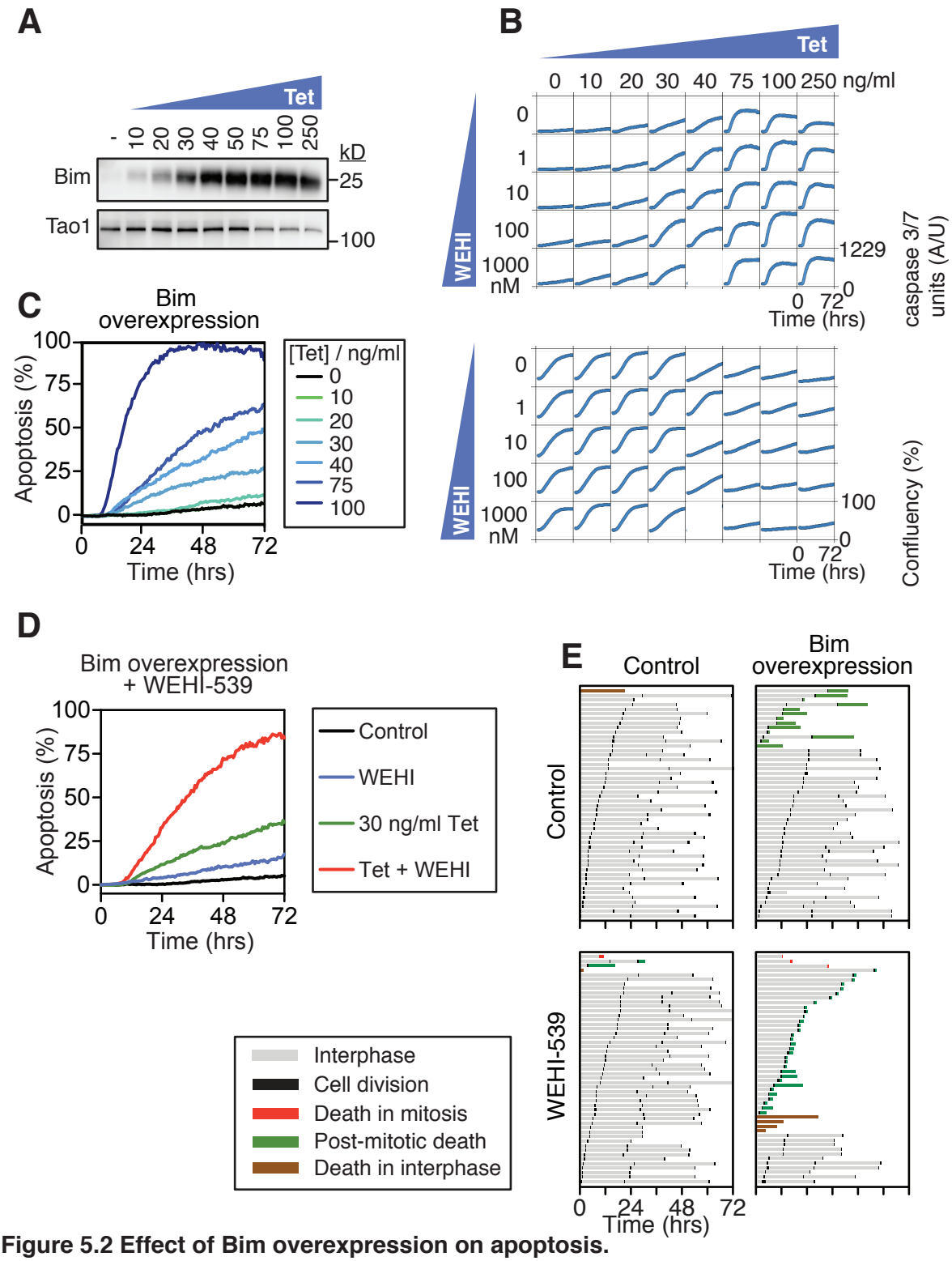

Figure 5.2 Effect of Bim overexpression on apoptosis.
(**A**) Immunoblot showing levels of Bim following incubation of RKO untagged- Bim cells with varying concentrations of tetracycline overnight.
(**B**) Concentration matrix plots measuring caspase 3/7 (A/U) and confluency (%) over a period of 72 hours when RKO Bim cells were exposed to tetracycline and WEHI-539.
(**C**) Line graph showing apoptosis (%) for RKO Bim cells treated with tetracycline for a period of 72 hours. Data is taken from (B).
(**D**) Line graph of the level of apoptosis (%) when overexpressing Bim (30 ng/ml tetracycline) and in the presence of 100 nM WEHI-539 for 72 hours in RKO- Bim cells.
(**E**) Cell fate profiles treated with the combination in (D). Time zero represents when imaging started.

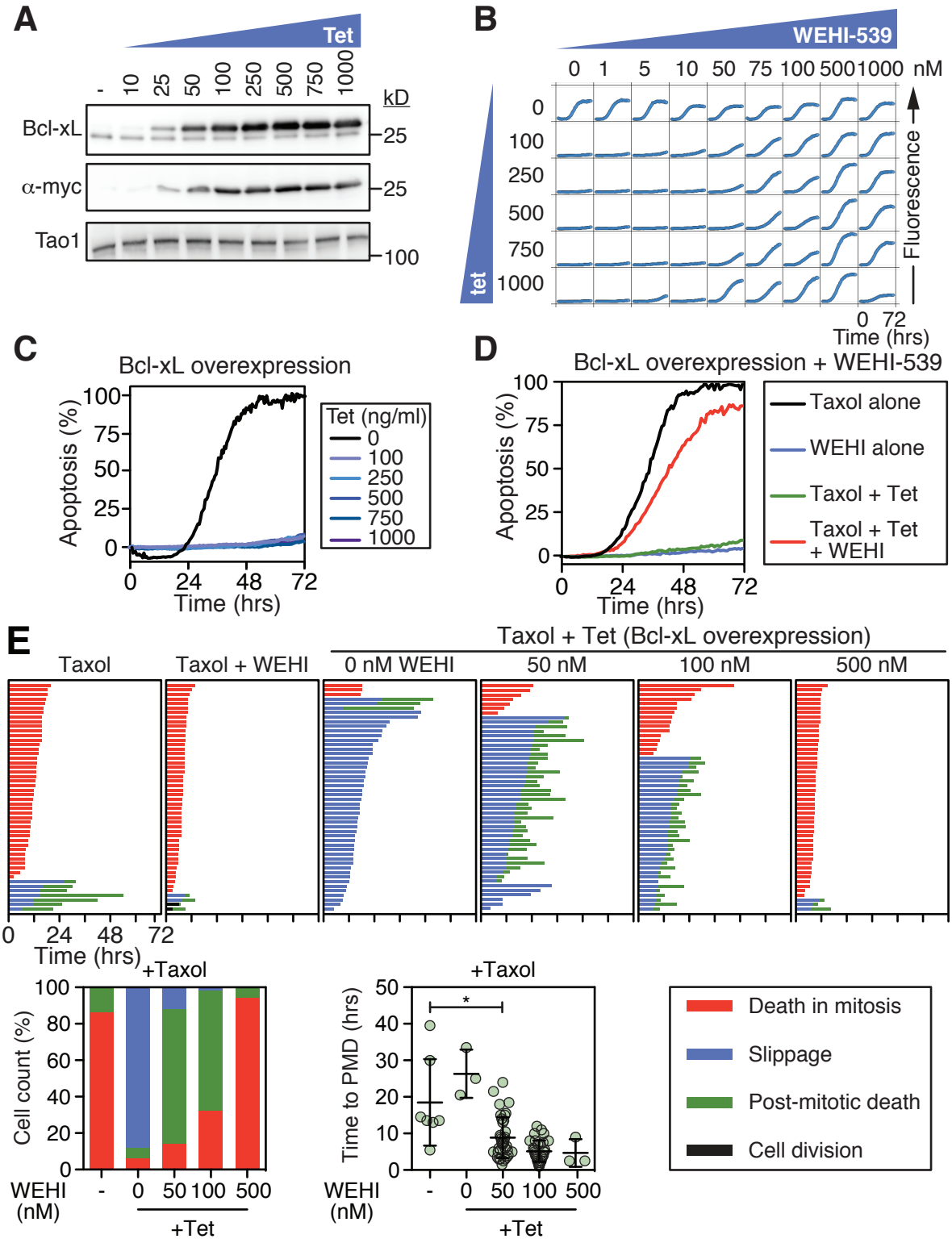

Figure 5.3 Effect of Bcl-xL overexpression on cell fate.

(**A**) Immunblot indicating the levels of myc-tagged Bcl-xL following overnight induction with varying concentrations of tetracycline in RKO myc-Bcl-xL cells.

(**B**) A concentration matix varying the levels of tetracycline and WEHI-539, measuring caspase 3/7 (A/U) over a 72 hour period for the cell line in (A).

(**C**) Line graph of % apoptosis for RKO myc-Bcl-xL cells treated with 100 nM Taxol and exposed to increasing concentrations of tetracycline.

(**D**) Line graph of % apoptosis for the overepression of Bcl-xL in the presence of 100 nM Taxol and 100 nM WEHI-539 in RKO myc-Bcl-xL cells.

(**E**) Cell fate profiles of the conditions depicted in (E) with the addition of various concentrations of WEHI-539. Time zero represents mitotic entry. Bar graph quantifies % cell death and the time to PMD is shown. Mann Whitney U test. *p<0.01.

et al., 2015) and see (Figure 5.3C)). When 100 nM WEHI-539 was added to this system, apoptosis was restored and levels were similar to Taxol-only treated cells (Figure 5.3D). This suggests that WEHI-539 inhibits Bcl-xL.

In previous studies, the overexpression of Bcl-xL resisted both mitotic and post-mitotic apoptosis in Taxol (Topham et al., 2015). Since the addition of WEHI-539 restores apoptosis, I asked whether the death was in mitosis or post-mitosis. To do this I analysed single cell behaviour over a 72 hour time period (Figure 5.3E). Consistent with Topham et al., RKO cells treated with Taxol alone gave 100% death, where 86% died in mitosis (Topham et al., 2015). Although the addition of WEHI-539 did not significantly alter the number of cells dying in mitosis or post-mitosis, DiM was accelerated from 12.7 to 7.7 hours. When Bcl-xL was overexpressed, a potent pro-survival effect was observed, where death was reduced to 12% and 88% of the cells analysed underwent slippage after an average mitotic arrest of 18.8 hrs. It was interesting to note that analysing cells at 50 nM, 100 nM and 500 nM of WEHI-539 showed a dose-dependent effect. At 50 nM, 88% did die, but of these, 84% died following exit from mitosis. When WEHI-539 was increased to 100 nM, although the total number of cells undergoing death was maximum at 100%, the number of cells dying following exit reduced to 68%, with the rest dying in mitosis. At both of these concentrations the time to PmD was accelerated. At 500 nM of WEHI-539, 94% died in mitosis after an average 9.5 hours, similar to control cells. This indicates that Bcl-xL is a potent pro-survival factor, exhibiting its effect in both mitosis and following exit.

5.24 Examining the effect of WEHI-539 on the interactions between Bcl-xL and its binding partner proteins

To further validate WEHI-539 as a Bcl-xL inhibitor, I looked at the interactions between Bcl-xL and its binding partners, where Bcl-xL interacts with Bim, Bid, Bad, Bax and Bak (Chen et al., 2005; Sattler et al., 1997). As WEHI-539 is a BH3 mimetic, it should compete with the proteins to bind in the BH3 domain, reducing the protein-protein interactions. To test this I expressed GFP- Bcl-xL in RKO cell lines using tetracycline and harvested cells for immunoprecipitation (Figure 5.4A). To detect interacting partners of the exogenous protein, a GFP-binder protein was used to pull down GFP-Bcl-xL (Rothbauer et al., 2007; Sloss et al., 2016). An immunoblot of the input samples for each condition confirmed the addition of protein sample prior to affinity purification (Figure 5.4B). Immunoblots of the immunoprecipitated proteins indicated that when exogenous GFP-Bcl-xL was expressed, Bim, Bad, Bak and Bax

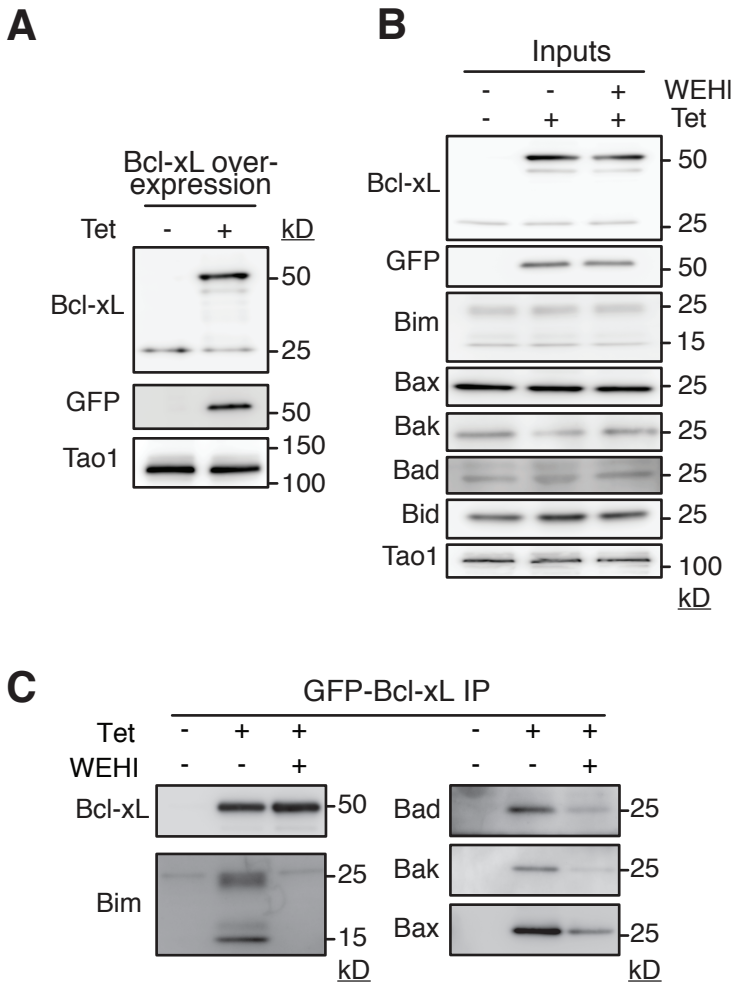

Figure 5.4 Effect of WEHI-539 on the interaction between Bcl-xL and its binding partners.
(**A**) Immunoblot showing the overexpression of GFP-Bcl-xL in RKO cells, following incubation with 100 ng/ml of tetracycline overnight.
(**B**) Immunoblot showing the input samples prior to affinity purification -/+ 100 ng/ml tetracycline and -/+ 100 nM WEHI-539, using the cell line in (A).
(**C**) An immunoblot showing the protein levels of Bcl-xL and its binding partners following overnight incubation with 100 ng/ml tetracycline and 100 nM WEHI-539, followed by affinity purification of the complexes, using the cell line in (A).

were affinity purified, thus confirming Bcl-xL interaction with these proteins (Figure 5.4C). In contrast, addition of 100 nM WEHI-539 inhibited immunoprecipitation of these proteins, suggesting that the agent interferes specifically with these interactions. This confirms that WEHI-539 is most likely docking in the BH3 domain of Bcl-xL, preventing the sequestration of the pro-apoptotic proteins.

5.3 Investigating the combination of WEHI-539 and antimitotics

Following confirmation of WEHI-539's specificity for Bcl-xL, I then used the inhibitor to study cellular fate following mitotic perturbation. The combination of antimitotics with inhibitors against the pro-survival proteins is not a new concept. Previous analyses have shown that the combination of ABT-737 and paclitaxel or an Eg5 inhibitor results in synergistic death (Bah et al., 2014; Chen et al., 2011; Kutuk and Letai, 2008; Oltersdorf et al., 2005; Shi et al., 2011). Studies focused on whole population apoptosis, with only some single cell analysis (Bah et al., 2014). Using single-cell tracking allows the careful observation of cellular behaviour over time, where these behaviours would not be observed if using techniques such as whole population apoptosis analysis (e.g. FACS, or annexin V assays). Furthermore, only Taxol and an Eg5 inhibitor have been previously analysed. Reports have also used ABT-737, which hits a number of pro-survival proteins and therefore, teasing apart the contribution of the individual apoptotic members to death is difficult. Together with previous evidences of synergy, and the fact that c-myc was shown to downregulate Bcl-xL in order to regulate DiM, this gives a sound rationale to study the combinatorial effect of Bcl-xL inhibition using WEHI-539 and antimitotics (including mitotic blockers and drivers) further.

5.31 The effect of Bcl-xL inhibition and mitotic blockers

Firstly, I gave focus to mitotic blockers which induce a mitotic arrest, preventing mitotic progression. I gave initial attention to the microtubule-targeting agents (MTA's) Taxol and nocodazole. These are part of the original class of antimitotics, where Taxol is used commonly in the clinic for treatment of breast and ovarian cancers, whilst nocodazole is used in cell biological contexts.

In the first instance, I concentrated on the microtubule-stabilising agent paclitaxel. I titrated various concentrations of paclitaxel along one axis, followed by WEHI-539 along the other, giving a total of 35 wells imaged (Figure 5.5A, left matrix). Again, to analyse the cell death quantitatively, the caspase 3/7 marker was used. From

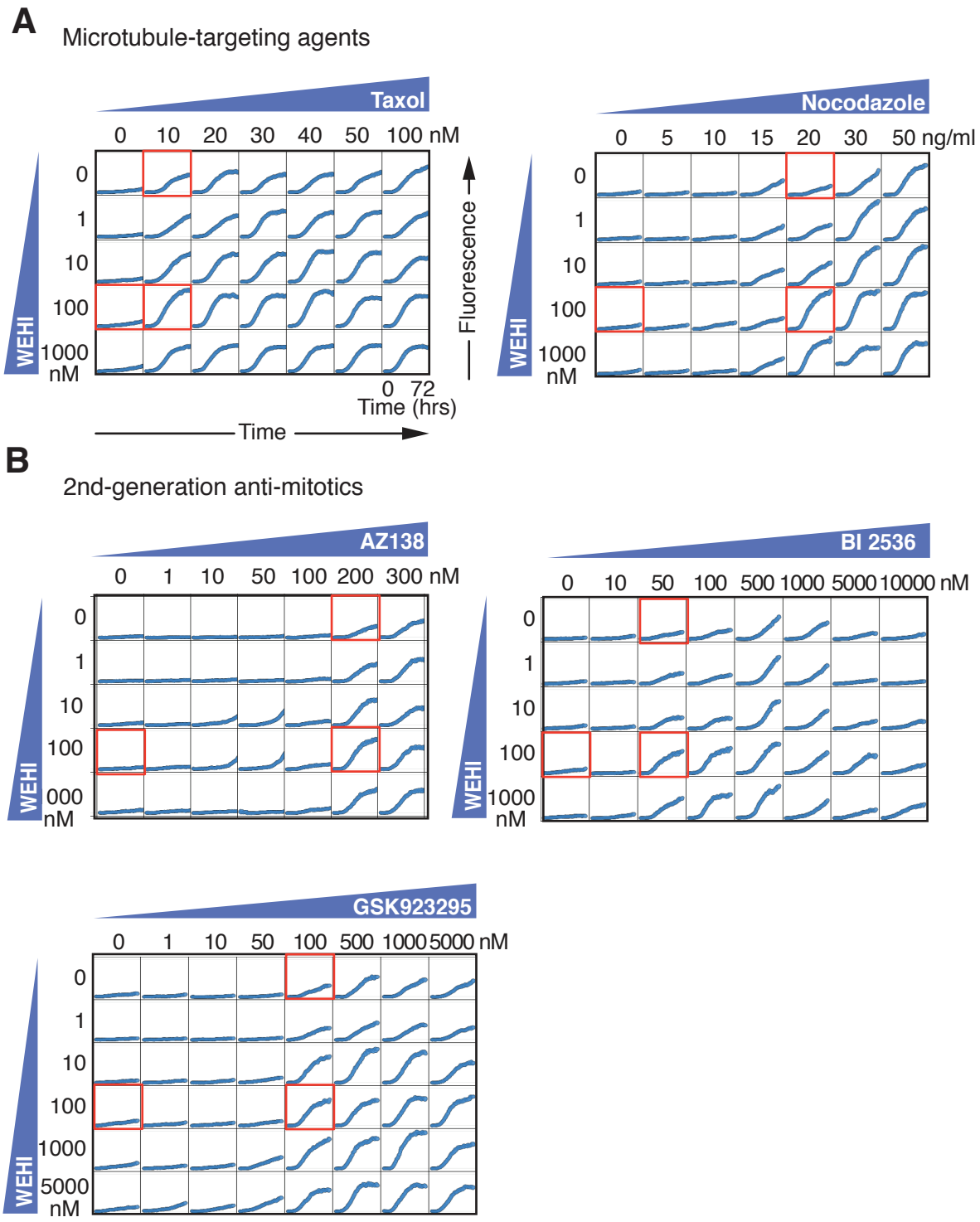

Figure 5.5 Effect of the combination of WEHI-539 and mitotic blockers.
(**A**) Dose matrix plots of microtubule-targeting agents Taxol and nocodazole against WEHI-539 over 72 hours, measuring caspase 3/7 (A/U), in RKO cells.
(**B**) Dose matrix plots of AZ138, BI 2536 and GSK923295 against WEHI-539 over 72 hours and measuring caspase 3/7 (A/U) activation, in RKO cells.

the concentration matrix, this allowed me to highlight the lowest concentration of Taxol for which the addition of WEHI-539 increased death, enabling me to carefully evaluate the contribution of Bcl-xL to the observed death. As highlighted, addition of separate treatments of 10 nM Taxol and 100 nM WEHI-539 resulted in 46% and 11% apoptosis respectively, but combining the drugs caused a potent induction of apoptosis (100%) (Figure 5.6A, left).

Next, I turned my attention to the microtubule-depolymerising mitotic blocker nocodazole. Under similar conditions, increasing the concentration of nocodazole gave rise to increasing apoptosis, evident after 15 ng/ml (Figure 5.5A, right matrix). From the matrix, the lowest concentration of nocodazole where the addition of WEHI-539 gave an increase in apoptosis was highlighted, here being 20 ng/ml and 100 nM WEHI-539, where 23% and 11% apoptosis was observed (Figure 5.6A, right). When the agents were combined 99% apoptosis was induced.

Following on from the microtubule-targeting agents, I next moved onto second-generation antimitotics, whose mechanism of action is similar to MTA's, with the induction of a mitotic arrest due to the perturbation of spindle assembly (Jackson et al., 2007; Keen and Taylor, 2009). This class of agents includes inhibitors targeting Eg5, Plk-1 and Cenp-E. Due to the similar effect on mitotic progression, I then asked whether combining these agents with Bcl-xL inhibition would result in an increased sensitisation to apoptosis.

Considering the motor protein Eg5, AZ138 exposure results in a monopolar spindle phenotype, activating the SAC and preventing mitotic progression (Gascoigne and Taylor, 2008). RKO cells were treated with increasing concentrations of AZ138, titrated against WEHI-539 (Figure 5.5B, top left). AZ138 resulted in little apoptosis until 200 nM, where 51% apoptosis was observed. This was further increased to 85% apoptosis with the addition of 100 nM WEHI-539 (Figure 5.7A, top). Furthermore, Plk-1 is a mitotic kinase, with functions implicated in mitotic entry (Zitouni et al., 2014). Upon targeting by genetic perturbation or small molecule inhibitors, cells arrest in mitosis due to the generation of a monopolar spindle, with failure to satisfy the SAC (Aspinall et al., 2015; Hanisch et al., 2006; Steegmaier et al., 2007; Sumara et al., 2004; Van Vugt et al., 2004). To inhibit Plk-1 I used BI2536 (Steegmaier et al., 2007). In a similar fashion to previous experiments, BI2536 was titrated against WEHI-539 (Figure 5.5B, right). At 50 nM BI2536, 100 nM of WEHI-539 enhanced apoptosis from 21% to 71%. (Figure 5.7A, middle). Interestingly at higher concentrations of BI2536, apoptosis was reduced, which has been indicated previously (Aspinall et al., 2015; Raab et al., 2015, 2014).

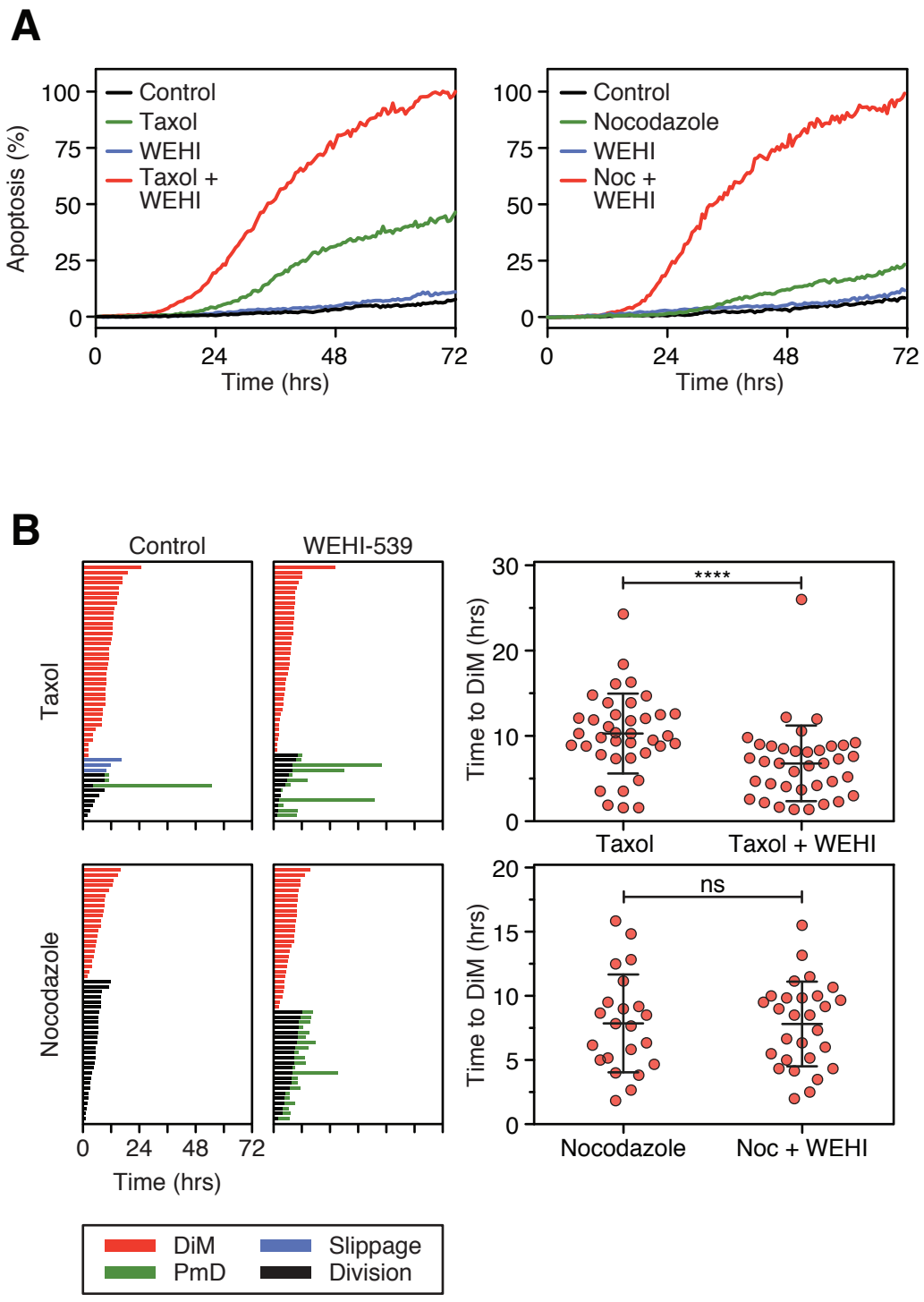

Figure 5.6 Analysing cell death in response to microtubule-targeting agents and WEHI-539.

(**A**) Line graphs measuring apoptosis (%) in response to Taxol (10 nM) or nocodazole (20 ng/ml) and WEHI-539 (100 nM), in RKO cells.

(**B**) Cell fate profiles of conditions in (A), with timing to DIM quantified. Time zero represents mitotic entry. Mann Whitney U test. ns $p>0.05$, ****$p<0.0001$.

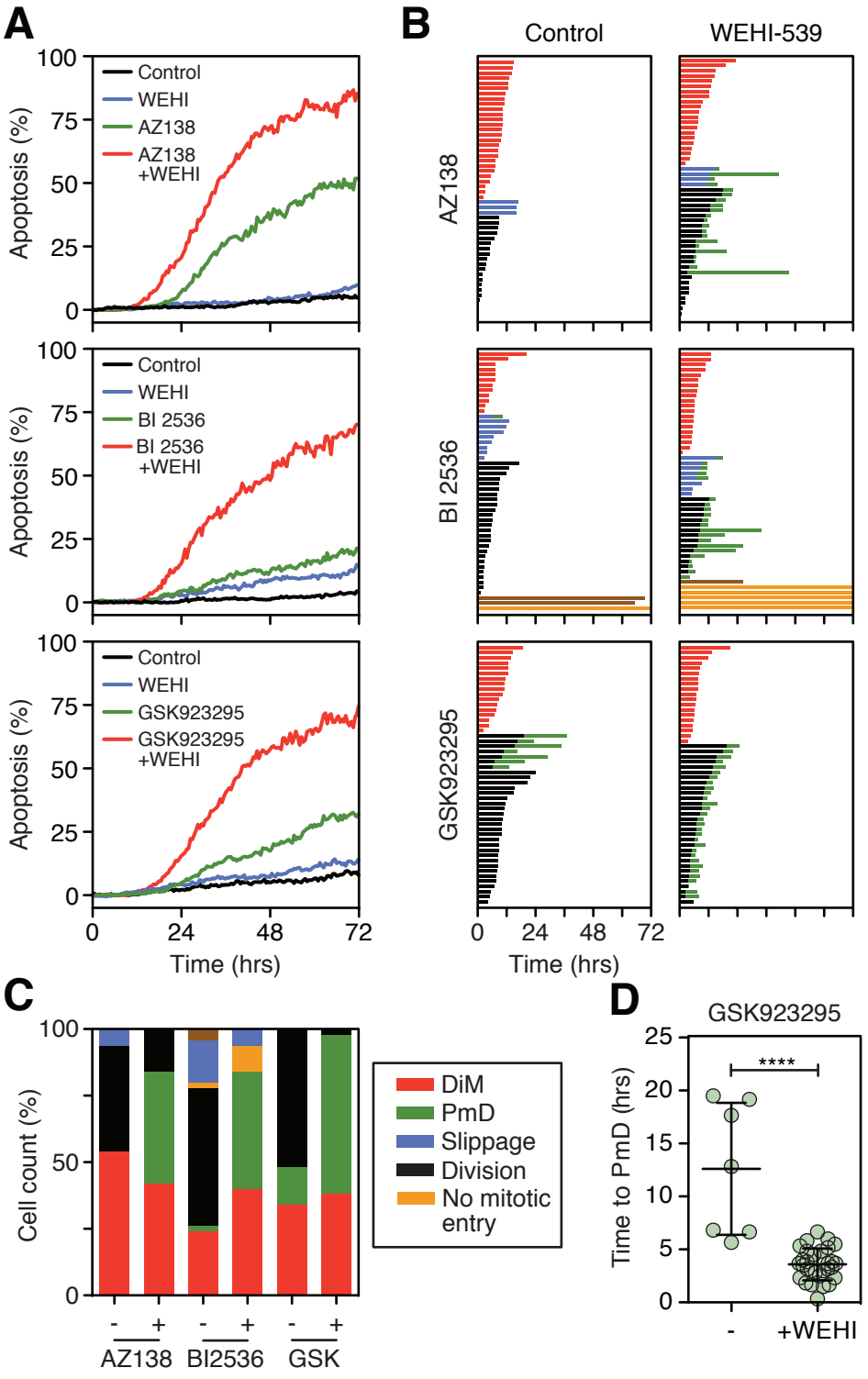

Figure 5.7 Analysis of cell fate with second generation anti-mitotics and WEHI-539 combination.

(**A**) Line graphs measuring apoptosis (%) for the combination of AZ138 (200nM), BI2536 (50 nM) or GSK923295 (100 nM) and WEHI-539 (100 nM), in RKO cells.

(**B**) Cell fate profiles of the conditions in (A). Time zero represents mitotic entry.

(**C**) Quantification of cellular fate, from (B).

(**D**) Quantification of time to PMD, from (B). Mann Whitney U test. ****p<0.0001.

The addition of WEHI-539 did not increase this further. Lastly, using the Cenp-E inhibitor GSK923295 (Wood et al., 2010), that was synthesised and characterised in Chapter 4, I titrated the two drugs against one another, with apoptosis evident with GSK923295 from 100 nM (Figure 5.5A, bottom left). At 100 nM of GSK923295, 32% of cells died, increasing to 75% with the addition of 100 nM WEHI-539 (Figure 5.7A, bottom).

Therefore, when considering the second-generation inhibitors against Eg5, Plk-1 and Cenp-E, each agent alone induced enhanced apoptosis with increasing concentrations. Importantly, the concentration matrix approach allowed the identification of cases where WEHI-539 was able to enhance cell death. In all cases, the combination of antimitotic and Bcl-xL inhibitor significantly enhanced the level of apoptosis.

5.32 Determining when cells are dying: in mitosis or post-mitosis

I have previously shown that in the Bcl-xL overexpressing cells, the addition of WEHI-539 accelerates PmD (Figure 5.3E) and also, when added to Taxol-treated cells, WEHI-539 increases the level of and reduces time to DiM ((Bah et al., 2014) and see (Figure 5.3E, 5.6B)). To see if WEHI-539 had an effect on both PmD and DiM with the mitotic blockers, I chose the lowest concentration of each blocker and together with the Bcl-xL inhibitor, plotted cell fate profiles. These were generated by analysing phase-contrast movies and following single cells over time. At the concentrations highlighted, a mixture of fates were obtained, including DiM, PmD, division and mitotic exit. This heterogeneity allowed me to analyse both DiM and PmD at the same time.

Firstly, considering Taxol, when RKO cells were exposed to 10 nM, 76% underwent DiM after a period of 10.3 hours. Furthermore, 12% underwent division after a prolonged arrest, and then arrested in the following interphase for the remainder of filming (Figure 5.6B, top). When 100 nM WEHI-539 was added, the cells that divided then underwent PmD after 10.6 hours. Of particular note, time to DiM was also accelerated from 10.3 to 6.8 hours. This infers again that Bcl-xL Is important for survival both during mitosis and following a perturbed mitosis. To confirm this observation, other combinations were analysed similarly. In nocodazole-treated cells, 44% died in mitosis, and 56% divided then arrested in interphase (Figure 5.6B, bottom). Upon addition of WEHI-539 the cells that divided then underwent death post-mitosis. There was no acceleration of timings to DiM here, indicating that Bcl-xL plays a role for survival following mitosis in this particular case. Although the mechanism of

WEHI-539 action with the two drugs may be different, these observations enhance those described previously (Leverson et al., 2015a).

I next analysed the second-generation inhibitors to determine where WEHI-539 was eliciting its effect. Treatment of cells with 200 nM AZ138 gave 54% DiM and 40% division (Figure 5.7B,C). After WEHI-539 was added although the number dying in mitosis was relatively unchanged, 58% died following division or exit with an average time of 6.9 hours. Furthermore, RKO cells treated with 50 nM BI2536 mostly showed a survival phenotype, where only 24% died in mitosis and 52% divided, with no resulting PmD. After exposure to WEHI-539, 42% died in interphase after exit or division. At higher concentrations of BI2536, for example 100 nM and 500nM, most of the cells underwent DiM or PmD following mitotic exit (Figure 5.8A, B). When cells were exposed to WEHI-539, PmD was accelerated. With 500 nM BI2536, time to PmD was reduced from 9.1 to 2.4 hours (Figure 5.8C). Lastly, at 100 nM GSK923295, 66% of cells divided, with 21% of these dying in the following interphase after 12.6 hours (Figure 5.7B,C). After WEHI-539 addition, 97% of those that divided underwent PmD after 3.6 hours. The striking acceleration to PmD with the GSK923295 and WEHI-539 combination (Figure 5.7D), indicates the importance of Bcl-xL for survival post-mitosis.

From the analysis, the prominent effect WEHI-539 has on PmD suggests the importance of Bcl-xL for survival following a mitotic arrest induced by MTA's or second-generation inhibitors. In general, there is little effect on timings or the level of DiM.

5.33 The effect of a WEHI-539 and mitotic driver combination

As with the second-generation inhibitors, which affect spindle assembly but have little effect on microtubule dynamics, a class of mitotic drivers have also been of interest. These include inhibitors of the kinases Aurora A, Aurora B and Mps1. It would be expected that targeting these kinases would activate the SAC, however, their role in spindle checkpoint function causes deficient cells to enter anaphase and exit an aberrant mitosis, in the presence of unaligned or non-segregated chromosomes (Keen and Taylor, 2009).

Inhibition of Aurora A induces a monopolar spindle (Glover et al., 1995; Manfredi et al., 2007) and targeting is of interest in a clinical setting (Nigg, 2001; Taylor and Peters, 2008), including with the inhibitor MLN8054 (Manfredi et al., 2007). Furthermore, studies on Aurora A inhibitors indicated for example, that ZM447439 had an increased preference for Aurora B, where cells were driven through an aberrant mitosis, overriding the SAC (Ditchfield et al., 2003; Keen and Taylor, 2009). This

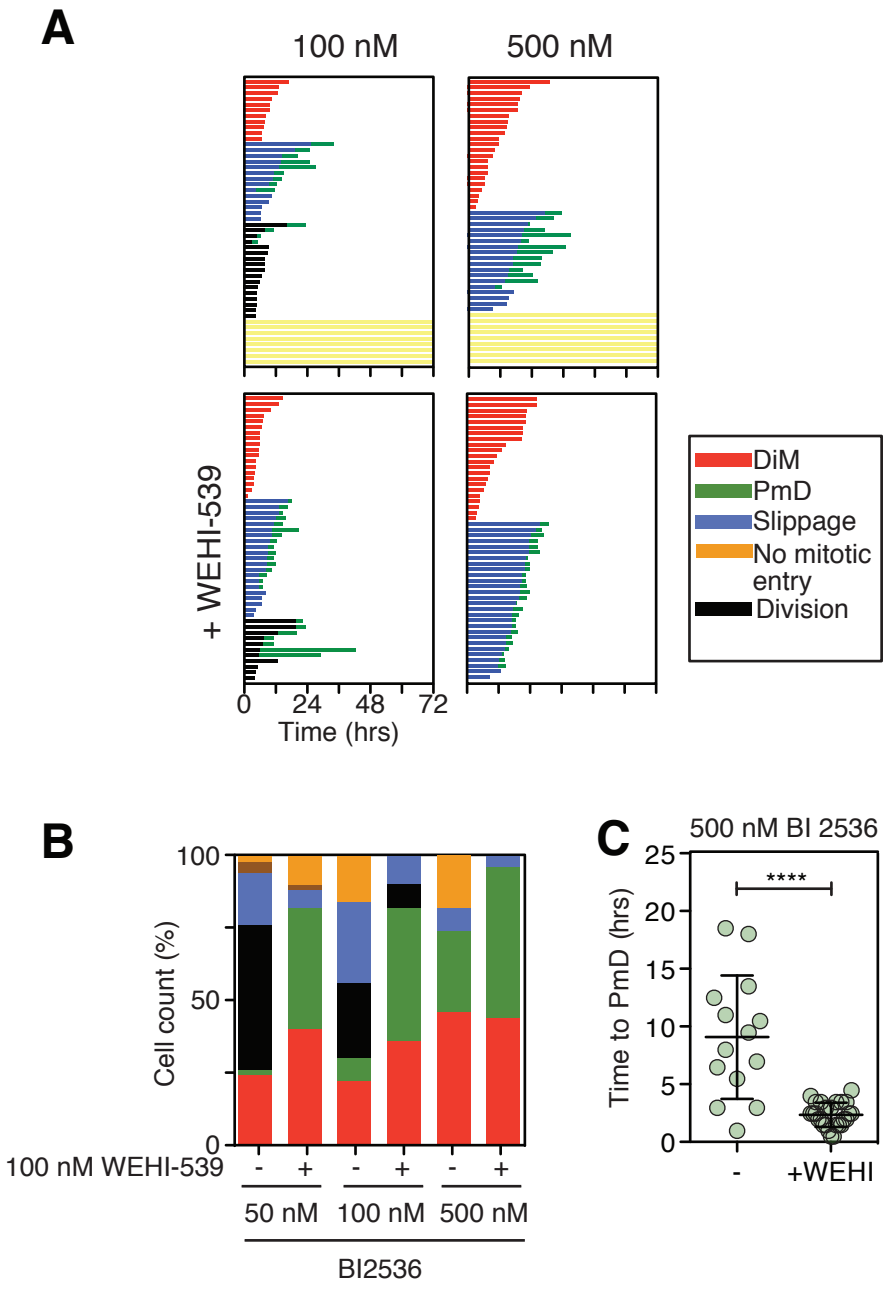

Figure 5.8 Analysing cellular fate with BI2536 and WEHI-539.
(**A**) Cell fate proiles of RKO cells treated with 100 or 500 nM of BI2536 and 100 nM WEHI-539. Time zero represents mitotic entry.
(**B**) Quantification of cell behaviour from (A) and from data in Figure 5.7B.

marked the first use of the term ‘mitotic driver’. Targeting other SAC components in a similar fashion led to the Mps1 inhibitor AZ3146 (Hewitt et al., 2010), where similarly cells override the checkpoint. Consequently, I chose to turn my attention to this class of inhibitors, driven by the lack of studies involving the combination of drivers and pro-survival inhibition. Thus, I next aimed to determine if the use of drivers and WEHI-539 together resulted in a synergistic effect in a similar way to that of the mitotic blockers.

Initially, I titrated various concentrations of the mitotic drivers MLN8054 (Aurora A), ZM447439 (Aurora B) and AZ3146 (Mps1) against WEHI-539 (Figure 5.9). At increasing concentrations of MLN8054 and ZM447439 the inhibitors induced little apoptosis alone. This is in contrast to the Mps1 inhibitor AZ3146, where at concentrations of 1 μM and above, late apoptosis was initiated (Figure 5.9, bottom). In contrast to the mitotic blockers, when WEHI-539 was combined with the mitotic drivers, little effect or enhancement of cell death was observed. However, when highlighting particular concentrations of the drivers and WEHI-539 concentrations, the AZ3146 and WEHI-539 combination did show a small increase in apoptosis (Figure 5.10A, bottom). Analysing this effect with single cell tacking confirmed that apoptosis was enhanced in this setting, where PmD increased from 38% to 62%, with an acceleration to death of 4 hours (Figure 5.10B). In contrast, for cells exposed to the Aurora A inhibitor, WEHI-539 had no observable impact on fate, with 100% dividing and surviving. With ZM447439, cells exited mitosis without dividing, with 72% of cells undergoing a second or third cytokinesis failure following interphase. When WEHI-539 was added to these cells, 6% underwent PmD but the majority were unaffected.

One possible explanation for the lack of WEHI-539-induced sensitivity to death is that the mitotic drivers were not added at sufficient concentration to inhibit the relevant kinase. One way this can be validated is to check the drug phenotype using cell fate profiling, with analysis of the cell behaviour at the concentrations in Figure 5.10A. I followed single cells for all conditions and compared the time in the first mitosis with untreated control cells (Figure 5.10B, 5.11A). Inhibiting Aurora A caused a slight delay in mitosis followed by division, with an increase from 0.3 hours to 0.9 hours. Aurora B inhibition also increased the time in the first mitosis to 0.9 hours, with a resulting cytokinesis failure. On the other hand, targeting Mps1 accelerated the time in the first mitosis to 0.26 hours. These deviations from normal mitotic timings suggest that the concentrations used do inhibit the kinases under analysis. Of particular note is the concentration of MLN8054 used. Previous studies have shown 1 μM inhibits Aurora

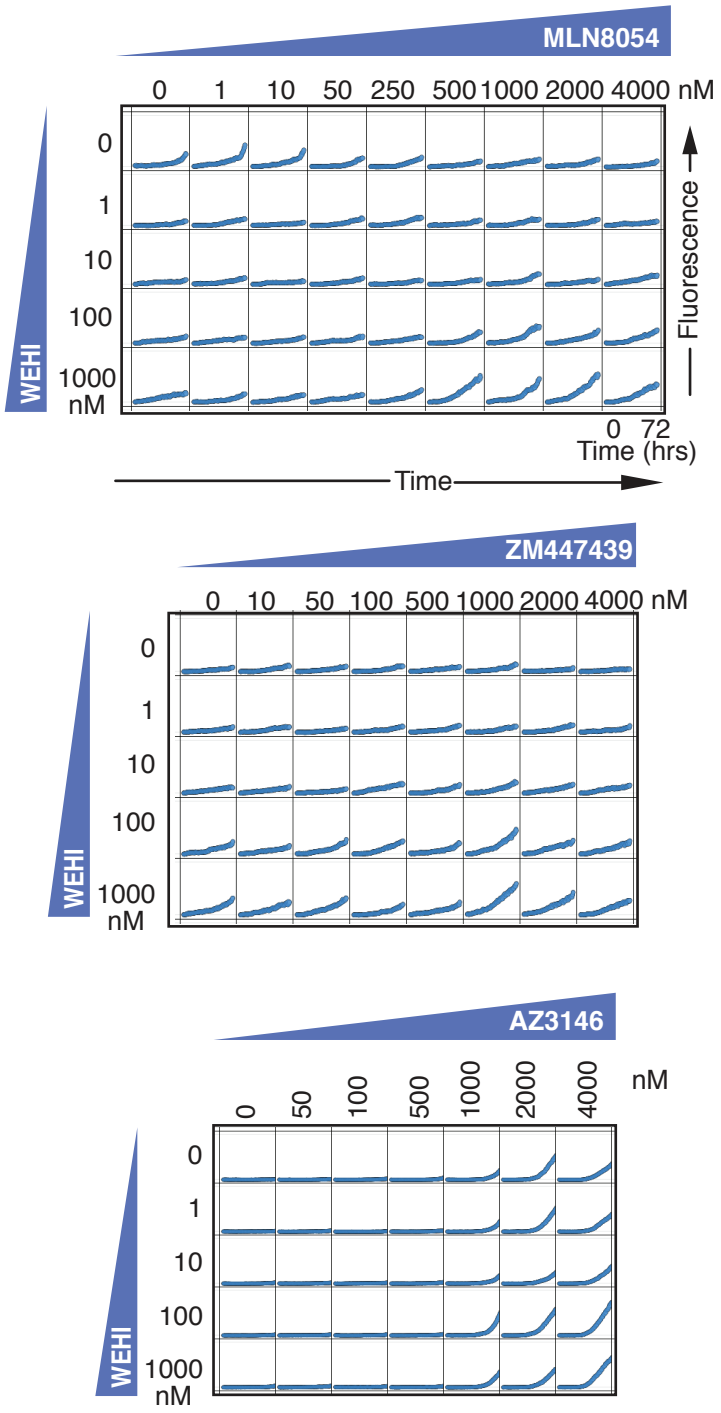

Figure 5.9 Effect of the combination of WEHI-539 and mitotic drivers.
Dose matrix plots of MLN8054, ZM447439 and AZ3146 when combined with WEHI-539. Caspase 3/7 (A/U) as fluorescence is measured over 72 hours, in RKO cells.

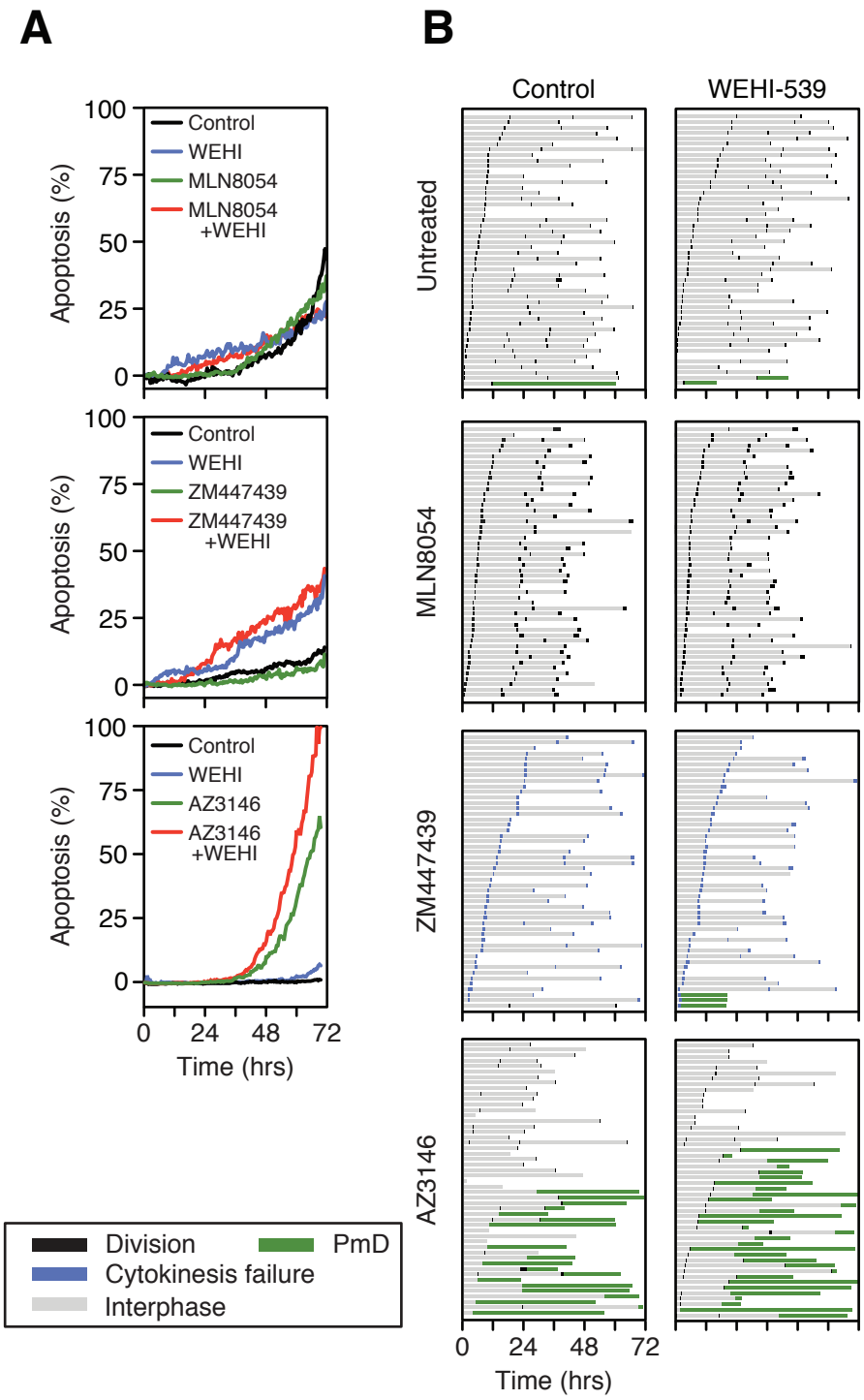

Figure 5.10 Analysis of cell fate with mitotic drivers and WEHI-539.
(**A**) Quantification of the time in the first mitosis for exposure of RKO cells to MLN8054 (250 nM), ZM447439 (2 µM), and AZ3146 (2 µM).
(**B**) Line graphs measuring apoptosis (%) for the combination of MLN8054 (250 nM), ZM447439 (2 µM), AZ3146 (2 µM) and WEHI-539 (100 nM).
(**C**) Cell fate profiles of the conditions in (B). Time zero represents when imaging started.

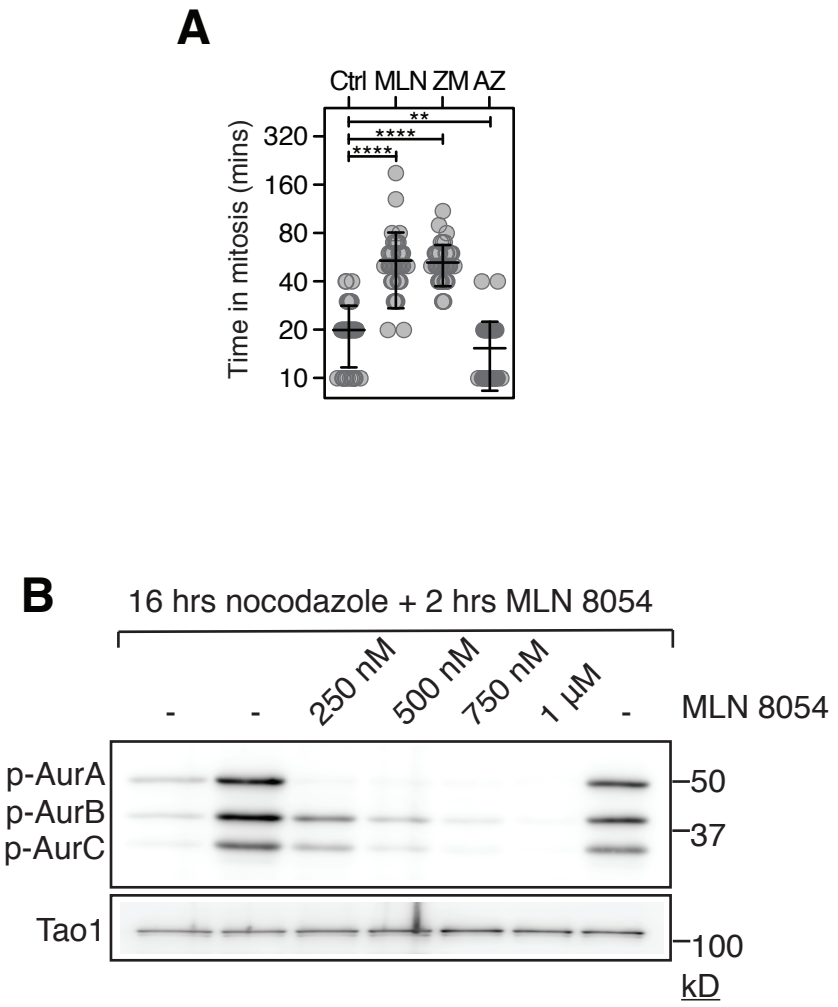

Figure 5.11 Effect of mitotic drivers on mitosis.
(**A**) Box and whisker plot showing the time in mitosis for control, MLN8054, ZM447439 and AZ3146 treated RKO cells. This is related to the conditions in Figure 5.10. Mann Whitney U test. **p<0.01, ***p<0.001, ****p<0.0001.
(**B**) Immunoblot for the protein levels of phosphorylated Aurora A, B and C when RKO cells were exposed to 30 ng/ml nocodazole for 16 hours and the Aurora A inhibitor, MLN8054 for 2 hours, followed by protein harvesting. A pan-Aurora antibody was used to detect endogenous levels of Aurora A/B/C when phosphorylated at either Thr288, Thr232 or Thr198 respectively.

A kinase activity (Manfredi et al., 2007), but here I indicated that 250 nM is sufficient to block its activity, as higher concentrations may also hit Aurora B and C (Figure 5.11B).

Therefore, although WEHI-539 is able to sensitise cells to mitotic blockers, there is little effect when combined with mitotic drivers. This indicates the importance of Bcl-xL for survival following a protracted mitosis, but when cells do not arrest and are driven through an abnormal mitosis, cells are less dependent upon Bcl-xL for survival.

5.34 Determining synergistic combinations

Based on the combinatorial studies, it is likely that there are synergistic combinations between the antimitotic blockers and WEHI-539. In order to define 'how synergistic' the combinations are, there are a number of models that can be used. These include: (i) Highest Single Agent (HSA) model; (ii) Bliss additivism model; (iii) Lowe model (Borisy et al., 2003). For purposes here, the Bliss model (Lehár et al., 2009; Wong et al., 2012) was chosen, where this assumes that the drugs inhibit independent sites, with mutually non-exclusive binding. Figure 5.12 gives an overview of how to calculate the synergy scores. For each individual matrix in Figures 5.5 and 5.9, the maximum fluorescence observed was noted (as caspase 3/7). Then, for each distinct well, the fluorescence for the 72 hour time point was expressed as a percentage of the maximum. From this, an *expected* synergy score for the combination of the two drugs was defined e.g. if drug A inhibition = 0.8 (i.e. 80% of the maximum for the experiment) and drug B = 0.2, then the *expected score* (C) = (0.8 + 0.2) – (0.8 x 0.2) = 0.84. If the actual response (D) was 0.9, then the *Bliss score* will be E = 0.9 – 0.84 x 100 = 6. This is a small positive value, but indicates a slight synergistic interaction for the combination. All scores for the individual wells were calculated similarly and then summated to give the *Bliss Sum*. Here, a positive value indicates *synergy*, a negative value *antagonism* and a score of zero indicates an *additive* interaction or zero interaction.

Initially, following this method, I then calculated Bliss Scores and Sums for the mitotic blockers and WEHI-539 combinations. Using Excel, I converted the Bliss Scores into heat maps, where green indicated synergy (positive value), red antagonism (negative value) and white no effect (zero number). Observing the heat maps in Figure 5.13 it is evident that for Taxol, most combinations are synergistic, indicated by the large number of green boxes. When the Bliss Score system was also applied to cells treated with nocodazole, AZ138, BI2536 and GSK923295, synergistic combinations were apparent in all matrices. If the heat maps are compared alongside the dose

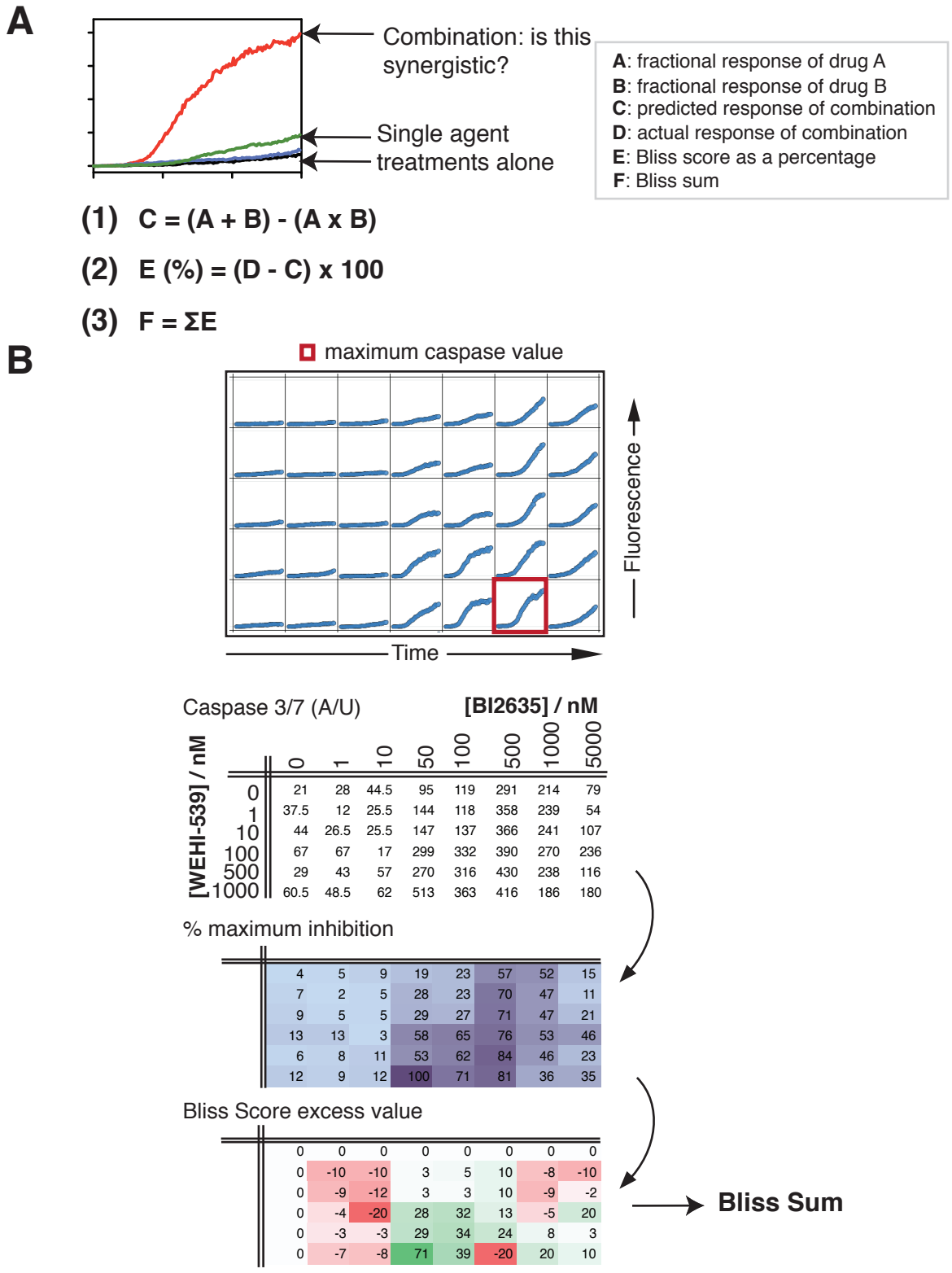

Figure 5.12 Calculating Bliss Scores and Sums.
(**A**) The formulae used for the determination of the Bliss Scores and Sums.
(**B**) The process by which the Bliss Sums were calculated. From the caspase 3/7 (A/U) profiles obtained from the IncuCyte® Zoom, the percentage of the maximum inhibition was calculated by identifying the maximum caspase value for the experiment. From this the expected and actual values were compared for each well, and then the Bliss Scores were summated to give the Bliss Sums.

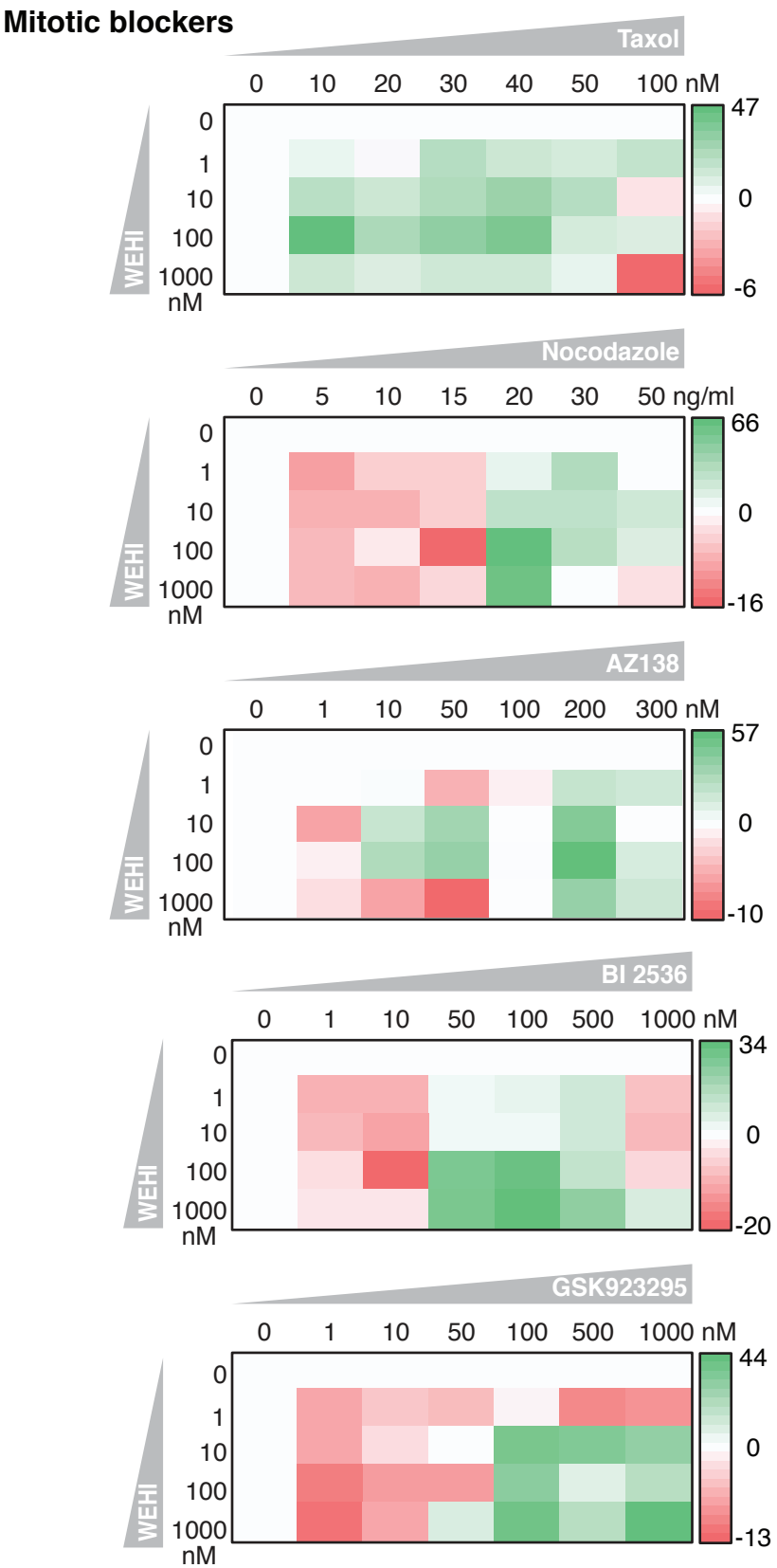

Figure 5.13 Determining Bliss Scores for mitotic blockers.
Using the method described in Figure 5.12, Bliss scores were calculated for the drug combinations of Taxol, nocodazole, AZ138, BI2536, GSK923295 with WEHI-539. From the Bliss Scores, heat maps were generated where green indicates positive (synergistic), and red, negative (antagonistic) scores.

matrices in Figure 5.5, they correlate well. For comparison, I calculated scores for the mitotic drivers similarly (Figure 5.14), and it became apparent that most interactions were antagonistic, indicated by the red boxes; an observation that also coincides with the dose matrices in Figure 5.9.

Bliss Scores were summated across the concentration matrix to give a Bliss Sum for each individual antimitotic and WEHI-539 combination (Figure 5.15). This enabled for comparison between all blockers and drivers. Overall, all mitotic blockers gave positive synergistic Bliss Sums, and the drivers negative antagonistic values. One exception was the Mps1 inhibitor, where a small positive value was seen. Thus, the Bliss Sums obtained were consistent with the observations made previously.

5.4 Investigating the role of Mcl-1 in survival

In order to understand why Bcl-xL inhibition only sensitises cells to mitotic blockers, but no significant effect is seen with the mitotic drivers, I turned my attention to another pro-survival factor Mcl-1. A likely explanation for the differential sensitivity stems from the redundancy that exists between Mcl-1 and Bcl-xL ((Eichhorn et al., 2014) and also see (Figure 5.1)). In contrast to other pro-survival proteins, Mcl-1 is degraded throughout a mitotic arrest (Harley et al., 2010; Millman and Pagano, 2011; Sloss et al., 2016; Wertz et al., 2011). Thus, in cases where cells undergo a mitotic arrest, Mcl-1 will be degraded, and cells will become increasingly dependent upon Bcl-xL for survival. Therefore, inhibition of Bcl-xL in these cases will largely tilt the balance towards death due to a reduced pro-survival/pro-apoptotic ratio. Conversely, in situations where Mcl-1 is not degraded (e.g. with the addition of mitotic drivers), the un-degraded pool of Mcl-1 would compensate for Bcl-xL inhibition to maintain pro-survival signalling.

5.41 Studying Mcl-1 levels in the presence of a mitotic blocker and driver

To confirm that Mcl-1 is compensating for the loss of Bcl-xL when cells are exposed to drivers, I compared the Mcl-1 protein levels following treatment with a mitotic blocker and a mitotic driver (Figure 5.16). RKO cells were treated with thymidine to synchronise in S phase for 16 hours. Following this, thymidine was washed out, and the antimitotic (either 20 ng/ml nocodazole or 2 μM ZM447439) was added. After a 10 hour incubation, when cells should be entering mitosis, samples were taken every 2 hours for both drug treatments and compared with the interphase population. For nocodazole-treated cells, which induce a mitotic arrest, Mcl-1 levels slowly declined in

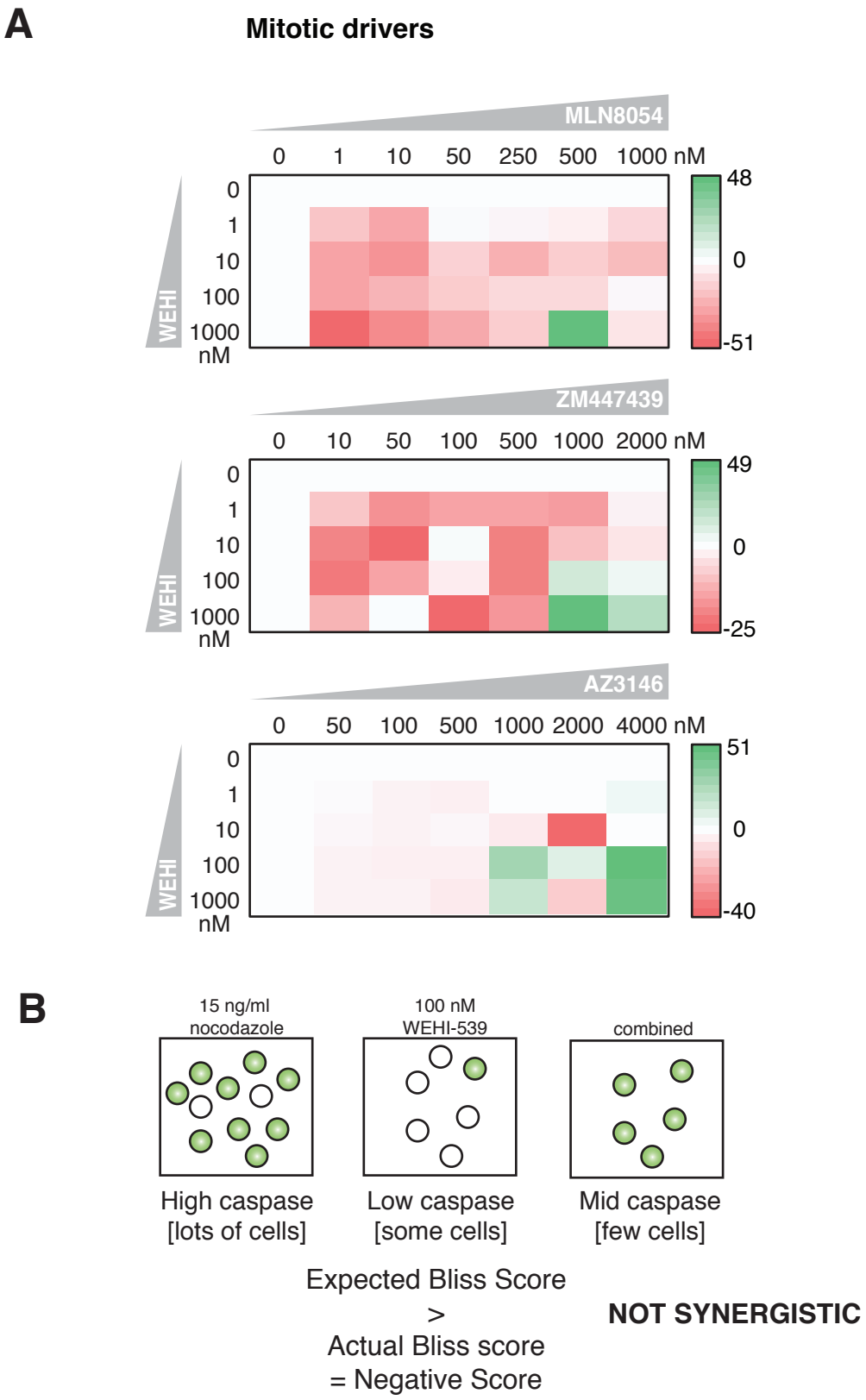

Figure 5.14 Effect of mitotic drivers and WEHI-539 combination on Bliss Scores. (**A**) Bliss Scores were calculated using the method in Figure 5.12 for the combination of the mitotic drivers MLN8054, ZM447439 and AZ3146 with WEHI-539. Positive (synergistic) Bliss Scores are shown in green, and negative (antagonistic) in red. (**B**) A representative diagram showing a scenario when the Bliss Scores may be negative, but where the interaction is classified as 'not synergistic' rather than 'antagonistic'.

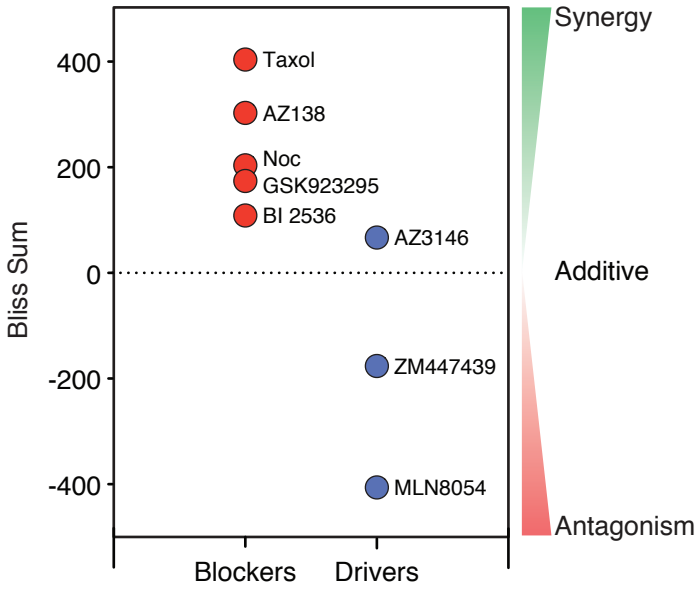

Figure 5.15 Bliss Sum analysis for mitotic blockers and drivers.
A scatter plot showing the Bliss Sum analysis for the mitotic blockers (red) and mitotic drivers (red) when in combination with WEHI-539. These were determined by the sumation of the Bliss excess values for each individual concentration matrix, shown in Figures 5.13 and 5.14.

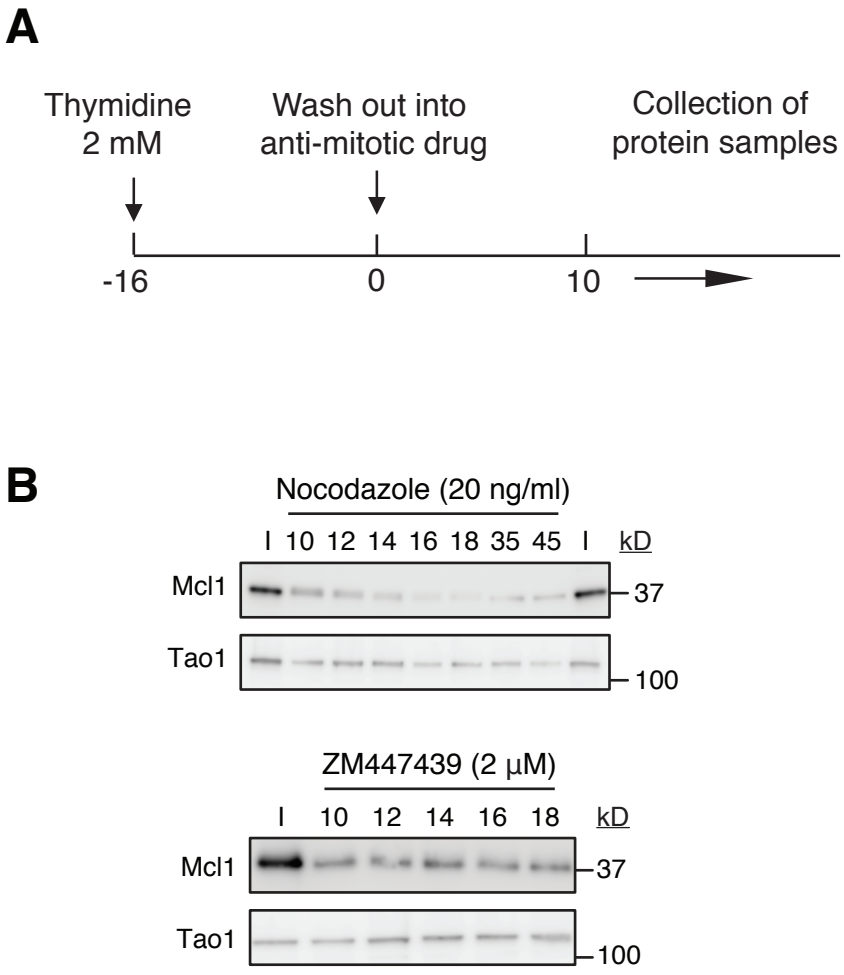

Figure 5.16 Effect of mitotic arrest on Mcl-1 levels.
(**A**) Schematic showing the experimental design following a single thymidine block in RKO cells for 16 hours, and washing into 20 ng/ml nocodazole or 2 µM ZM447439, with sample collection beginning at 10 hours after release.
(**B**) Immunoblot showing the levels of Mcl-1 following the protocol in (A), for nocodazole and ZM447439 exposure, with an interphase (I) control population shown. Times are given for when samples were collected.

comparison to the interphase population, which is consistent with previous observations ((Harley et al., 2010; Millman and Pagano, 2011; Sloss et al., 2016; Wertz et al., 2011) and see (Figure 5.16B)). However upon addition of ZM447439, Mcl-1 levels remained relatively stable over the time course. Cells exposed to the Aurora B inhibitor undergo slippage after a short period in mitosis and so it is likely that the majority of cells in this population analysed have exited and may be in an interphase state at the time of sampling.

Altogether this suggests that unlike the mitotic blockers, addition of mitotic drivers do not induce a decline of Mcl-1 levels. This implies that the sensitivity with WEHI-539 seen with the blockers is due to reduced Mcl-1 dependency and increased Bcl-xL dependency.

5.42 The effect of increasing or decreasing Mcl-1 expression on survival

To test the hypothesis that cells require Bcl-xL protection as Mcl-1 levels decline, two methods were used to functionally assess the effect of Mcl-1 level modulation. The first method involved overexpressing Mcl-1, where I rationalised that increasing Mcl-1 expression, thereby delaying Mcl-1 decline, may protect cells from death when exposed to WEHI-539 plus a mitotic blocker. The second method involved the suppression of Mcl-1, where cells should be more sensitive to death with WEHI-539 plus a mitotic driver.

Firstly, to examine the impact of increased Mcl-1 expression, I used an RKO cell line previously generated, expressing exogenous tetracycline-inducible GFP-tagged Mcl-1 ((Sloss et al., 2016) and see (Figure 5.17A)). Consistent with Figure 5.6B, cells exposed to 20 ng/ml nococdazole gave 17% PmD after 32 hours, with the majority undergoing division following a 4 hour arrest (Figure 5.17B). When Mcl-1 was overexpressed, little change on cell fate was observed. When nocodazole and WEHI-539 were combined, near maximal death was observed, where cells that divided ultimately underwent rapid PmD (68%) in 2.8 hrs. When Mcl-1 was overexpressed in this system, although no effect on the number of cells dying was apparent, the time to PmD was greatly increased to 17.5 hrs. This indicates the protective effect of Mcl-1 when expression is increased, with cells less sensitive to pharmacological inhibition of Bcl-xL.

Secondly, I tested whether suppression of Mcl-1 sensitised cells to death in the presence of a mitotic driver and WEHI-539. In Figure 5.10, WEHI-539 was unable to enhance apoptosis when cells were exposed to ZM447439. Therefore, I reasoned that

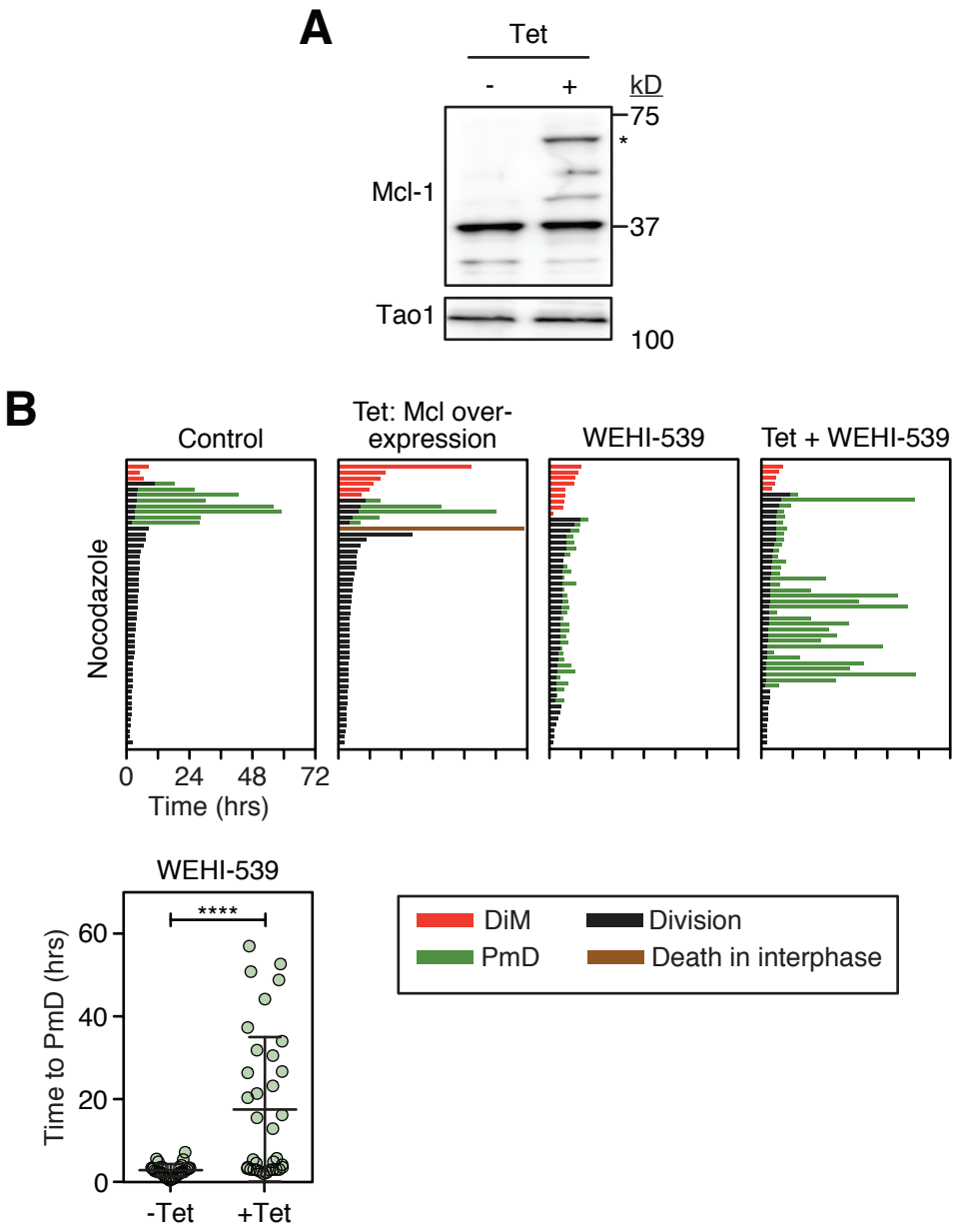

Figure 5.17 Effect of overexpression of Mcl-1 on post-mitotic death.
(**A**) Immunoblot for Mcl-1 following overnight tetracycline induction (1 µg/ml), for RKO cells overexpressing GFP-Mcl-1. * indicates the exogenous protein.
(**B**) Cell fate profiles for RKO cells overexpressing Mcl-1 in the presence of nocodazole (20 ng/ml) and WEHI-539 (100 nM). Time zero represents entry into mitosis. Time to PMD is quantified. Mann Whitney U test, ****p<0.0001.

if this insensitivity was due to the abundance of Mcl-1 in the system, then suppressing Mcl-1 in this context should sensitise Bcl-xL inhibited cells to ZM447439. As noted the co-suppression of Mcl-1 and Bcl-xL gives rise to high levels of apoptosis in untreated cells ((Topham et al., 2015) and see (Figure 5.1C,D)) and therefore, there is little room for comparison of cell fates. Due to this, I reduced the Mcl-1 siRNA concentration to 25 nM (rather than 66 nM normally used). Immunoblotting for Mcl-1 showed reduced levels of Mcl-1 upon siRNA transfection (Figure 5.18A). However, potent apoptosis was still observed with this reduced siRNA concentration and 100 nM WEHI-539, where 54% of these died very rapidly in mitosis within 0.7 hrs (Figure 5.18B). Upon addition of ZM447439 (2 μM), there was in fact, a slight protective effect on the cells, with fewer dying in mitosis (28%). Furthermore, under these conditions, 54% of cells died in interphase following cytokinesis failure, with an average time to death of 7.6 hrs, compared to 0.7 hours for the double suppression alone. The protection inferred by Aurora B inhibition may be as a result of telomere deprotection (Hayashi et al., 2012; Topham et al., 2015).

Since using RNAi-mediated suppression of Mcl-1 gave potent apoptosis, I turned to a recently described Mcl-1 inhibitor A-1210477 (Leverson et al., 2015b). The use of a small molecule inhibitor over the siRNA approach allows for rapid onset of inhibition, compared to 24-48 hours required for genetic perturbation. Also, this approach allows for titrated suppression of activity, which is very difficult to achieve with siRNA (Weiss et al., 2012). Due to these advantages I envisaged that I would be able to pick an Mcl-1/Bcl-xL inhibitor combination where there was a low level of apoptosis. Thus, I varied the concentration of A-1210477 against WEHI-539, measuring confluency and apoptosis induction (Figure 5.19A). From the dose matrix, I selected a combination of 2 μM A-1210477 and 100 nM WEHI-539 where minimal apoptosis was induced. The use of the inhibitors at these concentrations gave little or no effect when used on their own and only a small level of cell death was observed when added together. This allowed for the effect of a mitotic driver on apoptosis to be observed with facile comparison of cell fates. With the combined treatment of WEHI-539 and A-1210477, cell fate profiling revealed 38% of cells died post-mitosis with an average time to death of 35 hours, and 56% of cells divided 1-2 times during filming (Figure 5.19B, C). Consistent with previous results (Figure 5.10B), ZM447439 and 100 nM WEHI-539 together gave little apoptosis (Figure 5.19B). When A-1210477 was also added to this combination, apoptosis was enhanced and 86% died in interphase within 10 hours following mitotic exit. Therefore, when Bcl-xL and Aurora B are dually

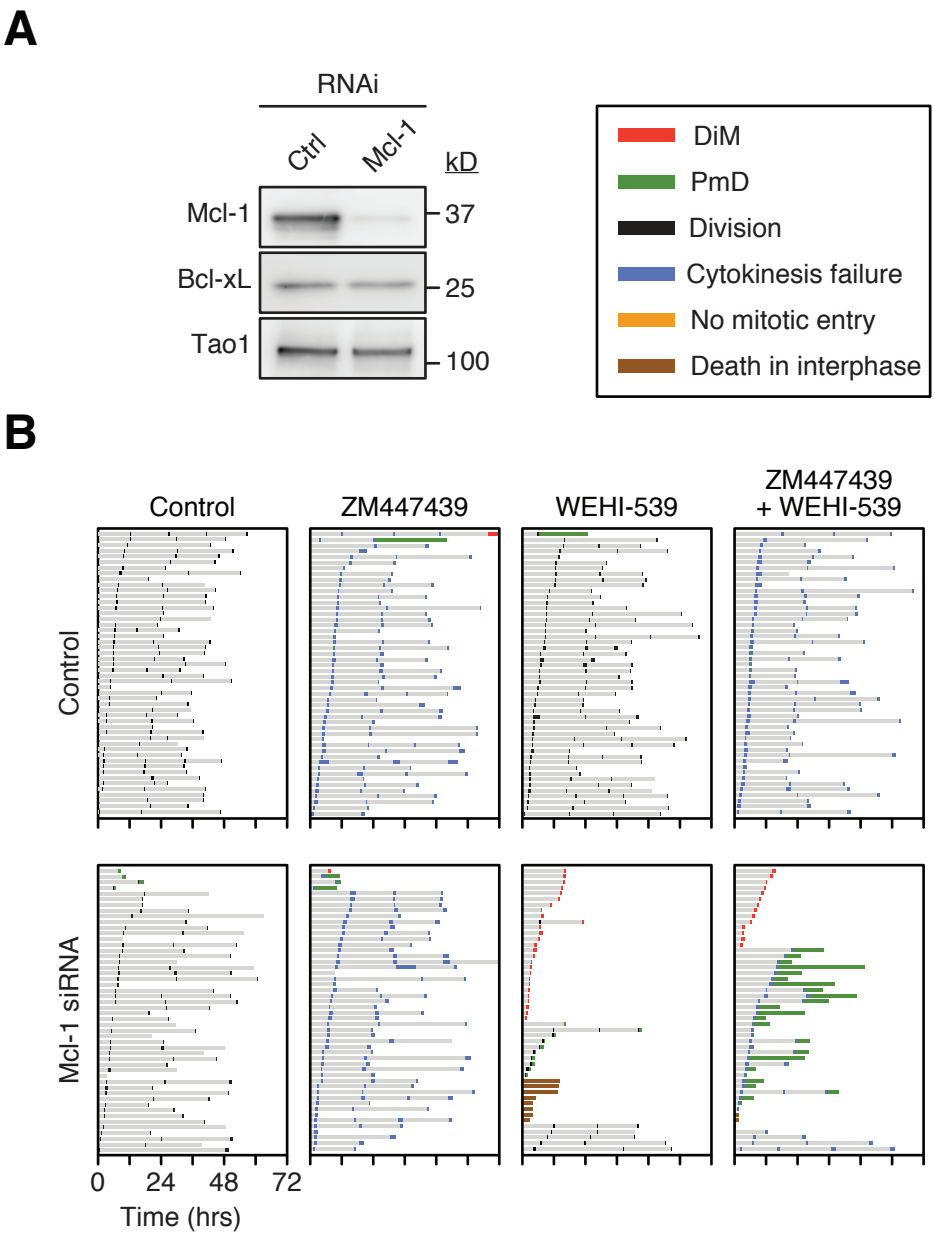

Figure 5.18 Effect of co-inhibition of Mcl-1 and Bcl-xL on ZM447439-treated RKO cells.
(**A**) Immunoblot showing Mcl-1 protein levels following siRNA transfection for 48 hours. (**B**) Cell fate profiles showing the behaviour of RKO cells following treatment with ZM447439 (2 μM), WEHI-539 (100 nM) and Mcl1 siRNA (25 nM), over a 72 hour period. Time zero represents when imaging started.

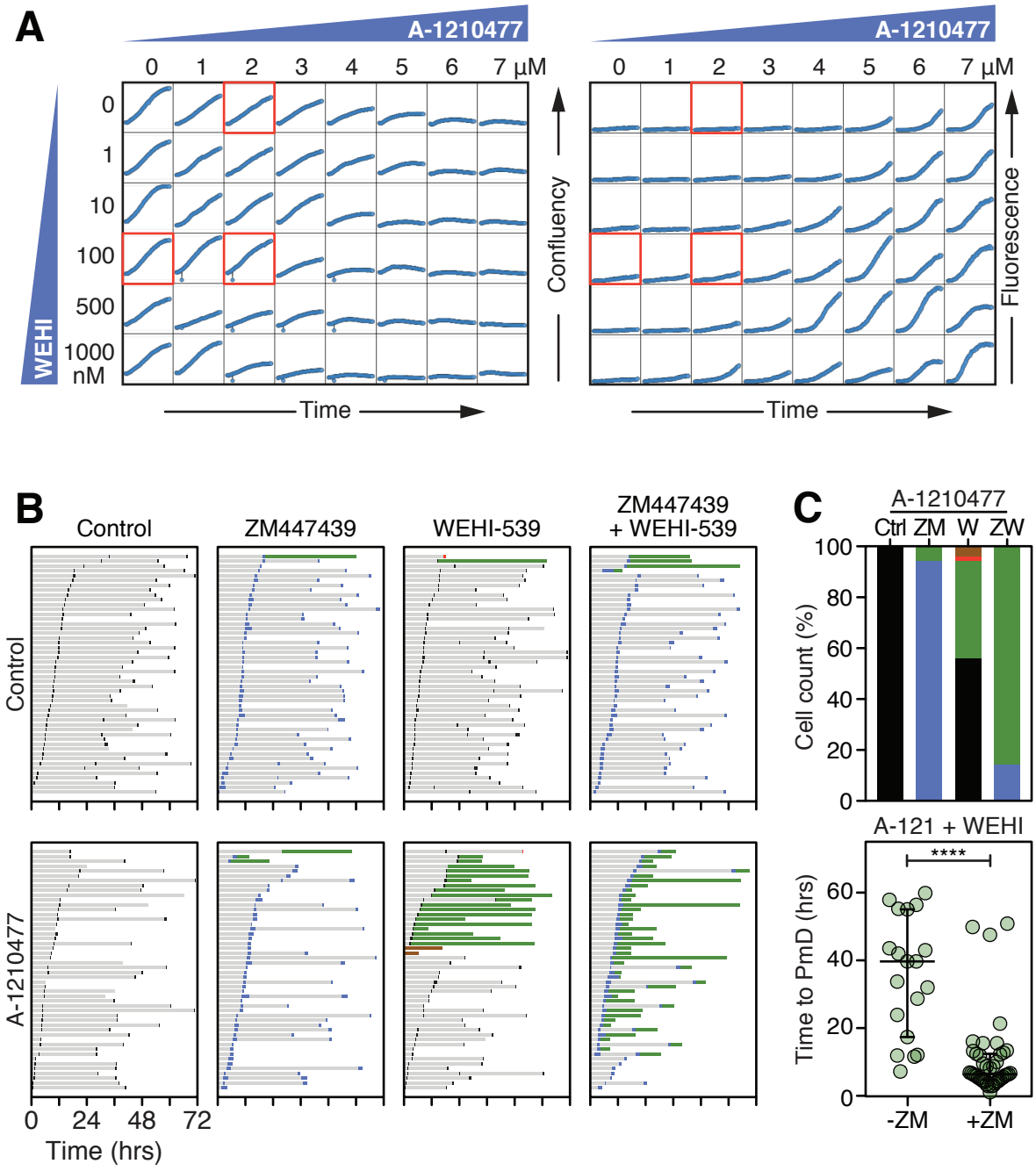

Figure 5.19 Effect of co-treatment with A-1210477/WEHI-539 and ZM447439.
(**A**) Dose matrix plots measuring confluency and caspase 3/7 (A/U) over 72 hours, for the titration of A-1210477 against WEHI-539, in RKO cells.
(**B**) Cell fate profiles for conditions identified in (A) and treatment with ZM447439 (2 µM). Time zero represents when imaging started. The number of cells undergoing different fates is quantified. Time to PMD for WEHI-539/ A-1210477 combination and WEHI-539/ A-1210477/ZM447439 combination is quantified. Mann Whitney U test, ****p<0.0001.

inhibited, Mcl-1 is able to maintain post-mitotic survival following cytokinesis failure. Thus, when cells exhibit a mitotic arrest, dependency upon Bcl-xL for survival is due to the reduced levels of Mcl-1.

5.43 Using Mcl-1 deficient DLD-1 cells to analyse the effect of ZM447439 and WEHI-539

My previous experiments have shown redundancy between Mcl-1 and Bcl-xL and have suggested that Mcl-1 compensation is a possible reason for the lack of synergy between WEHI-539 and mitotic drivers. I therefore questioned whether WEHI-539 could further increase death in combination with a mitotic driver in cells with diminished levels of Mcl-1 and that are largely dependent on Bcl-xL. The colon cancer cell line DLD-1 is a prime candidate for this (Sloss et al., 2016). To test this, I exposed DLD-1 cells to 2 μM of ZM447439, which resulted in 34% of cells undergoing death. Of these, 18% died in mitosis, 76% post-mitosis and 6% died in interphase as filming commenced (Figure 5.20). As anticipated, 62% of the total population underwent multiple cytokinesis failures (slippage), showing that ZM447439 was functioning as expected in these cells. In comparison to the RKO cells where WEHI-539 was benign, DLD-1 cells exposed to 100 nM WEHI-539 exhibited some death, with 26% dying post-mitosis. However, when ZM447439 and WEHI-539 were combined, 76% apoptosis was seen, with 93% of these dying following exit in the subsequent interphase. This infers that in the absence of Mcl-1 function and with a mitotic driver, post-mitotic survival is dependent upon Bcl-xL functioning.

Taken together, modulating Mcl-1 levels has revealed that Bcl-xL and Mcl-1 have overlapping functions. The lack of synergy seen for the combination of mitotic drivers and WEHI-539 can be explained by the presence of the pro-survival Mcl-1 exhibiting a protective function in these cells. The differences between the RKO and DLD-1 cell lines are highlighted due to contrasting dependencies upon pro-survival proteins, confirming the inter- and intra-line heterogenetic response to antimitotics (Gascoigne and Taylor, 2008).

5.5 Summary

In this chapter I found that Bcl-xL inhibition using WEHI-539 was able to sensitise cells to antimitotics dependent on the context. When studying both mitotic blockers and mitotic drivers, I discovered that Bcl-xL repression was only able to enhance apoptosis in response to mitotic blockers, reasoning that this was due to the

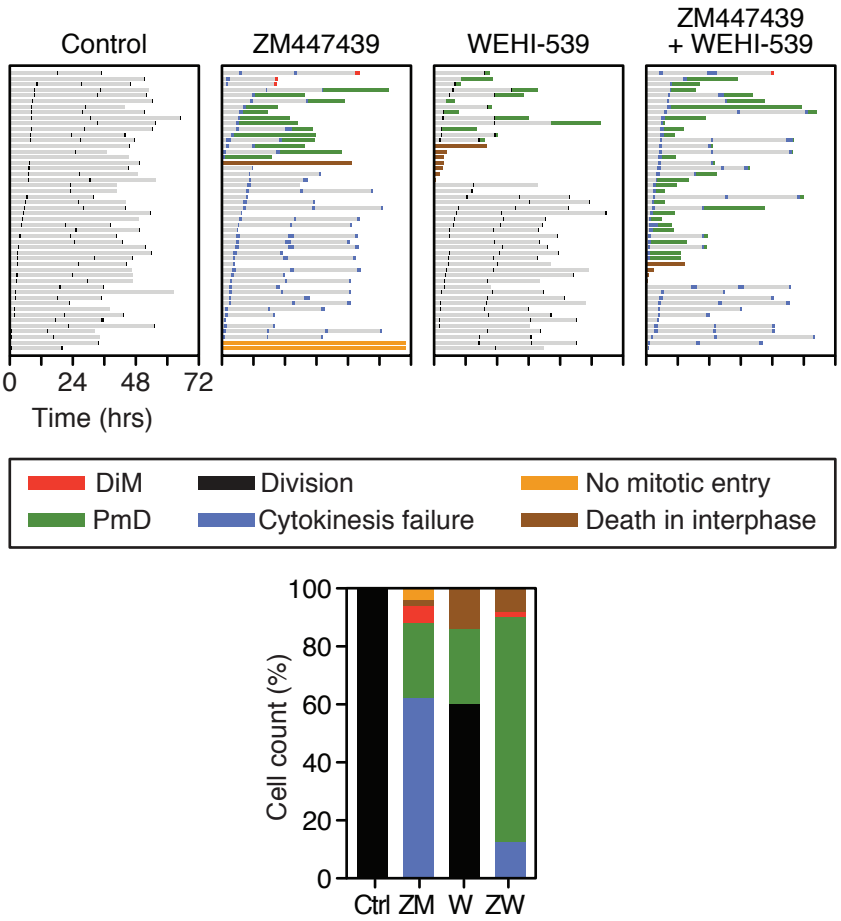

Figure 5.20 Effect of ZM447439 and WEHI-539 exposure on cell death in DLD-1 cells. Cell fate profiles of DLD-1 cells treated with ZM447439 (2 µM) and WEHI-539 (100 nM). TIme zero represents when imaging started. The number of cells undergoing each fate is quantified.

decreased dependency of cells on Mcl-1 throughout the mitotic arrest. This was further confirmed when Bcl-xL inhibition was seen to be ineffective with mitotic drivers, indicated by Mcl-1 levels remaining prominent. Through methods including overexpression of Mcl-1, suppression of Mcl-1 and utilising a cell line with diminished dependency upon Mcl-1, I established that the Mcl-1/Bcl-xL ratio is important in determining sensitivity to the antimitotic plus WEHI-539 combination. Through the use of a specific Bcl-xL inhibitor WEHI-539 I was able to see the subtle effects of Bcl-xL on post-mitotic survival following a protracted mitosis. Titration of protein levels is not as facile with siRNA, and therefore the effects I uncovered here were not seen previously when genetic perturbation was used (Bah et al., 2014). See Appendix 2 and 3 for the corresponding published papers (Bennett et al., 2016; Topham et al., 2015).

5.6 Discussion

5.61 The concept of synergy and the overlapping functioning between Mcl-1 and Bcl-xL

Throughout mitosis, proteins are prone to post-translational modifications such as phosphorylation and proteolysis, as transcription and translation are largely suppressed (Barr et al., 2011; Nigg, 2001; Pines, 2006). These modifications can influence activity and progression through mitosis. In the case of the apoptotic machinery, several proteins of this family undergo post-translational modifications, such as phosphorylation, including Bcl-xL (Bah et al., 2014). Mcl-1 is also phosphorylated, but unlike other apoptotic members it has been suggested that this may stimulate its proteasome-mediated degradation during a mitotic arrest (Harley et al., 2010; Sloss et al., 2016; Wertz et al., 2011). However, the exact mechanism of degradation is not fully known, with many E3 ubiquitin ligases being implicated (Sloss et al., 2016; Stewart et al., 2010). This degradation pushes the balance towards apoptosis, with an increase in DiM in many cases (Shi et al., 2011; Topham et al., 2015; Tunquist et al., 2010).

The general rationale behind combining antimitotics and BH3 mimetics stems from studies eluding to the role of the intrinsic apoptotic pathway in the mechanism of antimitotics (Allan and Clarke, 2007; Andersen et al., 2009; Gascoigne and Taylor, 2008; Shi et al., 2008). The combination tips the balance towards the pro-apoptotic proteins and increases the potential for apoptosis. Previously, it had been shown that combining ABT-737 with Taxol or an Eg5 inhibitor gives a synergistic response in cancer cell lines, patient derived tumour cells, and animal models (Bah et al., 2014;

Chen et al., 2011; Kutuk and Letai, 2008; Oltersdorf et al., 2005; Shi et al., 2011; Tan et al., 2011). Studying a wide range of mitotic blockers in cell culture, I was able to confirm this observation with a specific Bcl-xL inhibitor WEHI-539, where in most cases Bcl-xL was important for post-mitotic survival. However, no synergy was apparent with mitotic drivers plus WEHI-539 in this thesis. It should be noted that although a negative score is given for some combinations of mitotic drivers/blockers and WEHI-539 (indicated by red in the heat maps, Figures 5.13, 5.14), the interaction is *not* antagonistic. The caspase 3/7 reading detected by the IncuCyte® is dependent upon the number of cells within a well and therefore, two wells may give different readings yet have the same level of death (Figure 5.14B). For example, if cells are treated with 15 ng/ml nocodazole, some death will occur, and with 100 nM WEHI-539 little death will occur. However, even though the combination gives a similar level of death to nocodazole alone, the well with combined treatments may initially have fewer cells, giving a lower caspase 3/7 reading than nocodazole alone. Consequently, even though there is no additional effect (i.e. no increased death) of the combined treatment compared with nocodazole alone, when calculating the Bliss Score, a negative value is given. The interaction is therefore classified as 'not synergistic'.

Sometimes BH3 mimetics are not effective, which may be because of the redundancy between the pro-survival proteins, for example where Mcl-1 expression confers resistance to ABT-737 (Chen et al., 2007; Konopleva et al., 2006; Tahir et al., 2007; van Delft et al., 2006). Indeed, redundancy between Mcl-1 and Bcl-xL has been well documented by modulating the levels of both proteins (Eichhorn et al., 2014; Eno et al., 2012; Topham et al., 2015) and this was the most likely explanation for the differential sensitivity between mitotic blockers and drivers with WEHI-539. When exposed to mitotic blockers, the resulting mitotic arrest was accompanied by Mcl-1 levels declining, meaning that cells were highly dependent upon Bcl-xL when they exited mitosis (Figure 5.21). In contrast, the mitotic drivers did not induce an arrest, but drove cells through an aberrant mitosis (Keen and Taylor, 2009). This meant that cells were dependent upon both Mcl-1 and Bcl-xL for survival and thus, the inhibition of Bcl-xL did not enhance death significantly. This hypothesis was further confirmed by the co-inhibition of both Bcl-xL and Mcl-1 in the presence of an Aurora B inhibitor (Figures 5.18, 5.19). Here, PmD timings were accelerated and high levels of death were seen. The synergistic behaviour seen here is specific to the RKO cell line, as other cell lines will likely express different levels of the apoptotic proteins and therefore this differential dependency will influence the redundancy observed. This was exemplified where the

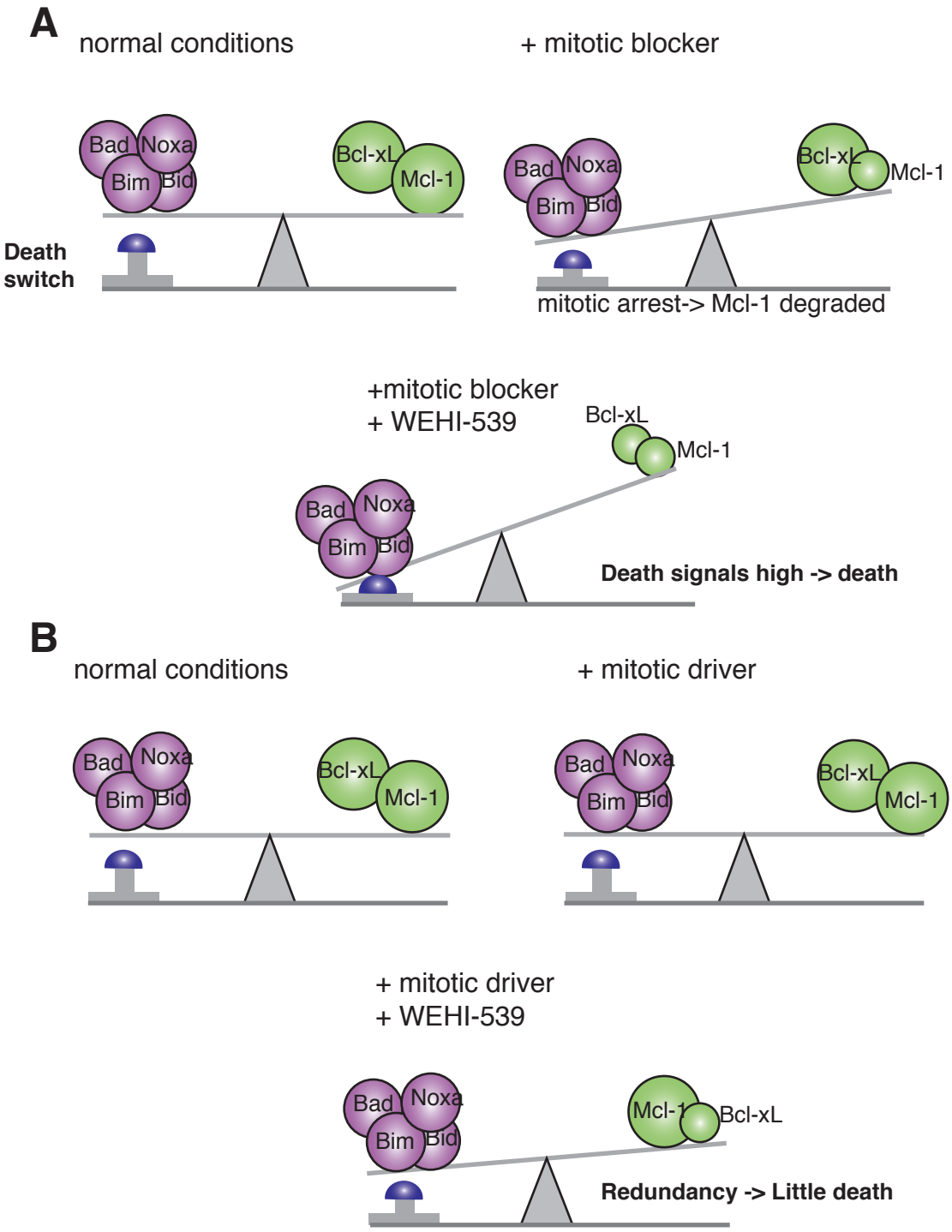

Figure 5.21 The balance between pro- and anti-apoptotic proteins and the redundancy between Mcl-1 and Bcl-xL determines cell survival.
(**A**) Under basal conditions in the cell, pro- and anti-apoptotic proteins are balanced. When exposed to a mitotic blocker, Mcl-1 levels decline and Bcl-xL dependency increases. WEHI-539 therefore enhances death.
(**B**) If in the presence of a mitotic driver, cell death is not enhanced by WEHI-539 since Mcl-1 levels are sufficient to maintain survival.

DLD-1 cell line does in fact show synergistic behaviour with drivers and WEHI-539 due to the increased dependency upon Bcl-xL over Mcl-1. This is in contrast to the RKO cell line which is equally dependent upon both proteins and therefore does not show this synergy. Further testing would involve many cell lines with differential expression. Therefore, mitotic blockers are unique in that they reduce the redundancy through Mcl-1 degradation, something that cannot be recapitulated with the mitotic drivers.

5.62 The post-mitotic response

The levels of Mcl-1 to Bcl-xL (i.e. the Mcl-1/Bcl-xL ratio) are important in determining the sensitivity to antimitotics and Bcl-xL inhibition, and this study has revealed the importance of both pro-survival proteins in promoting survival following and during a perturbed mitosis. Mcl-1 has been previously described as a mitotic 'death timer' (Haschka et al., 2015; Tunquist et al., 2010). Indeed, when Mcl-1 was overexpressed in my system, DiM was also delayed by five hours (Figure 5.17B), establishing its requirement for survival during a prolonged mitosis. Additionally, the importance of Mcl-1 in post-mitotic survival has also been indicated, where Mcl-1 RNAi in slippage-prone DLD-1 cells increased PmD when cells were exposed to AZ138 and also the overexpression of Mcl-1 delayed death following slippage (Sloss et al., 2016). In addition to this observation, I revealed that in the presence of Bcl-xL inhibition and increased Mcl-1 expression, nocodazole-treated cells exhibited an extended time to PmD (Figure 5.17B). I have repeatedly indicated that when Bcl-xL is inhibited in the presence of low concentrations of antimitotics, increased PmD is widespread. In some cases, DiM is increased and timings are accelerated, particularly in the presence of Taxol (Figure 5.6B). Therefore, both Mcl-1 and Bcl-xL are important for survival in mitosis and post-mitosis.

A premature exit from mitosis confers resistance to death and to microtubule-targeting agents (Bekier et al., 2009; Gascoigne and Taylor, 2008; Shin et al., 2003; Swanton et al., 2007; Tao et al., 2005; Taylor and McKeon, 1997). Often a limiting factor regarding the efficacy of anticancer agents is the lack of apoptosis induction during or after a mitotic arrest. This has been evidenced in cell culture and mouse studies with taxanes (Milross et al., 1996; Shi et al., 2008), where a mitotic arrest was not followed by PmD. In the examples in my thesis, it is noted that exposure of cells to antimitotics results in various phenotypes. Often, some cells undergo DiM, whilst some slip. PmD was a rare occurrence at the low drug concentrations studied here. When PmD was seen (e.g. with GSK923295, Figure 5.7B) then the timings to death were

relatively long (12.6 hours) and levels were low (14%), implying that a premature exit does stimulate a slight protective function and resistance to apoptosis. Furthermore, when these cells were exposed to WEHI-539, the cells that were previously resistant to death, then underwent rapid post-mitotic death (3.6 hours). This concept was also evidenced by studies where delaying slippage increased post-mitotic death (Sloss et al., 2016), again consistent with the notion that a premature exit confers resistance to PmD- where the longer the mitotic arrest, the increased likelihood that post-mitotic responses will be activated. Consequently, this contributes to the view that mitotic exit (slippage) is a good therapeutic target (Huang et al., 2009; Zasadil et al., 2014). It may be that the combination of mitotic blockers with Bcl-xL inhibition could overcome this apoptotic resistance, as Mcl-1 levels decline in this situation, resulting in increased dependency upon Bcl-xL.

5.63 Mitosis as a stress

In the absence of any other cytotoxic insult, the simultaneous suppression of both Mcl-1 (either with siRNA or A-1210477) and Bcl-xL results in potent apoptosis ((Eichhorn et al., 2014; Topham et al., 2015) and see (Figure 5.1C,D)). This confirms the functional redundancy between the pro-survival members in this system, since repression of only one pro-survival member does not result in significant apoptosis. Interestingly, when cells were lacking both Mcl-1 and Bcl-xL, apoptosis occurred either in mitosis or rapidly following exit ((Topham et al., 2015) and see (Figure 5.18B)). Additionally, when Bim was overexpressed in the presence of WEHI-539, cells died rapidly following mitotic exit (Figure 5.2E). This indicates that even without an additional cytotoxic insult, the lack of pro-survival functioning can induce death both in mitosis and post-mitosis. Thus, in these cases, mitosis itself is sufficient to activate apoptosis.

During mitosis, many processes occur such as cellular architecture modifications, changes in chromosome condensation and the halting of transcription and translation. These changes make the mitotic process a vulnerable state for the cell. Therefore, it is not surprising that further perturbations in mitosis e.g. reduced pro-survival functioning, can cause additional damage to the cells, resulting in apoptosis. These mitotic stress signals may be as a result of DNA damage or telomere deprotection mechanisms (Hayashi et al., 2012; Imreh et al., 2011; Topham et al., 2015). Under certain conditions, it is likely that upon mitotic entry, telomere deprotection causes DNA damage (Hayashi et al., 2012). The kinase Aurora B

removes the protective TRF2 from telomeres, and this exposed telomere gives rise to caspase-dependent DNA damage responses (Colin et al., 2015; Hain et al., 2016; Hayashi et al., 2012). Furthermore, when TRF2 was overexpressed or Aurora B inhibited, in the presence of Mcl-1 and Bcl-xL repression, DiM was reduced (Topham et al., 2015). Similarly, I have also shown that when Mcl-1 is depleted in the presence of WEHI-539, Aurora B inhibition resulted in a delay in apoptosis (Figure 5.18B). Further experimentation may reveal if the observed death in cells with little pro-survival functioning is a result of telomere deprotection.

Other potential inducers of cell death may arise from metabolic changes. A mitotic arrest is accompanied by mitophagy, where ATP levels are reduced, resulting in AMPK activation (Doménech et al., 2015). This is accompanied by a metabolic change from oxidative respiration to glycolysis. Consequently, when pro-survival functioning is lacking, the metabolic changes in a mitotic arrest may cause sufficient stress to induce apoptosis.

5.64 Bcl-xL inhibition in the clinic

5.641 Combination chemotherapy

Understanding the effect of taxanes is important if the associated issues are to be overcome, including undesirable side effects, resistance and the inability to predict responsiveness. One important matter that is essential to understand is the stage of the cell cycle at which paclitaxel, for example, affects cells. Studies involving the combination of docetaxel and an Mps1 inhibitor (NTRC 0066-0) inferred that they act synergistically and with an increase in multipolar spindles (Maia et al., 2015). Therefore, the likely mechanism by which docetaxel elicits its effect is via mitosis. When breast cancer tissue samples were exposed to Taxol *in vivo*, abnormal mitoses with multipolar spindles were apparent (Zasadil et al., 2014). Together, these observations are consistent with the notion that taxanes act in mitosis. However, this theory has been questioned by others. Some have suggested the action of paclitaxel is in interphase (Weaver, 2014). However, cell culture studies signify that clinically relevant taxane concentrations don't cause death in interphase (Janssen et al., 2013; Zasadil et al., 2014). Nevertheless, tumour models indicated a low mitotic index following paclitaxel exposure, implying the absence of a mitotic arrest (Janssen et al., 2013; Orth et al., 2011). However, it is not clear how paclitaxel would elicit its action in interphase. In general, my studies have reiterated the importance of taxanes in mitosis

and therefore, understanding the dynamics of how these drugs influence this phase is beneficial to understanding the interactions with combination therapies.

When combined with mitotic blockers, WEHI-539 exposed Bcl-xL as an important pro-survival factor. Death following an abnormal mitosis was increased, but also time to DiM was decreased in the case of paclitaxel (Figure 5.6). This has been suggested previously, where inhibiting pro-survival functioning in the presence of antimitotics increased apoptosis (Bah et al., 2014; Leverson et al., 2015b; Shi et al., 2011; Tan et al., 2011). Clinically, the combination of Bcl-xL inhibitors and antimitotics may therefore be advantageous. I gave particular interest to highlighting combinations of antimitotics plus WEHI-539 where Bcl-xL inhibition was able to enhance apoptosis, specifically when the antimitotic was used at the lowest dose possible. For example, GSK923295 alone would have to be used at a higher dose (>500 nM), to induce apoptosis to the same level as a 100 nM dose with 100 nM WEHI-539 elicits (Figure 5.5B). This is important when considering a major drawback of agents such as Taxol is peripheral neuropathy (Dumontet and Jordan, 2010; Rowinsky et al., 1993) and reducing doses of these agents should result in milder side effects. Whilst the inhibition of Bcl-xL causes thrombocytopenia (Roberts et al., 2012; Tse et al., 2008) due to the detrimental effect on platelet survival (Mason et al., 2007; Zhang et al., 2007), these toxicity problems may be manageable with the lower doses in combination with mitotic blockers.

Furthermore, although WEHI-539 is effective in cells, it lacks the efficacy and chemical stability needed for efficiency *in vivo* and therefore similar testing would need to be carried out with the improved A-1155463 and A-13311852 (Leverson et al., 2015a). In fact, studies have indicated these agents displayed enhanced efficacy when in combination with docetaxel. Additionally, the Bcl-xL overexpression assay used in Figure 5.3 may allow for the screening of potential new inhibitors of Bcl-xL. As the overexpression of Bcl-xL protected against apoptosis in the presence of Taxol, WEHI-539 was able to reverse this. Compounds which mimic the activity of WEHI-539 would be taken forward as potential Bcl-xL inhibitors. Later testing would make use of *in vivo* animal models, patient-derived xenograft models (PDX) and perhaps patient samples to test the response following this combination strategy.

5.642 Biomarkers for efficacy

Clinically, in order for the antimitotic combination to be successful, potential biomarkers need to be identified for noting patients likely to respond to treatment.

Those with low levels (or low dependency) of Mcl-1 may respond to the antimitotic plus Bcl-xL inhibitor combination, whether the antimitotic is a blocker or driver. However, if patients have high Mcl-1 dependency they may not respond to a mitotic driver and Bcl-xL inhibitor, but may show success with a mitotic blocker with or without a BH3 mimetic combination. Therefore, it is important that patients are screened for the Bcl-xL/Mcl-1 ratios prior to therapy. Although in this study I have focused on Bcl-xL and Mcl-1, it may be that Bcl-2 dependency is important for survival in a subset of cancers and so this cannot be dismissed. However, Bcl-2 has yet to be implicated for DiM in response to antimitotics (Li et al., 2005; Shi et al., 2011).

The requirement for biomarkers is further reiterated by studies in ovarian cancer cell lines, where high Bcl-xL expression conferred resistance to taxanes, and those with increased Bcl-xL/Mcl-1 ratios had higher Bliss Sums when navitoclax and Taxol were combined (Wong et al., 2012). These observations indicate that patients with high Bcl-xL/Mcl-1 ratio would likely respond better in trials with antimitotics and Bcl-xL inhibitors. To further this evaluation, the use of other cell lines with differential dependency upon the apoptotic proteins will be required.

While it may be unlikely that inhibiting a single pro-survival protein will be clinically effective, there may be cases where a particular cancer is reliant on one protein for survival. For example, ABT-199 has been approved for the treatment of chronic lymphocytic leukemia (CLL), which is a cancer reliant upon Bcl-2 for survival (http://www.fda.gov/NewsEvents/Newsroom/PressAnnouncements/ucm4 95253.htm). Furthermore, genes encoding both Bcl-xL and Mcl-1 are amplified in a number of cancers, making them likely candidates for target therapy (Beroukhim et al., 2010). Therefore, in these cases, single agent therapy may be effective.

Although the ratio of Bcl-xL/Mcl-1 is important, the levels of the pro-apoptotic proteins also have to be considered. Both the pro- and anti-apoptotic proteins undergo post-translational modifications in mitosis, including caspase-9, Bid, Bcl-xL and Bim (Allan and Clarke, 2007; Poruchynsky et al., 1998; Sakurikar et al., 2012; Upreti et al., 2008; Wan et al., 2014; Wang et al., 2014) and due to the functional redundancy that exists, it is likely that the interplay between all members that determines sensitivity to antimitotics. As some cancers exhibit overexpression of many Bcl-2 members (Beroukhim et al., 2010), further detailed studies need to explore the factors that confer sensitivity or resistance to chemotherapy. One method of predicting sensitivity to chemotherapeutics is via BH3 profiling or dynamic BH3 profiling (Montero et al., 2015; Ryan et al., 2010). This method measures how close to the apoptotic threshold a cell

is, i.e. how 'primed' a cell is to death. Dynamic BH3 profiling (DBP) has been used to foresee initial changes in death signalling that occur upon exposure to chemotherapeutic drugs (Montero et al., 2015). In this particular study, the authors indicated that DBP could be used to predict *in vitro* and *in vivo* responses, and eventually it may be able to predict patient responses in the clinic.

An additional biomarker of efficacy of BH3 mimetics may be the state of association of, for example Bcl-xL:Bim complexes (or similar), since the level of priming encountered depends on the relative association or proteins with their binding partners (Certo et al., 2006). A higher association results in an increased sensitivity to agents such as the BH3 mimetics, exemplified in studies with A-1155463 (Punnoose et al., 2016). Therefore it may be that inhibitors of Bcl-xL will be more efficacious in patients where Bcl-xL:Bim association is higher. Consequently, these approaches may be used in predicting patient response to the antimitotic plus Bcl-xL inhibitor approach described here.

This chapter has confirmed the role of the intrinsic apoptotic pathway in the mechanism of antimitotics. The use of WEHI-539 in combination with antimitotics has been exploited, showing an enhancement of cell death. The study has highlighted the requirement for biomarkers in order to predict when the antimitotic plus Bcl-xL inhibitor combination will be most effective, with focus on the difference between mitotic blockers and drivers and the role of Mcl-1. Therefore, these observations may be used clinically to devise improved anticancer strategies.

Chapter 6: Discussion

6.1 Overview

Antimitotic agents targeting tubulin are used extensively during cancer chemotherapy but their use is complicated by issues regarding predictability, resistance and toxicity (Dumontet and Jordan, 2010; Rowinsky et al., 1993). My thesis has focused on the interplay between mitosis and apoptosis, with a view to identifying strategies by which mitosis could be exploited to improve the efficacy of existing antimitotic agents. In order to achieve this, I focused on three areas:

(i) *Establishing new methods of anticancer therapy:* this involved the examination of the ability to target Bub1 kinase with a novel inhibitor 2OH-BNPP1 in *in vitro* and cell-based settings;

(ii) *The establishment of an assay to induce aneuploidy*: this encompassed the use of a synthesised Cenp-E inhibitor GSK923295 to induce chromosome misalignment, followed by checkpoint override to missegregate chromosomes and generate daughter cells with unequal chromosome numbers;

(iii) *Understanding how antimitotics cause cell death:* this involved testing the ability of Bcl-xL inhibition with WEHI-539 to sensitise cells to antimitotic agents, including mitotic blockers and mitotic drivers. Furthermore, this enabled the role of Bcl-xL in survival during mitosis and post-mitosis to be examined.

The initial aims of the project were to address the issues associated with the lack of efficacy of newly developed mitotic agents. Given that Taxol is thought to elicit its action via mitotic arrest-induced apoptosis, second-generation inhibitors were developed to mimic this mechanism. Unfortunately, such agents against Cenp-E, Plk-1 and Eg5 for example, have failed to elicit the expected clinical effect (Komlodi-Pasztor et al., 2012; Mitchison, 2012). Consequently, I asked whether targeting the checkpoint protein Bub1 would be beneficial. Upon initiation of the project, the importance of the kinase activity of Bub1 was not fully known, and there were no *bona fide* Bub1 kinase inhibitors. I tested the ability of the only published inhibitor, 2OH-BNPP1, to target Bub1. I also aimed to establish Bub1 kinase's role in the SAC. In doing so, this may have determined whether inhibiting Bub1 may give improved effects over other mitotic

agents. However, this was unsuccessful due to the lack of evidence of 2OH-BNPP1 inhibiting Bub1 in cells. Indeed, I may have used the Bub1 interphase assay in Figure 3.11 or modelling studies to identify new potential lead compounds for Bub1 inhibition, however, at this time, we became aware that Bayer had patented a series of Bub1 inhibitors and in collaboration with Erich Nigg's lab were characterising these in cell based assays. This work was later published, describing two compounds namely BAY-320 and BAY-524 (Baron et al., 2016). These compounds did exhibit activity in cells, where the H2A phosphorylation signal was reduced upon exposure, and at 3-7 μM they exhibited synergy with paclitaxel, similar to results published with previous Mps1 inhibitors (Janssen et al., 2009; Maia et al., 2015). Furthermore, selectivity profiles indicated even at 10 μM, the compounds showed little activity towards other kinases (Baron et al., 2016). Therefore, given the specificity and efficacy of these compounds, and the known difficulty in developing specific kinase inhibitors (Hanks and Hunter, 1995), I feel my decision to terminate this project was well justified.

Following on from this, I chose to study another aspect of mitotic perturbation, that is chromosome misseegregation and the resulting aneuploidy. Aneuploidy is a hallmark of cancers (Mitelman, 2014), yet the causes and consequences of this karyotype remain vague. The lack of suitable assays to study this phenomenon led to the proposal of the Cenp-E/Mps1 inhibitor approach, where success was proven with 98% of chromosomes missegregating at least one chromosome (Bennett et al., 2015). Following generation of the assay within the lab, other groups including that of Angelika Amon, were heavily studying aneuploidy and therefore, it was realised that our group lacked the expertise to be competitive in this area. It was suggested that I may have taken the project in the direction of a chemical synthesis route, with the potential generation of improved Cenp-E inhibitors. The kinetic resolution method described would have allowed for GSK923295-analogues to be developed, however, there was no guarantee these would have been more effective. For the purposes of studying mitosis, GSK923295 was suitable, and notably, concentrations of 50-100 nM were sufficient to inhibit Cenp-E in these assays, meaning potency was not an issue that needed to be addressed. Consequently, I used GSK923295 as an antimitotic in my final part of my thesis.

Furthermore, the final aspect of mitotic perturbation I studied was the effect of antimitotics on cell fate. Despite advances, the mechanisms that control the fate of cells when exposed to antimitotics are lacking in detail. Recently, c-myc was found to drive the expression of the members of the intrinsic apoptotic network, and in doing so,

controls death in mitosis upon mitotic perturbation (Topham et al., 2015). c-myc downregulates Bcl-xL, and this sensitises cells to antimitotic agents, and therefore, it was hypothesised that targeting Bcl-xL in the presence of antimitotics would sensitise cells to death, which was confirmed by my studies, in particular with mitotic blockers. I determined that the Mcl-l/Bcl-xL ratio is important in influencing sensitivity to mitotic drivers and blockers, an observation which has not been seen previously. This finding may allow for the identification of possible biomarkers that will confer resistance or sensitivity, but also will allow for possible drug combinations to be identified. In order to do so, this will be expanded to other cell lines and eventually tested *in vivo*, to definitively link the Bcl-xL/Mcl-1 ratio with the synergistic effect seen. Therefore, this project was very successful.

Furthermore, my studies have highlighted the advantage of the single-cell tracking approach. Whole-population analysis masks subtle cellular behaviour which can only be observed with a single-cell approach. For example, the caspase readout used throughout is only a crude analytical method for cell death, but to truly understand the biology in regards to mitosis, the single-cell analysis approach is vital. This was particularly important when studying the role of Bcl-xL in mitotic and post-mitotic survival.

6.2 Concluding remarks

The deregulation of the cell cycle is a common feature of cancers and therefore targeting the cell cycle in anticancer therapy has been of major interest (Manchado et al., 2012). Targeting has focused on many aspects of the cycle including cell cycle entry, mitotic entry, spindle assembly, the SAC and mitotic exit, where proteins and processes controlling these are often disrupted in cancer. For example, further exacerbating the level of genomic instability by targeting the SAC is thought to be a promising strategy in chemotherapy due to the already high levels of aneuploidy and CIN often associated with cancer (Weaver and Cleveland, 2006). Our understanding of aneuploidy has advanced over the past years, with the possibility of targeting aneuploidy as an anticancer strategy being acknowledged. Possible targeting strategies include the use of compounds such as the energy-stress inducing AICAR, which target pathways that are essential for the survival of aneuploidy cells (Tang et al., 2011). Further compounds which target aneuploidy are now being developed (Santaguida and Amon, 2015).

Further studies have also indicated that perhaps Taxol does not induce death due to a prolonged mitotic arrest. Paclitaxel accumulates intracellularly up to 100-fold, in comparison to serum levels (Zasadil et al., 2014), and this characteristic may contribute to its efficacy. Studies indicated that at the clinical concentrations encountered in tumours, Taxol did not induce a mitotic arrest, but in fact, the cytotoxic effect was as a result of chromosome missegregation on multipolar spindles. It is this mitotic defect that induces the tumour regression effect, indicating that Taxol effects mitosis in a number of different ways. Therefore, the mitotic arrest that is stimulated with the second-generation inhibitors may not be sufficient for antitumour effects. However, development and testing is still in its infancy, so it is premature to discount these agents. Evidence from Plk-1 inhibitor studies indicates that dosing at low concentrations causes chromosome missegregation (Lera and Burkard, 2012), similar to the effects seen with paclitaxel. Therefore, similar effects may be seen with other second-generation inhibitors with further experimentation.

It is most likely that combination chemotherapy will be the most successful approach in cancer treatment rather than single-agent treatment. The combination will allow for overall improved efficacy, whilst maintaining toxicity at a more manageable level. Challenges will be faced, including validating targets within tumours, the appropriate dosage and schedule and most importantly, identifying patients who are most likely to be sensitive and benefit from treatment- where problems still exist due to the heterogeneity. With the emergence of new possible targets and inhibitors beyond the traditional microtubule-targeting agents, it may be that we are closer to devising novel and improved anticancer strategies.

7 References

Abrieu, A., Kahana, J.A., Wood, K.W., Cleveland, D.W., 2000. CENP-E as an essential component of the mitotic checkpoint in vitro. Cell 102, 817–26.

Adams, J.M., Cory, S., 2007. The Bcl-2 apoptotic switch in cancer development and therapy. Oncogene 26, 1324–1337.

Adams, R.R., Wheatleya, S.P., Gouldsworthy, A.M., Kandels-Lewis, S.E., Carmena, M., Smythe, C., Gerloff, D.L., Earnshaw, W.C., 2000. INCENP binds the Aurora-related kinase AIRK2 and is required to target it to chromosomes, the central spindle and cleavege furrow. Curr. Biol. 10, 1075–1078.

Agarwal, R., Gonzalez-Angulo, A.M., Myhre, S., Carey, M., Lee, J.S., Overgaard, J., Alsner, J., Stemke-Hale, K., Lluch, A., Neve, R.M., Kuo, W.L., Sorlie, T., Sahin, A., Valero, V., Keyomarsi, K., Gray, J.W., Borresen-Dale, A.L., Mills, G.B., Hennessy, B.T., 2009. Integrative analysis of cyclin protein levels identifies cyclin B1 as a classifier and predictor of outcomes in breast cancer. Clin. Cancer Res. 15, 3654–3662.

Alaimo, P., Shogren-Knaak, M., Shokat, K., 2001. Chemical genetic approaches for the elucidation of signaling pathways. Curr. Opin. Chem. Biol. 360–367.

Alizadeh, A., Elsen, M., Davis, R., Ma, C., Lossos, I., Rosenwald, A., Boldrick, J., Sabet, H., Tran, T., Yu, X., Powell, J., Yang, L., Marti, G., Moore, T., Hudson Jr, J., Lu, L., Lewis, D., Tibshirani, R., Sherlock, G., Chan, W., Greiner, T., Weisenburger, D., Armitage, J., Warnke, R., Levy, R., Wilson, W., Grever, M., Byrd, J., Botstein, D., Brown, P., Staudt, L., 2009. Distinct types of diffuse large B-cell lymphoma identified by gene expression profiling. Gene Expr. 105, 3671–3678.

Allan, L.A., Clarke, P.R., 2007. Phosphorylation of Caspase-9 by CDK1/Cyclin B1 Protects Mitotic Cells against Apoptosis. Mol. Cell 26, 301–310.

Amundson, S.A., Myers, T.G., Scudiero, D., Lines, C.C., Kitada, S., Reed, J.C., Fornace, A.J., 2000. An Informatics Approach Identifying Markers of Chemosensitivity in Human Cancer Cell Lines An Informatics Approach Identifying Markers of Chemosensitivity in Human. Cancer Res. 6101–6110.

Andersen, J.L., Johnson, C.E., Freel, C.D., Parrish, A.B., Day, J.L., Buchakjian, M.R., Nutt, L.K., Thompson, J.W., Moseley, M.A., Kornbluth, S., 2009. Restraint of apoptosis during mitosis through interdomain phosphorylation of caspase-2. EMBO J. 28, 3216–3227.

Anderson, E., Larsson, K., Kirk, O., 1998. One Biocatalyst–Many Applications: The Use of Candida Antarctica B-Lipase in Organic Synthesis. Biocatal. Biotransformation 16, 181–204.

Arbour, N., Vanderluit, J.L., Le Grand, J.N., Jahani-Asl, A., Ruzhynsky, V.A., Cheung, E.C.C., Kelly, M.A., MacKenzie, A.E., Park, D.S., Opferman, J.T., Slack, R.S., 2008. Mcl-1 is a key regulator of apoptosis during CNS development and after DNA damage. J. Neurosci. 28, 6068–78.

Asghar, A., Lajeunesse, A., Dulla, K., Combes, G., Thebault, P., Nigg, E.A., Elowe, S., 2015. Bub1 autophosphorylation feeds back to regulate kinetochore docking and promote localized substrate phosphorylation. Nat. Commun. 6, 8364.

Aspinall, C.F., Zheleva, D., Tighe, A., Taylor, S.S., 2015. Mitotic entry: Non-genetic heterogeneity exposes the requirement for Plk1. Oncotarget 6, 36472–88.

Bah, N., Maillet, L., Ryan, J., Dubreil, S., Gautier, F., Letai, A., Juin, P., Barillé-Nion, S., 2014. Bcl-xL controls a switch between cell death modes during mitotic arrest. Cell Death Dis. 5, e1291.

Bai, L., Smith, D.C., Wang, S., 2014. Pharmacology & Therapeutics Small-molecule SMAC mimetics as new cancer therapeutics. Pharmacol. Ther. 144, 82–95.

Baker, D.J., Jin, F., Jeganathan, K.B., van Deursen, J.M., 2009. Whole Chromosome Instability Caused by Bub1 Insufficiency Drives Tumorigenesis through Tumor Suppressor Gene Loss of Heterozygosity. Cancer Cell 16, 475–486.
Baron, A.P., von Schubert, C., Cubizolles, F., Siemeister, G., Hitchcock, M., Mengel, A., Schroder, J., Fernández-Montalván, A., von Nussbaum, F., Mumberg, D., Nigg, E.A., 2016. Probing the catalytic functions of Bub1 kinase using the small molecule inhibitors BAY-320 and BAY-524. Elife 5, 1–26.
Barr, F.A., Elliott, P.R., Gruneberg, U., 2011. Protein phosphatases and the regulation of mitosis. J. Cell Sci. 124, 2323–34.
Basso, K., Margolin, A.A., Stolovitzky, G., Klein, U., Dalla-Favera, R., Califano, A., 2005. Reverse engineering of regulatory networks in human B cells. Nat. Genet. 37, 382–390.
Bayliss, R., Fry, A., Haq, T., Yeoh, S., 2012. On the molecular mechanisms of mitotic kinase activation. Open Biol. 2, 120136.
Bekier, M.E., Fischbach, R., Lee, J., Taylor, W.R., 2009. Length of mitotic arrest induced by microtubule-stabilizing drugs determines cell death after mitotic exit. Mol. Cancer Ther. 8, 1646–1654.
Bellingham, R., Buswell, A.M., Choudary, B.M., Gordon, A.H., Moore, S.O., Peterson, M., Sasse, M., Shamji, A., Urquhart, M.W.J., 2010. Discovery and Development of an Efficient, Scalable, and Robust Route to the Novel CENP-E Inhibitor GSK923295A. Org. Process Res. Dev. 14, 1254–1263.
Bennett, A., Bechi, B., Tighe, A., Thompson, S., Procter, D.J., Taylor, S.S., 2015. Cenp-E inhibitor GSK923295: Novel synthetic route and use as a tool to generate aneuploidy. Oncotarget 6, 20921–20932.
Bennett, A., Sloss, O., Topham, C., Nelson, L., Tighe, A., Taylor, S.S., 2016. Inhibition of Bcl-xL sensitizes cells to mitotic blockers, but not mitotic drivers. Open Biol. 6, 160134.
Berardo, M.D., Elledge, R.M., de Moor, C., Clark, G.M., Osborne, C.K., Allred, D.C., 1998. Bcl-2 and Apoptosis in Lymph Node Positive Breast Carcinoma. Cancer 82, 1296–302.
Bernard, P., Maure, J.F., Javerzat, J.P., 2001. Fission yeast Bub1 is essential in setting up the meiotic pattern of chromosome segregation. Nat. Cell Biol. 3, 522–526.
Beroukhim, R., Mermel, C.H., Porter, D., Wei, G., Raychaudhuri, S., Donovan, J., Barretina, J., Boehm, J.S., Dobson, J., Urashima, M., Mc Henry, K.T., Pinchback, R.M., Ligon, A.H., Cho, Y.-J., Haery, L., Greulich, H., Reich, M., Winckler, W., Lawrence, M.S., Weir, B.A., Tanaka, K.E., Chiang, D.Y., Bass, A.J., Loo, A., Hoffman, C., Prensner, J., Liefeld, T., Gao, Q., Yecies, D., Signoretti, S., Maher, E., Kaye, F.J., Sasaki, H., Tepper, J.E., Fletcher, J.A., Tabernero, J., Baselga, J., Tsao, M.-S., Demichelis, F., Rubin, M.A., Janne, P.A., Daly, M.J., Nucera, C., Levine, R.L., Ebert, B.L., Gabriel, S., Rustgi, A.K., Antonescu, C.R., Ladanyi, M., Letai, A., Garraway, L.A., Loda, M., Beer, D.G., True, L.D., Okamoto, A., Pomeroy, S.L., Singer, S., Golub, T.R., Lander, E.S., Getz, G., Sellers, W.R., Meyerson, M., 2010. The landscape of somatic copy-number alteration across human cancers. Nature 463, 899–905.
Beug, S.T., Cheung, H.H., LaCasse, E.C., Korneluk, R.G., 2012. Modulation of immune signalling by inhibitors of apoptosis. Trends Immunol. 33, 535–545.
Biesecker, L.G., Spinner, N.B., 2013. A genomic view of mosaicism and human disease. Nat. Rev. Genet. 14, 307–20.
Biggins, S., Murray, A.W., 2001. The budding yeast protein kinase Ipl1/Aurora allows the absence of tension to activate the spindle checkpoint. Genes Dev. 15, 3118–29.
Billen, L.P., Kokoski, C.L., Lovell, J.F., Leber, B., Andrews, D.W., 2008. Bcl-XL inhibits membrane permeabilization by competing with Bax. PLoS Biol. 6, 1268–1280.

Birkbak, N.J., Eklund, A.C., Li, Q., McClelland, S.E., Endesfelder, D., Tan, P., Tan, I.B., Richardson, A.L., Szallasi, Z., Swanton, C., 2011. Paradoxical relationship between chromosomal instability and survival outcome in cancer. Cancer Res. 71, 3447–3452.

Bischoff, J.R., Al., E., 1998. A homologue of Drosophila is oncogenic and amplified in human colorectal cancers. EMBO J. 17, 3052–3065.

Bishop, A.C., Kung, C., Shah, K., Witucki, L., Shokat, K.M., Liu, Y., 1999. Generation of Monospecific Nanomolar Tyrosine Kinase Inhibitors via a Chemical Genetic Approach Generation of Monospecific Nanomolar Tyrosine Kinase Inhibitors via a Chemical Genetic Approach. J. Am. Chem. Soc. 121, 627–631.

Bishop, A.C., Ubersax, J.A., Petsch, D.T., Matheos, D.P., Gray, N.S., Blethrow, J., Shimizu, E., Tsien, J.Z., Schultz, P.G., Rose, M.D., Wood, J.L., Morgan, D.O., Shokat, K.M., 2000. A chemical switch for inhibitor-sensitive alleles of any protein kinase. Nature 407, 395–401.

Bisswanger, H., 2014. Enzyme assays. Perspect. Sci. 1, 41–55.

Blangy, A., Lane, H., D'Herin, P., Harper, M., Kress, M., Nigg, E., 1995. Phosphorylation by p34(cdc2) Regulates Spindle Association of Human Eg5, a Kinesin-Related Motor Essential for Bipolar Spindle Formation In Vivo. Cell 63, 1159–1169.

Boise, L.H., Gonzalez-Garcia, M., Postema, C.E., Ding, L., Lindsten, T., Turka, L.A., Mao, X., Nunez, G., Thompson, C.B., 1993. Bcl-X, a Bcl-2 Related Gene That Functions As a Dominant Regulator of Apoptotic Cell Death. Cell 74, 597–608.

Borisy, A.A., Elliott, P.J., Hurst, N.W., Lee, M.S., Lehar, J., Price, E.R., Serbedzija, G., Zimmermann, G.R., Foley, M.A., Stockwell, B.R., Keith, C.T., 2003. Systematic discovery of multicomponent therapeutics. Proc. Natl. Acad. Sci. U. S. A. 100, 7977–7982.

Boutros, R., Dozier, C., Ducommun, B., 2006. The when and wheres of CDC25 phosphatases. Curr. Opin. Cell Biol. 18, 185–191.

Boveri, T., 2008. Concerning the origin of malignant tumours by Theodor Boveri. Translated and annotated by Henry Harris. J. Cell Sci. 121, 1–84.

Boveri, T., 1914. Zur Frage der Entstehung maligner Tumoren. Fischer, Jena.

Boveri, T., 1902. Ueber mehrpolige Mitosen als Mittel zur Analyse des Zellkerns. Verh Phys-med Ges Würzbg. NF 35, 67–90.

Brito, D.A., Rieder, C.L., 2006. Mitotic Checkpoint Slippage in Humans Occurs via Cyclin B Destruction in the Presence of an Active Checkpoint. Curr. Biol. 16, 1194–1200.

Brooks, H.B., Geeganage, S., Kahl, S.D., Montrose, C., Sittampalam, S., Smith, M.C., Weidner, J.R., 2012. Basics of Enzymatic Assays for HTS. Assay Guid. Man. 3–4.

Brown, J., Wilson, G., 2003. Apoptosis genes and resistance to cancer therapy: what does the experimental and clinical data tell us? Cancer Biol. Ther. 2, 477–90.

Brown, J.M., Attardi, L.D., 2005. The role of apoptosis in cancer development and treatment response. Nat. Rev. Cancer 5, 231–237.

Brown, K.D., Coulson, R.M.R., Yen, T.J., Cleveland, D.W., 1994. Cyclin-like accumulation and loss of the putative kinetochore motor CENP-E results from coupling continuous synthesis with specific degradation at the end of mitosis. J. Cell Biol. 125, 1303–1312.

Brown, K.D., Wood, K.W., Cleveland, D.W., 1996. The kinesin-like protein CENP-E is kinetochore-associated throughout poleward chromosome segregation during anaphase-A. J. Cell Sci. 109, 961–9.

Brunelle, J.K., Letai, A., 2009. Control of mitochondrial apoptosis by the Bcl-2 family. J. Cell Sci. 122, 437–441.

Carmena, M., Wheelock, M., Funabiki, H., Earnshaw, W.C., 2012. The chromosomal passenger complex (CPC): from easy rider to the godfather of mitosis. Nat. Rev.

Mol. Cell Biol. 13, 789–803.
Castedo, M., Perfettini, J.L., Roumier, T., Andreau, K., Medema, R., Kroemer, G., 2004. Cell death by mitotic catastrophe: a molecular definition. Oncogene 23, 2825–2837.
Certo, M., Del Gaizo Moore, V., Nishino, M., Wei, G., Korsmeyer, S., Armstrong, S. a, Letai, A., 2006. Mitochondria primed by death signals determine cellular addiction to antiapoptotic BCL-2 family members. Cancer Cell 9, 351–65.
Chakravarty, A., Shinde, V., Tabernero, J., Cervantes, A., Cohen, R.B., Dees, E.C., Burris, H., Infante, J.R., Macarulla, T., Elez, E., Andreu, J., Rodriguez-Braun, E., Rosello, S., Von Mehren, M., Meropol, N.J., Langer, C.J., ONeil, B., Bowman, D., Zhang, M., Danaee, H., Faron-Yowe, L., Gray, G., Liu, H., Pappas, J., Silverman, L., Simpson, C., Stringer, B., Tirrell, S., Veiby, O.P., Venkatakrishnan, K., Galvin, K., Manfredi, M., Ecsedy, J.A., 2011. Phase I assessment of new mechanism-based pharmacodynamic biomarkers for MLN8054, a small-molecule inhibitor of Aurora A kinase. Cancer Res. 71, 675–685.
Chan, G.K.T., Schaar, B.T., Yen, T.J., 1998. Characterization of the kinetochore binding domain of CENP-E reveals interactions with the kinetochore proteins CENP-F and hBUBR1. J. Cell Biol. 143, 49–63.
Chan, J.Y., 2011. A clinical overview of centrosome amplification in human cancers. Int. J. Biol. Sci. 7, 1122–1144.
Chan, K.-S., Koh, C.-G., Li, H.-Y., 2012. Mitosis-targeted anti-cancer therapies: where they stand. Cell Death Dis. 3, e411.
Chang, J., Wooten, E., Tsimelzon, A., Hilsenbeck, S., Gutierrez, M., Elledge, R., Mohsin, S., Osborne, C., Chamness, G., Allred, D., O'Connell, P., 2003. Gene expression profiling for the prediction of therapeutic response to docetaxel in patients with breast cancer. Mech. Dis. 362, 362–369.
Cheeseman, I.M., Chappie, J.S., Wilson-Kubalek, E.M., Desai, A., 2006. The Conserved KMN Network Constitutes the Core Microtubule-Binding Site of the Kinetochore. Cell 127, 983–997.
Chen, J., Jin, S., Abraham, V., Huang, X., Liu, B., Mitten, M.J., Nimmer, P., Lin, X., Smith, M., Shen, Y., Shoemaker, a. R., Tahir, S.K., Zhang, H., Ackler, S.L., Rosenberg, S.H., Maecker, H., Sampath, D., Leverson, J.D., Tse, C., Elmore, S.W., 2011. The Bcl-2/Bcl-XL/Bcl-w Inhibitor, Navitoclax, Enhances the Activity of Chemotherapeutic Agents In Vitro and In Vivo. Mol. Cancer Ther. 10, 2340–2349.
Chen, J.G., Horwitz, S.B., 2002. Differential mitotic responses to microtubule-stabilizing and -destabilizing drugs. Cancer Res. 62, 1935–1938.
Chen, L., Willis, S.N., Wei, A., Smith, B.J., Fletcher, J.I., Hinds, M.G., Colman, P.M., Day, C.L., Adams, J.M., Huang, D.C.S., 2005. Differential targeting of prosurvival Bcl-2 proteins by their BH3-only ligands allows complementary apoptotic function. Mol. Cell 17, 393–403.
Chen, R.-H., 2004. Phosphorylation and activation of Bub1 on unattached chromosomes facilitate the spindle checkpoint. EMBO J. 23, 3113–21.
Chen, S., Dai, Y., Harada, H., Dent, P., Grant, S., 2007. Mcl-1 down-regulation potentiates ABT-737 lethality by cooperatively inducing Bak activation and Bax translocation. Cancer Res. 67, 782–791.
Cheng, E., Levine, B., Boise, L., Thompson, C., Hardwick, J., 1996. Bax-independent inhibition of apoptosis by Bcl-xL. Nature 379, 554–556.
Chipuk, J.E., Moldoveanu, T., Llambi, F., Parsons, M.J., Green, D.R., 2010. The BCL-2 Family Reunion. Mol. Cell 37, 299–310.
Chu, R., Terrano, D.T., Chambers, T.C., 2012. Cdk1/cyclin B plays a key role in mitotic arrest-induced apoptosis by phosphorylation of Mcl-1, promoting its degradation and freeing Bak from sequestration. Biochem. Pharmacol. 83, 199–206.
Chung, V., Heath, E.I., Schelman, W.R., Johnson, B.M., Kirby, L.C., Lynch, K.M.,

Botbyl, J.D., Lampkin, T.A., Holen, K.D., 2012. First-time-in-human study of GSK923295, a novel antimitotic inhibitor of centromere-associated protein E (CENP-E), in patients with refractory cancer. Cancer Chemother. Pharmacol. 69, 733–41.
Cimini, D., 2008. Merotelic kinetochore orientation, aneuploidy, and cancer. Biochim. Biophys. Acta - Rev. Cancer 1786, 32–40.
Cimini, D., Howell, B., Maddox, P., Khodjakov, A., Degrassi, F., Salmon, E.D., 2001. Merotelic kinetochore orientation is a major mechanism of aneuploidy in mitotic mammalian tissue cells. J. Cell Biol. 152, 517–527.
Cimini, D., Tanzarella, C., Degrassi, F., 1999. Differences in malsegregation rates obtained by scoring ana-telophases or binucleate cells. Mutagenesis 14, 563–568.
Clarke, P., Tyler, K., 2003. Reovirus-induced apoptosis: A minireview. Apoptosis 8, 141–150.
Cleary, M.L., Smith, S.D., Sklar, J., 1988. Cloning and Structural Analysis of cDNAs for bcl-2 and a Hybrid bcl-2 / Immunoglobulin Transcript Resulting from the t (14;18) Translocation. Cell 47, 19–28.
Clute, P., Pines, J., 1999. Temporal and spatial control of cyclin B1 destruction in metaphase. Nat. Cell Biol. 1, 82–87.
Cochran, J.C., Krzysiak, T.C., Gilbert, S.P., 2006. Pathway of ATP hydrolysis by monomeric kinesin Eg5. Biochemistry 45, 12334–44.
Cohen, P., 2000. The regulation of protein function by multisite phosphorylation--a 25 year update. Trends Biochem. Sci. 25, 596–601.
Colin, D.J., Hain, K.O., Allan, L.A., Clarke, P.R., 2015. Cellular responses to a prolonged delay in mitosis are determined by a DNA damage response controlled by Bcl-2 family proteins. Open Biol. 5, 140156.
Colombo, R., Caldarelli, M., Mennecozzi, M., Giorgini, M.L., Sola, F., Cappella, P., Perrera, C., Re Depaolini, S., Rusconi, L., Cucchi, U., Avanzi, N., Bertrand, J.A., Bossi, R.T., Pesenti, E., Galvani, A., Isacchi, A., Colotta, F., Donati, D., Moll, J., 2010. Targeting the mitotic checkpoint for cancer therapy with NMS-P715, an inhibitor of MPS1 kinase. Cancer Res. 70, 10255–10264.
Cooke, C., Schaar, B., Yen, T., Earnshaw, W., 1997. Localization of CENP-E in the fibrous corona and outer plate of mammalian kinetochores from prometaphase through anaphase. Chromosoma 106, 446–55.
Cory, S., Adams, J.M., 2002. The Bcl2 family: regulators of the cellular life-or-death switch. Nat. Rev. Cancer 2, 647–656.
Crasta, K., Huang, P., Morgan, G., Winey, M., Surana, U., 2006. Cdk1 regulates centrosome separation by restraining proteolysis of microtubule-associated proteins. EMBO J. 25, 2551–2563.
Crook, N.E., Clem, R.J., Miller, L.K., 1993. An apoptosis-inhibiting baculovirus gene with a zinc finger-like motif. J. Virol. 67, 2168–2174.
Czabotar, P.E., Lee, E.F., van Delft, M.F., Day, C.L., Smith, B.J., Huang, D.C.S., Fairlie, W.D., Hinds, M.G., Colman, P.M., 2007. Structural insights into the degradation of Mcl-1 induced by BH3 domains. Proc. Natl. Acad. Sci. U. S. A. 104, 6217–22.
Czabotar, P.E., Lessene, G., Strasser, A., Adams, J.M., 2014. Control of apoptosis by the BCL-2 protein family: implications for physiology and therapy. Nat. Rev. Mol. Cell Biol. 15, 49–63.
Dai, W., Wang, Q., Liu, T., Haploinsufficiency, B., Yang, Y., Xu, M., Rao, C. V, 2004. Slippage of Mitotic Arrest and Enhanced Tumor Development in Mice with BubR1 Haploinsufficiency Advances in Brief Slippage of Mitotic Arrest and Enhanced Tumor Development in Mice with. Cancer Res. 64, 440–445.
Daum, J.R., Potapova, T.A., Sivakumar, S., Daniel, J.J., Flynn, J.N., Rankin, S., Gorbsky, G.J., 2011. Cohesion Fatigue Induces Chromatid Separation in Cells

Delayed at Metaphase. Curr. Biol.
Davids, M., Letai, A., 2013. ABT-199: A New Hope for Selective BCL-2 Inhibition. Cancer Cell 23, 139–141.
De Antoni, A., Pearson, C., Cimini, D., Canman, J., Sala, V., Nezi, L., Mapelli, M., Sironi, L., Faretta, M., Salmon, E., Musacchio, A., 2005. The Mad1/Mad2 Complex as a Template for Mad2 Activation in the Spindle Assembly Checkpoint. Curr. Biol. 15, 214–225.
de Lange, T., 2009. How telomeres solve the end-protection problem. Science 326, 948–52.
Delbridge, A.R.D., Grabow, S., Strasser, A., Vaux, D.L., 2016. Thirty years of BCL-2: translating cell death discoveries into novel cancer therapies. Nat. Rev. Cancer 16, 99–109.
Deng, J., Carlson, N., Takeyama, K., Dal Cin, P., Shipp, M., Letai, A., 2007. BH3 Profiling Identifies Three Distinct Classes of Apoptotic Blocks to Predict Response to ABT-737 and Conventional Chemotherapeutic Agents. Cancer Cell 12, 171–185.
Desagher, S., Osen-Sand, A., Nichols, A., Eskes, R., Montessuit, S., Lauper, S., Maubdrell, K., Antonsson, B., Martinou, J.-C., 1999. Bid-induced conformational changes of Bax is responsible for mitochondrial cytochrome c release during apoptosis. J.Cell Biol. 144, 891–901.
Deveraux, Q., Takahashi, R., Salvesen, G., Reed, J., 1997. X-linked IAP is a direct inhibitor of cell-death proteases. Nature 388, 300–4.
Díaz-Martínez, L.A., Karamysheva, Z.N., Warrington, R., Li, B., Wei, S., Xie, X.-J., Roth, M.G., Yu, H., 2014. Genome-wide siRNA screen reveals coupling between mitotic apoptosis and adaptation. EMBO J. 33, 1–17.
Ding, Q., Huo, L., Yang, J.Y., Xia, W., Wei, Y., Liao, Y., Chang, C.J., Yang, Y., Lai, C.C., Lee, D.F., Yen, C.J., Chen, Y.J.R., Hsu, J.M., Kuo, H.P., Lin, C.Y., Tsai, F.J., Li, L.Y., Tsai, C.H., Hung, M.C., 2008. Down-regulation of myeloid cell leukemia-1 through inhibiting Erk/Pin 1 pathway by sorafenib facilitates chemosensitization in breast cancer. Cancer Res. 68, 6109–6117.
Ditchfield, C., Johnson, V.L., Tighe, A., Ellston, R., Haworth, C., Johnson, T., Mortlock, A., Keen, N., Taylor, S.S., 2003. Aurora B couples chromosome alignment with anaphase by targeting BubR1, Mad2, and Cenp-E to kinetochores. J. Cell Biol. 161, 267–280.
Doménech, E., Maestre, C., Esteban-martínez, L., Partida, D., Pascual, R., Fernández-Miranda, G., Seco, E., Campos-Olivas, R., Pérez, M., Megias, D., Allen, K., López, M., Saha, A.K., Velasco, G., Rial, E., Méndez, R., Boya, P., Salazar-Roa, M., Malumbres, M., 2015. AMPK and PFKFB3 mediate glycolysis and survival in response to mitophagy during mitotic arrest. Nat. Cell Biol. 17, 1304–1316.
Domina, A.M., Vrana, J.A., Gregory, M.A., Hann, S.R., Craig, R.W., 2004. MCL1 is phosphorylated in the PEST region and stabilized upon ERK activation in viable cells, and at additional sites with cytotoxic okadaic acid or taxol. Oncogene 23, 5301–5315.
Drukman, S., Kavallaris, M., 2002. Microtubule alterations and resistance to tubulin-binding agents (Review). Int. J. Oncol. 21, 621–628.
Du, J., Kelly, A., Funabiki, H., Patel, D., 2012. Structural Basis for Recognition of H3T3ph and Smac/DIABLO N-terminal Peptides by Human Survivin. Structure 20, 185–195.
Du, L., Lyle, C.S., Chambers, T.C., 2005. Characterization of vinblastine-induced Bcl-xL and Bcl-2 phosphorylation: evidence for a novel protein kinase and a coordinated phosphorylation/dephosphorylation cycle associated with apoptosis induction. Oncogene 24, 107–117.
Dumontet, C., Jordan, M.A., 2010. Microtubule-binding agents: a dynamic field of

cancer therapeutics. Nat. Rev. Drug Discov. 9, 790–803.
Earnshaw, W.C., Bernat, R.L., 1991. Chromosomal passengers: toward an integrated view of mitosis. Chromosoma 100, 139–146.
Eckelman, B.P., Salvesen, G.S., Scott, F.L., 2006. Human inhibitor of apoptosis proteins: why XIAP is the black sheep of the family. EMBO Rep. 7, 988–94.
Edlich, F., Banerjee, S., Suzuki, M., Cleland, M.M., Arnoult, D., Wang, C., Neutzner, A., Tjandra, N., Youle, R.J., 2011. Bcl-xL retrotranslocates Bax from the mitochondria into the cytosol. Cell 145, 104–116.
Eichhorn, J.M., Alford, S.E., Sakurikar, N., Chambers, T.C., 2014. Molecular analysis of functional redundancy among anti-apoptotic Bcl-2 proteins and its role in cancer cell survival. Exp. Cell Res. 322, 415–24.
Eischen, C.M., Woo, D., Roussel, M.F., Cleveland, J.L., 2001. Apoptosis Triggered by Myc-Induced Suppression of Bcl-X L or Bcl-2 Is Bypassed during Lymphomagenesis Apoptosis Triggered by Myc-Induced Suppression of Bcl-X L or Bcl-2 Is Bypassed during Lymphomagenesis. Mol. Cell. Biol. 21, 5063–5070.
Elmore, S., 2007. Apoptosis: A Review of Programmed Cell Death. Toxicol. Pathol. 35, 495–516.
Engström, K., Vallin, M., Syrén, P.-O., Hult, K., Bäckvall, J.-E., 2011. Mutated variant of Candida antarctica lipase B in (S)-selective dynamic kinetic resolution of secondary alcohols. Org. Biomol. Chem. 9, 81–2.
Eno, C.O., Zhao, G., Olberding, K.E., Li, C., 2012. The Bcl-2 proteins Noxa and Bcl-xL co-ordinately regulate oxidative stress-induced apoptosis. Biochem. J. 444, 69–78.
Estornes, Y., Bertrand, M.J.M., 2015. Seminars in Cell & Developmental Biology IAPs, regulators of innate immunity and inflammation. Semin. Cell Dev. Biol. 39, 106–114.
Evans, T., Rosenthal, E.T., Youngblom, J., Distel, D., Hunt, T., 1983. Cyclin: A protein specified by maternal mRNA in sea urchin eggs that is destroyed at each cleavage division. Cell 33, 389–396.
Ferenz, N.P., Gable, A., Wadsworth, P., 2010. Mitotic functions of kinesin-5. Semin. Cell Dev. Biol. 21, 255–9.
Fernius, J., Hardwick, K.G., 2007. Bub1 kinase targets Sgo1 to ensure efficient chromosome biorientation in budding yeast mitosis. PLoS Genet. 3, e213.
Flemming, W., 1881. Studien uber Regeneration der Gewebe. Aus dem Anat. Inst. Kiel 4-42, 60-6.
Frykman, H., Ohrner, N., Norin, T., Hult, K., 1993. S-ethyl thiooctanoate as acyl donor in lipase catalysed resolution of secondary alcohols. Tetrahedron Lett. 34, 1367–1370.
Fukahara, S., Rowley, J., 1978. Chromosome 14 translocations in non-Burkitt lymphomas. Int. J. Cancer 22, 14–21.
Fulda, S., Vucic, D., 2012. Targeting IAP proteins for therapeutic intervention in cancer. Nat. Rev. Drug Discov. 11, 109–24.
Ganem, N.J., Godinho, S. a, Pellman, D., 2009. A mechanism linking extra centrosomes to chromosomal instability. Nature 460, 278–82.
Ganem, N.J., Pellman, D., 2012. Linking abnormal mitosis to the acquisition of DNA damage. J. Cell Biol. 199, 871–881.
Gascoigne, K.E., Taylor, S.S., 2009. How do anti-mitotic drugs kill cancer cells? J. Cell Sci. 122, 2579–85.
Gascoigne, K.E., Taylor, S.S., 2008. Cancer cells display profound intra- and interline variation following prolonged exposure to antimitotic drugs. Cancer Cell 14, 111–22.
Geigl, J.B., Obenauf, A.C., Schwarzbraun, T., Speicher, M.R., 2008. Defining “chromosomal instability.” Trends Genet. 24, 64–69.

Gennerich, A., Vale, R.D., 2009. Walking the walk: how kinesin and dynein coordinate their steps. Curr. Opin. Cell Biol. 21, 59–67.
Ghanem, A., Aboul-Enein, H.Y., 2005. Application of lipases in kinetic resolution of racemates. Chirality 17, 1–15.
Gianni, L., Zambetti, M., Clark, K., Baker, J., Cronin, M., Wu, J., Mariani, G., Rodriguez, J., Carcangiu, M., Watson, D., Valagussa, P., Rouzier, R., Symmans, W.F., Ross, J.S., Hortobagyi, G.N., Pusztai, L., Shak, S., 2005. Gene expression profiles in paraffin-embedded core biopsy tissue predict response to chemotherapy in women with locally advanced breast cancer. J. Clin. Oncol. 23, 7265–7277.
Girdler, F., Gascoigne, K.E., Eyers, P. a, Hartmuth, S., Crafter, C., Foote, K.M., Keen, N.J., Taylor, S.S., 2006. Validating Aurora B as an anti-cancer drug target. J. Cell Sci. 119, 3664–75.
Gjertsen, B.T., Schöffski, P., 2014. Discovery and development of the Polo-like kinase inhibitor volasertib in cancer therapy. Leukemia 11–19.
Glaser, S.P., Lee, E.F., Trounson, E., Gores, G.J., Kaufmann, S.H., Bouillet, P., Wei, A., Fairlie, W.D., Izon, D.J., Zuber, J., Rappaport, A.R., Herold, M.J., Alexander, W.S., Lowe, S.W., Robb, L., 2012. Anti-apoptotic Mcl-1 is essential for the development and sustained growth of acute myeloid leukemia Anti-apoptotic Mcl-1 is essential for the development and sustained growth of acute myeloid leukemia. Genes Dev. 26, 120–125.
Glinsky, G. V, Berezovska, O., Glinskii, A.B., 2005. Microarray analysis identifies a death-from- cancer signature predicting therapy failure in patients with multiple types of cancer. J. Clin. Invest. 115, 1503–1521.
Glotzer, M., Murray, A.W., Kirschner, M.W., 1991. Cyclin is degraded by the ubiquitin pathway. Nature 349, 132–138.
Glover, D., Leibowitz, M., McLean, D., Parry, H., 1995. Mutations in aurora Prevent Centrosome Separation Leading to the Formation of Monopolar Spindles. Cell 81, 95–105.
Golsteyn, R.M., Mundt, K.E., Fry, A.M., Nigg, E.A., 1995. Cell-Cycle Regulation of the Activity and Subcellular-Localization of Plk1, A Human Protein-Kinase Implicated in Mitotic Spindle Function. J. Cell Biol. 129, 1617–1628.
Gordon, D.J., Resio, B., Pellman, D., 2012. Causes and consequences of aneuploidy in cancer. Nat. Rev. Genet. 13, 189–203.
Goshima, G., Vale, R.D., 2003. The roles of microtubule-based motor proteins in mitosis: comprehensive RNAi analysis in the Drosophila S2 cell line. J. Cell Biol. 162, 1003–16.
Goto, H., Yasui, Y., Kawajiri, A., Nigg, E.A., Terada, Y., Tatsuka, M., Nagata, K. ichi, Inagaki, M., 2003. Aurora-B regulates the cleavage furrow-specific vimentin phosphorylation in the cytokinetic process. J. Biol. Chem. 278, 8526–8530.
Gotor-Fernández, V., Brieva, R., Gotor, V., 2006. Lipases: Useful biocatalysts for the preparation of pharmaceuticals. J. Mol. Catal. B Enzym. 40, 111–120.
Gottesman, M.M., 2002. Mechanisms of cancer drug resistance. Annu. Rev. Med. 53, 615–627.
Grabow, S., Delbridge, A.R.D., Valente, L.J., Strasser, A., 2014. MCL-1 but not BCL-XL is critical for the development and sustained expansion of thymic lymphoma in p53-deficient mice. Blood 124, 3939–3946.
Grabsch, H., Takeno, S., Parsons, W.J., Pomjanski, N., Boecking, A., Gabbert, H.E., Mueller, W., 2003. Overexpression of the mitotic checkpoint genes BUB1, BUBR1, and BUB3 in gastric cancer - Association with tumour cell proliferation. J. Pathol. 200, 16–22.
Grabsch, H.I., Askham, J.M., Morrison, E.E., Pomjanski, N., Lickvers, K., Parsons, W.J., Boecking, A., Gabbert, H.E., Mueller, W., 2004. Expression of BUB1 protein in gastric cancer correlates with the histological subtype, but not with DNA ploidy

or microsatellite instability. J. Pathol. 202, 208–214.
Gudimchuk, N., Vitre, B., Kim, Y., Kiyatkin, A., Cleveland, D.W., Ataullakhanov, F.I., Grishchuk, E.L., 2013. Kinetochore kinesin CENP-E is a processive bi-directional tracker of dynamic microtubule tips. Nat. Cell Biol. 15, 1079–1088.
Gyrd-Hansen, M., Meier, P., 2010. IAPs : from caspase inhibitors to modulators of NF-κ B , inflammation and cancer. Nat. Publ. Gr. 10, 561–574.
Hacker, G., 2000. The morphology of apoptosis. Cell Tissue Res. 301, 5–17.
Hagting, A., Jackman, M., Simpson, K., Pines, J., 1999. Translacation of cyclin B1 to the nucleus at prophase requires a aphosphorylation-dependent nuclear import signal. Curr. Biol. 9, 680–689.
Hain, K.O., Colin, D.J., Rastogi, S., Allan, L.A., Clarke, P.R., 2016. Prolonged mitotic arrest induces a caspase-dependent DNA damage response at telomeres that determines cell survival. Sci. Rep. 6, 26766.
Haldar, S., Jena, N., Croce, C., 1995. Inactivation of Bcl-2 by phosphorylation. Proc. Natl. Acad. Sci. 92, 4507–4511.
Hanahan, D., Weinberg, R.A., 2011. Hallmarks of cancer: The next generation. Cell 144, 646–674.
Hanisch, A., Wehner, A., Nigg, E., Sillje, H., 2006. Different Plk1 Functions Show Distinct Dependencies on Polo-Box Domain-mediated Targeting. Mol. Biol. Cell 17, 448–459.
Hanks, S.K., Hunter, T., 1995. The eukaryotic protein kinase superfamily : kinase (catalytic) domam structure and classification. FASEB J. 9, 576–596.
Harley, M.E., Allan, L.A., Sanderson, H.S., Clarke, P.R., 2010. Phosphorylation of Mcl-1 by CDK1–cyclin B1 initiates its Cdc20-dependent destruction during mitotic arrest. EMBO J. 29, 2407–2420.
Harvey, M., McArthur, M., Montgomery Jr, C., Butel, J., Bradley, A., Donehower, L., 1993. Spontaneous and carcinogen-induced tumorigenesis in p53-deficient mice. Nat. Genet. 5, 225–229.
Haschka, M.D., Soratroi, C., Kirschnek, S., Häcker, G., Hilbe, R., Geley, S., Villunger, A., Fava, L.L., 2015. The NOXA–MCL1–BIM axis defines lifespan on extended mitotic arrest. Nat. Commun. 6, 6891.
Hassold, T., Hunt, P., 2001. To err (meiotically) is human: the genesis of human aneuploidy. Nat. Rev. Genet. 2, 280–291.
Hauf, S., Cole, R.W., LaTerra, S., Zimmer, C., Schnapp, G., Walter, R., Heckel, A., Van Meel, J., Rieder, C.L., Peters, J.M., 2003. The small molecule Hesperadin reveals a role for Aurora B in correcting kinetochore-microtubule attachment and in maintaining the spindle assembly checkpoint. J. Cell Biol. 161, 281–294.
Hayashi, M.T., Cesare, A.J., Fitzpatrick, J.A.J., Lazzerini-Denchi, E., Karlseder, J., 2012. A telomere-dependent DNA damage checkpoint induced by prolonged mitotic arrest. Nat. Struct. Mol. Biol. 19, 387–394.
Hayden, J.H., Bowser, S.S., Rieder, C.L., 1990. Kinetochores capture astral microtubules during chromosome attachment to the mitotic spindle: Direct visualization in live newt lung cells. J. Cell Biol. 111, 1039–1045.
Heald, R., Khodjakov, A., 2015. Thirty years of search and capture: The complex simplicity of mitotic spindle assembly. J. Cell Biol. 211, 1103–1111.
Heilig, C.E., Loffler, H., Mahlknecht, U., Janssen, J.W.G., Ho, A.D., Jauch, A., Kramer, A., 2010. Chromosomal instability correlates with poor outcome in patients with myelodysplastic syndromes irrespectively of the cytogenetic risk group. J. Cell. Mol. Med. 14, 895–902.
Hempen, P.M., Kurpad, H., Calhoun, E.S., Abraham, S., Kern, S.E., 2003. A double missense variation of the BUB1 gene and a defective mitotic spindle checkpoint in the pancreatic cancer cell line Hs766T. Hum. Mutat. 21, 445.
Hewitt, L., Tighe, A., Santaguida, S., White, A.M., Jones, C.D., Musacchio, A., Green,

S., Taylor, S.S., 2010. Sustained Mps1 activity is required in mitosis to recruit O-Mad2 to the Mad1-C-Mad2 core complex. J. Cell Biol. 190, 25–34.
Higgins, J.M.G., 2013. Chromosome segregation: Learning to let go. Curr. Biol. 23, R883–R885.
Hitchcock, M., Mengel, A., Richter, A., Briem, H., Eis, K., Pütter, V., Siemeister, G., Prechtl, S., AE Fernandez-Montalvan, C.S., 2013. Substituted benzylpyrazoles WO2013092512.
Hochegger, H., Takeda, S., Hunt, T., 2008. Cyclin-dependent kinases and cell-cycle transitions : does one fit all ? Nat. Rev. Mol. Cell Biol. 9, 910–916.
Holland, A.J., Cleveland, D.W., 2012. Losing balance: the origin and impact of aneuploidy in cancer. EMBO Rep. 13, 501–514.
Holland, A.J., Cleveland, D.W., 2009. Boveri revisited: chromosomal instability, aneuploidy and tumorigenesis. Nat. Rev. Mol. Cell Biol. 10, 478–487.
Holtrich, U.W.E., Wolf, G., Brauninger, A., Karnq, T., Bohme, B., Rjbsamen-waigmann, H., Strebhardt, K., 1994. Induction and down-regulation of PLK, a human serine/threonine kinase expressed in proliferating cells and tumors. Proc. Natl. Acad. Sci. 91, 1736–1740.
Holy, T.E., Leibler, S., 1994. Dynamic instability of microtubules as an efficient way to search in space. Pro. Natl. Aca. Sci., USA 91, 5682–5685.
Horvitz, H., 1999. Genetic control of programmed cell death in the nematode Caenorhabditis elegans. Cancer Res. 1, 1701s–1706s.
Huang, H.C., Shi, J., Orth, J.D., Mitchison, T.J., 2009. Evidence that Mitotic Exit Is a Better Cancer Therapeutic Target Than Spindle Assembly. Cancer Cell 16, 347–358.
Huszar, D., Theoclitou, M.-E., Skolnik, J., Herbst, R., 2009. Kinesin motor proteins as targets for cancer therapy. Cancer Metastasis Rev. 28, 197–208.
Ichim, G., Lopez, J., Ahmed, S.U., Muthalagu, N., Giampazolias, E., Delgado, M.E., Haller, M., Riley, J.S., Mason, S.M., Athineos, D., Parsons, M.J., VandeKooij, B., Bouchier-Hayes, L., Chalmers, A.J., Rooswinkel, R.W., Oberst, A., Blyth, K., Rehm, M., Murphy, D.J., Tait, S.W.G., 2015. Limited Mitochondrial Permeabilization Causes DNA Damage and Genomic Instability in the Absence of Cell Death. Mol. Cell 57, 860–872.
Imreh, G., Norberg, H.V., Imreh, S., Zhivotovsky, B., 2011. Chromosomal breaks during mitotic catastrophe trigger γH2AX-ATM-p53-mediated apoptosis. J. Cell Sci. 124, 2951–63.
Inoshita, S., Takeda, K., Hatai, T., Terada, Y., Sano, M., Hata, J., Umezawa, A., Ichijo, H., 2002. Phosphorylation and inactivation of myeloid cell leukemia 1 by JNK in response to oxidative stress. J. Biol. Chem. 277, 43730–43734.
Inoué, S., Salmon, E.D., 1995. Force generation by microtubule assembly/disassembly in mitosis and related movements. Mol. Biol. Cell 6, 1619–40.
Invitrogen, 2010. Flp-In System.
Iringer, S., Piatti, S., Michaelis, C., Nasmyth, K., 1995. Genes involved in sister chromatid separation are needed for beta-type cyclin proteolysis in budding yeast. Cell 81, 269–277.
Jablonski, S.A., Chan, G.K., Cooke, C.A., Earnshaw, W.C., Yen, T.J., 1998. The hBUB1 and hBUBR1 kinases sequentially assemble onto kinetochores during prophase with hBUBR1 concentrating at the kinetochore plates in mitosis. Chromosoma 107, 386–96.
Jackman, M., Lindon, C., Nigg, E.A., Pines, J., 2003. Active cyclin B1-Cdk1 first appears on centrosomes in prophase. Nat. Cell Biol. 5, 143–148.
Jackson, J.R., Patrick, D.R., Dar, M.M., Huang, P.S., 2007. Targeted anti-mitotic therapies: can we improve on tubulin agents? Nat. Rev. Cancer 7, 107–17.
Jacobson, M.D., Weil, M., Raff, M.C., 1997. Programmed Cell Death in Animal

Development. Cell 88, 347–354.
James, N.D., Sydes, M.R., Clarke, N.W., Mason, M.D., Dearnaley, D.P., Spears, M.R., Ritchie, A.W.S., Parker, C.C., Russell, J.M., Attard, G., De Bono, J., Cross, W., Jones, R.J., Thalmann, G., Amos, C., Matheson, D., Millman, R., Alzouebi, M., Beesley, S., Birtle, A.J., Brock, S., Cathomas, R., Chakraborti, P., Chowdhury, S., Cook, A., Elliott, T., Gale, J., Gibbs, S., Graham, J.D., Hetherington, J., Hughes, R., Laing, R., McKinna, F., McLaren, D.B., O'Sullivan, J.M., Parikh, O., Peedell, C., Protheroe, A., Robinson, A.J., Srihari, N., Srinivasan, R., Staffurth, J., Sundar, S., Tolan, S., Tsang, D., Wagstaff, J., Parmar, M.K.B., 2016. Addition of docetaxel, zoledronic acid, or both to first-line long-term hormone therapy in prostate cancer (STAMPEDE): Survival results from an adaptive, multiarm, multistage, platform randomised controlled trial. Lancet 387, 1163–1177.
Janssen, A., Beerling, E., Medema, R., van Rheenen, J., 2013. Intravital FRET Imaging of Tumor Cell Viability and Mitosis during Chemotherapy. PLoS One 8.
Janssen, A., Kops, G.J.P.L., Medema, R.H., 2009. Elevating the frequency of chromosome mis-segregation as a strategy to kill tumor cells. Proc. Natl. Acad. Sci. U. S. A. 106, 19108–13.
Janssen, A., van der Burg, M., Szuhai, K., Kops, G.J.P.L., Medema, R.H., 2011. Chromosome Segregation Errors as a Cause of DNA Damage and Structural Chromosome Aberrations. Science 333, 1895–1898.
Jeganathan, K., Malureanu, L., Baker, D.J., Abraham, S.C., Van Deursen, J.M., 2007. Bub1 mediates cell death in response to chromosome missegregation and acts to suppress spontaneous tumorigenesis. J. Cell Biol. 179, 255–267.
Johnson, V.L., Scott, M.I.F., Holt, S. V, Hussein, D., Taylor, S.S., 2004. Bub1 is required for kinetochore localization of BubR1, Cenp-E, Cenp-F and Mad2, and chromosome congression. J. Cell Sci. 117, 1577–89.
Jordan, M.A., Toso, R.J., Thrower, D., Wilson, L., 1993. Mechanism of mitotic block and inhibition of cell proliferation by taxol at low concentrations. Proc. Natl. Acad. Sci. U. S. A. 90, 9552–6.
Jordan, M.A., Wendell, K., Gardiner, S., Jordan, M.A., Wendell, K., Gardiner, S., Derry, W.B., Copp, H., Wilson, L., 1996. Mitotic Block Induced in HeLa Cells by Low Concentrations of Paclitaxel (Taxol) Results in Abnormal Mitotic Exit and Apoptotic Cell Death. Cancer Res. 56, 816–825.
Jordan, M.A., Wilson, L., 2004. Microtubules as a target for anticancer drugs. Nat. Rev. Cancer 4, 253–265.
Kaitna, S., Mendoza, M., Jantsch-Plunger, V., Glotzer, M., 2000. Incenp and an Aurora-like kinase form a complex essential for chromosome segregation and efficient completion of cytokinesis. Curr. Biol. 10, 1172–1181.
Kaitna, S., Pasierbek, P., Jantsch, M., Loidl, J., Glotzer, M., 2002. The Aurora B kinase, AIR-2, regulates kinetochores during mitosis and is required for separation of homologous chromosomes during meiosis. Curr. Biol. 12, 798–812.
Kallio, M.J., McCleland, M.L., Stukenberg, P.T., Gorbsky, G.J., 2002. Inhibition of Aurora B kinase blocks chromosome segregation, overrides the spindle checkpoint, and perturbs microtubule dynamics in mitosis. Curr. Biol. 12, 900–905.
Kaman, J., Van der Eycken, J., Peter, A., Fulop, F., 2001. Enzymatic resolution of bicyclic 1, 3-amino alcohols in organic media. Tetrahedron: Asymmetry 12, 625–631.
Kang, J., Yang, M., Li, B., Qi, W., Zhang, C., Shokat, K.M., Tomchick, D.R., Machius, M., Yu, H., 2008. Structure and substrate recruitment of the human spindle checkpoint kinase Bub1. Mol. Cell 32, 394–405.
Kapoor, T.M., Lampson, M.A., Hergert, P., Cameron, L., Cimini, D., Salmon, E.D., McEwen, B.F., Khodjakov, A., 2006. Chromosomes can congress to the metaphase plate before biorientation. Science 311, 388–91.

Kawabata, T., Tanimura, S., Asai, K., Kawasaki, R., Matsumaru, Y., Kohno, M., 2012. Up-regulation of pro-apoptotic protein Bim and down-regulation of anti-apoptotic protein Mcl-1 cooperatively mediate enhanced tumor cell death induced by the combination of ERK kinase (MEK) inhibitor and microtubule inhibitor. J. Biol. Chem. 287, 10289–300.
Kawashima, S.A., Yamagishi, Y., Honda, T., Ishiguro, K., Watanabe, Y., 2010. Phosphorylation of H2A by Bub1 prevents chromosomal instability through localizing shugoshin. Science 327, 172–7.
Keen, N., Taylor, S., 2009. Mitotic drivers—inhibitors of the Aurora B Kinase. Cancer Metastasis Rev. 28, 185–195.
Kelly, A., Ghenoiu, C., Xue, J., Zierhut, C., Kimura, H., Funabiki, H., 2010. Survivin Reads Phosphorylated Histone H3 Threonine 3 to Activate the Mitotic Kinase Aurora B Alexander. Science 330, 235–239.
Kelly, G., Strasser, A., 2011. The essential role of evasion from cell death in cancer. Adv. Cancer Res. 111, 39–96.
Kerr, J., Wyllie, A., Currie, A., 1972. Apoptosis: a Basic Biological Phenomenon With Wideranging Implications in Tissue Kinetics. Br. J. Cancer 26, 239–257.
Kiefer, M., Brauer, M., Powers, V., Wu, J., Umansky, S., Tomei, D., Barr, P., 1995. Modulation of apoptosis by the widely distributed Bcl-2 homologue Bak. Nature 374, 736–739.
Kim, Y., Heuser, J.E., Waterman, C.M., Cleveland, D.W., 2008. CENP-E combines a slow, processive motor and a flexible coiled coil to produce an essential motile kinetochore tether. J. Cell Biol. 181, 411–419.
Kim, Y., Holland, A.J., Lan, W., Cleveland, D.W., 2010. Aurora kinases and protein phosphatase 1 mediate chromosome congression through regulation of CENP-E. Cell 142, 444–455.
King, E.M.J., Rachidi, N., Morrice, N., Hardwick, K.G., Stark, M.J.R., 2007. Ipl1p-dependent phosphorylation of Mad3p is required for the spindle checkpoint response to lack of tension at kinetochores. Genes Dev. 21, 1163–1168.
King, R.W., Peters, J.M., Tugendreich, S., Rolfe, M., Hieter, P., Kirschner, M.W., 1995. A 20s complex containing CDC27 and CDC16 catalyzes the mitosis-specific conjugation of ubiquitin to cyclin B. Cell 81, 279–288.
Kirschner, M.W., Mitchison, T.J., 1986. Beyond self assembly: from microtubules to morphogenesis. Cell 45, 329–342.
Kischkel, F.C., Hellbardt, S., Behrmann, I., Germer, M., Pawlita, M., Krammer, P.H., Peter, M.E., 1995. Cytotoxicity-dependent APO-1 (Fas/CD95)-associated proteins form a death-inducing signaling complex (DISC) with the receptor. EMBO J. 14, 5579–88.
Kitajima, T., Hauf, S., Ohsugi, M., 2005. Human Bub1 defines the persistent cohesion site along the mitotic chromosome by affecting Shugoshin localization. Curr. Biol. 15, 353–359.
Kiyomitsu, T., Obuse, C., Yanagida, M., 2007. Human Blinkin/AF15q14 is required for chromosome alignment and the mitotic checkpoint through direct interaction with Bub1 and BubR1. Dev. Cell 13, 663–76.
Klebig, C., Korinth, D., Meraldi, P., 2009. Bub1 regulates chromosome segregation in a kinetochore-independent manner. J. Cell Biol. 185, 841–58.
Knowlton, A.L., Lan, W., Stukenberg, P.T., 2006. Aurora B Is Enriched at Merotelic Attachment Sites, Where It Regulates MCAK. Curr. Biol. 16, 1705–1710.
Kobayashi, S., Lee, S.H., Meng, X.W., Mott, J.L., Bronk, S.F., Werneburg, N.W., Craig, R.W., Kaufmann, S.H., Gores, G.J., 2007. Serine 64 phosphorylation enhances the antiapoptotic function of Mcl-1. J. Biol. Chem. 282, 18407–18417.
Kodama, Y., Taura, K., Miura, K., Schnabl, B., Osawa, Y., Brenner, D.A., 2009. Antiapoptotic Effect of c-Jun N-terminal Kinase-1 through Mcl-1 Stabilization in

TNF-Induced Hepatocyte Apoptosis. Gastroenterology 136, 1423–1434.
Kollareddy, M., Zheleva, D., Dzubak, P., Brahmkshatriya, P.S., Lepsik, M., Hajduch, M., 2012. Aurora kinase inhibitors: Progress towards the clinic. Invest. New Drugs 30, 2411–2432.
Komlodi-Pasztor, E., Sackett, D.L., Fojo, A.T., 2012. Inhibitors targeting mitosis: Tales of how great drugs against a promising target were brought down by a flawed rationale. Clin. Cancer Res. 18, 51–63.
Konopleva, M., Contractor, R., Tsao, T., Samudio, I., Ruvolo, P.P., Kitada, S., Deng, X., Zhai, D., Shi, Y.X., Sneed, T., Verhaegen, M., Soengas, M., Ruvolo, V.R., McQueen, T., Schober, W.D., Watt, J.C., Jiffar, T., Ling, X., Marini, F.C., Harris, D., Dietrich, M., Estrov, Z., McCubrey, J., May, W.S., Reed, J.C., Andreeff, M., 2006. Mechanisms of apoptosis sensitivity and resistance to the BH3 mimetic ABT-737 in acute myeloid leukemia. Cancer Cell 10, 375–388.
Kornev, A.P., Haste, N.M., Taylor, S.S., Eyck, L.F. Ten, 2006. Surface comparison of active and inactive protein kinases identifies a conserved activation mechanism. Proc. Natl. Acad. Sci. U. S. A. 103, 17783–17788.
Koss, B., Morrison, J., Perciavalle, R.M., Singh, H., Rehg, J.E., Williams, R.T., Opferman, J.T., 2013. Requirement for antiapoptotic MCL-1 in the survival of BCR-ABL B-lineage acute lymphoblastic leukemia. Blood 122, 1587–1598.
Kozopas, K.M., Yang, T., Buchan, H.L., Zhou, P., Craig, R.W., 1993. MCL1, a gene expressed in programmed myeloid cell differentiation, has sequence similarity to BCL2. Proc. Natl. Acad. Sci. U. S. A. 90, 3516–20.
Krek, W., Nigg, E., 1992. Cell cycle regulation of vertebrate p34(cdc2) activity: identification of Thr161 as an essential in vivo phosphorylation site. New Biol. 4, 323–329.
Krenn, V., Wehenkel, A., Li, X., Santaguida, S., Musacchio, A., 2012. Structural analysis reveals features of the spindle checkpoint kinase Bub1-kinetochore subunit Knl1 interaction. J. Cell Biol. 196, 451–467.
Kung, P.-P., Martinez, R., Zhu, Z., Zager, M., Blasina, A., Rymer, I., Hallin, J., Xu, M., Carroll, C., Chionis, J., Wells, P., Kozminski, K., Fan, J., Guicherit, O., Huang, B., Cui, M., Liu, C., Huang, Z., Sistla, A., Yang, J., Murray, B.W., 2014. Chemogenetic Evaluation of the Mitotic Kinesin CENP-E Reveals a Critical Role in Triple-Negative Breast Cancer. Mol. Cancer Ther. 13, 2104–15.
Kusakabe, K.I., Ide, N., Daigo, Y., Itoh, T., Yamamoto, T., Hashizume, H., Nozu, K., Yoshida, H., Tadano, G., Tagashira, S., Higashino, K., Okano, Y., Sato, Y., Inoue, M., Iguchi, M., Kanazawa, T., Ishioka, Y., Dohi, K., Kido, Y., Sakamoto, S., Ando, S., Maeda, M., Higaki, M., Baba, Y., Nakamura, Y., 2015. Discovery of imidazo[1,2- b]pyridazine derivatives: Selective and orally available Mps1 (TTK) kinase inhibitors exhibiting remarkable antiproliferative activity. J. Med. Chem. 58, 1760–1775.
Kutuk, O., Letai, A., 2010. Displacement of Bim by Bmf and Puma rather than increase in Bim level mediates paclitaxel-induced apoptosis in breast cancer cells. Cell Death Differ. 17, 1624–1635.
Kutuk, O., Letai, A., 2008. Alteration of the mitochondrial apoptotic pathway is key to acquired paclitaxel resistance and can be reversed by ABT-737. Cancer Res. 68, 7985–7994.
Kuukasjärvi, T., Karhu, R., Tanner, M., Nupponen, N., Pennanen, S., Kallioniemi, A., Kallioniemi, O., Isola, J., 1997. Genetic Heterogeneity and Clonal Evolution Underlying Development of Asynchronous Metastasis in Human Breast Cancer. Cancer Res. 57, 1597–1604.
Kwon, M., Godinho, S.A., Chandhok, N.S., Ganem, N.J., Azioune, A., Thery, M., Pellman, D., 2008. Mechanisms to suppress multipolar divisions in cancer cells with extra centrosomes. Genes Dev. 22, 2189–2203.

Labi, V., Erlacher, M., Krumschnabel, G., Manzl, C., Tzankov, A., Pinon, J., Egle, A., Villunger, A., 2010. Apoptosis of leukocytes triggered by acute DNA damage promotes lymphoma formation. Genes Dev. 24, 1602–1607.
Lampson, M.A., Cheeseman, I.M., 2011. Sensing centromere tension: Aurora B and the regulation of kinetochore function. Trends Cell Biol. 21, 133–140.
Lanni, J.S., Jacks, T., 1998. Characterization of the p53-dependent postmitotic checkpoint following spindle disruption. Mol. Cell. Biol. 18, 1055–64.
Lara-Gonzalez, P., Taylor, S.S., 2012. Cohesion fatigue explains why pharmacological inhibition of the APC/C induces a spindle checkpoint-dependent mitotic arrest. PLoS One 7, e49041.
Lara-Gonzalez, P., Westhorpe, F.G., Taylor, S.S., 2012. The spindle assembly checkpoint. Curr. Biol. 22, R966–80.
Lawrence, C.J., Dawe, R.K., Christie, K.R., Cleveland, D.W., Dawson, S.C., Endow, S.A., Goldstein, L.S.B., Goodson, H. V, Hirokawa, N., Howard, J., Malmberg, R.L., McIntosh, J.R., Miki, H., Mitchison, T.J., Okada, Y., Reddy, A.S.N., Saxton, W.M., Schliwa, M., Scholey, J.M., Vale, R.D., Walczak, C.E., Wordeman, L., 2004. A standardized kinesin nomenclature. J. Cell Biol. 167, 19–22.
Leeson, P., Oncology, H., Hospital, C., 1912. Chemical beauty contest. Nature 481, 455–456.
Lehár, J., Krueger, A.S., Avery, W., Heilbut, A.M., Johansen, L.M., Price, E.R., Rickles, R.J., Short, G.F., Staunton, J.E., Jin, X., Lee, M.S., Zimmermann, G.R., Borisy, A. a, 2009. Synergistic drug combinations tend to improve therapeutically relevant selectivity. Nat. Biotechnol. 27, 659–666.
Lengauer, C., Kinzler, K.W., Vogelstein, B., 1998. Genetic instabilities in human cancers. Nature 396, 643–649.
Lens, S.M.A., Voest, E.E., Medema, R.H., 2010. Shared and separate functions of polo-like kinases and aurora kinases in cancer. Nat. Rev. Cancer 10, 825–841.
Lera, R.F., Burkard, M.E., 2012. High mitotic activity of polo-like kinase 1 is required for chromosome segregation and genomic integrity in human epithelial cells. J. Biol. Chem. 287, 42812–42825.
Lessene, G., Czabotar, P.E., Colman, P.M., 2008. BCL-2 family antagonists for cancer therapy. Nat. Rev. Drug Discov. 7, 989–1000.
Lessene, G., Czabotar, P.E., Sleebs, B.E., Zobel, K., Lowes, K.N., Adams, J.M., Baell, J.B., Colman, P.M., Deshayes, K., Fairbrother, W.J., Flygare, J.A., Gibbons, P., Kersten, W.J.A., Kulasegaram, S., Moss, R.M., Parisot, J.P., Smith, B.J., Street, I.P., Yang, H., Huang, D.C.S., Watson, K.G., 2013. Structure-guided design of a selective BCL-X(L) inhibitor. Nat. Chem. Biol. 9, 390–7.
Letai, A., Bassik, M.C., Walensky, L.D., Sorcinelli, M.D., Weiler, S., Korsmeyer, S.J., 2002. Distinct BH3 domains either sensitize or activate mitochondrial apoptosis, serving as prototype cancer therapeutics. Cancer Cell 2, 183–192.
Leverson, J.D., Phillips, D.C., Mitten, M.J., Boghaert, E.R., Diaz, D., Tahir, S.K., Belmont, L.D., Nimmer, P., Xiao, Y., Ma, X.M., Lowes, K.N., Kovar, P., Chen, J., Jin, S., Smith, M., Xue, J., Zhang, H., Oleksijew, A., Magoc, T.J., Vaidya, K.S., Albert, D.H., Tarrant, J.M., La, N., Wang, L., Tao, Z.-F., Wendt, M.D., Sampath, D., Rosenberg, S.H., Tse, C., Huang, D.C.S., Fairbrother, W.J., Elmore, S.W., Souers, A.J., 2015a. Exploiting selective BCL-2 family inhibitors to dissect cell survival dependencies and define improved strategies for cancer therapy. Sci. Transl. Med. 7, 279ra40.
Leverson, J.D., Zhang, H., Chen, J., Tahir, S.K., Phillips, D.C., Xue, J., Nimmer, P., Jin, S., Smith, M., Xiao, Y., Kovar, P., Tanaka, A., Bruncko, M., Sheppard, G.S., Wang, L., Gierke, S., Kategaya, L., Anderson, D.J., Wong, C., Eastham-Anderson, J., Ludlam, M.J.C., Sampath, D., Fairbrother, W.J., Wertz, I., Rosenberg, S.H., Tse, C., Elmore, S.W., Souers, A.J., 2015b. Potent and selective small-molecule

MCL-1 inhibitors demonstrate on-target cancer cell killing activity as single agents and in combination with ABT-263 (navitoclax). Cell Death Dis. 6, e1590.
Li, H., Zhu, H., Xu, C., Yuan, J., 1998. 1998 LI Cleavage of BID by Caspase 8 Mediates the Mitochondrial Damage in the Fas Pathway of Apoptosis. Cell 94, 491–501.
Li, R., Moudgil, T., Ross, H.J., Hu, H.-M., 2005. Apoptosis of non-small-cell lung cancer cell lines after paclitaxel treatment involves the BH3-only proapoptotic protein Bim. Cell Death Differ. 12, 292–303.
Li, R., Murray, A.W., 1991. Feedback control of mitosis in budding yeast. Cell 66, 519–31.
Li, X., Nicklas, R.B., 1995. Mitotic forces control a cell-cycle checkpoint. Nature 373, 630–632.
Lin, E.Y., Orlofsky, A., Berger, M.S., Prystowsky, M.B., 1993. Characterization of A1, a novel hemopoietic-specific early-response gene with sequence similarity to bcl-2. J. Immunol. 151, 1979–88.
Lin, Z., Jia, L., Tomchick, D.R., Luo, X., Yu, H., 2014. Substrate-Specific Activation of the Mitotic Kinase Bub1 through Intramolecular Autophosphorylation and Kinetochore Targeting. Structure 22, 1616–1627.
Lindon, C., Pines, J., 2004. Ordered proteolysis in anaphase inactivates Plk1 to contribute to proper mitotic exit in human cells. J. Cell Biol. 164, 233–241.
Lindqvist, A., van Zon, W., Karlsson Rosenthal, C., Wolthuis, R.M.F., 2007. Cyclin B1-Cdk1 activation continues after centrosome separation to control mitotic progression. PLoS Biol. 5, e123.
Lingle, W.L., Lutz, W.H., Ingle, J.N., Maihle, N.J., Salisbury, J.L., 1998. Centrosome hypertrophy in human breast tumors: implications for genomic stability and cell polarity. Proc. Natl. Acad. Sci. U. S. A. 95, 2950–5.
Lipinski, C., Lombardo, F., Dominy, B., Feeney, P., 2012. Experimental and computational approaches to estimate solubility and permeability in drug discovery and development setting. Adv. Drug Deliv. Rev. 64, 4–17.
Liu, F., Stanton, J.J., Wu, Z., Piwnica-Worms, H., 1997. The human Myt1 kinase preferentially phosphorylates Cdc2 on threonine 14 and localizes to the endoplasmic reticulum and Golgi complex. Mol. Cell. Biol. 17, 571–83.
Liu, H., Rankin, S., Yu, H., 2013. Phosphorylation-enabled binding of SGO1-PP2A to cohesin protects sororin and centromeric cohesion during mitosis. Nat. Cell Biol. 15, 40–9.
Liu, X., Dai, S., Zhu, Y., Marrack, P., Kappler, J.W., Street, J., 2003. The Structure of a Bcl-x L / Bim Fragment Complex : Implications for Bim Function. Immunity 19, 341–352.
Liu, X., Kim, C.N., Yang, J., Jemmerson, R., Wang, X., 1996. Induction of apoptotic program in cell-free extracts: Requirement for dATP and cytochrome c. Cell 86, 147–157.
Liu, Z., Ling, K., Wu, X., Cao, J., Liu, B., Li, S., Si, Q., Cai, Y., Yan, C., Zhang, Y., Weng, Y., 2009. Reduced expression of cenp-e in human hepatocellular carcinoma. J. Exp. Clin. Cancer Res. 28, 156.
Locksley, R.M., Killeen, N., Lenardo, M.J., 2001. The TNF and TNF Receptor Superfamilies. Cell 104, 487–501.
Lohka, M.J., Hayes, M.K., Maller, J.L., 1988. Purification of maturation-promoting factor, an intracellular regulator of early mitotic events. Proc. Natl. Acad. Sci. U. S. A. 85, 3009–3013.
Lolli, G., Johnson, L.N., 2005. CAK-Cyclin-Dependent Activating Kinase: A key kinase in cell cycle control and a target for Drugs? Cell Cycle 4, 572–577.
Lopez, J., Tait, S.W.G., 2015. Mitochondrial apoptosis: killing cancer using the enemy within. Br. J. Cancer 112, 957–62.
Lowe, S.W., Ruley, H.E., Jacks, T., Housman, D.E., 1993. P53-Dependent Apoptosis

Modulates the Cytotoxicity of Anticancer Agents. Cell 74, 957–967.
Maia, A.R.R., Man, J. De, Boon, U., Janssen, A., Song, J., Omerzu, M., Sterrenburg, J.G., Prinsen, M.B.W., Willemsen-Seegers, N., van Doornmalen, A.M., Uitdehaag, J.C.M., Kops, G.J., Jonkers, J., Buijsman, R.C., Zaman, G.J., Medema, R.H., 2015. Inhibition of the spindle assembly checkpoint kinase TTK enhances the efficacy of docetaxel in a triple negative breast cancer model. Ann. Oncol. 26, 2180–92.
Malumbres, M., 2011. Physiological Relevance of Cell Cycle Kinases. Physiol. Rev. 91, 973–1007.
Manchado, E., Guillamot, M., Malumbres, M., 2012. Killing cells by targeting mitosis. Cell Death Differ. 19, 369–377.
Manfredi, M.G., Ecsedy, J.A., Meetze, K.A., Balani, S.K., Burenkova, O., Chen, W., Galvin, K.M., Hoar, K.M., Huck, J.J., LeRoy, P.J., Ray, E.T., Sells, T.B., Stringer, B., Stroud, S.G., Vos, T.J., Weatherhead, G.S., Wysong, D.R., Zhang, M., Bolen, J.B., Claiborne, C.F., 2007. Antitumor activity of MLN8054, an orally active small-molecule inhibitor of Aurora A kinase. Proc. Natl. Acad. Sci. U. S. A. 104, 4106–4111.
Manning, G., 2002. The Protein Kinase Complement of the Human Genome. Science 298, 1912–1934.
Mao, Y., Abrieu, A., Cleveland, D.W., 2003. Activating and silencing the mitotic checkpoint through CENP-E-dependent activation/inactivation of BubR1. Cell 114, 87–98.
Mao, Y., Desai, A., Cleveland, D.W., 2005. Microtubule capture by CENP-E silences BubR1-dependent mitotic checkpoint signaling. J. Cell Biol. 170, 873–880.
Marcus, A.I., Peters, U., Thomas, S.L., Garrett, S., Zelnak, A., Kapoor, T.M., Giannakakou, P., 2005. Mitotic kinesin inhibitors induce mitotic arrest and cell death in taxol-resistant and -sensitive cancer cells. J. Biol. Chem. 280, 11569–11577.
Marivin, A., Berthelet, J., Plenchette, S., Dubrez, L., 2012. The Inhibitor of Apoptosis (IAPs) in Adaptive Response to Cellular Stress. Cells 1, 711–37.
Mason, K.D., Carpinelli, M.R., Fletcher, J.I., Collinge, J.E., Hilton, A.A., Ellis, S., Kelly, P.N., Ekert, P.G., Metcalf, D., Roberts, A.W., Huang, D.C.S., Kile, B.T., 2007. Programmed Anuclear Cell Death Delimits Platelet Life Span. Cell 128, 1173–1186.
Maurer, U., Charvet, C., Wagman, A.S., Dejardin, E., Green, D.R., 2006. Glycogen synthase kinase-3 regulates mitochondrial outer membrane permeabilization and apoptosis by destabilization of MCL-1. Mol. Cell 21, 749–760.
Mayer, T.U., 1999. Small Molecule Inhibitor of Mitotic Spindle Bipolarity Identified in a Phenotype-Based Screen. Science 286, 971–974.
Mazumdar, M., Sundareshan, S., Misteli, T., 2004. Human chromokinesin KIF4A functions in chromosome condensation and segregation. J. Cell Biol. 166, 613–620.
McClelland, S.E., Burrell, R.A., Swanton, C., 2009. Chromosomal instability: A composite phenotype that influences sensitivity to chemotherapy. Cell Cycle 8, 3262–3266.
McDonnell, T., Deane, N., Platt, F., Nunez, G., Jaeger, U., McKearn, J., Korsmeyer, S., 1989. bcl-2-immunoglobulin transgenic mice demonstrate extended B cell survival and follicular lymphoproliferation. Cell 57, 79–88.
McEwen, B.F., Chan, G.K., Zubrowski, B., Savoian, M.S., Sauer, M.T., Yen, T.J., 2001. CENP-E is essential for reliable bioriented spindle attachment, but chromosome alignment can be achieved via redundant mechanisms in mammalian cells. Mol. Biol. Cell 12, 2776–2789.
McGuinness, B.E., Hirota, T., Kudo, N.R., Peters, J.M., Nasmyth, K., 2005. Shugoshin

prevents dissociation of cohesin from centromeres during mitosis in vertebrate cells. PLoS Biol. 3, 0433–0449.
McKeown, M.R., Bradner, J.E., 2014. Therapeutic strategies to inhibit MYC. Cold Spring Harb. Perspect. Med. 4.
Meraldi, P., Sorger, P.K., 2005. A dual role for Bub1 in the spindle checkpoint and chromosome congression. EMBO J. 24, 1621–33.
Michalak, E.M., Vandenberg, C.J., Delbridge, A.R.D., Wu, L., Scott, C.L., Adams, J.M., Strasser, A., 2010. Apoptosis-promoted tumorigenesis: gamma-irradiation-induced thymic lymphomagenesis requires Puma-driven leukocyte death. Genes Dev. 24, 1608–1613.
Michel, L.S., Liberal, V., Chatterjee, A., Kirchwegger, R., Pasche, B., Gerald, W., Dobles, M., Sorger, P.K., Murty, V. V, Benezra, R., 2001. MAD2 haplo-insufficiency causes premature anaphase and chromosome instability in mammalian cells. Nature 409, 355–359.
Millman, S.E., Pagano, M., 2011. MCL1 meets its end during mitotic arrest. EMBO Rep. 12, 384–5.
Milross, C.G., Mason, K. a, Hunter, N.R., Chung, W.K., Peters, L.J., Milas, L., 1996. Relationship of mitotic arrest and apoptosis to antitumor effect of paclitaxel. J. Natl. Cancer Inst. 88, 1308–1314.
Minn, A.J., Boise, L.H., Thompson, C.B., 1996. Expression of Bcl-x(L) and loss of p53 can cooperate to overcome a cell cycle checkpoint induced by mitotic spindle damage. Genes Dev. 10, 2621–2631.
Minn, B.A.J., Rudin, C.M., Boise, L.H., Thompson, C.B., 1995. Expression of Bcl-xL Can Confer a Multidrug Resistance Phenotype. Blood 86, 1903–1911.
Minor, L., 2006. Handbook of Assay Development in Drug Discovery. Taylor and Francis Group.
Mitchison, T.J., 2012. The proliferation rate paradox in antimitotic chemotherapy. Mol. Biol. Cell 23, 1–6.
Mitchison, T.J., Kirschner, M., 1984. Dynamic instability of microtubule growth. Nature 312, 237–242.
Mitelman, 2014. Mitelman Database of Chromosome Aberrations and Gene Fusions in Cancer [WWW Document]. URL http://cgap.nci.nih.gov/Chromosomes/Mitelman
Montero, J., Sarosiek, K. a., DeAngelo, J.D., Maertens, O., Ryan, J., Ercan, D., Piao, H., Horowitz, N.S., Berkowitz, R.S., Matulonis, U., Jänne, P. a., Amrein, P.C., Cichowski, K., Drapkin, R., Letai, A., 2015. Drug-Induced Death Signaling Strategy Rapidly Predicts Cancer Response to Chemotherapy. Cell 160, 977–989.
Morel, C., Carlson, S.M., White, F.M., Davis, R.J., 2009. Mcl-1 integrates the opposing actions of signaling pathways that mediate survival and apoptosis. Mol. Cell. Biol. 29, 3845–3852.
Mori, T., Kinoshita, Y., Watanabe, A., Yamaguchi, T., Hosokawa, K., Honjo, H., 2006. Retention of paclitaxel in cancer cells for 1 week in vivo and in vitro. Cancer Chemother. Pharmacol. 58, 665–672.
Morrow, C.J., Tighe, A., Johnson, V.L., Scott, M.I.F., Ditchfield, C., Taylor, S.S., 2005. Bub1 and aurora B cooperate to maintain BubR1-mediated inhibition of APC/CCdc20. J. Cell Sci. 118, 3639–52.
Moustafa-Kamal, M., Gamache, I., Lu, Y., Li, S., Teodoro, J.G., 2013. BimEL is phosphorylated at mitosis by Aurora A and targeted for degradation by βTrCP1. Cell Death Differ. 20, 1393–403.
Muchmore, S., Sattler, M., Liang, H., Meadows, R., Harlan, J., Yoon, H., Nettesheim, D., Chang, B., Thompson, C., Wong, S., Ng, S., Fesik, S., 1996. X-ray and NMR structure of human Bcl-xL, an inhibitor of programmed cell death. Nature 381, 335–341.
Mullard, A., 2012. Protein–protein interaction inhibitors get into the groove. Nat. Rev.

Drug Discov. 11, 173–175.
Muller, P.A.J., Vousden, K.H., 2014. Mutant p53 in cancer: New functions and therapeutic opportunities. Cancer Cell 25, 304–317.
Murray, S., Briasoulis, E., Linardou, H., Bafaloukos, D., Papadimitriou, C., 2012. Taxane resistance in breast cancer: Mechanisms, predictive biomarkers and circumvention strategies. Cancer Treat. Rev. 38, 890–903.
Musacchio, A., Salmon, E.D., 2007. The spindle-assembly checkpoint in space and time. Nat. Rev. Mol. Cell Biol. 8, 379–93.
Nakagawa, T., Kollmeyer, T.M., Morlan, B.W., Anderson, S.K., Bergstralh, E.J., Davis, B.J., Asmann, Y.W., Klee, G.G., Ballman, K. V., Jenkins, R.B., 2008. A tissue biomarker panel predicting systemic progression after PSA recurrence post-definitive prostate cancer therapy. PLoS One 3.
Nakano, K., Vousden, K.H., 2001. PUMA, a novel proapoptotic gene, is induced by p53. Mol. Cell 7, 683–694.
Ndubaku, C., Varfolomeev, E., Wang, L., Zobel, K., Lau, K., Elliott, L.O., Maurer, B., Fedorova, A. V, Dynek, J.N., Koehler, M., Hymowitz, S.G., Tsui, V., Deshayes, K., Fairbrother, W.J., Flygare, J.A., Vucic, D., 2009. Antagonism of c-IAP and XIAP proteins is required for efficient induction of cell death by small-molecule IAP antagonists. ACS Chem. Biol. 4, 557–566.
Ni Chonghaile, T., Sarosiek, K.A., Vo, T., Ryan, J.A., Richardson, P., Tai, Y., Mitsiades, C.S., Matulonis, U.A., Drapkin, R., Stone, R., Deangelo, D.J., Mcconkey, D.J., Sallan, S.E., Silverman, L., Hirsch, M.S., Carrasco, D.R., Letai, A., 2011. Pretreatment Mitochondrial Priming Correlates with Clinical Response to Cytotoxic Chemotherapy Triona. Science 334, 1129–1133.
Ni Chonghaile, T., Sarosiek, K.A., Vo, T., Ryan, J.A., Tammareddi, A., Del, V., Moore, G., Deng, J., Anderson, K., Tai, Y., Mitsiades, C.S., Matulonis, U.A., Stone, R., Deangelo, D.J., Mcconkey, D.J., Sallan, S.E., Silverman, L., Hirsch, M.S., Carrasco, D.R., Letai, A., 2012. Pretreatment Mitochondrial Priming Correlates with Clinical Response to Cytotoxic Chemotherapy. Science 334, 1129–1133.
Nicholson, J.M., Cimini, D., 2011. How Mitotic Errors Contribute to Karyotypic Diversity in Cancer, Advances in Cancer Research. Elsevier Inc.
Nigg, E.A., 2001. Mitotic kinases as regulators of cell division and its checkpoints. Nat. Rev. Mol. Cell Biol. 2, 21–32.
Nigg, E.A., 1995. Cyclin-dependent protein kinases: key regulators of the eukaryotic cell cycle. BioEssays 17, 471–480.
Nolen, B., Taylor, S., Ghosh, G., 2004. Regulation of protein kinases: Controlling activity through activation segment conformation. Mol. Cell 15, 661–675.
Nurse, P., 1990. Universal control mechanism regulating onset of M-phase. Nature 344, 503–508.
Nyati, S., Schinske-Sebolt, K., Pitchiaya, S., Chekhovskiy, K., Chator, A., Chaudhry, N., Dosch, J., Van Dort, M.E., Varambally, S., Kumar-Sinha, C., Nyati, M.K., Ray, D., Walter, N.G., Yu, H., Ross, B.D., Rehemtulla, A., 2015. The kinase activity of the Ser/Thr kinase BUB1 promotes TGF-β signaling. Sci. Signal. 8, ra1.
O 'Gorman, S., Fox, D.T., Wahl, G.M., 1991. Recombinase-Mediated Gene Activation and Site-Specific Integration in Mammalian Cells. Source Sci. New Ser. 251, 1351–1355.
O'Connor, L., Strasser, A., O'Reilly, L.A., Hausmann, G., Adams, J.M., Cory, S., Huang, D.C.S., 1998. Bim: A novel member of the Bcl-2 family that promotes apoptosis. EMBO J. 17, 384–395.
O'Farrell, P.H., 2001. Triggering the all-or-nothing switch into mitosis. Trends Cell Biol. 11, 512–519.
O'Neill, K.L., Huang, K., Zhang, J., Chen, Y., Luo, X., 2016. Inactivation of prosurvival Bcl-2 proteins activates Bax / Bak through the outer mitochondrial membrane.

Genes Dev 30, 973–988.
O'Neill, M., Beecher, D., Mangan, D., Rowan, A.S., Monte, A., Sroka, S., Modregger, J., Hundle, B., Moody, T.S., 2012. A novel lipase enzyme panel exhibiting superior activity and selectivity over lipase B from Candida antarctica for the kinetic resolution of secondary alcohols. Tetrahedron: Asymmetry 23, 583–586.
Oda, E., 2000. Noxa, a BH3-Only Member of the Bcl-2 Family and Candidate Mediator of p53-Induced Apoptosis. Science 288, 1053–1058.
Ohashi, A., Ohori, M., Iwai, K., Nambu, T., Miyamoto, M., Kawamoto, T., Okaniwa, M., 2015. A novel time-dependent CENP-E inhibitor with potent antitumor activity. PLoS One 10, 1–19.
Okada, H., Mak, T.W., 2004. Pathways of apoptotic and non-apoptotic death in tumour cells. Nat. Rev. Cancer 4, 592–603.
Olopade, O., Adeyanju, M., Safa, A., Hagos, F., Mick, R., Thompson, C., Recant, W., 1997. Overexpression of BCL-x protein in primary breast cancer is associated with high tumor grade and nodal metastases. Cancer J. Sci. Am. 3, 230–7.
Oltersdorf, T., Elmore, S.W., Shoemaker, A.R., Armstrong, R.C., Augeri, D.J., Belli, B.A., Bruncko, M., Deckwerth, T.L., Dinges, J., Hajduk, P.J., Joseph, M.K., Kitada, S., Korsmeyer, S.J., Kunzer, A.R., Letai, A., Li, C., Mitten, M.J., Nettesheim, D.G., Ng, S., Nimmer, P.M., O'Connor, J.M., Oleksijew, A., Petros, A.M., Reed, J.C., Shen, W., Tahir, S.K., Thompson, C.B., Tomaselli, K.J., Wang, B., Wendt, M.D., Zhang, H., Fesik, S.W., Rosenberg, S.H., 2005. An inhibitor of Bcl-2 family proteins induces regression of solid tumours. Nature 435, 677–681.
Oltvai, Z.N., Milliman, C.L., Korsemeyer, S.J., 1993. Bcl-2 Heterodimerizes in-Vivo With a Conserved Homolog, Bax, That Accelerates Programmed Cell-Death. Cell 74, 609–619.
Orrenius, C., Mattson, A., Norin, T., 1994. Preparation of 1-pyridinylethanols of high enantiomeric purity by lipase catalysed transesterifications. Tetrahedron: Asymmetry 5, 1363–1366.
Orrenius, C., Ohrner, N., Rottici, D., Mattson, A., Hult, K., Norin, T., 1995. Candida antarctica lipase B catalysed kinetic resolutions: Substrate structure requirements for the preparation of enantiomerically enriched secondary alcanols. Tetrahedron: Asymmetry 6, 1217–1220.
Orth, J., Kohler, R., Foijer, F., Sorger, P., Weissleder, R., Mitchison, T., 2011. Analysis of mitosis and anti-mitotic drug responses in tumors by in vivo microscopy and single-cell pharmacodynamics. Cancer Res. 71, 4608–4616.
Orth, J.D., Loewer, A., Lahav, G., Mitchison, T.J., 2012. Prolonged mitotic arrest triggers partial activation of apoptosis, resulting in DNA damage and p53 induction. Mol. Biol. Cell 23, 567–576.
Packham, G., White, E.L., Eischen, C.M., Yang, H., Parganas, E., Ihle, J.N., Grillot, D.A.M., Zambetti, G.P., Nunez, G., Cleveland, J.L., 1998. Selective regulation of Bcl-X(L) by a Jak kinase-dependent pathway is bypassed in murine hematopoietic malignancies. Genes Dev. 12, 2475–2487.
Parker, L.L., Atherton-fessler, S.U.E., Piwnica-worms, H., 1992. Weel Is a Dual-Specificity Kinase That Phosphorylates. Cell 89, 2917–2921.
Perera, D., Taylor, S.S., 2010. Sgo1 establishes the centromeric cohesion protection mechanism in G2 before subsequent Bub1-dependent recruitment in mitosis. J. Cell Sci. 123, 653–9.
Perera, D., Tilston, V., Hopwood, J. a, Barchi, M., Boot-Handford, R.P., Taylor, S.S., 2007. Bub1 maintains centromeric cohesion by activation of the spindle checkpoint. Dev. Cell 13, 566–79.
Petitjean, A., Mathe, E., Kato, S., Ishioka, C., Tavtigian, S., Hainaut, P., Olivier, M., 2007. Impact of Mutant p53 Functional Properties on Mutation Patterns and Tumor Phenotype: Lessons from Recent Developments in the IARC TP53

Database. Hum. Mutat. 28, 622–629.
Pihan, G.A., Purohit, A., Wallace, J., Knecht, H., Woda, B., Quesenberry, P., Doxsey, S.J., 1998. Centrosome Defects and Genetic Instability in Malignant Tumors Centrosome Defects and Genetic Instability in Malignant Tumors. Cancer Res. 58, 3974–3985.
Piidkzdingrrotbtiti, I.L., Orrenius, C., Mattson, A., Norin, T., 1994. Preparation of 1-Pyridinylethanols of High Enantiomeric by Lipase Catalysed Transesterifications. Tetrahedron: Asymmetry 5, 1363–1366.
Pines, J., 2006. Mitosis: A matter of getting rid of the right protein at the right time. Trends Cell Biol. 16, 55–63.
Pinna, L.A., Ruzzene, M., 1996. How do protein kinases recognize their substrates? Biochim. Biophys. Acta - Mol. Cell Res. 1314, 191–255.
Poruchynsky, M.S., Wang, E.E., Rudin, C.M., Blagosklonny, M. V., Fojo, T., 1998. Bcl-x(L) is phosphorylated in malignant cells following microtubule disruption. Cancer Res. 58, 3331–3338.
Punnoose, E., Leverson, J., Peale, F., Boghaert, E., Belmont, L., Tan, N., Young, A., Mitten, M., Ingalla, E., Darbonna, W., Oleksijew, A., Tapang, P., Yue, P., Oeh, J., Lee, L., Maiga, S., Fairbrother, W., Amiot, M., Souers, A., Sampath, D., 2016. Expression profile of BCL-2, BCL-XL and MCL-1 predicts pharmacological response to the BCL-2 selective antagonist venetoclax in multiple myeloma models. Mol. Cancer Ther. 15, 1132–44.
Putkey, F.R., Cramer, T., Morphew, M.K., Silk, A.D., Johnson, R.S., McIntosh, J.R., Cleveland, D.W., 2002. Unstable kinetochore-microtubule capture and chromosomal instability following deletion of CENP-E. Dev. Cell 3, 351–65.
Qi, W., Yu, H., 2007. KEN-box-dependent degradation of the Bub1 spindle checkpoint kinase by the anaphase-promoting complex/cyclosome. J. Biol. Chem. 282, 3672–9.
Qian, X., McDonald, A., Zhou, H.-J., Adams, N.D., Parrish, C.A., Duffy, K.J., Fitch, D.M., Tedesco, R., Ashcraft, L.W., Yao, B., Jiang, H., Huang, J.K., Marin, M. V., Aroyan, C.E., Wang, J., Ahmed, S., Burgess, J.L., Chaudhari, A.M., Donatelli, C.A., Darcy, M.G., Ridgers, L.H., Newlander, K.A., Schmidt, S.J., Chai, D., Colón, M., Zimmerman, M.N., Lad, L., Sakowicz, R., Schauer, S., Belmont, L., Baliga, R., Pierce, D.W., Finer, J.T., Wang, Z., Morgan, B.P., Morgans, D.J., Auger, K.R., Sung, C.-M., Carson, J.D., Luo, L., Hugger, E.D., Copeland, R. a., Sutton, D., Elliott, J.D., Jackson, J.R., Wood, K.W., Dhanak, D., Bergnes, G., Knight, S.D., 2010. Discovery of the First Potent and Selective Inhibitor of Centromere-Associated Protein E: GSK923295. ACS Med. Chem. Lett. 1, 30–34.
Quintyne, N., Reing, J., Hoffelder, D., Gollin, S., Saunders, W., 2005. Spindle Multipolarity Is Prevented by Centrosomal Clustering. Science 307, 127–129.
Raab, M., Krämer, A., Hehlgans, S., Sanhaji, M., Kurunci-Csacsko, E., Dötsch, C., Bug, G., Ottmann, O., Becker, S., Pachl, F., Kuster, B., Strebhardt, K., 2015. Mitotic arrest and slippage induced by pharmacological inhibition of Polo-like kinase 1. Mol. Oncol. 9, 140–154.
Raab, M., Pachl, F., Krämer, A., Kurunci-Csacsko, E., Dötsch, C., Knecht, R., Becker, S., Kuster, B., Strebhardt, K., 2014. Quantitative chemical proteomics reveals a Plk1 inhibitor-compromised cell death pathway in human cells. Cell Res. 1–4.
Rath, O., Kozielski, F., 2015. Kinesins and cancer. Kinesins and Cancer 12, 1–271.
Reed, J., Miyashita, T., Takayama, S., Wang, H., Sato, T., Krajewski, S., Aime-Sempe, C., Bodrug, S., Kitada, S., Hanada, M., 1996. BCL-2 family proteins: regulators of cell death involved in the pathogenesis of cancer and resistance to therapy. J. Cell Biochem. 60, 23–32.
Reed, J.C., Stein, C., Subasinghe, C., Haldar, S., Croce, C.M., Yum, S., Cohen, J., 1990. Antisense-mediated inhibition of BCL2 protooncogene expression and

leukemic cell growth and survival: comparison of phosphodiester and phosphorothiolate oligonucleotides. Cancer Res 50, 6565–6570.
Renehen, A., Booth, C., Potten, C., 2001. What is apoptosis and why is it important? BMJ 322, 1536–1538.
Ricke, R.M., Jeganathan, K.B., van Deursen, J.M., 2011. Bub1 overexpression induces aneuploidy and tumor formation through Aurora B kinase hyperactivation. J. Cell Biol. 193, 1049–64.
Rieder, C., Maiato, H., 2004. Stuck in Division or Passing through : What Happens When Cells Cannot Review. Dev. Cell 7, 637–651.
Rieder, C.L., Alexander, S.P., 1990. Kinetochores are transported poleward along a single astral microtubule during chromosome attachment to the spindle in newt lung cells. J. Cell Biol. 110, 81–95.
Rieder, C.L., Cole, R.W., Khodjakov, A., Sluder, G., 1995. The checkpoint delaying anaphase in response to chromosome monoorientation is mediated by an inhibitory signal produced by unattached kinetochores. J. Cell Biol. 130, 941–948.
Rieder, C.L., Schultz, a, Cole, R., Sluder, G., 1994. Anaphase onset in vertebrate somatic cells is controlled by a checkpoint that monitors sister kinetochore attachment to the spindle. J. Cell Biol. 127, 1301–10.
Rivera, N.R., Hsiao, Y., Cowen, J. a., McWilliams, C., Armstrong, J., Yasuda, N., Hughes, D.L., 2001. Highly Efficient Synthesis of 2-Amino-3-Pyridinecarboxaldehyde. Synth. Commun. 31, 1573–1579.
Roberts, A.W., Davids, M.S., Pagel, J.M., Kahl, B.S., Puvvada, S.D., Gerecitano, J.F., Kipps, T.J., Anderson, M.A., Brown, J.R., Gressick, L., Wong, S., Dunbar, M., Zhu, M., Desai, M.B., Cerri, E., Enschede, S.H., Humerickhouse, R.A., Wierda, W.G., Seymour, J.F., 2015. Targeting BCL2 with Venetoclax in Relapsed Chronic Lymphocytic Leukemia. N. Engl. J. Med. 374, 311–322.
Roberts, A.W., Seymour, J.F., Brown, J.R., Wierda, W.G., Kipps, T.J., Khaw, S.L., Carney, D.A., He, S.Z., Huang, D.C.S., Xiong, H., Cui, Y., Busman, T.A., McKeegan, E.M., Krivoshik, A.P., Enschede, S.H., Humerickhouse, R., 2012. Substantial susceptibility of chronic lymphocytic leukemia to BCL2 inhibition: Results of a phase I study of navitoclax in patients with relapsed or refractory disease. J. Clin. Oncol. 30, 488–496.
Roberts, B.T., Farr, K.A., Hoyt, M.A., 1994. The Saccharomyces cerevisiae checkpoint gene BUB1 encodes a novel protein kinase. Mol. Cell. Biol. 14, 8282–91.
Rothbauer, U., Zolghadr, K., Muyldermans, S., Schepers, A., Cardoso, M.C., Leonhardt, H., 2007. A Versatile Nanotrap for Biochemical and Functional Studies with Fluorescent Fusion Proteins. Mol. Cell. Proteomics 7, 282–289.
Rotticci, D., Rotticci-Mulder, J.C., Denman, S., Norin, T., Hult, K., 2001. Improved enantioselectivity of a lipase by rational protein engineering. Chembiochem 2, 766–770.
Rouf, A., Gupta, P., Aga, M.A., Kumar, B., Parshad, R., Taneja, S.C., 2011. Cyclic trans-beta-amino alcohols: Preparation and enzymatic kinetic resolution. Tetrahedron: Asymmetry 22, 2134–2143.
Rowinsky, E., Donehower, R., 1995. Paclitaxel (Taxol). N. Engl. J. Med. 332, 1004–1014.
Rowinsky, E., Eisenhauer, E., Chaudhry, V., Arbuck, S., Donehower, R., 1993. Clinical toxicities encountered with paclitaxel (Taxol). Semin. Oncol. 20, 1–15.
Russell, P., Nurse, P., 1984. cdc25+ Functions as an Inducer in the M itotic Control of Fission Yeast. Cell 45, 145–153.
Ryan, J.A., Brunelle, J.K., Letai, A., 2010. Heightened mitochondrial priming is the basis for apoptotic hypersensitivity of CD4+ CD8+ thymocytes. Proc. Natl. Acad. Sci. U. S. A. 107, 12895–900.
Saelens, X., Festjens, N., Vande Walle, L., van Gurp, M., van Loo, G., Vandenabeele,

P., 2004. Toxic proteins released from mitochondria in cell death. Oncogene 23, 2861–2874.
Sáez, A.J.G., Villunger, A., 2016. MOMP in the absence of BH3-only proteins. Genes Dev 30, 878–880.
Sakurikar, N., Eichhorn, J.M., Chambers, T.C., 2012. Cyclin-dependent kinase-1 (Cdk1)/cyclin B1 dictates cell fate after mitotic arrest via phosphoregulation of antiapoptotic Bcl-2 proteins. J. Biol. Chem. 287, 39193–204.
Salmela, A., Kallio, M., 2013. Mitosis as an anti-cancer drug target. Chromosoma 122, 431–449.
Santaguida, S., Amon, A., 2015. Short- and long-term effects of chromosome mis-segregation and aneuploidy. Nat. Rev. Mol. Cell Biol. 16, 473–485.
Santamaría, D., Barrière, C., Cerqueira, A., Hunt, S., Tardy, C., Newton, K., Cáceres, J.F., Dubus, P., Malumbres, M., Barbacid, M., 2007. Cdk1 is sufficient to drive the mammalian cell cycle. Nature 448, 811–815.
Sattler, M., Liang, H., Nettesheim, D., Meadows, R.P., Harlan, J.E., Eberstadt, M., Yoon, H.S., Shuker, S.B., Chang, B.S., Minn, A.J., Thompson, C.B., Fesik, S.W., 1997. Structure of Bcl-xL-Bak peptide complex: recognition between regulators of apoptosis. Science 275, 983–6.
Saxton, W.M., Stemple, D.L., Leslie, R.J., Salmon, E.D., Zavortink, M., McIntosh, J.R., 1984. Tubulin dynamics in cultured mammalian cells. J. Cell Biol. 99, 2175–2186.
Schaar, B.T., Chan, G.K.T., Maddox, P., Salmon, E.D., Yen, T.J., 1997. CENP-E function at kinetochores is essential for chromosome alignment. J. Cell Biol. 139, 1373–1382.
Schliekelman, M., Cowley, D.O., O'Quinn, R., Oliver, T.G., Lu, C., Salmon, E.D., Van Dyke, T., 2009. Impaired Bub1 function in vivo compromises tension-dependent checkpoint function leading to aneuploidy and tumorigenesis. Cancer Res. 69, 45–54.
Sedlak, T.W., Oltvai, Z.N., Yang, E., Wang, K., Boise, L.H., Thompson, C.B., Korsmeyer, S.J., 1995. Multiple Bcl-2 family members demonstrate selective dimerizations with Bax. Proc. Natl. Acad. Sci. 92, 7834–7838.
Sekar, G., Kamble, R.M., Singh, V.K., 1999. Enantiomerically pure N -aryl- β -amino alcohols by enzymatic resolution. Tetrahedron: Asymmetry 10, 12–15.
Seki, A., Coppinger, J.A., Jang, C.-Y., Yates, J.R., Fang, G., 2008. Bora and the kinase Aurora a cooperatively activate the kinase Plk1 and control mitotic entry. Science 320, 1655–1658.
Senft, D., Weber, A., Saathoff, F., Berking, C., Heppt, M. V, Kammerbauer, C., Rothenfusser, S., Kellner, S., Kurgyis, Z., Besch, R., Häcker, G., 2015. In non-transformed cells Bak activates upon loss of anti-apoptotic Bcl-X L and Mcl-1 but in the absence of active BH3-only proteins. Nat. Publ. Gr. 6, 1–11. doi:10.1038/cddis.2015.341
Sentman, C.L., Shutter, J.R., Hockenbery, D., Kanagawa, O., Korsmeyer, S.J., 1991. Bcl-2 Inhibits Multiple Forms of Apoptosis But Not Negative Selection in Thymocytes. Cell 67, 879–888.
Sharp-Baker, H., Chen, R.H., 2001. Spindle checkpoint protein Bub1 is required for kinetochore localization of Mad1, Mad2, Bub3, and CENP-E, independently of its kinase activity. J. Cell Biol. 153, 1239–50.
Shi, J., Orth, J.D., Mitchison, T., 2008. Cell type variation in responses to antimitotic drugs that target microtubules and kinesin-5. Cancer Res. 68, 3269–3276.
Shi, J., Zhou, Y., Huang, H.-C., Mitchison, T.J., 2011. Navitoclax (ABT-263) accelerates apoptosis during drug-induced mitotic arrest by antagonizing Bcl-xL. Cancer Res. 71, 4518–26.
Shichiri, M., Yoshinaga, K., Hisatomi, H., Sugihara, K., Hirata, Y., 2002. Genetic and epigenetic inactivation of mitotic checkpoint genes hBUB1 and hBUBR1 and their

relationship to survival. Cancer Res. 62, 13–17.
Shin, H.J., Baek, K.H., Jeon, A.H., Park, M.T., Lee, S.J., Kang, C.M., Lee, H.S., Yoo, S.H., Chung, D.H., Sung, Y.C., McKeon, F., Lee, C.W., 2003. Dual roles of human BubR1, a mitotic checkpoint kinase, in the monitoring of chromosomal instability. Cancer Cell 4, 483–497.
Shiozaki, E., Chai, J., Rigotti, D., Riedl, S., Li, P., Srinivasula, S., Alnemri, E., Fairman, R., Shi, Y., 2003. Mechanism of XIAP-mediated inhibition of caspase-9. Mol. Cell 11, 519–527.
Silk, A.D., Zasadil, L.M., Holland, A.J., Vitre, B., Cleveland, D.W., Weaver, B.A., 2013. Chromosome missegregation rate predicts whether aneuploidy will promote or suppress tumors. Proc. Natl. Acad. Sci. U. S. A. 110, E4134–41.
Slee, E.A., Harte, M.T., Kluck, R.M., Wolf, B.B., Casiano, C.A., Newmeyer, D.D., Wang, H., Reed, J.C., Nicholson, D.W., Alnemri, E.S., Green, D.R., Martin, S.J., 1999. Ordering the Cytochrome c–initiated Caspase Cascade: Hierarchical Activation of Caspases-2, -3, -6, -7, -8, and -10 in a Caspase-9–dependent Manner. J. Cell Biol. 144, 281–292.
Sloss, O., Topham, C., Diez, M., Taylor, S., 2016. Mcl-1 dynamics influence mitotic slippage and death in mitosis. Oncotarget 7, 5176–5192.
Sodir, N.M., Swigart, L.B., Karnezis, A.N., Hanahan, D., Evan, G.I., Soucek, L., 2011. Endogenous Myc maintains the tumor microenvironment. Genes Dev. 25, 907–916.
Solomon, M.J., Glotzer, M., Lee, T.H., Philippe, M., Kirschner, M.W., 1990. Cyclin activation of p34cdc2. Cell 63, 1013–1024.
Solomon, M.J., Lee, T., Kirschner, M.W., 1992. Role of phosphorylation in p34cdc2 activation: identification of an activating kinase. Mol. Biol. Cell 3, 13–27.
Sotiriou, C., Neo, S., McShane, L., 2003. Breast cancer classification and prognosis based on gene expression profiles from a population-based study. Proc. Natl. Acad. Sci. 100, 10393–10398.
Souers, A.J., Leverson, J.D., Boghaert, E.R., Ackler, S.L., Catron, N.D., Chen, J., Dayton, B.D., Ding, H., Enschede, S.H., Fairbrother, W.J., Huang, D.C.S., Hymowitz, S.G., Jin, S., Khaw, S.L., Kovar, P.J., Lam, L.T., Lee, J., Maecker, H.L., Marsh, K.C., Mason, K.D., Mitten, M.J., Nimmer, P.M., Oleksijew, A., Park, C.H., Park, C.-M., Phillips, D.C., Roberts, A.W., Sampath, D., Seymour, J.F., Smith, M.L., Sullivan, G.M., Tahir, S.K., Tse, C., Wendt, M.D., Xiao, Y., Xue, J.C., Zhang, H., Humerickhouse, R.A., Rosenberg, S.H., Elmore, S.W., 2013. ABT-199, a potent and selective BCL-2 inhibitor, achieves antitumor activity while sparing platelets. Nat. Med. 19, 202–208.
Steegmaier, M., Hoffmann, M., Baum, A., Lenart, P., Petronczki, M., Krssak, M., Gurtler, U., Garin-Chesa, P., Lieb, S., Quant, J., Grauert, M., Adolf, G.R., Kraut, N., Peters, J.M., Rettig, W.J., 2007. BI 2536, a Potent and Selective Inhibitor of Polo-like Kinase 1, Inhibits Tumor Growth In Vivo. Curr. Biol. 17, 316–322.
Steinbeck, R.G., 2001. Pathologic mitoses and pathology of mitosis in tumorigenesis. Eur. J. Histochem. 45, 311–318.
Stevens, D., Gassmann, R., Oegema, K., Desai, A., 2011. Uncoordinated loss of chromatid cohesion is a common outcome of extended metaphase arrest. PLoS One 6, e22969.
Stewart, M.L., Fire, E., Keating, A.E., Walensky, L.D., 2010. The MCL-1 BH3 helix is an exclusive MCL-1 inhibitor and apoptosis sensitizer. Nat. Chem. Biol. 6, 595–601.
Stewart, S., Fang, G., 2005. Destruction box-dependent degradation of Aurora B is mediated by the anaphase-promoting complex/cyclosome and Cdh1. Cancer Res. 65, 8730–8735.
Strasser, A., Whittingham, S., Vaux, D.L., Bath, M.L., Adams, J.M., Cory, S., Harris, A.W., 1991. Enforced BCL2 expression in B-lymphoid cells prolongs antibody

responses and elicits autoimmune disease. Proc. Natl. Acad. Sci. U. S. A. 88, 8661–5.
Strausfield, U., Labbe, J.C., Fesquet, D., Cavadore, J.C., Picard, A., Sadhu, K., Russell, P., Doree, M., 1991. Dephosphorylation and activation of a p34cdc2/cyclin B complex in vitro by human CDC25 protein. Nature 351, 242–245.
Strebhardt, K., Ullrich, A., 2006. Targeting polo-like kinase 1 for cancer therapy. Nat. Rev. Cancer 6, 321–330.
Sudakin, V., Ganoth, D., Dahan, A., Heller, H., Hershko, J., Luca, F.C., Ruderman, J. V, Hershko, A., 1995. The Cyclosome, a Large Complex Containing Cyclin-Selective Ubiquitin Ligase Activity, Targets Cyclins for Destruction at the End of Mitosis. Mol. Biol. Cell 6, 185–197.
Sumara, I., Gimenez-Abian, J., Gerlich, D., Hirota, T., Kraft, C., de la Torre, C., Ellenberg, J., Peters, J., 2004. Roles of Polo-like kinase 1 in Assembly of Functional Mitotic Spindles. Curr. Biol. 14, 1712–1722.
Swanton, C., Marani, M., Pardo, O., Warne, P.H., Kelly, G., Sahai, E., Elustondo, F., Chang, J., Temple, J., Ahmed, A.A., Brenton, J.D., Downward, J., Nicke, B., 2007. Regulators of Mitotic Arrest and Ceramide Metabolism Are Determinants of Sensitivity to Paclitaxel and Other Chemotherapeutic Drugs. Cancer Cell 11, 498–512.
Swanton, C., Nicke, B., Schuett, M., Eklund, A.C., Ng, C., Li, Q., Hardcastle, T., Lee, A., Roy, R., East, P., Kschischo, M., Endesfelder, D., Wylie, P., Kim, S.N., Chen, J.-G., Howell, M., Ried, T., Habermann, J.K., Auer, G., Brenton, J.D., Szallasi, Z., Downward, J., 2009. Chromosomal instability determines taxane response. Proc. Natl. Acad. Sci. U. S. A. 106, 8671–8676.
Swanton, C., Tomlinson, I., Downward, J., 2006. Chromosomal Instability , Colorectal Cancer and Taxane Resistance. Cell Cycle 818–823.
Tahir, S.K., Yang, X., Anderson, M.G., Morgan-Lappe, S.E., Sarthy, A. V., Chen, J., Warner, R.B., Ng, S.C., Fesik, S.W., Elmore, S.W., Rosenberg, S.H., Tse, C., 2007. Influence of Bcl-2 family members on the cellular response of small-cell lung cancer cell lines to ABT-737. Cancer Res. 67, 1176–1183.
Takai, N., Hamanaka, R., Yoshimatsu, J., Miyakawa, I., 2005. Polo-like kinases (Plks) and cancer. Oncogene 24, 287–291.
Tan, N., Malek, M., Zha, J., Yue, P., Kassees, R., Berry, L., Fairbrother, W.J., Sampath, D., Belmont, L.D., 2011. Navitoclax Enhances the Efficacy of Taxanes in Non-Small Cell Lung Cancer Models. Clin. Cancer Res. 17, 1394–1404.
Tanaka, K., Mukae, N., Dewar, H., van Breugel, M., James, E.K., Prescott, A.R., Antony, C., Tanaka, T.U., 2005. Molecular mechanisms of kinetochore capture by spindle microtubules. Nature 434, 987–994.
Tang, Y., Williams, B.R., Siegel, J.J., Amon, A., 2011. The energy and proteotoxic stress-inducing compounds AICAR and 17-AAG antagonize proliferation in aneuploid cells. Cell 144, 499–512.
Tang, Z., Shu, H., Qi, W., Mahmood, N.A., Mumby, M.C., Yu, H., 2006. PP2A Is Required for Centromeric Localization of Sgo1 and Proper Chromosome Segregation. Dev. Cell 10, 575–585.
Tang, Z., Sun, Y., Harley, S.E., Zou, H., Yu, H., 2004. Human Bub1 protects centromeric sister-chromatid cohesion through Shugoshin during mitosis. Proc. Natl. Acad. Sci. U. S. A. 101, 18012–7.
Tannous, B.A., Kerami, M., Van Der Stoop, P.M., Kwiatkowski, N., Wang, J., Zhou, W., Kessler, A.F., Lewandrowski, G., Hiddingh, L., Sol, N., Lagerweij, T., Wedekind, L., Niers, J.M., Barazas, M., Nilsson, R.J.A., Geerts, D., De Witt Hamer, P.C., Hagemann, C., Vandertop, W.P., Van Tellingen, O., Noske, D.P., Gray, N.S., W??rdinger, T., 2013. Effects of the selective MPS1 inhibitor MPS1-IN-3 on

glioblastoma sensitivity to antimitotic drugs. J. Natl. Cancer Inst. 105, 1322–1331.
Tanudji, M., Shoemaker, J., Italien, L.L., Russell, L., Chin, G., Schebye, X.M., 2004. Gene Silencing of CENP-E by Small Interfering RNA in HeLa Cells Leads to Missegregation of Chromosomes after a Mitotic Delay. Mol. Biol. Cell 15, 3771–3781.
Tao, W., South, V.J., Zhang, Y., Davide, J.P., Farrell, L., Kohl, N.E., Sepp-Lorenzino, L., Lobell, R.B., 2005. Induction of apoptosis by an inhibitor of the mitotic kinesin KSP requires both activation of the spindle assembly checkpoint and mitotic slippage. Cancer Cell 8, 49–59.
Tao, Z., Hasvold, L., Wang, L., Wang, X., Petros, A.M., Park, C.H., Boghaert, E.R., Catron, N.D., Chen, J., Colman, P.M., Czabotar, P.E., Deshayes, K., Fairbrother, W.J., Flygare, J.A., Hymowitz, S.G., Jin, S., Judge, R.A., Koehler, M.F.T., Kovar, P.J., Lessene, G., Mitten, M.J., Ndubaku, C.O., Nimmer, P., Purkey, H.E., Oleksijew, A., Phillips, D.C., Sleebs, B.E., Smith, B.J., Smith, M.L., Tahir, S.K., Watson, K.G., Xiao, Y., Xue, J., Zhang, H., Zobel, K., Rosenberg, S.H., Tse, C., Leverson, J.D., Elmore, S.W., Souers, A.J., 2014. Discovery of a Potent and Selective BCL - X. ACS Med. Chem. Lett. 5, 1088–1093.
Tardif, K.D., Rogers, A., Cassiano, J., Roth, B.L., Cimbora, D.M., McKinnon, R., Peterson, A., Douce, T.B., Robinson, R., Dorweiler, I., Davis, T., Hess, M.A., Ostanin, K., Papac, D.I., Baichwal, V., McAlexander, I., Willardsen, J.A., Saunders, M., Christophe, H., Kumar, D. V., Wettstein, D.A., Carlson, R.O., Williams, B.L., 2011. Characterization of the Cellular and Antitumor Effects of MPI-0479605, a Small-Molecule Inhibitor of the Mitotic Kinase Mps1. Mol. Cancer Ther. 10, 2267–2275.
Tatsuka, M., Katayama, H., Ota, T., Tanaka, T., Odashima, S., Suzuki, F., Terada, Y., 1998. Multinuclearity and Increased Ploidy Caused by Overexpression of the Aurora- and Ipi 1-like Midbody-associated Protein Mitotic Kinase in Human Cancer Cells. Cancer Res. 58, 4811–4816.
Taylor, S., Ha, E., McKeon, F., 1998. The human homologue of Bub3 is required for kinetochore localization of Bub1 and a Mad3/Bub1-related protein kinase. J. Cell Biol. 142, 1–11.
Taylor, S., Peters, J.-M., 2008. Polo and Aurora kinases: lessons derived from chemical biology. Curr. Opin. Cell Biol. 20, 77–84.
Taylor, S.S., Hussein, D., Wang, Y., Elderkin, S., Morrow, C.J., 2001. Kinetochore localisation and phosphorylation of the mitotic checkpoint components Bub1 and BubR1 are differentially regulated by spindle events in human cells. J. Cell Sci. 114, 4385–4395.
Taylor, S.S., McKeon, F., 1997. Kinetochore localization of murine Bub1 is required for normal mitotic timing and checkpoint response to spindle damage. Cell 89, 727–35.
Terrano, D.T., Upreti, M., Chambers, T.C., 2010. Cyclin-dependent kinase 1-mediated Bcl-xL/Bcl-2 phosphorylation acts as a functional link coupling mitotic arrest and apoptosis. Mol. Cell. Biol. 30, 640–56.
Thompson, S., Compton, D., 2011. Chromosomes and cancer cells. Chromosom. Res. 19, 433–444.
Thompson, S.L., Compton, D.A., 2010. Proliferation of aneuploid human cells is limited by a p53-dependent mechanism. J. Cell Biol. 188, 369–381.
Thompson, S.L., Compton, D.A., 2008. Examining the link between chromosomal instability and aneuploidy in human cells. J. Cell Biol. 180, 665–672.
Tighe, A., Johnson, V.L., Taylor, S.S., 2004. Truncating APC mutations have dominant effects on proliferation, spindle checkpoint control, survival and chromosome stability. J. Cell Sci. 117, 6339–6353.
Titus, J., 2012. Mitotic Spindle Assembly : The Role of Motor Proteins, in: eLS. pp. 1–7.

Todt, F., Cakir, Z., Reichenbach, F., Emschermann, F., Lauterwasser, J., Kaiser, A., Ichim, G., Tait, S.W., Frank, S., Langer, H.F., Edlich, F., 2015. Differential retrotranslocation of mitochondrial Bax and Bak. EMBO J. 34, 67–80.
Tomasini, R., Mak, T.W., Melino, G., 2008. The impact of p53 and p73 on aneuploidy and cancer. Trends Cell Biol. 18, 244–252.
Topham, C., Tighe, A., Ly, P., Bennett, A., Sloss, O., Nelson, L., Ridgway, R.A., Huels, D., Littler, S., Schandl, C., Sun, Y., Bechi, B., Procter, D.J., Sansom, O.J., Cleveland, D.W., Taylor, S.S., 2015. MYC Is a Major Determinant of Mitotic Cell Fate. Cancer Cell 28, 129–140.
Topham, C.H., Taylor, S.S., 2013. Mitosis and apoptosis: how is the balance set? Curr. Opin. Cell Biol. 25, 780–5.
Torres, E.M., Sokolsky, T., Tucker, C.M., Chan, L.Y., Boselli, M., Dunham, M.J., Amon, A., 2007. Effects of aneuploidy on cellular physiology and cell division in haploid yeast. Science 317, 916–24.
Torres, E.M., Williams, B.R., Amon, A., 2008. Aneuploidy: Cells losing their balance. Genetics 179, 737–746.
Toyoshima-Morimoto, F., Taniguchi, E., Nishida, E., 2002. Plk1 promotes nuclear translocation of human Cdc25C during prophase. EMBO Rep. 3, 341–348.
Tse, C., Shoemaker, A.R., Adickes, J., Anderson, M.G., Chen, J., Jin, S., Johnson, E.F., Marsh, K.C., Mitten, M.J., Nimmer, P., Roberts, L., Tahir, S.K., Xiao, Y., Yang, X., Zhang, H., Fesik, S., Rosenberg, S.H., Elmore, S.W., 2008. ABT-263: A Potent and Orally Bioavailable Bcl-2 Family Inhibitor. Cancer Res. 68, 3421–3428.
Tsujimoto, Y., 1989. Stress-resistance conferred by high level of bcl-2 alpha protein in human B lymphoblastoid cell. Oncogene 4, 1331–6.
Tsukahara, T., Tanno, Y., Watanabe, Y., 2010. Phosphorylation of the CPC by Cdk1 promotes chromosome bi-orientation. Nature 467, 719–723.
Tunquist, B.J., Woessner, R.D., Walker, D.H., 2010. Mcl-1 stability determines mitotic cell fate of human multiple myeloma tumor cells treated with the kinesin spindle protein inhibitor ARRY-520. Mol. Cancer Ther. 9, 2046–56.
Uchiumi, T., Longo, D.L., Ferris, D.K., 1997. Cell cycle regulation of the human polo-like kinase (PLK) promoter. J. Biol. Chem. 272, 9166–9174.
Uetake, Y., Sluder, G., 2010. Prolonged prometaphase blocks daughter cell proliferation despite normal completion of mitosis. Curr. Biol. 20, 1666–1671.
Uhlmann, F., Lottspeich, F., Nasmyth, K., 1999. Sister-chromatid separation at anaphase onset is promoted by cleavage of the cohesin subunit Scc1. Nature 400, 37–42.
Uhlmann, F., Wernic, D., Poupart, M.A., Koonin, E. V, Nasmyth, K., 2000. Cleavage of cohesin by the CD clan protease separin triggers anaphase in yeast. Cell 103, 375–386.
Upreti, M., Galitovskaya, E.N., Chu, R., Tackett, A.J., Terrano, D.T., Granell, S., Chambers, T.C., 2008. Identification of the major phosphorylation site in Bcl-xL induced by microtubule inhibitors and analysis of its functional significance. J. Biol. Chem. 283, 35517–25.
van Delft, M.F., Huang, D.C.S., 2006. How the Bcl-2 family of proteins interact to regulate apoptosis. Cell Res. 16, 203–13.
van Delft, M.F., Wei, A.H., Mason, K.D., Vandenberg, C.J., Chen, L., Czabotar, P.E., Willis, S.N., Scott, C.L., Day, C.L., Cory, S., Adams, J.M., Roberts, A.W., Huang, D.C.S., 2006. The BH3 mimetic ABT-737 targets selective Bcl-2 proteins and efficiently induces apoptosis via Bak/Bax if Mcl-1 is neutralized. Cancer Cell 10, 389–399.
Van Vugt, M.A., Bras, A., Medema, R.H., 2004. Polo-like kinase-1 controls recovery from a G2 DNA damage-induced arrest in mammalian cells. Mol. Cell 15, 799–811.

van't Veer, L., Dai, H., van de Vijver, M., He, Y., Hart, A., Mao, M., Peterse, H., van der Kooy, K., Marton, M., Witteveen, A., Schreiber, G., Kerkhoven, R., Roberts, C., Linsley, P., Bernards, R., Friend, S., 2002. Gene expression profiling predicts clinical outcome of breast cancer. Nature 415, 530–536.

Vanden Berghe, T., Linkermann, A., Jouan-Lanhouet, S., Walczak, H., Vandenabeele, P., Berghe, T. Vanden, Linkermann, A., Jouan-Lanhouet, S., Walczak, H., Vandenabeele, P., 2014. Regulated necrosis: the expanding network of non-apoptotic cell death pathways. Nat. Rev. Mol. Cell Biol. 15, 135–47.

Varadarajan, S., Vogler, M., Butterworth, M., Dinsdale, D., Walensky, L.D., Cohen, G.M., 2013. Evaluation and critical assessment of putative MCL-1 inhibitors. Cell Death Differ. 20, 1475–84.

Varfolomeev, E., Goncharov, T., Maecker, H., Zobel, K., Komuves, L., Deshayes, K., Vucic, D., 2012. Cellular Inhibitors of Apoptosis Are Global Regulators of NF-κB and MAPK Activation by Members of the TNF Family of Receptors. Sci Signal 5, ra22.

Vaux, D., Cory, S., Adams, J., 1988. Bcl-2 gene promotes haemopoetic cell survival and cooperates with c-myc to immortalize pre-B cells. Nature 335, 440–44.

Villunger, A., Labi, V., Bouillet, P., Adams, J., Strasser, A., 2011. Can the analysis of BH3-only protein knockout mice clarify the issue of " direct versus indirect " activation of Bax and Bak ? Cell Death Differ. 18, 1545–1546.

Vo, T., Ryan, J., Carrasco, R., Neuberg, D., Rossi, D.J., Stone, R., Deangelo, D.J., Frattini, M.G., Letai, A., 2013. Relative Mitochondrial Priming of Malignant Myeloblasts and Normal HSCs Determines Chemotherapeutic Success in AML. Cell 151, 617–632.

Vogler, M., Weber, K., Dinsdale, D., Schmitz, I., Schulze-Osthoff, K., Dyer, M.J.S., Cohen, G.M., 2009. Different forms of cell death induced by putative BCL2 inhibitors. Cell Death Differ. 16, 1030–1039.

Vucic, D., Fairbrother, W.J., 2007. The inhibitor of apoptosis proteins as therapeutic targets in cancer. Clin. Cancer Res. 13, 5995–6000.

Wan, L., Tan, M., Yang, J., Inuzuka, H., Dai, X., Wu, T., Liu, J., Shaik, S., Chen, G., Deng, J., Malumbres, M., Letai, A., Kirschner, M.W., Sun, Y., Wei, W., 2014. APCCdc20 suppresses apoptosis through targeting Bim for ubiquitination and destruction. Dev. Cell 29, 377–391.

Wang, F., Dai, J., Daum, J.R., Niedzialkowska, E., Banerjee, B., Stukenberg, P.T., Gorbsky, G.J., Higgins, J.M.G., 2010. Histone H3 Thr-3 phosphorylation by Haspin positions Aurora B at centromeres in mitosis. Science 330, 231–235.

Wang, F., Ulyanova, N.P., van der Waal, M.S., Patnaik, D., Lens, S.M.A., Higgins, J.M.G., 2011. A positive feedback loop involving Haspin and Aurora B promotes CPC accumulation at centromeres in mitosis. Curr. Biol. 21, 1061–9.

Wang, P., Lindsay, J., Owens, T.W., Mularczyk, E.J., Warwood, S., Foster, F., Streuli, C.H., Brennan, K., Gilmore, A.P., 2014. Phosphorylation of the proapoptotic BH3-only protein Bid primes mitochondria for apoptosis during mitotic arrest. Cell Rep. 7, 661–71.

Warren, C., Brady, M., Johnston, R., Hanna, J., Hardwick, K., Spencer, F., 2002. Distinct Chromosome Segregation Roles for Spindle Checkpoint Proteins. Mol. Biol. Cell 13, 3029–3041.

Watanabe, N., Arai, H., Nishihara, Y., Taniguchi, M., Watanabe, N., Hunter, T., Osada, H., 2004. M-phase kinases induce phospho-dependent ubiquitination of somatic Wee1 by SCF(beta-TrCP). Proc. Natl. Acad. Sci. 101, 4419–4424.

Watanabe, Y., 2005. Shugoshin: guardian spirit at the centromere. Curr. Opin. Cell Biol. 17, 590–5.

Weaver, B.A., 2014. How Taxol/paclitaxel kills cancer cells. Mol. Biol. Cell 25, 2677–81.

Weaver, B.A., 2003. Centromere-associated protein-E is essential for the mammalian mitotic checkpoint to prevent aneuploidy due to single chromosome loss. J. Cell Biol.
Weaver, B.A., Cleveland, D.W., 2006. Does aneuploidy cause cancer? Curr. Opin. Cell Biol. 18, 658–667.
Weaver, B.A., Cleveland, D.W., 2005. Decoding the links between mitosis, cancer, and chemotherapy: The mitotic checkpoint, adaptation, and cell death. Cancer Cell 8, 7–12.
Weaver, B.A., Silk, A.D., Montagna, C., Verdier-Pinard, P., Cleveland, D.W., 2007. Aneuploidy Acts Both Oncogenically and as a Tumor Suppressor. Cancer Cell 11, 25–36.
Weiss, E., Winey, M., 1996. The Saccharomyces cerevisiae spindle pole body duplication gene MPS1 is part of a mitotic checkpoint. J. Cell Biol. 132, 111–23.
Weiss, W., Taylor, S., Shokat, K., 2012. Recognizing and exploiting differences between RNAi and small-molecule inhibitors. Nat. Chem. Biol. 29, 997–1003.
Welburn, J.P.I., Vleugel, M., Liu, D., Yates, J.R., Lampson, M.A., Fukagawa, T., Cheeseman, I.M., 2010. Aurora B Phosphorylates Spatially Distinct Targets to Differentially Regulate the Kinetochore-Microtubule Interface. Mol. Cell 38, 383–392.
Wells, J.A., McClendon, C.L., 2007. Reaching for high-hanging fruit in drug discovery at protein-protein interfaces. Nature 450, 1001–9.
Wengner, A.M., Siemeister, G., Koppitz, M., Schulze, V., Kosemund, D., Klar, U., Stoeckigt, D., Neuhaus, R., Lienau, P., Bader, B., Prechtl, S., Raschke, M., Frisk, A.-L., von Ahsen, O., Michels, M., Kreft, B., von Nussbaum, F., Brands, M., Mumberg, D., Ziegelbauer, K., 2016. Novel Mps1 Kinase Inhibitors with Potent Antitumor Activity. Mol. Cancer Ther. 15, 583–592.
Wertz, I.E., Kusam, S., Lam, C., Okamoto, T., Sandoval, W., Anderson, D.J., Helgason, E., Ernst, J.A., Eby, M., Liu, J., Belmont, L.D., Kaminker, J.S., O'Rourke, K.M., Pujara, K., Kohli, P.B., Johnson, A.R., Chiu, M.L., Lill, J.R., Jackson, P.K., Fairbrother, W.J., Seshagiri, S., Ludlam, M.J.C., Leong, K.G., Dueber, E.C., Maecker, H., Huang, D.C.S., Dixit, V.M., 2011. Sensitivity to antitubulin chemotherapeutics is regulated by MCL1 and FBW7. Nature 471, 110–114.
Westhorpe, F.G., Diez, M. a., Gurden, M.D.J., Tighe, A., Taylor, S.S., 2010. Re-evaluating the role of Tao1 in the spindle checkpoint. Chromosoma 119, 371–379.
Westhorpe, F.G., Tighe, A., Lara-Gonzalez, P., Taylor, S.S., 2011. p31comet-mediated extraction of Mad2 from the MCC promotes efficient mitotic exit. J. Cell Sci. 124, 3905–3916.
Williams, B.R., Prabhu, V.R., Hunter, K.E., Glazier, C.M., Whittaker, C.A., Housman, D.E., Amon, A., 2008. Aneuploidy Affects Proliferation and Spontaneous Immortalization in Mammalian Cells. Science 322, 703–710.
Willis, S., Fletcher, J., Kaufmann, T., van Delft, M., Chen, L., Czabotar, P., Ierino, H., Lee, E., Fairlie, W., Bouillet, P., Strasser, A., Kluck, R., Adams, J., Huang, D., 2007. Apoptosis Initiated When BH3 Ligands Engage Multiple Bcl-2 Homologs, Not Bax or Bak. Science 315, 856–859.
Wollman, R., Cytrynbaum, E.N., Jones, J.T., Meyer, T., Scholey, J.M., Mogilner, A., 2005. Efficient chromosome capture requires a bias in the "search-and-capture" process during mitotic-spindle assembly. Curr. Biol. 15, 828–832.
Wong, F.Y., Liem, N., Xie, C., Yan, F.L., Wong, W.C., Wang, L., Yong, W.P., 2012. Combination Therapy with Gossypol Reveals Synergism against Gemcitabine Resistance in Cancer Cells with High BCL-2 Expression. PLoS One 7, 1–10.
Wood, K.W., Lad, L., Luo, L., Qian, X., Knight, S.D., Nevins, N., Brejc, K., Sutton, D., Gilmartin, A.G., Chua, P.R., Desai, R., Schauer, S.P., McNulty, D.E., Annan, R.S., Belmont, L.D., Garcia, C., Lee, Y., Diamond, M.A., Faucette, L.F., Giardiniere, M.,

Zhang, S., Sun, C.-M., Vidal, J.D., Lichtsteiner, S., Cornwell, W.D., Greshock, J.D., Wooster, R.F., Finer, J.T., Copeland, R.A., Huang, P.S., Morgans, D.J., Dhanak, D., Bergnes, G., Sakowicz, R., Jackson, J.R., 2010. Antitumor activity of an allosteric inhibitor of centromere-associated protein-E. Proc. Natl. Acad. Sci. U. S. A. 107, 5839–44.

Wood, K.W., Sakowicz, R., Goldstein, L.S., Cleveland, D.W., 1997. CENP-E is a plus end-directed kinetochore motor required for metaphase chromosome alignment. Cell 91, 357–66.

Woods, A., Sherwin, T., Sasse, R., MacRae, T.H., Baines, A.J., Gull, K., 1989. Definition of individual components within the cytoskeleton of Trypanosoma brucei by a library of monoclonal antibodies. J. Cell Sci. 93 (Pt 3), 491–500.

Xiang, Z., Luo, H., Payton, J.E., Cain, J., Ley, T.J., Opferman, J.T., Tomasson, M.H., 2010. Mcl1 haploinsufficiency protects mice from Myc -induced acute myeloid leukemia. J. Clin. Invest. 120, 2109–2118.

Yamagishi, Y., Honda, T., Tanno, Y., Watanabe, Y., 2012a. Two Histone Marks Establish the Inner Centromere and Chromosome Bi-Orientation. Science 239, 1–6.

Yamagishi, Y., Yang, C.-H., Tanno, Y., Watanabe, Y., 2012b. MPS1/Mph1 phosphorylates the kinetochore protein KNL1/Spc7 to recruit SAC components. Nat. Cell Biol. 14, 746–752.

Yamaguchi, S., Decottignies, A., Nurse, P., 2003. Function of Cdc2p-dependent Bub1p phosphorylation and Bub1p kinase activity in the mitotic and meiotic spindle checkpoint. EMBO J. 22, 1075–87.

Yamamoto, K., Ichijo, H., Korsmeyer, S.J., 1999. BCL-2 is phosphorylated and inactivated by an ASK1/Jun N-terminal protein kinase pathway normally activated at G(2)/M. Mol. Cell. Biol. 19, 8469–78.

Yang, E., Zha, J.P., Jockel, J., Boise, L.H., Thompson, C.B., Korsmeyer, S.J., 1995. Bad, a Heterodimeric Partner for Bcl-X(L) and Bcl-2, Displaces Bax and Promotes Cell-Death. Cell 80, 285–291.

Yao, X., Abrieu, A., Zheng, Y., Sullivan, K.F., Cleveland, D.W., 2000. CENP-E forms a link between attachment of spindle microtubules to kinetochores and the mitotic checkpoint. Nat. Cell Biol. 2, 484–91.

Yen, T.J., Compton, D.A., Wise, D., Zinkowski, R.P., Brinkley, B.R., Earnshaw, W.C., Cleveland, D.W., 1991. CENP-E, a novel human centromere-associated protein required for progression from metaphase to anaphase. EMBO J. 10, 1245–54.

Yen, T.J., Li, G., Schaar, B.T., Szilak, I., Cleveland, D.W., 1992. CENP-E is a putative kinetochore motor that accumulates just before mitosis. Nature 359, 536–539.

Yu, J., Zhang, L., Hwang, P.M., Kinzler, K.W., Vogelstein, B., 2001. PUMA induces the rapid apoptosis of colorectal cancer cells. Mol. Cell 7, 673–682.

Yuan, J., Horlin, A., Hock, B., Stutte, H., Rubsamen-Waigmann, H., Strebhardt, K., 1997. Polo-Like Kinase, A Novel Marker For Cellular Proliferation. Am. J. Pathol. 150, 1165–1172.

Yvon, A.C., Wadsworth, P., Jordan, M.A., 1999. Taxol Suppresses Dynamics of Individual Microtubules in Living Human Tumor Cells. Mol. Biol. Cell 10, 947–959.

Zasadil, L.M., Andersen, K.A., Yeum, D., Rocque, G.B., Wilke, L.G., Tevaarwerk, A.J., Raines, R.T., Burkard, M.E., Weaver, B.A., 2014. Cytotoxicity of paclitaxel in breast cancer is due to chromosome missegregation on multipolar spindles. Sci. Transl. Med. 6, 229ra43.

Zhang, H., Nimmer, P.M., Tahir, S.K., Chen, J., Fryer, R.M., Hahn, K.R., Iciek, L.A., Morgan, S.J., Nasarre, M.C., Nelson, R., Preusser, L.C., Reinhart, G.A., Smith, M.L., Rosenberg, S.H., Elmore, S.W., Tse, C., 2007. Bcl-2 family proteins are essential for platelet survival. Cell Death Differ. 14, 943–51.

Zhu, C., Zhao, J., Bibikova, M., Leverson, J., Bossy-Wetzel, E., Fan, J.-B., Abraham,

R., Jiang, W., 2005. Functional Analysis of Human Microtubule-based Motor Proteins, the Kinesins and Dyneins, in Mitosis/Cytokinesis Using RNA Interference. Mol. Biol. Cell 16, 3187–3199.

Zitouni, S., Nabais, C., Jana, S.C., Guerrero, A., Bettencourt-Dias, M., 2014. Polo-like kinases: structural variations lead to multiple functions. Nat. Rev. Mol. Cell Biol. 15, 433–452.

8 Appendix

8.1 Appendix 1

Bennett, A., Bechi, B., Tighe, A., Thompson, S., Procter, D.J., Taylor, S.S.
Cenp-E inhibitor GSK923295: Novel synthetic route and use as a tool to generate aneuploidy
2015, Oncotarget

Cenp-E inhibitor GSK923295: Novel synthetic route and use as a tool to generate aneuploidy

Ailsa Bennett[1], Beatrice Bechi[2], Anthony Tighe[1], Sarah Thompson[1], David J. Procter[2], Stephen S. Taylor[1]

[1]Faculty of Life Sciences, University of Manchester, United Kingdom

[2]School of Chemistry, University of Manchester, United Kingdom

Correspondence to:
Stephen S. Taylor, **e-mail:** stephen.taylor@manchester.ac.uk

Keywords: *Chromosome Section, spindle assembly checkpoint, Mps1, aneuploidy, chromosome instability, Cenp-E*

Received: *July 02, 2015* ***Accepted:*** *July 24, 2015* ***Published:*** *August 06, 2015*

ABSTRACT

Aneuploidy is a common feature of cancer, with human solid tumour cells typically harbouring abnormal chromosome complements. The aneuploidy observed in cancer is often caused by a chromosome instability phenotype, resulting in genomic heterogeneity. However, the role aneuploidy and chromosome instability play in tumour evolution and chemotherapy response remains poorly understood. In some contexts, aneuploidy has oncogenic effects, whereas in others it is anti-proliferative and tumour-suppressive. Dissecting fully the role aneuploidy plays in tumourigenesis requires tools and facile assays that allow chromosome missegregation to be induced experimentally in cells that are otherwise diploid and chromosomally stable. Here, we describe a chemical biology approach that induces low-level aneuploidy across a large population of cells. Specifically, cells are first exposed to GSK923295, an inhibitor targeting the mitotic kinesin Cenp-E; while the majority of chromosomes align at the cell's equator, a small number cluster near the spindle poles. By then driving these cells into anaphase using AZ3146, an inhibitor targeting the spindle checkpoint kinase Mps1, the polar chromosomes are missegregated. This results in, on average, two chromosome missegregation events per division, and avoids trapping chromosomes in the spindle midzone, which could otherwise lead to DNA damage. We also describe an efficient route for the synthesis of GSK923295 that employs a novel enzymatic resolution. Together, the approaches described here open up new opportunities for studying cellular responses to aneuploidy.

INTRODUCTION

Aneuploidy is defined as a karyotype with a chromosome number that deviates from the expected. For example, individuals with Down Syndrome have three copies of chromosome 21 instead of two, leading to developmental disabilities and shortened life expectancy. Aneuploidy can arise due to unequal chromosome segregation during mitosis and meiosis, generating daughter cells with extensive gene copy number changes. The consequences of the chromosomal imbalance manifest at the cellular level. In yeast, aneuploidy induces proteotoxic stress, suppresses proliferation and reduces fitness [1–4]. Similarly, in mammalian cells, aneuploidy is anti-proliferative and sensitizes cells to compounds that interfere with protein folding [5–7].

Despite aneuploidy's anti-proliferative potential, it is a common feature of cancers and indeed, Boveri suggested over 100 years ago that aneuploidy might promote tumour formation [8–10]. In mice, artificial induction of aneuploidy can act either as a tumour promoter or a tumour suppressor, depending on the context [11–13]. An emerging view is that while a low level of aneuploidy provides enough genetic variation to fuel tumour evolution, excessive chromosome instability creates genetic chaos, which is detrimental to fitness [14, 15]. Nevertheless, because aneuploidy is anti-proliferative in non-transformed cells, understanding how cancer cells tolerate aneuploidy is a key question.

Defining the acute and chronic effects of chromosome missegregation requires tools and assays to generate aneuploidy in otherwise diploid, chromosomally stable cells so that the short and long term consequences on cellular physiology can be studied. A current approach to induce chromosome missegregation involves arresting cells in mitosis with drugs that block spindle assembly, e.g. the microtubule targeting agent nocodazole or Eg5/KSP kinesin inhibitors such as monastrol [16–19]. Following washout, spindle assembly leads to chromosome segregation but with maloriented chromosomes that missegregate [16]. While effective, a monastrol-washout has a major impact on spindle assembly and only gives rise to one chromosome missegregation event every three divisions [19]. Moreover, these chromosomes can often get trapped in the cleavage furrow or form micronuclei, leading to DNA damage, in turn causing chromosome translocations as well as whole chromosome aneuploidies [20, 21]. Other methods of generating aneuploidies includes the use of topoisomerase II inhibitors [22], but again this approach induces DNA damage leading to chromosome translocations. Dissecting aneuploidy without the complication of DNA damage therefore requires new approaches.

Cenp-E (Centromere Associated Protein-E), is a plus-end directed kinesin-7 motor protein, required for chromosome segregation in both mitosis and meiosis [23]. Cenp-E localises to kinetochores throughout mitosis, with phosphorylation by Aurora kinases A and B, plus the opposing function of protein phosphatase 1, imposing important regulatory control [24–26]. Cenp-E function aids chromosome alignment by moving chromosomes from the spindle poles to the metaphase plate [25]. Specifically, by linking the unattached kinetochores on mono-oriented chromosomes to an adjacent, mature kinetochore fibre, Cenp-E mediates congression of polar chromosomes prior to biorientation [27].

When Cenp-E expression is perturbed using antibody injections, immunodepletions, anti-sense, siRNA or gene deletion approaches, complete chromosome alignment is inhibited [28–30]. This is consistent with even a single unattached kinetochore being sufficient to prevent anaphase onset [31–33]. Cenp-E inhibition leads to persistent activation of the spindle assembly checkpoint (SAC), in turn leading to a mitotic arrest [29, 34, 35]. Cenp-E may also play a direct role in the SAC; Cenp-E binds and, in the absence of bound microtubules, activates the SAC kinase BubR1 [36, 37].

In the quest to develop novel antimitotic chemotherapy agents, mitotic kinesins are attractive targets [38]. To explore Cenp-E's potential, small molecule inhibitors that disrupt Cenp-E function have been developed [39, 40]. A high throughput library screen seeking compounds that inhibited the microtubule-stimulated ATPase activity of Cenp-E led to the development of GSK923295 [40]. GSK923295 is an allosteric inhibitor of Cenp-E that prevents ATP hydrolysis, thus stabilizing the enzyme in a conformation with increased affinity for microtubule binding [41]. Cells treated with GSK923295 assemble bipolar spindles and align most of their chromosomes. However, a number remain clustered near the spindle poles, leading to SAC arrest and apoptosis [41].

We reasoned that in combination with drugs that override the SAC, GSK923295 would be a useful tool to efficiently generate whole chromosomes aneuploidies, without the risk of DNA damage. Here we describe a novel approach to synthesize GSK923295, together with an assay that induces on average two chromosome missegregation events per cell division without trapping chromosomes in the cleavage furrow.

RESULTS

Enzymatic resolution facilitates an asymmetric synthesis of GSK923295

To experimentally induce whole chromosome aneuploidies, we set out to synthesise the Cenp-E inhibitor, GSK923295 by following previously published routes [40, 42]. A key step involves resolution of racemic 1-(2-amino-3-pyridinyl)ethanol (Fig. 1, compound **2**) to obtain enantiomerically pure 1*S*-(2-amino-3-pyridinyl)ethanol (*(S)*–**2**) for subsequent reaction with an intermediate (**1**), ultimately producing GSK923295 (**6**). In our hands, the published preparative HPLC resolution method was inefficient and therefore we explored other options. Previously, a mutated variant of *Candida antarctica* lipase B was shown to successfully resolve aromatic secondary alcohols [43], so we explored a similar strategy. *Candida antarctica* lipase B (CALB) enzyme was added to a racemic mixture of (**2**), with excess S-ethyl thiohexanoate **3**, under solvent free conditions, at 39°C (Fig. 1). The progress of the reaction was monitored using HPLC. The enzyme specifically reacted with the (*R*)-enantiomer over a 12-hour period, leaving the (*S*)-enantiomer unreacted. The ester and alcohol were each obtained in 50% yield, and the alcohol *(S)*–**2** in > 99% enantiomeric excess (ee). Purification by column chromatography then yielded pure 1*S*-(2-amino-3-pyridinyl)ethanol (*(S)*–**2**). The pure (*S*)-enantiomer was then reacted with phenacyl chloride (**1**) to give the pyridyl imidazole (**5**). Methods used for subsequent steps to GSK923295 (**6**) were as published [44–47]. Our synthetic studies employing a lipase in a kinetic resolution, illustrate the (*R*) specificity of the enzyme and provide a convenient and reliable synthesis of the Cenp-E inhibitor GSK923295.

GSK923295 inhibits chromosome alignment

To characterise the synthesized inhibitor, diploid DLD-1 colon cancer cells were treated with 50 nM

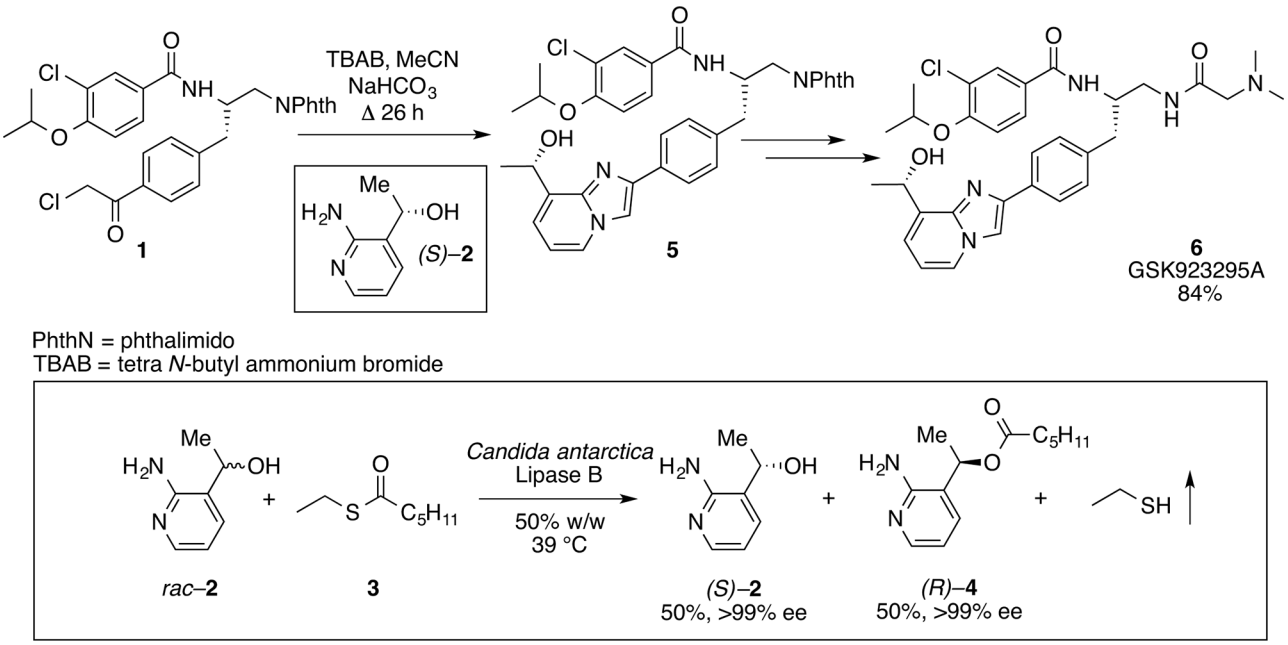

Figure 1: Resolution of racemic mixture to synthesise GSK923295. The desired (*S*)-enantiomer (**2**) was obtained by the resolution of the racemic mixture of 1-(2-amino-3-pyridinyl)ethanol (*rac*-**2**), through the reaction with S-ethyl thiohexanoate at 39°C with *Candida Antarctica* Lipase B enzyme (50% w/w). The pure enantiomer (**2**) and the intermediate (**1**) then reacted to give the pyridyl imidazole (**5**), with subsequent reactions yielding GSK923295 (**6**).

GSK923295. After four hours, cells were fixed and stained to detect Bub1, tubulin and the DNA, then analysed by immunofluorescence microscopy (Fig. 2A). Consistent with previous reports [41], in the presence of GSK923295, bipolar spindles formed and while the majority of chromosomes aligned at metaphase, a few remained close to the spindle poles. The kinetochores of these unaligned chromosomes stained strongly for Bub1, indicating that they were not correctly attached to spindle microtubules [48, 49]. Thus, our preparation of GSK923295 yields the expected cellular phenotype.

To identify minimal concentrations and exposure times required to induce a potent chromosome misalignment phenotype, HeLa cells were first treated with varying concentrations of GSK923295 for four hours then fixed and analysed by fluorescence microscopy (Fig. 2B). 100 mitotic cells for each condition were assigned to one of four different stages of mitosis, namely prophase, prometaphase, metaphase and anaphase. Cells with unaligned chromosomes were classified as prometaphase. In the control populations, on average 12% were in prophase, 21% prometaphase, 29% metaphase and 38% in anaphase. At 50 nM, the number in prometaphase increased to 94%, with no obvious metaphase or anaphase figures (Fig. 2B). Many of these prometaphase figures typically had bipolar spindles with many aligned chromosomes but a few polar chromosomes, similar to the situation in DLD-1 cells (Fig. 2A). This phenotype did not appear to change at concentrations above 50 nM. Next, we treated HeLa cells with 50 nM GSK923295 then analysed them at various time points as described above. Within two hours of treatment, > 95% of cells were in prometaphase, indicating a complete block of metaphase and anaphase (Fig. 2C). We observed a similar result in DLD-1 cells, with ~91% of cells scored as prometaphase by two hours of exposure (Fig. 2C). Thus, in both HeLa and DLD-1 cells, a two-hour exposure of 50 nM GSK923295 is sufficient to induce a potent chromosome misalignment phenotype.

We next set out to determine whether GSK923295-mediated inhibition of Cenp-E is reversible by asking whether cells completed chromosome alignment following drug washout. HeLa cells were treated with 50 nM GSK923295 for four hours, washed twice with PBS then fresh media added. At various time points, chromosome alignment was analysed as above (Fig. 2D). In the control population, where the inhibitor was not washed out, 96% of the mitotic cells were scored as prometaphase. By contrast, following a 30-minute period after washout, 54% were classified as prometaphase, 19% metaphase, and 19% anaphase. Therefore, following washout of GSK923295 chromosome alignment appears to recover. Moreover, the presence of anaphase figures indicates SAC satisfaction. Thus, Cenp-E function can be restored following washout of GSK923295, indicating that the drug is reversible.

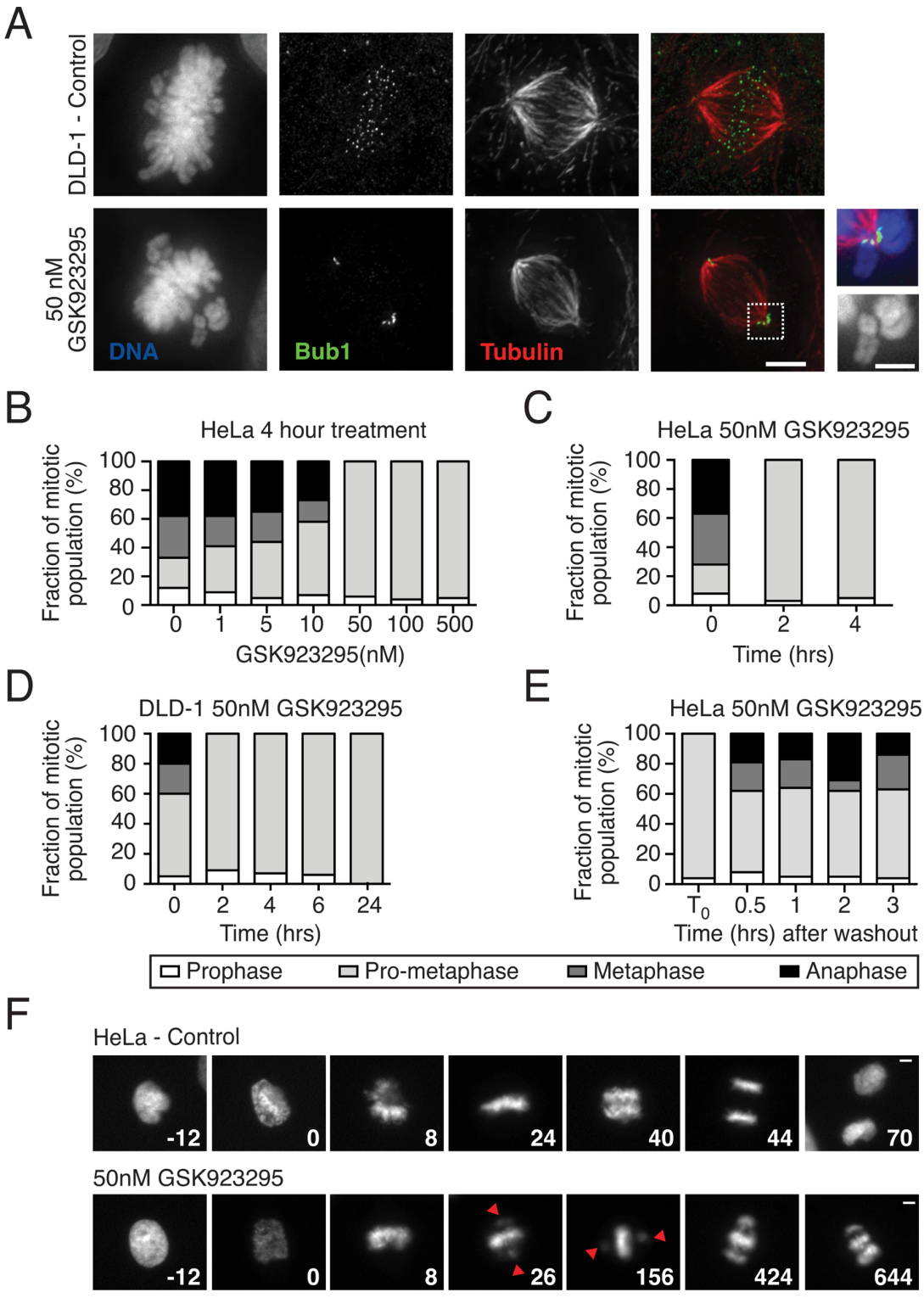

Figure 2: GSK923295 induces chromosome misalignment. A. Immunofluorescence images of DLD-1 cells treated with 50 nM GSK923295 for four hours, fixed and stained for DNA (blue), Bub1 (green) and tubulin (red), with insets showing unaligned chromosome(s). Bar: 5 μm or 2.5 μm for increased magnification. **B.** A bar chart quantifying the number of cells in each mitotic phase following exposure of HeLa cells to GSK923295 at various concentrations. **C.** Quantification of the number of HeLa cells in each mitotic phase over a time course, following 50 nM GSK923295 treatment. **D.** The number of DLD-1 cells in each stage of mitosis over time after 50 nM GSK923295 treatment. **E.** Treatment of HeLa cells with 50 nM GSK923295, and classification of 100 mitotic cells after no washout (control), or at various times following wash-out. **F.** Time lapse sequences of control and 50 nM Cenp-E inhibitor treated HeLa GFP Histone-H2B cells. Time zero represents nuclear envelope break down. Bar: 5 μm.

GSK923295 induces mitotic arrest

The lack of obvious metaphases and anaphases in GSK923295-treated cultures is consistent with persistent activation of the SAC and mitotic arrest. Indeed, Cenp-E inhibition has been shown to activate the SAC [23, 29]. However, it is conceivable that GSK923295-treated cells also slip out mitosis without completing chromosome alignment and undergoing sister chromatid disjunction [50]. To distinguish between these two possibilities, we turned to time-lapse microscopy, analysing HeLa cells expressing a GFP-tagged histone to visualize the chromosomes in living cells (Fig. 2F). HeLa GFP Histone-H2B cells were treated with 50 nM GSK923295 then analysed by time-lapse fluorescence microscopy, acquiring images every 2 minutes, marking nuclear envelope break-down (NEBD) at time zero. In the representative control cell shown in Fig. 2F, chromosome alignment was complete by 24 minutes and chromosome segregation apparent by 40 minutes, such that by 70 minutes the daughter cells had returned to interphase. In the GSK923295-treated cell, most chromosomes had aligned by 26 minutes but at least 1 chromosome was visible near each of the two spindle poles. This configuration persisted for several hours until chromosomes started to "fall off" the metaphase plate, resulting in more chromosomes/chromatids near the spindle poles (Fig. 2F, see 424 and 644 mins). This is highly reminiscent of cohesion fatigue [51, 52], a phenomenon whereby aligned chromosomes are eventually peeled apart by spindle forces, during a metaphase delay. Note that the HeLa cell line used here is particularly prone to cohesion fatigue [51–53]. Once cohesion fatigue occurs, satisfaction of the SAC is impossible and indeed, the cell shown eventually underwent slippage (not shown), but other cells in the population were shown to undergo apoptosis. Thus, GSK923295-mediated inhibition of Cenp-E does indeed lead to a prolonged mitotic arrest, which in the first instance appears to be caused by blocking complete chromosome congression.

GSK923295 induces death in mitosis and post-mitotic apoptosis

Cell fate in response to anti-mitotic agents varies considerably depending on the cell line studied, the anti-mitotic drug used and the drug concentration applied [54]. Moreover, genetically identical cells can undergo different fates despite identical environmental conditions. The time-lapse analysis above shows that HeLa cells undergo a prolonged mitotic arrest, then cohesion fatigue followed by mitotic exit (in the representative example). To determine whether this was the dominant phenotype, HeLa cells treated with 50 nM GSK923295 were analysed by flow cytometry at various time points to determine DNA content (Fig. 3A). After an eight-hour exposure, the vast majority of cells had 4c DNA contents, consistent with an inability to undergo a normal cell division. At later time points, and in particular by 48 hours, the majority of cells had sub-2c DNA contents, indicating extensive apoptosis (Fig. 3A). Thus, although 50 nM GSK923295 only initially leads to misalignment of a few chromosomes (Fig. 2A), which are in principle capable of alignment (Fig. 2E), we suggest that the subsequent cohesion fatigue generates single chromatids that cannot align (Fig. 2F), thereby leading to persistent activation of the SAC, in turn leading to extensive apoptosis.

As mentioned above, the HeLa cells used here are particularly sensitive to cohesion fatigue [51, 52]. Thus, the prolonged mitotic arrest and subsequent death observed in may be a reflection of cohesion fatigue rather than prolonged Cenp-E inhibition. Therefore we turned to RKO cells, a diploid colon cancer cell line that appears to be more resistant to cohesion fatigue (not shown). When exposed to taxol, nocoazole or an Eg5 inhibitor, RKO cells typically undergo death in mitosis [54]. To determine the long-term effects of GSK923295 on RKO cells, time-lapse imaging was performed over a 72 hour period. Proliferation and apoptosis were analysed by confluence based measurements and caspase 3/7 fluorescent probes. While concentrations of 50 nM and below appeared relatively benign, 100 nM GSK923295 inhibited proliferation and induced apoptosis (Fig. 3B). To determine when cells treated with 100 nM were dying, we inspected the image sequences and used phase contrast morphology to monitor mitosis and generated cell fate profiles as described previously [54]. Briefly, each fate profile represents 50 cells with the colour of the line showing the fate of the cell in the period of imaging, and the length of the line is the time taken to undergo the particular cell behaviour. In the control population, cells underwent, on average, three cell divisions during 72 hours. Consistent with the HeLa time-lapse and FACS data, GSK923295 treated RKO cells underwent mitotic arrest. 40% of the cells then died in mitosis after an average arrest time of 11.91 hours. Cohesion fatigue was not obvious in these cells, but higher resolution time-lapse microscopy would be required to definitively conclude this. Strikingly, despite the continued presence of GSK923295, 26% of the cells divided after an arrest of 15.22 hours, yielding two daughter cells. Interestingly, only one of these cells entered a second mitosis. Of the rest, 24% died in the subsequent interphase, while the remainder remained arrested in interphase for the remainder of the experiment.

Sequential Cenp-E and Mps1 inhibition generates aneuploid daughter cells

Our analysis confirms that GSK923295-treated cells assembly bipolar spindles and, while the majority of chromosomes align, a few remain clustered near

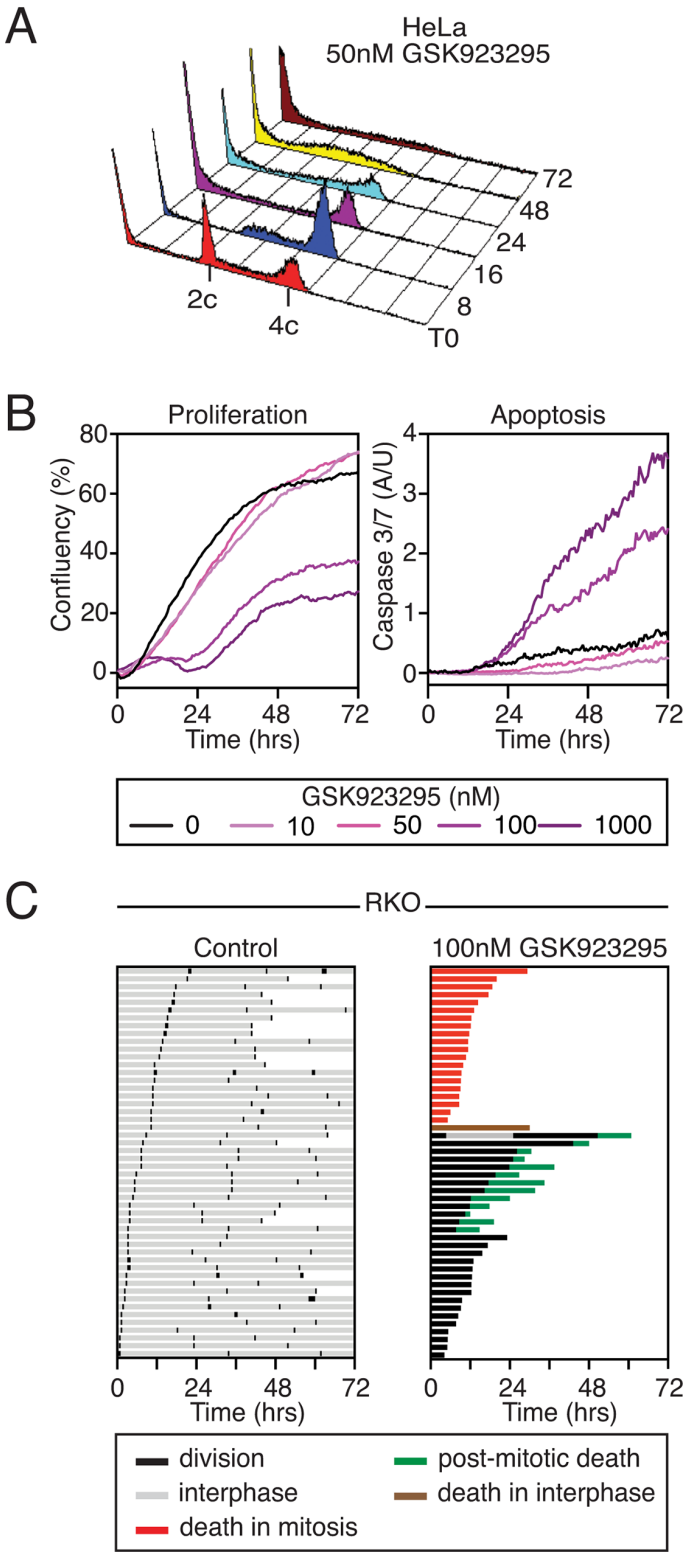

Figure 3: GSK923295 causes cell death. A. DNA content histograms of HeLa cells treated with 50 nM GSK923295, over a time course. **B.** Line graph showing percent confluency and caspase 3/7 activation of RKO cells treated with varying Cenp-E inhibitor concentrations. **C.** Fate profiles for untreated and Cenp-E inhibitor treated RKO cells. One bar represents one cell.

the spindle poles. We reasoned that driving these cells into anaphase by overriding the SAC should induce missegregation of the polar chromosomes, thereby generating aneuploid daughter cells. To test this, DLD-1 Histone-H2B- mCherry cells were treated with 50 nM GSK923295 for 4 hours and then analysed by time-lapse imaging (Fig. 4A). Metaphase cells with polar chromosomes were identified and 2 μM of AZ3146, an Mps1 kinase inhibitor, was added to override the SAC [55]. As predicted, AZ3146 induced anaphase onset in the cells with polar chromosomes leading to obvious non-disjunction events (Arrows in Fig. 4A, Supplemental Movie S1). Importantly, lagging chromosomes were not observed (Arrowheads in Fig. 4A, lower panels). By contrast, addition of AZ3146 in the absence of GSK923295 resulted in anaphases with chromosomes near the poles and in the midzone that appeared to get stretched between the two separating masses (Fig. 4A, Supplemental Movie S2). To confirm that this strategy also induces chromosome missegregation in diploid cells we repeated the analysis in HCT116 cells. Quantitation of time-lapse sequences showed that 98% of the anaphases observed in GSK923295-AZ3146-treated cultures underwent anaphase with unaligned chromosomes (Fig. 4B). To confirm that these cells completed cytokinesis, HCT116 cells were exposed to GSK923295 for 4 hours and mitotic-arrested cells isolated by selective detachment. Flow cytometry analysis showed that the vast majority of the isolated cells had 4c DNA contents consistent with mitotic arrest (Fig. 4C). Two hours after addition of AZ3146 the vast majority of cells had 2c DNA contents, indicating that they had completed chromosome segregation and cytokinesis. To confirm that these cells were aneuploid, we performed *in situ* fluorescent hybridization on interphase cells following sequential GSK923295-AZ3146 exposure, using probes to detect the centromeres of chromosomes 6 and 7 (Fig. 4D). We focussed on cell pairs to enrich for daughters. In control populations, we typically saw two foci for each of the probes. In drug-treated populations, we often saw cell pairs where one cell had three foci for one of the probes while the adjacent cell only had 1, i.e. a 3+1 foci pattern (Fig. 4D), indicating a missegregation event. Quantitation showed that ~9% of cells missegregated chromosome 6 or 7. By contrast, following a monastrol washout, only ~2% of cells had 3+1 foci. Multiplying these rates by the total number of chromosomes per cell to calculate how often any chromosome missegregates indicates cells treated with sequential GSK923295-AZ3146 exposure missegregate ~2 chromosomes per division, compared to monastrol washout where less than 50% of divisions result in a single missegregation event (42%). Missegregation in untreated populations is rare, with only one missegregation event in 100 divisions.

DISCUSSION

Chiral amino alcohols are important building blocks for medicinal chemistry and drug discovery [56–58]. In particular, 1*S*-(2-amino-3-pyridinyl)ethanol *(S)*–**2** is a crucial component in the synthetic route to GSK923295. However, access to amino alcohol motifs in enantiopure form, using either asymmetric synthetic methods or resolution, is often difficult thus reducing the overall efficiency of syntheses. We show here that an enzyme-based kinetic resolution using CALB, efficiently and reproducibly gives the maximum 50% yield of the required 1*S*-(2-amino-3-pyridinyl)ethanol (*S)*–**2** in high enantiomeric excess. A previously reported route to GSK923295 involved resolution of *rac*–**2** by chiral HPLC [40]; a process that we found to be unsatisfactory. In turn, our asymmetric biocatalytic approach has resulted in an efficient and convenient route to GSK923295. Our novel asymmetric approach has the potential to deliver novel compounds inspired by GSK923295.

We set out to use GSK923295 in conjunction with the Mps1 inhibitor AZ3146 to efficiently induce whole chromosome aneuploidies without major disruption to the spindle and without inducing DNA damage. Consistent with previous reports [41], our data shows that GSK923295 does not prevent spindle assembly but efficiently and rapidly prevents complete chromosome alignment. Importantly, GSK923295 is reversible; following washout, the remaining chromosomes align and anaphase occurs in a timely manner. While this suggests that GSK923295 does not induce irreparable damage, note that prolonged mitotic arrest in the presence of a functional spindle can induce cohesion fatigue, which is irreversible [51, 52].This can be avoided either by short mitotic arrests or selecting cell lines that are more resistant to cohesion fatigue. Indeed, when overriding the SAC in GSK923295-treated DLD-1 cells, the majority of chromosomes appeared to segregate normally. Importantly however, the polar chromosomes missegregated giving rise to aneuploid daughters. Although Cenp-E is required to maintain the integrity of kinetochore-microtubule interactions on bioriented chromosomes [59, 60], when we triggered anaphase in GSK923295-arrested cells, we did not observe lagging chromosomes or bridges. Thus, in contrast to nocodazole and monastrol washouts, the approach we describe is promising in terms of inducing whole chromosome aneuploidies without concomitant DNA damage. Moreover, interphase FISH indicates that the sequential GSK923295-AZ3146 exposure gave rise to ~2 chromosome missegregation events per division, and is thus about five-fold more efficient than a monastrol-washout-based strategy.

The chemical biology approach we describe here to induce aneuploidy has several advantages over molecular genetic approaches. Small molecular inhibitors can efficiently induce highly penetrant effects

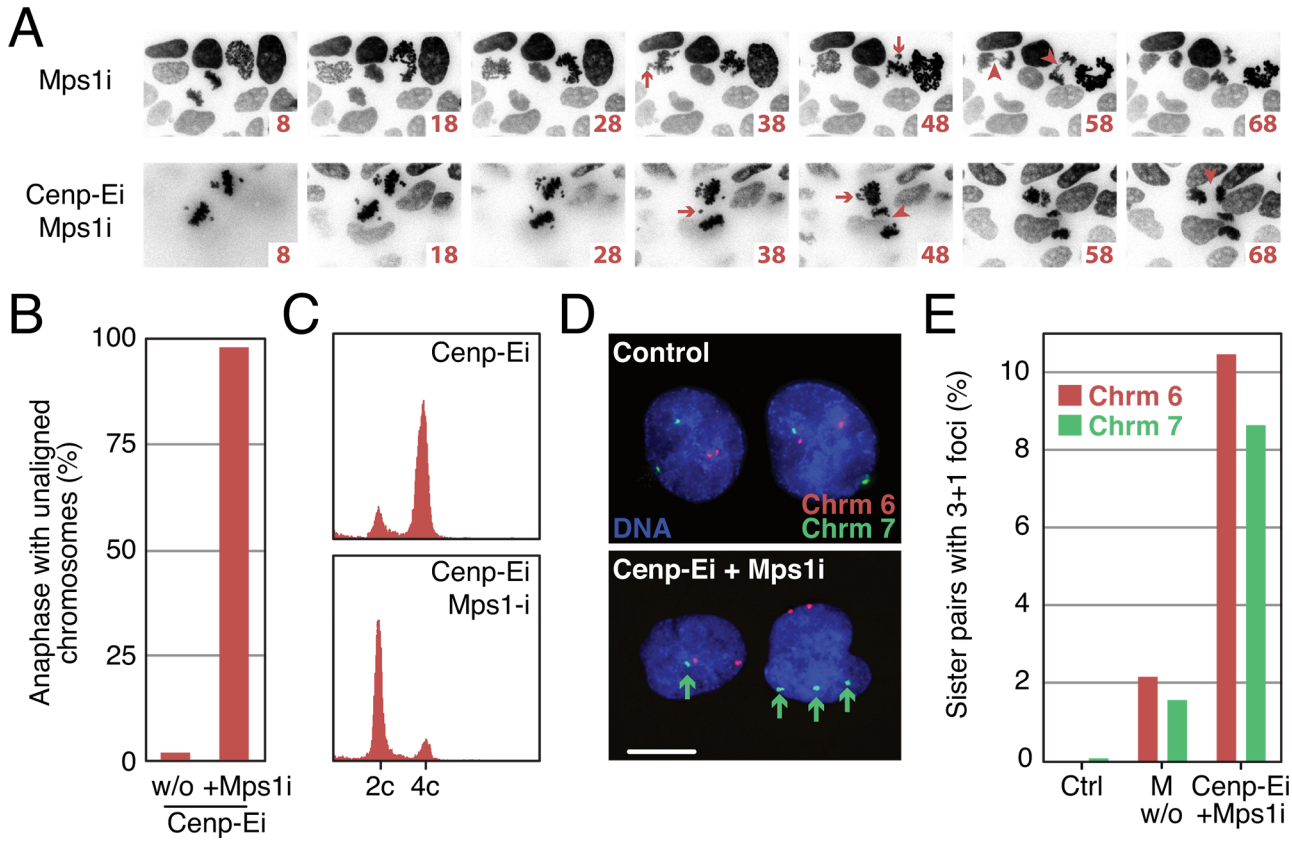

Figure 4: Sequential Cenp-E and Mps1 inhibition generates aneuploid daughter cells. A. Time lapse sequences of DLD-1 histone-H2B-mCherry cells treated with the Mps1 inhibitor alone or Cenp-E inhibitor treated cells, washed into the Mps1 inhibitor. Arrows indicate mitotic defects: unaligned chromosomes/lagging chromosomes. **B.** Quantification of the number of anaphases in HCT-116 cells with unaligned chromosomes after treatment with Cenp-E inhibitor alone or Cenp-E inhibitor and Mps1 inhibitor combined. **C.** DNA content histograms of Cenp-E and Cenp-E and Mps1 inhibitors treated cells. **D.** FISH analysis labelling chromosomes 6 and 7 in control and Cenp-E and Mps1 inhibitor treated cells. Bar: 10 μm. **E.** Bar chart quantifying the number of pairs of daughter cells with 3+1 foci under control, monastrol washout (100 μM), and Cenp-E and Mps1 inhibitor treated conditions.

across whole cell populations, facilitating, for example, large-scale bio- chemical experiments that are more difficult to achieve with RNAi. And indeed, we show that > 95% of cells treated with GSK923295-AZ3146 missegregate at least one chromosome. Inhibitors can easily be combined with other modalities, such as RNAi. This may facilitate RNAi screens for cellular responses to aneuploidy. Inhibitors inactivate their targets with rapid onset, allowing loss-of-function experiments to be conducted with precise temporal control. Consequently, the assay we describe here involves short time courses that can be used to avoid issues such as cohesion fatigue. Finally, small-molecule regimens can easily be transferred from one cell type or even species to another, including specialized cell types, which are not amenable to RNAi-based strategies. This could facilitate aneuploidy induction in specialised cell types, such as stem cells, or in existing lines expressing specific biosensors and reporters.

Interestingly, when RKO cells were exposed to GSK923295, 26% arrested in mitosis but then eventually divided. Whether these dividing cells aligned all their chromosomes before committing to anaphase, or whether they underwent anaphase with unaligned chromosomes is not known. Distinguishing between these two possibilities is important; the first possibility implies SAC satisfaction while the latter implies SAC exhaustion. High-resolution time-lapse imaging will be required to address this. Following division in the presence of GSK923295, the vast majority of cells then failed to undergo another mitosis, indicating a robust cell cycle arrest. Again, determining whether the dividing cells underwent anaphase with unaligned chromosomes or not will be required to determine why these cells engaged post-mitotic anti-proliferative responses. If chromosome segregation was completed, then it could be the prolonged arrest was sufficient to induce the subsequent G1 arrest [61]. If anaphase was initiated with unaligned chromosomes, then DNA damage and/or aneuploidy could be the cause [19, 20]. Distinguishing between these possibilities is an important area for future experimentation. Moreover, the chemical biology

approaches we describe here have potential in terms of understanding how cells respond to chromosome missegregation and tolerate aneuploidy.

MATERIALS AND METHODS

Synthesis

All synthetic methods were as described previously [42]. All chemicals were purchased from Sigma. In a closed reaction vessel equipped with bleach trap, *S*-ethyl thiohexanoate (10 mmol) (**3**) was added to racemic 1-(2-aminophenyl)ethanol (1 mmol) (*rac*–**2**) and the CALB enzyme preparation (50% w/w). The reaction proceeded at 39°C and was monitored *via* HPLC analysis (Chiralcel OD-H; Heptane: ethanol 90:10, 0.1% IPAM; Flow: 0.8 mL/min). After completion at 12 hours, the enzyme was removed by filtration. The mixture was then purified by column chromatography (ethyl acetate as eluent) to give ester (*R*)–**4** and the unreacted alcohol (*S*)–**2**.

(*S*)-1-(2-amino-3-pyridinyl)ethanol ((*S*)–2)

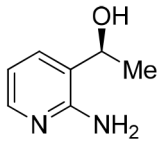

Unreacted alcohol (*S*)–**2**. Colourless oil. RT = 10.8 min. Yield: 50%. *ee*: > 99%. $[\alpha]_D$ = -0.5° (ethanol, c = 1.00).

(*R*)-1-(2-amino-3-pyridinyl)ethyl hexanoate ((*R*)–4)

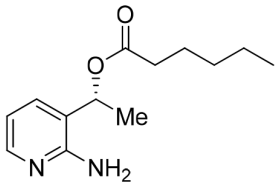

Ester (*R*)–**4** obtained from reacting alcohol *(R)*–**2**. Colourless oil. RT = 7.1 min. Yield: 50%. ^{1}H NMR (400 MHz, $CDCl_3$) δ 0.78–0.86 (m, 3H, $CO(CH_2)_4CH_3$), 1.18–1.30 (m, 4H, $CO(CH_2)_2(CH_2)_2CH_3$), 1.49–1.59 (m, 5H, $COCH_2CH_2(CH_2)_2CH_3$), $OCHCH_3$), 2.23–2.29 (m, 2H, $COCH_2(CH_2)_3CH_3$), 5.15 (s, 2H, NH_2), 5.82 (q, *J* = 6.8 Hz, 1H, $OCHCH_3$), 6.58 (dd, J = 5.2, 7.8 Hz, 1H, H-5), 7.40–7.41 (m, 1H, H-4), 7.86–7.88 (m, 1H, H-6). ^{13}C NMR (100 MHz, $CDCl_3$) δ 13.9 ($CO(CH_2)_4CH_3$), 19.1 (CH_3CHOH), 22.3 ($CO(CH_2)_3CH_2CH_3$), 24.6 ($CO(CH_2)_2CH_2$), 31.1 ($COCH_2CH_2CH_2$), 34.3 ($COCH_2CH_2$), 68.9 (CH_3CHOH), 113.6 (*C*H-5), 119.9 (*C*-3), 136.2 (*C*H-4), 146.4 (*C*H-6), 156.4 (*C*-2). 173.3 (*C*O).

Cell lines

DLD-1, HeLa, RKO and HCT-116 cell lines were cultured in DMEM plus 10% fetal calf serum (LifeTechnologies), 2 mM glutamine, 100 U/mL penicillin, and 100 U/mL streptomycin (Lonza) at 37°C in a humidified 5% CO_2 atmosphere. DLD-1 Histone-H2B-mCherry were as described previously [62]. Small molecule inhibitors dissolved in DMSO were as follows: GSK923295, Cenp-E inhibitor (in house); AZ3146, Mps1 inhibitor (Tocris); Monastrol, Eg5 inhibitor (Sigma).

Immunofluorescence

Cells were plated at 8 × 10^4 cells/mL on 19 mm (VWR International) coverslips at 500 µL. After overnight incubation, the Cenp-E inhibitor was added for various time periods. Cells were fixed with 1% formaldehyde, quenched with glycine, and then permeabilised with PBST (PBS and 0.1% Triton X-100). For microtubule staining the PEM buffer was used. Cells were pre-extracted with 100 mM Pipes, 1 mM $MgCl_2$, 0.1 mM $CaCl_2$, and 0.1% Triton X-100 for 90 seconds, followed by fixation with 4% formaldehyde in PEM buffer for 10 minutes. Cells were then incubated with sheep anti-Bub1 SB1.3 [49] and with mouse anti-tubulin TAT1 [63], for 30 minutes, and then washed and incubated with secondary antibodies Cy2-, and Cy3-, antisheep/mouse (Millipore) for 30 minutes. Hoechst 33358 (Sigma) at 1 µg/mL was then added to the cells, followed by mounting onto slides with 90% glycerol and 20 mM Tris-HCl, pH 8.0. Images were taken at room temperature with a restoration microscope (DeltaVision RT; Applied Precision) using a 100x 1.40 NA Plan Apo objective and a filter set (Sedat Quad; Chroma Technology Corp.). Images were captured with a charge-coupled device camera (CoolSNAP HQ; Photometrics) with a z-optical spacing of 0.2 µm. Raw images were then deconvolved with the SoftWorx software (Applied Precision), and these were then processed, and PhotoShop (Adobe) was used to analyse the images.

Time lapse

Cells were plated at 8 × 10^4 cells/mL in a 24 well plate (Corning) at a volume of 500 µL. 16 hours later DMSO (control) or Cenp-E inhibitor (50 nM) were added. Cells were then imaged every 2 minutes using a Zeiss Axiovert 200 microscope, with an automated PZ-2000 stage (Applied Biosystems), with cells maintained at 37°C and a continuous flow of 5% CO_2. Images were acquired with a 60x objective. All the shutters, filter wheels and point visiting were driven by MetaMorph software (Universal imaging). Images were taken with a camera (CoolSNAP HQ; Photometrics) and processed with Photoshop (Adobe), and Quicktime (Apple).

FACS

The method was as previous [48]. After harvesting, samples were fixed in 100% ethanol at −20°C overnight, and after washing with PBS, cells were resuspended in propidium iodide (40 μg/mL) and RNase (50 μg/mL), leaving at room temperature for 30 minutes. Flow cytometric analysis was performed measuring DNA content of at least 10, 000 cells using a Cyan ADP (Beckman Coulter), and Summit 4.3 was used for data analysis.

Proliferation and apoptosis assays

For the cell proliferation, caspase 3/7 activation and the phase imaging, cells were plated in a 96 well plate (Greiner Bio-One) at a density of 1×10^5 cells/mL, with 100 μL per well. The IncuCyte ZOOM (Essen BioSciences) was used to image the cells, according to the manufacturer's instructions. Prism (GraphPad) was used for the analysis and fate profiling.

Interphase FISH

HCT-116 cells were plated at a density of 8×10^4 cells/mL onto glass coverslips. After drug treatment, cells were washed and 75 mM potassium chloride was added. Samples were fixed with methanol-acetic acid (3:1). Alpha-satellite probes for chromosomes 6 and 7 (MP Biomedicals and Cytocell) were used consistent with the manufacturers protocol. Chromosome signals in 300 nuclei were scored according to [16]. FISH images were acquired as 0.25 μm optical sections with the 60x 1.4 NA objective and are projections of four to five merged planes in the z-axis.

ACKNOWLEDGMENTS

We thank members of the Taylor lab for technical advice and comments on the manuscript.

FUNDING

AB is funded by a studentship from Cancer Research UK and a University of Manchester Presidential Scholarship. BB and DJP are supported by Knowledge Transfer and Established Career Fellowships, respectively, from the Engineering and Physical Sciences Research Council. SST is supported by a Cancer Research UK Senior Fellowship.

CONFLICTS OF INTEREST

The authors declare no conflicts.

REFERENCES

1. Torres EM, Sokolsky T, Tucker CM, Chan LY, Boselli M, Dunham MJ, Amon A. Effects of aneuploidy on cellular physiology and cell division in haploid yeast. Science. 2007; 317:916–924.
2. Oromendia AB, Dodgson SE, Amon A. Aneuploidy causes proteotoxic stress in yeast. Genes Dev. 2012; 26:2696–2708.
3. Siegel JJ, Amon A. New Insights into the Troubles of Aneuploidy. Annu Rev Cell Dev Biol. 2012; 28:189–214.
4. Oromendia AB, Amon A. Aneuploidy: implications for protein homeostasis and disease. Dis Model Mech. 2014; 7:15–20.
5. Torres EM, Williams BR, Amon A. Aneuploidy: Cells losing their balance. Genetics. 2008; 179:737–746.
6. Williams BR, Prabhu VR, Hunter KE, Glazier CM, Whittaker Ca, Housman DE, Amon A. Aneuploidy affects proliferation and spontaneous immortalization in mammalian cells. Science. 2008; 322:703–710.
7. Tang Y, Williams BR, Siegel JJ, Amon A. The energy and proteotoxic stress-inducing compounds AICAR and 17-AAG antagonize proliferation in aneuploid cells. Cell. 2011; 144:499–512.
8. Boveri T. Ueber mehrpolige Mitosen als Mittel zur Analyse des Zellkerns. Verh Phys-med Ges Würzburg NF. 1902; 35:67–90.
9. Boveri T. Zur Frage der Entstehung maligner Tumoren. Fischer, Jena. 1914; .
10. Boveri T. Concerning the origin of malignant tumours by Theodor Boveri. Translated and annotated by Henry Harris. J Cell Sci. 2008; 121:1–84.
11. Weaver BA, Silk AD, Montagna C, Verdier-Pinard P, Cleveland DW. Aneuploidy Acts Both Oncogenically and as a Tumor Suppressor. Cancer Cell. 2007; 11:25–36.
12. Holland AJ, Cleveland DW. Boveri revisited: chromosomal instability, aneuploidy and tumorigenesis. Nat Rev Mol Cell Biol. 2009; 10:478–487.
13. Silk AD, Zasadil LM, Holland AJ, Vitre B, Cleveland DW, Weaver BA. Chromosome missegregation rate predicts whether aneuploidy will promote or suppress tumors. Proc Natl Acad Sci U S A. 2013; 110:E4134–4141.
14. Birkbak NJ, Eklund AC, Li Q, McClelland SE, Endesfelder D, Tan P, Tan IB, Richardson AL, Szallasi Z, Swanton C. Paradoxical relationship between chromosomal instability and survival outcome in cancer. Cancer Res. 2011; 71:3447–3452.
15. Holland AJ, Cleveland DW. Losing balance: the origin and impact of aneuploidy in cancer. EMBO Rep. 2012; 13:501–514.
16. Cimini D, Tanzarella C, Degrassi F. Differences in malsegregation rates obtained by scoring ana-ztelophases or binucleate cells. Mutagenesis. 1999; 14:563–568.

17. Cimini D, Howell B, Maddox P, Khodjakov A, Degrassi F, Salmon ED. Merotelic kinetochore orientation is a major mechanism of aneuploidy in mitotic mammalian tissue cells. J Cell Biol. 2001; 152:517–527.
18. Knowlton AL, Lan W, Stukenberg PT. Aurora B Is Enriched at Merotelic Attachment Sites, Where It Regulates MCAK. Curr Biol. 2006; 16:1705–1710.
19. Thompson SL, Compton DA. Examining the link between chromosomal instability and aneuploidy in human cells. J Cell Biol. 2008; 180:665–672.
20. Janssen A, van der Burg M, Szuhai K, Kops GJPL, Medema RH. Chromosome Segregation Errors as a Cause of DNA Damage and Structural Chromosome Aberrations. Science. 2011; 333:1895–1898.
21. Ganem NJ, Pellman D. Linking abnormal mitosis to the acquisition of DNA damage. J Cell Biol. 2012; 199:871–881.
22. Clarke DJ, Giménez-Abián JF, Tönnies H, Neitzel H, Sperling K, Downes CS, Johnson RT. Creation of monosomic derivatives of human cultured cell lines. Proc Natl Acad Sci U S A. 1998; 95:167–171.
23. Schaar BT, Chan GK, Maddox P, Salmon ED, Yen TJ. CENP-E function at kinetochores is essential for chromosome alignment. J Cell Biol. 1997; 139:1373–1382.
24. Yen TJ, Li G, Schaar BT, Szilak I, Cleveland DW. CEN-E is a putative kinetochore motor that accumulates just before mitosis. Nature. 1992; 359:536–539.
25. Wood KW, Sakowicz R, Goldstein LS, Cleveland DW. CENP-E is a plus end-directed kinetochore motor required for metaphase chromosome alignment. Cell. 1997; 91:357–366.
26. Kim Y, Holland AJ, Lan W, Cleveland DW. Aurora kinases and protein phosphatase 1 mediate chromosome congression through regulation of CENP-E. Cell. 2010; 142:444–455.
27. Kapoor TM, Lampson MA, Hergert P, Cameron L, Cimini D, Salmon ED, McEwen BF, Khodjakov A. Chromosomes can congress to the metaphase plate before biorientation. Science. 2006; 311:388–392.
28. Yen TJ, Compton DA, Wise D, Zinkowski RP, Brinkley BR, Earnshaw WC, Cleveland DW. CENP-E, a novel human centromere-associated protein required for progression from metaphase to anaphase. EMBO J. 1991; 10:1245–1254.
29. Yao X, Abrieu A, Zheng Y, Sullivan KF, Cleveland DW. CENP-E forms a link between attachment of spindle microtubules to kinetochores and the mitotic checkpoint. Nature Cell Biol. 2000; 2:484–491.
30. Weaver BA. Centromere-associated protein-E is essential for the mammalian mitotic checkpoint to prevent aneuploidy due to single chromosome loss. J Cell Biol. 2003; 162:551–563.
31. Rieder CL, Salmon ED. Motile kinetochores and polar ejection forces dictate chromosome position on the vertebrate mitotic spindle. J Cell Biol. 1994; 124:223–233.
32. Li X, Nicklas RB. Mitotic forces control a cell-cycle checkpoint. Nature. 1995; 373.
33. Rieder CL, Cole RW, Khodjakov A, Sluder G. The checkpoint delaying anaphase in response to chromosome monoorientation is mediated by an inhibitory signal produced by unattached kinetochores. J Cell Biol. 1995; 130:941–948.
34. Abrieu A, Kahana JA, Wood KW, Cleveland DW. CENP-E as an essential component of the mitotic checkpoint *in vitro*. Cell. 2000; 102:817–826.
35. Lara-Gonzalez P, Westhorpe F, Taylor S. The Spindle Assembly Checkpoint. Curr Biol. 2012; 22:R966–R980.
36. Mao Y, Abrieu A, Cleveland DW. Activating and silencing the mitotic checkpoint through CENP-E-dependent activation/inactivation of BubR1. Cell. 2003; 114:87–98.
37. Mao Y, Desai A, Cleveland DW. Microtubule capture by CENP-E silences BubR1-dependent mitotic checkpoint signaling. J Cell Biol. 2005; 170:873–880.
38. Huszar D, Theoclitou M-E, Skolnik J, Herbst R. Kinesin motor proteins as targets for cancer therapy. Cancer Metastasis Rev. 2009; 28:197–208.
39. Ding X, Yan F, Yao P, Yang Z, Wan W, Wang X, Liu J, Gao X, Abrieu A, Zhu T, Zhang J, Dou , Yao X. Probing CENP-E function in chromosome dynamics using small molecule inhibitor syntelin. Cell Res. 2010; 20:1386–1389.
40. Qian X, Mcdonald A, Zhou H-J, Adams ND, Parrish CA, Duffy KJ, Fitch DM, Tedesco R, Ashcraft LW, Yao B, Jiang H, Huang JK, Marin MV, Aroyan CE, Wang J, Ahmed S, et al. Discovery of the First Potent and Selective Inhibitor of Centromere-Associated Protein, E: GSK923295. ACS Med Chem Lett. 2010; 1:30–34.
41. Wood KW, Lad L, Luo L, Qian X, Knight SD, Nevins N, Brejc K, Sutton D, Gilmartin AG, Chua PR, Desai R, Schauer SP, McNulty DE, Annan RS, Belmont LD, Garcia C, et al. Antitumor activity of an allosteric inhibitor of centromere-associated protein-E. Proc Natl Acad Sci U S A. 2010; 107:5839–5844.
42. Bellingham R, Buswell AM, Choudary BM, Gordon AH, Moore SO, Peterson M, Sasse M, Shamji A, Urquhart MWJ. Discovery and Development of an Efficient, Scalable, and Robust Route to the Novel CENP-E Inhibitor GSK923295A. Org Process Res Dev. 2010; 14:1254–1263.
43. Engström K, Vallin M, Syrén P-O, Hult K, Bäckvall J-E. Mutated variant of Candida antarctica lipase B in (S)-selective dynamic kinetic resolution of secondary alcohols. Org Biomol Chem. 2011; 9:81–82.
44. Frykman H, Ohrner N, Norin T, Hult K. S-ethyl thiooctanoate as acyl donor in lipase catalysed resolution of secondary alcohols. Tetrahedron Lett. 1993; 34:1367–1370.

45. Orrenius C, Mattson A, Norin T. Preparation of 1-pyridinylethanols of high enantiomeric purity by lipase catalysed transesterifications. Tetrahedron Asymmetry. 1994; 5:1363–1366.

46. Orrenius C, Ohrner N, Rottici D, Mattson A, Hult K, Norin T. Candida antarctica lipase B catalysed kinetic resolutions: Substrate structure requirements for the preparation of enantiomerically enriched secondary alcohols. Tetrahedron Asymmetry. 1995; 6:1217–1220.

47. Rivera NR, Hsiao Y, Cowen JA, McWilliams C, Armstrong J, Yasuda N, Hughes DL. Highly Efficient Synthesis of 2-Amino-3-Pyridinecarboxaldehyde. Synth Commun. 2001; 31:1573–1579.

48. Taylor SS, McKeon F. Kinetochore localization of murine Bub1 is required for normal mitotic timing and checkpoint response to spindle damage. Cell. 1997; 89:727–735.

49. Taylor SS, Hussein D, Wang Y, Elderkin S, Morrow CJ. Kinetochore localisation and phosphorylation of the mitotic checkpoint components Bub1 and BubR1 are differentially regulated by spindle events in human cells. J Cell Sci. 2001; 114:4385–4395.

50. Tanudji M, Shoemaker J, Italien LL, Russell L, Chin G, Schebye XM. Gene Silencing of CENP-E by Small Interfering RNA in HeLa Cells Leads to Missegregation of Chromosomes after a Mitotic Delay. Mol Biol Cell. 2004; 15:3771–3781.

51. Daum John R, Potapova Tamara A, Sivakumar S, Daniel Jeremy J, Flynn Jennifer N, Rankin S, Gorbsky Gary J. Cohesion Fatigue Induces Chromatid Separation in Cells Delayed at Metaphase. Curr Biol. 2011; 21:1018–1024.

52. Stevens D, Gassmann R, Oegema K, Desai A. Uncoordinated loss of chromatid cohesion is a common outcome of extended metaphase arrest. PLOS ONE. 2011; 6:e22969.

53. Lara-Gonzalez P, Taylor SS. Cohesion fatigue explains why pharmacological inhibition of the APC/C induces a spindle checkpoint-dependent mitotic arrest. PLOS ONE. 2012; 7:e49041.

54. Gascoigne KE, Taylor SS. Cancer cells display profound intra- and interline variation following prolonged exposure to antimitotic drugs. Cancer Cell. 2008; 14:111–122.

55. Hewitt L, Tighe A, Santaguida S, White AM, Jones CD, Musacchio A, Green S, Taylor SS. Sustained Mps1 activity is required in mitosis to recruit O-Mad2 to the Mad1-C-Mad2 core complex. J Cell Biol. 2010; 190:25–34.

56. Sekar G, Kamble RM, Singh VK. Enantiomerically pure N -aryl-β-amino alcohols by enzymatic resolution. Tetrahedron Asymmetry. 1999; 10:3663–3666.

57. Kaman J, Van der Eycken J, Peter A, Fulop F. Enzymatic resolution of bicyclic 1 , 3-amino alcohols in organic media. Tetrahedron Asymmetry. 2001; 12:625–631.

58. Rouf A, Gupta P, Aga MA, Kumar B, Parshad R, Taneja SC. Cyclic trans-beta-amino alcohols: Preparation and enzymatic kinetic resolution. Tetrahedron Asymmetry. 2011; 22:2134–2143.

59. McEwen BF, Chan GK, Zubrowski B, Savoian MS, Sauer MT, Yen TJ. CENP-E is essential for reliable bioriented spindle attachment, but chromosome alignment can be achieved via redundant mechanisms in mammalian cells. Mol Biol Cell. 2001; 12:2776–2789.

60. Putkey FR, Cramer T, Morphew MK, Silk AD, Johnson RS, McIntosh JR, Cleveland DW. Unstable kinetochore-microtubule capture and chromosomal instability following deletion of CENP-E. Dev Cell. 2002; 3:351–365.

61. Uetake Y, Sluder G. Prolonged prometaphase blocks daughter cell proliferation despite normal completion of mitosis. Curr Biol. 2010; 20:1666–1671.

62. Tighe A, Staples O, Taylor S. Mps1 kinase activity restrains anaphase during an unperturbed mitosis and targets Mad2 to kinetochores. J Cell Biol. 2008; 181:893–901.

63. Woods A, Baines AJ, Gull K. A high molecular mass phosphoprotein defined by a novel monoclonal antibody is closely associated with the intermicrotubule cross bridges in the Trypanosoma brucei cytoskeleton. J Cell Sci. 1992; 103:665–675.

8.2 Appendix 2

Topham, C., Tighe, A., Ly, P., Bennett, A., Sloss, O., Nelson, L., Ridgway, R.A., Huels, D., Littler, S., Schandl, C., Sun, Y., Bechi, B., Procter, D.J., Sansom, O.J., Cleveland, D.W., Taylor, S.S.

MYC is a major determinant of mitotic cell fate

2015, Cancer Cell

Cancer Cell
Article

CellPress

MYC Is a Major Determinant of Mitotic Cell Fate

Caroline Topham,[1,5] Anthony Tighe,[1,5] Peter Ly,[2] Ailsa Bennett,[1] Olivia Sloss,[1] Louisa Nelson,[1] Rachel A. Ridgway,[3] David Huels,[3] Samantha Littler,[1] Claudia Schandl,[1] Ying Sun,[2] Beatrice Bechi,[4] David J. Procter,[4] Owen J. Sansom,[3] Don W. Cleveland,[2] and Stephen S. Taylor[1,*]
[1]Faculty of Life Sciences, University of Manchester, Oxford Road, Manchester M13 9PT, UK
[2]Ludwig Institute for Cancer Research and Department of Cellular and Molecular Medicine, University of California at San Diego, La Jolla, CA 92093, USA
[3]Cancer Research UK Beatson Institute, Garscube Estate, Glasgow G61BD, UK
[4]School of Chemistry, University of Manchester, Oxford Road, Manchester M13 9PL, UK
[5]Co-first author
*Correspondence: stephen.taylor@manchester.ac.uk
http://dx.doi.org/10.1016/j.ccell.2015.06.001

SUMMARY

Taxol and other antimitotic agents are frontline chemotherapy agents but the mechanisms responsible for patient benefit remain unclear. Following a genome-wide siRNA screen, we identified the oncogenic transcription factor Myc as a taxol sensitizer. Using time-lapse imaging to correlate mitotic behavior with cell fate, we show that Myc sensitizes cells to mitotic blockers and agents that accelerate mitotic progression. Myc achieves this by upregulating a cluster of redundant pro-apoptotic BH3-only proteins and suppressing pro-survival Bcl-xL. Gene expression analysis of breast cancers indicates that taxane responses correlate positively with Myc and negatively with Bcl-xL. Accordingly, pharmacological inhibition of Bcl-xL restores apoptosis in Myc-deficient cells. These results open up opportunities for biomarkers and combination therapies that could enhance traditional and second-generation antimitotic agents.

INTRODUCTION

Antimitotic drugs are frontline treatments for breast, ovarian, and lung cancer, as well as various hematological malignancies (Dumontet and Jordan, 2010). These drugs bind tubulin and inhibit microtubule dynamics, and although many cancers initially respond well, some are intrinsically resistant and others acquire resistance (Murray et al., 2012). Predicting which cancers will respond is hampered by our limited understanding of the molecular mechanisms responsible for patient benefit (Gascoigne and Taylor, 2009; Weaver, 2014). At high concentrations, antimitotic drugs disrupt spindle assembly, leading to mitotic arrest by persistent activation of the spindle assembly checkpoint (SAC) (Lara-Gonzalez et al., 2012). SAC activation blocks the anaphase promoting complex/cyclosome (APC/C), thereby preventing ubiquitination and degradation of cyclin B1, in turn maintaining the mitotic state. Following prolonged arrest, cells either die in mitosis or undergo "slippage," returning to interphase without completing cell division (Brito and Rieder, 2006). Following slippage, p53-dependent post-mitotic responses then induce cell cycle arrest, senescence, or apoptosis (Rieder and Maiato, 2004). At lower taxol concentrations, the SAC becomes satisfied, allowing cells to progress through mitosis, albeit with spindle abnormalities and chromosome segregation errors (Zasadil et al., 2014). Bypassing both death in mitosis (DiM) and post-mitotic responses can fuel chromosome instability and taxane resistance (A'Hern et al., 2013).

The competing-networks model helps explain whether a cell either dies in mitosis or undergoes slippage (Gascoigne and Taylor, 2008). According to this model, two independent networks dictate mitotic cell fate, one slowly generating a death signal, the other slowly degrading cyclin B1, leading to slippage. During a

Significance

Antimitotic agents such as the taxanes are used widely to treat various cancers. To address limitations with these agents, a new generation of inhibitors that disrupt mitosis without affecting microtubule dynamics is being evaluated, including drugs targeting mitotic kinesins and mitotic kinases. However, we still have limited understanding of the mechanisms that dictate cell fate in response to mitotic disruption. Here we show that Myc drives expression of an apoptotic network that sensitizes breast, ovarian, lung, and colon cancer cells to drugs that both activate and override the spindle assembly checkpoint. Moreover, we show that Myc promotes both p53-independent death in mitosis and p53-dependent post-mitotic responses. Our results raise opportunities to explore biomarkers and combination therapies aimed at enhancing antimitotic efficacy.

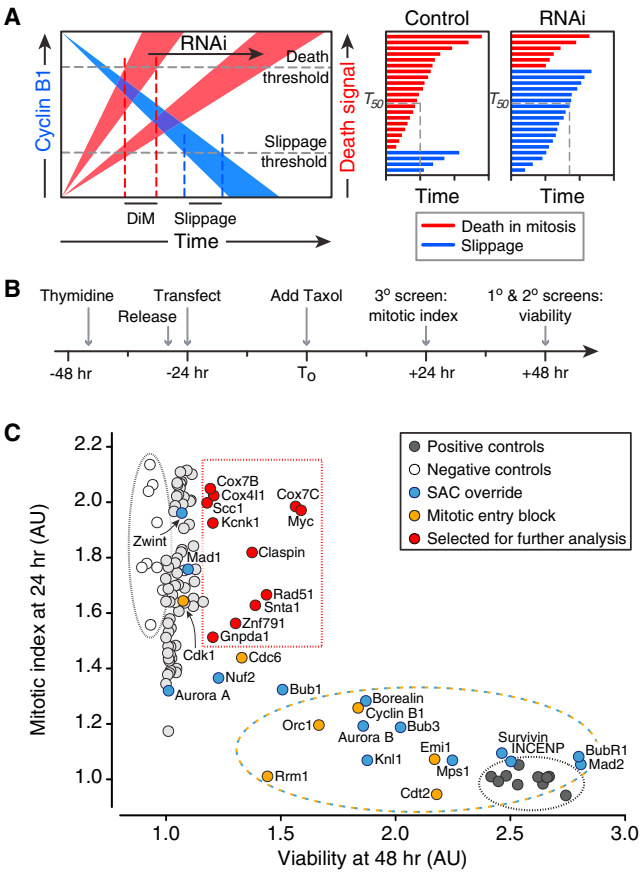

Figure 1. A Genome-wide siRNA Screen for Regulators of Mitotic Cell Fate

(A) Rationale for the screen based on the competing-networks model.

(B) Timeline of siRNA transfection procedure.

(C) Scatterplot of mitotic index at 24 hr against viability at 48 hr.

See also Figure S1 and Tables S1 and S2.

prolonged arrest, these networks work in opposite directions: while cell death signals become stronger, cyclin B1 levels slowly fall due to incomplete penetrance of SAC-mediated APC/C inhibition (Brito and Rieder, 2006). Both networks have thresholds and the fate of the cell is dictated by which threshold is breached first. Whereas our understanding of the mechanisms regulating cyclin B1 degradation is well advanced, less is known about death in mitosis. It involves the intrinsic apoptosis pathway; however, how this is regulated during mitosis is unclear (Topham and Taylor, 2013). The nature of the apoptotic trigger is also unclear, but DNA damage seems a likely candidate, with one source being partial activation of caspase-activated DNase (CAD), caused by cytochrome c leakage from mitochondria (Orth et al., 2012). A second source is telomere deprotection, driven by the mitotic kinase Aurora B (Hayashi et al., 2012). In light of our limited understanding regarding the mechanisms responsible for apoptosis during a mitotic arrest, we adopted an unbiased approach and screened a genome-wide library for siRNAs that suppress taxol-induced cell death. To define how genes identified in the screen modulate antimitotic responses, we then used single-cell time-lapse imaging to directly correlate mitotic behavior with subsequent cell fate.

RESULTS

A Genome-wide Screen for Regulators of Mitotic Cell Fate

The competing-networks model predicts that suppressing death signals during mitotic arrest provides more time for cyclin B1 degradation, thereby shifting cell fate from death to slippage (Figure 1A). To test this, we screened an siRNA library to identify genes required for DiM. Because slippage results in cell survival, we based the screen on a viability assay (Figure S1A). To maximize the assay's dynamic range, we treated RKO cells, which predominantly undergo DiM (Gascoigne and Taylor, 2008), with a saturating concentration of taxol to ensure maximal mitotic blockage and apoptotic response. We also synchronized the cells to maximize cell death by 48 hr (Figure 1B). The primary screen identified 325 hits (Figure S1B). To filter out off-target hits, we performed a secondary screen using a pool of four different siRNAs, yielding 100 hits. Because taxol-induced death requires mitotic entry and robust spindle checkpoint activation, we predicted that in addition to DiM genes, the screen would also uncover genes required for cell cycle progression and SAC function. Indeed, we identified all the known SAC components, several kinetochore proteins required for SAC function and the entire chromosomal passenger complex, plus several genes required for mitotic entry (Figure 1C). To distinguish cell cycle and SAC genes from potential DiM genes, we performed a tertiary screen measuring mitotic index at 24 hr (Figure 1B) and plotted it against viability at 48 hr (Figure 1C). To hone in on potential DiM genes, we focused on hits with a high mitotic index at 24 hr and a substantial viability score at 48 hr (Figure 1C). Time-lapse microscopy showed that siRNA pools targeting *KCNK1*, *ZNF791*, *SNTA1*, and *MYC* shifted cell fate from death to slippage (Figure S1C). Importantly, mitotic exit was not accelerated, indicating inhibition of apoptosis rather than SAC override.

Myc Is a Regulator of Cell Fate following Prolonged Mitotic Arrest

Of the four hits, we first focused on *MYC*, which encodes the bHLH-Zip transcription factor c-Myc (hereafter Myc). Myc, a potent oncogene deregulated in many cancers, regulates a multitude of genes via both transcriptional amplification and co-factor-dependent activation/repression (Conacci-Sorrell et al., 2014; Eilers and Eisenman, 2008; Hann, 2014; Wolf et al., 2015). Myc thus drives numerous biological pathways including proliferation, biogenesis, and metabolism which, when deregulated, promote transformation and tumorigenesis. Because Myc can also drive apoptosis, primarily via the ARF-MDM2-p53 pathway (Lowe et al., 2004; McMahon, 2014), we considered it an attractive candidate for a DiM gene. To validate Myc as a bona fide on-target hit, we deconvolved the siRNA pools, identifying four distinct siRNAs that repressed Myc and inhibited DiM (Figures S1D and S2A). When combined, these four siRNAs reduced Myc protein levels by 90% and shifted cell fate in favor of slippage (Figures 2A and 2B). In nine control experiments, quantitating 100 cells per population, 82% of cells underwent DiM, while 18% slipped (Figure 2C). In five Myc RNAi populations, 45% of cells died, while 55% slipped. Moreover, titrating the siRNAs revealed a correlation between Myc protein levels and cell fate (Figure 2D). In addition, an RNAi-resistant Myc transgene

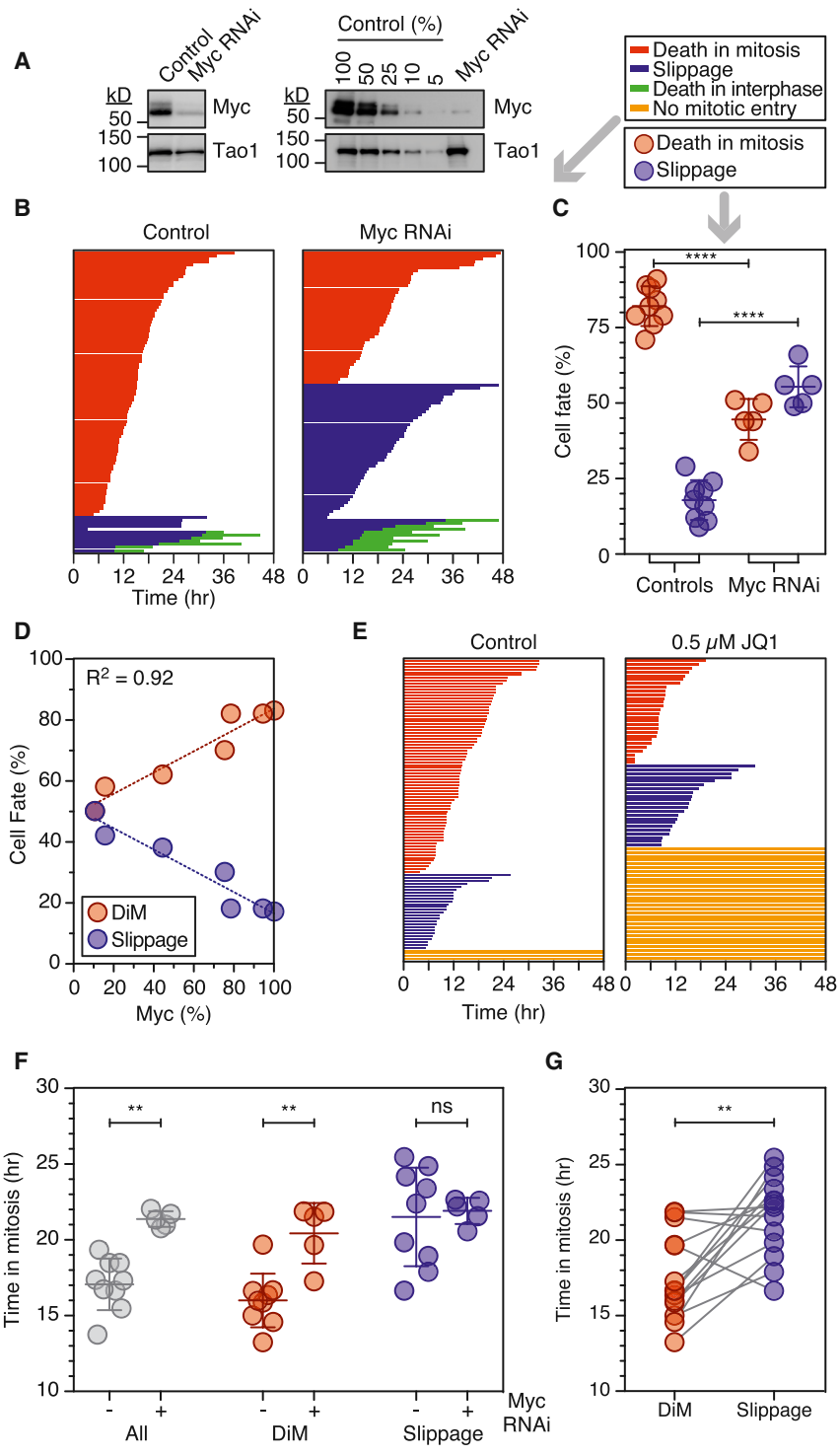

Figure 2. Myc Is a Regulator of Mitotic Cell Fate

(A) Immunoblots showing Myc inhibition.

(B) Fate profiles of RKO cells exposed to 0.1 μM taxol following Myc RNAi.

(C) Cell fate in nine control and five Myc RNAi populations.

(D) Correlation between Myc protein levels and cell fate.

(E) Fate profiles of RKO cells exposed to 0.1 μM taxol and 0.5 μM JQ1.

(F) Time spent arrested in mitosis; entire population (gray), cells that die (red), and cells that slip (blue).

(G) Time arrested in mitosis with lines connecting cells from the same population. **p < 0.01, ****p < 0.0001.

See also Figure S2.

reverted the fate profile back toward DiM (Figure S2B). To further validate Myc, we turned to non-RNAi modalities, in particular the small molecules DMSO and JQ1 (Figure S2C). DMSO, which blocks transcriptional elongation of *MYC* (Eick and Bornkamm, 1986), efficiently suppressed Myc in RKO cells (Figure S2C) and reduced DiM from 92% to 58% (Figure S2D). JQ1 displaces the Brd4 transcriptional elongation factor from the *MYC* promoter (Filippakopoulos et al., 2010; McKeown and Bradner, 2014) and accordingly JQ1 inhibited Myc expression in RKO cells (Figure S2C). This was accompanied by a substantial effect on proliferation (Figure 2E). However, of the cells that did enter mitosis, only 56% were killed by taxol, demonstrating a shift in favor of slippage (Figure 2E). Significantly, a Myc cDNA resisted the DMSO and JQ1 effects and restored DiM (Figure S2D). To determine whether Myc's role in DiM depends on its ability to modulate gene expression, we turned to Omomyc, a mutant bHLH-Zip domain that sequesters Myc in complexes unable to bind to E-boxes (Soucek et al., 2002). Inducing Omomyc in RKO cells inhibited DiM (Figure S2B), indicating that Myc most likely promotes DiM via its canonical role as a transcription factor. Interestingly Myc V394D, which cannot bind the Miz1 transcriptional repressor (Wiese et al., 2013), rescued Myc RNAi (Figure S2B), suggesting that Myc promotes DiM largely via transcriptional activation. Taking together the RNAi data, the DMSO, JQ1, and Omomyc experiments, we conclude that Myc is a key determinant of cell fate following prolonged mitotic arrest.

Using Myc to Test the Competing-Networks Model

The competing-networks model predicts that suppressing mitotic death provides more time for cyclin B1 degradation, thus shifting the balance toward slippage. A corollary is that the average time spent in mitosis should increase (Figure 1A). Consistently, whereas controls spent 17.1 hr arrested in mitosis, Myc-deficient cells spent 21.3 hr (Figure 2F) arrested in mitosis. Moreover, when we compared the cells that died, controls took 16.0 hr, whereas Myc-deficient cells took 20.4 hr; thus, even if a cell did not

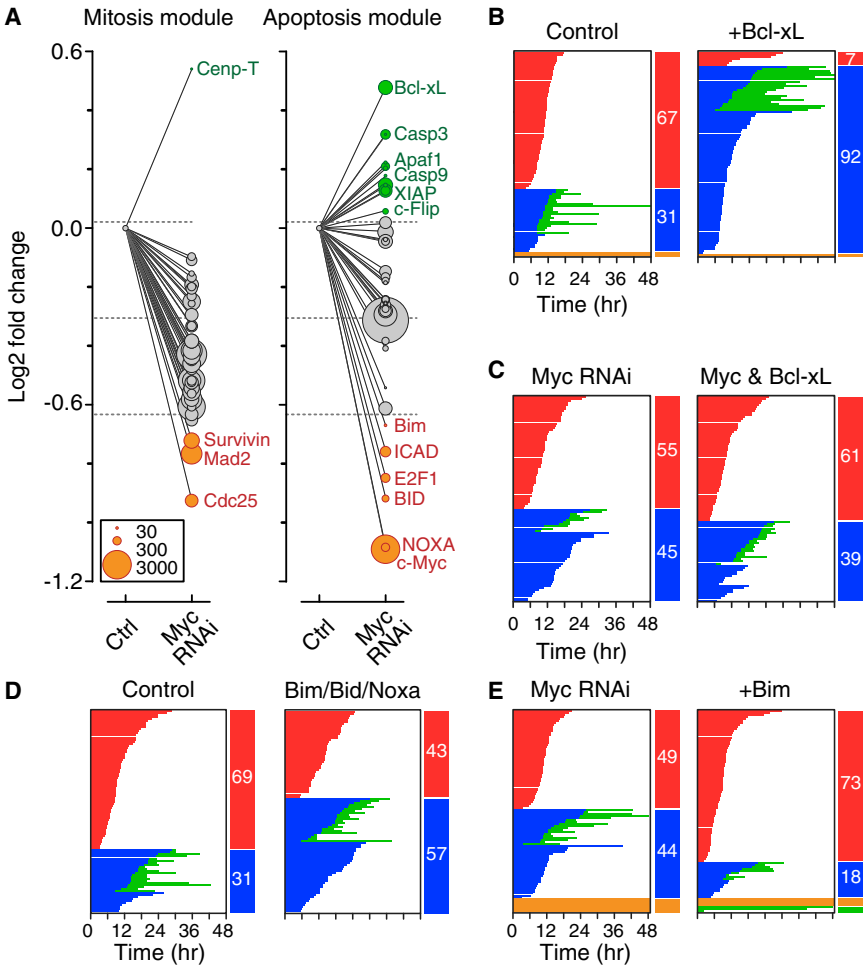

Figure 3. A Cluster of Redundant BH3-Only Proteins Promote Death in Mitosis

(A) Gene expression changes following Myc RNAi; y axis shows the fold change and circle sizes reflect the number of transcripts detected. Horizontal lines represent mean ± 1 SD.

(B–E) Fate profiles of RKO cells exposed to 0.1 μM taxol following tet-induced overexpression of Bcl-xL (B); RNAi-mediated co-repression of Myc and Bcl-xL (C); RNAi-mediated co-repression of Bim, Bid, and Noxa (D); and tet-induced overexpression of Bim following Myc RNAi (E).

See also Figure S3 and Table S3.

escape death, inhibiting Myc delayed its onset. Slippage typically took longer than DiM (Figure 2G) and the time from mitotic entry to slippage was not significantly affected by Myc RNAi (Figure 2F), consistent with the notion that the two competing networks are independent, and that Myc influences the death pathway but not the slippage pathway.

Myc Inhibition Deregulates an Apoptosis Module

To define how Myc promotes DiM, we interrogated mitosis and apoptosis gene expression modules using Nanostring technology. With the exception of Cenp-T, all the mitosis genes were suppressed following Myc RNAi (Figure 3A), reflecting Myc's role as a transcriptional amplifier and/or cell cycle driver. Of the three notably repressed genes, Survivin and Mad2 promote chromosome alignment and SAC function. Consistently, in the absence of taxol, whereas overall mitotic timing was normal in Myc RNAi cells, chromosome alignment was delayed slightly and anaphase onset slightly accelerated (Figure S3A). Nevertheless, despite these subtle effects on an unperturbed mitosis, Figure 2 clearly demonstrates that Myc-deficient cells mount a robust SAC response in 100 nM taxol, suggesting that mitotic deregulation is unlikely to account for the shift in cell fate. We therefore turned to the apoptosis module, which included 12 upregulated and six downregulated genes (Figure 3A). Because Myc RNAi promotes survival, the dominant effectors are likely to be upregulated pro-survival genes and/or downregulated pro-death genes. Of the upregulated genes, Bcl-xL is a well-established pro-survival factor, while three of the downregulated genes, namely Bid, Bim, and Noxa, encode BH3-only pro-apoptotic proteins (Figure 3A). Because these are Myc effectors in other contexts (McMahon, 2014), we analyzed them in more detail.

BH3-Only Pro-apoptotic Proteins Are Redundant Effectors of Myc

Consistent with Myc's known ability to repress Bcl-xL (Eischen et al., 2001), Myc RNAi elevated Bcl-xL protein levels in RKO cells (Figure S3B). Ectopic overexpression of Bcl-xL suppressed both DiM and post-mitotic apoptosis (Figures 3B and S3C), supporting the notion that Bcl-xL is a potent mitotic survival factor (Bah et al., 2014; Minn et al., 1996; Upreti et al., 2008). However, ectopic Bcl-xL enhanced survival more potently than Myc RNAi, suggesting that other consequences of Myc inhibition attenuate the pro-survival effect of increased Bcl-xL (Eichhorn et al., 2014). Indeed, whereas Mcl1 transcripts fell only marginally upon Myc RNAi, Mcl1 protein levels fell substantially (Figures S3B and S3E), possibly due to deregulation of factors involved in Mcl1 turnover. However, in taxol-arrested cells, this residual Mcl1 appeared to resist mitotic degradation (Figure S3E). Nevertheless, despite these complexities, we reasoned that Bcl-xL upregulation alone is unlikely to explain the Myc RNAi phenotype, and therefore we turned our attention to the downregulated pro-death genes.

The downregulated BH3-only proteins (Figure 3A), namely Bid, Bim, and Noxa, are known to be upregulated by Myc, either directly or via the ARF-MDM2-p53 pathway (McMahon, 2014). If Bid, Bim, and Noxa are important Myc DiM effectors, then their inhibition should mimic Myc RNAi. However, because they did not manifest in the screen they are unlikely to be essential for DiM. Indeed, repression of each in isolation or in pairs had little effect on mitotic fate (Figure S3G). In contrast, co-repression of Bim, Bid, and Noxa tipped the balance in favor of slippage (Figure 3D), consistent with them being redundant

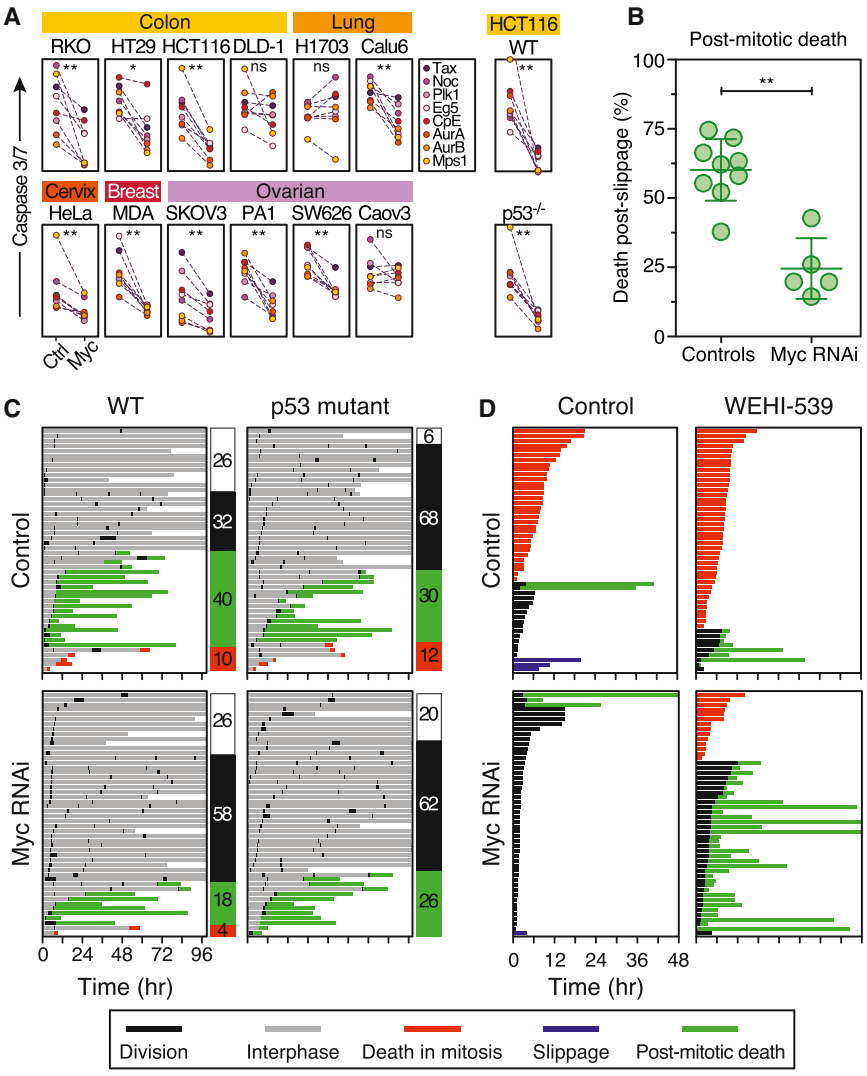

Figure 4. Myc Promotes Post-mitotic Death

(A) Apoptosis induction in cell lines indicated exposed to various antimitotic agents following Myc RNAi.

(B) Graph quantitating death following slippage in the presence of 0.1 μM taxol.

(C) Fate profiles of wild-type and p53-deficient HCT116 cells following Myc RNAi then exposed to the Mps1 inhibitor AZ3146 (2 μM). Numbers indicate percentage of cells that undergo one division (white), multiple divisions (black), post-mitotic death (green), and DiM (red).

(D) Fate profiles of RKO cells exposed to 10 nM taxol in combination with 100 nM WEHI-539. In (C), 0 hr is when imaging started.*$p < 0.05$, **$p < 0.01$. See also Figure S4 and Table S4.

downstream effectors of Myc. A corollary is that overexpression of any one should revert the Myc RNAi phenotype. Indeed, transgenic Bim restored DiM in Myc RNAi cells (Figures 3E and S3H). Consistent with the competing-networks concept, Bim/Bid/Noxa RNAi extended mitotic timing, whereas induction of Bim accelerated the onset of DiM (Figure S3I). We conclude therefore that Bim, Bid, and Noxa are redundant Myc effectors required for DiM.

MYC Sensitizes Various Cancer Lines to Antimitotic Drugs

To test the role of Myc in a wider context, we inhibited Myc in 12 cell lines derived from colon, lung, breast, cervical, and ovarian cancers (Figure S4A), then exposed them to a panel of antimitotic drugs including agents targeting Eg5/KSP, Plk1, Cenp-E, Aurora A, Aurora B, and Mps1. To monitor apoptosis, we used time-lapse imaging to measure caspase-3/7 activity. The effects of inhibiting Myc were strikingly consistent, significantly attenuating apoptosis in nine lines (Figure 4A). Interestingly, Myc inhibition had little effect in three lines, namely DLD-1, H1703, and Caov-3. The competing-networks model may explain these exceptions. DLD-1 cells slip very quickly (Gascoigne and Taylor, 2008); therefore, despite inhibiting DiM, slippage would be expected to continue such that Myc RNAi has little effect. Conversely, H1703 cells die very quickly and rarely slip, suggesting that despite delaying DiM, slippage may not be fast enough to permit exit. Nevertheless, Myc promotes apoptosis in a variety of cancer lines exposed to various antimitotic agents.

MYC Promotes Apoptosis following Slippage

In contrast to taxol, drugs targeting Aurora B and Mps1 drive cells through an aberrant mitosis (Keen and Taylor, 2009), suggesting that Myc also promotes apoptosis following slippage. Indeed, following exit from a prolonged taxol arrest, Myc RNAi reduced cell death from 60% to 25% (Figure 4B). Moreover, in response to an Mps1 inhibitor, Myc RNAi reduced post-mitotic apoptosis from 40% to 18% (Figure 4C) and enhanced colony formation (Figure S4B). Canonical Myc-driven apoptosis involves the ARF-MDM2-p53 pathway; however, because p53 is disengaged during mitosis, Myc-dependent DiM is likely p53-independent. Indeed, Myc RNAi suppressed apoptosis in p53-deficient HCT116 cells treated with mitotic blockers (Figure 4A). Consistent with p53 restraining further cell cycle progression following an aberrant mitosis (Thompson and Compton, 2010), p53 deletion increased the number of HCT116 cells entering a second mitosis from 32% to 68% (Figure 4C). However, apoptosis was only slightly affected by p53 loss, 30% versus 40% in controls, indicating that post-mitotic apoptosis is largely p53-independent. Interestingly, whereas Myc RNAi only had a marginal effect on post-mitotic apoptosis in p53-deficient cells, it increased the number of p53-proficient cells entering a second mitosis from 32% to 58% (Figure 4C). Thus, following an aberrant mitosis, Myc not only enhances post-mitotic apoptosis but also suppresses cell cycle progression, possibly via the ARF-MDM2-p53 pathway.

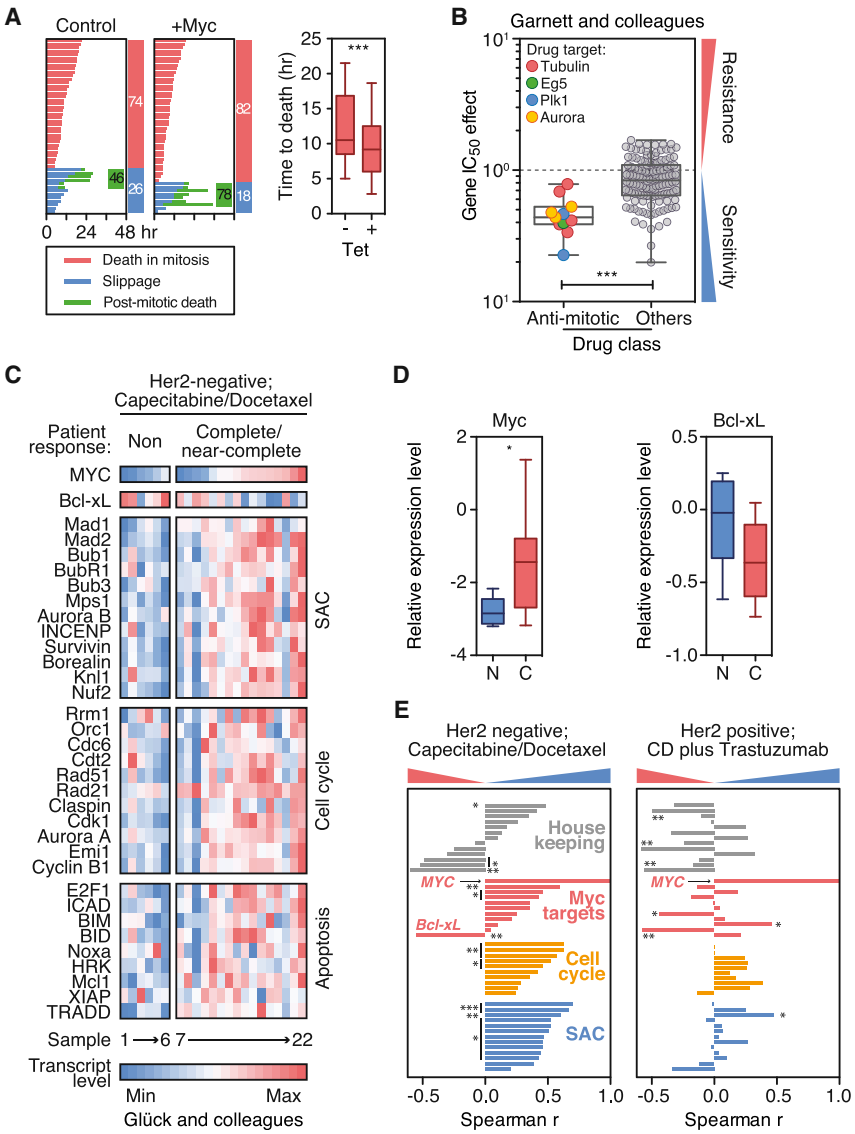

Figure 5. Overexpression of Myc Sensitizes Cancer Cells to Antimitotic Agents

(A) Fate profiles and box-and-whisker plot showing time to DiM in RKO cells exposed to 0.1 μM taxol following tet-induced overexpression of Myc.

(B) Gene IC_{50} effects for *MYC* comparing antimitotic agents with other drugs.

(C) Heatmaps showing gene expression profiles of 22 breast tumors (six non-responders and 16 complete/near-complete responders) treated with capecitabine and docetaxel.

(D) Box-and-whisker plots showing Myc and Bcl-xL expression levels in non-responsive (N) and responsive tumors (C).

(E) Bar graphs showing correlations between *MYC* and the SAC, cell cycle, and apoptosis genes. *p < 0.05, **p < 0.01, ***p < 0.001.

See also Figure S5 and Tables S5 and S6.

Myc Enhances Survival in Low-Dose Taxol

In breast cancers, taxol does not accumulate to concentrations high enough to induce prolonged mitotic arrest; rather cells progress through mitosis, albeit with chromosome segregation errors (Zasadil et al., 2014). Because Myc promotes post-mitotic death, we reasoned that Myc would also influence low-dose taxol responses. To test this, we reduced the taxol concentration to 10 nM (Figure S4C), a concentration in cell culture medium that results in intracellular concentrations similar to those measured in breast cancer (Zasadil et al., 2014). In 10 nM taxol, most RKO cells died in mitosis but 31% divided, indicating that the taxol concentration was "on the edge" (Figure 4D). Of those that divided, 12.5% died in the next interphase. Strikingly, Myc RNAi cells spent considerably less time in mitosis then divided, indicating that the SAC became satisfied (Figure 4D). Consistently, Myc RNAi slightly accelerated anaphase onset during an unperturbed mitosis (Figure S3A). Following division in 10 nM taxol, Myc RNAi cells survived, at least for the duration of the experiment. These divisions are unlikely to be normal; indeed, when we added 100 nM WEHI-539, a selective Bcl-xL inhibitor (Lessene et al., 2013), all the cells that divided subsequently died (Figures 4D and S4C). Thus, inhibiting Myc enhances survival in low-dose taxol but this can be ameliorated by inhibition of Bcl-xL.

Tumor Cells Overexpressing MYC Are Sensitive to Antimitotic Agents

Because inhibiting Myc suppresses apoptosis in response to antimitotic agents, we asked whether elevating Myc expression had the opposite effect. Indeed, tet-induction of a Myc transgene in RKO cells accelerated DiM by 2.3 hr and reduced slippage, albeit modestly (Figure 5A). Moreover, of the cells that slipped, overexpressing Myc increased post-mitotic death from 46% to 78%. Consistently, overexpressing Myc in Rat1a cells enhances colcemid-induced apoptosis (Li and Dang, 1999). To examine Myc overexpression in a wider context, we interrogated the Genomics of Drug Sensitivity in Cancer database (Garnett et al., 2012), which describes 665 cell lines, 47 of which overexpress Myc, in response to 141 drugs, 11 of which target microtubules or mitotic regulators. The mean half-maximal inhibitory concentration (IC_{50}) effect for the 11 antimitotic drugs was 0.47 compared to 0.83 for the other 130 drugs (Figures 5B and S5A), confirming that tumor cells overexpressing Myc are more sensitive to antimitotic agents compared to drugs in general.

To determine whether the Myc overexpression effect extended to patient chemotherapy responses, we interrogated microarray datasets from XeNA, a clinical trial examining response rates in women with operable, early stage breast cancer receiving neoadjuvant capecitabine plus the antimitotic agent docetaxel (Glück et al., 2012). Tumors from patients showing complete or near-complete responses tended to have elevated Myc (Figures 5C and 5D). Next, we analyzed the SAC

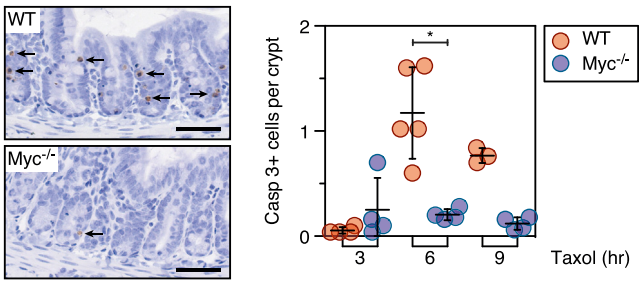

Figure 6. *MYC*-Deficient Crypts Are Resistant to Taxol-Induced Apoptosis

Immunohistochemical staining and quantitation of cleaved caspase 3 in intestinal sections from wild-type and *MYC* mutant mice following 3, 6, and 9 hr exposure to taxol. Bar represents 50 μm. *$p < 0.05$.

and cell cycle genes identified by the siRNA screen (Figure 1C), and the Myc regulated genes identified by our Nanostring analysis (Figure 3A). Although there was no obvious overall correlation between Myc and several housekeeping genes, Myc correlated positively with the SAC, cell cycle, and apoptosis genes (Figures 5C and 5E). Moreover, the SAC, cell cycle, and Myc clusters were elevated in the responsive tumors (Figure S5B). The elevation was not simply due to a global increase in gene expression because Bcl-xL displayed a negative correlation (Figures 5C–5E), consistent with Myc-induced suppression (Figure 3A). Moreover, the correlation between Myc and cell cycle/SAC genes was not simply due to increased proliferation, because Her2-positive tumors did not show a similar pattern (Figures 5E and S5C). These results suggest that a positive response to antimitotic chemotherapy requires entry into mitosis, a robust SAC response, and the ability to undergo Myc-dependent apoptosis.

Myc Is Required for Taxol-Induced Apoptosis in Mouse Intestinal Crypts

The correlation between Myc expression and chemotherapy responses is provocative. However, Her2-negative breast cancers include various tumor subtypes and XeNA used multiple chemotherapy agents. We therefore turned to a genetically constrained model system that allows single agent exposure to validate the role of Myc in the context of an intact tissue. Mice harboring a conditional *MYC* allele provided such a system (Phesse et al., 2014). *AhCre*$^{+}$ *MYC*$^{fl/fl}$ mice were injected with β-napthoflavone to delete *MYC* in the small intestine. Four days later, taxol was administered to induce mitotic arrest and then apoptosis was measured with caspase 3 staining (Radulescu et al., 2010). In Myc-deficient intestines, we observed 0.2 apoptotic cells per intestinal crypt compared to 1.2 in Myc-proficient controls (Figure 6). We conclude therefore that Myc is a determinant of mitotic cell fate in the mouse intestine.

Interrogating Kcnk1, Snta1, and Znf791

The transcript profiling and functional experiments indicate that Myc enhances DiM by suppressing Bcl-xL and upregulating BH3-only proteins (Figure 3). However, a defining feature of Myc is its ability to modulate numerous genes thereby influencing various biological processes, including biosynthesis and metabolism pathways (Conacci-Sorrell et al., 2014; Eilers and Eisenman, 2008). Consequently, Myc targets not included in the Nanostring analysis could contribute to the phenotype. Moreover, the screen identified *KCNK1*, *ZNF791* and *SNTA1* (Figure S1C), but it is not immediately obvious how they might modulate apoptosis. To address these issues, we deconvolved the Kcnk1, Znf791, and Snta1 siRNA pools. In each case, only a single siRNA sequence enhanced viability, suggesting that they were "off-target" hits (Figure S1D). When transfected in isolation, the active Znf791 and Snta1 siRNAs accelerated mitotic exit rather than delaying DiM (Figure S1E). In contrast, the active Kcnk1 siRNA induced a Myc-like phenotype, suppressing DiM without accelerating mitotic exit. Therefore, to identify the target of this siRNA, and to interrogate Myc target genes not included in the Nanostring analysis, we turned to global gene expression profiling.

Egr1 Promotes Death in Mitosis

RKO cells were transfected with Myc, Kcnk1, and Snta1 siRNAs and then cDNA libraries were sequenced using Illumina HiSeq technology. Myc RNAi induced numerous changes, with 955 downregulated genes and 1,214 upregulated genes (Figure 7A). The effect on Myc itself was relatively modest, possibly reflecting negative auto-regulation (Conacci-Sorrell et al., 2014). Gene ontology analysis highlighted ribosome biogenesis, metabolism, gene expression, cell cycle, and apoptosis pathways (Figure S6C), consistent with known Myc functions. The Kcnk1 siRNA affected 424 genes, with *KCNK1* itself one of the most repressed (Figure 7A). Whereas gene ontology analysis also highlighted metabolism and biosynthesis pathways, the p values and fold enrichment scores were substantially lower (Figure S6C), indicating that DiM can be suppressed without major effects on metabolism and biosynthesis pathways.

To understand how the active Kcnk1 siRNA suppresses DiM, we focused on the 58 downregulated genes in common with Myc (Figure 7B). Only two were repressed more than 2-fold in both conditions, namely *SNORD102* and *EGR1*. Of these, Egr1, a zinc finger transcription factor, stands out as it is an established Myc target required for Myc-dependent, p53-independent apoptosis, and it cooperates with Myc to upregulate Bim and Noxa (Boone et al., 2011; Wirth et al., 2014). We reasoned therefore that the Kcnk1 siRNA might suppress DiM via inhibition of Egr1. Consistently, transcript profiling indicated that Bim, Bid, and Noxa were reduced following Kcnk1 siRNA (not shown). To test directly whether Egr1 promotes DiM, we transfected RKO cells with siRNAs specifically targeting Egr1. Strikingly, this shifted cell fate from DiM to slippage in a manner comparable to Myc siRNA (Figure 7C). Thus, these observations identify *EGR1* as a "DiM" gene and suggest that *KCNK1* manifested in the screen because of off-target activity toward Egr1.

Myc Modulates DNA Damage Accumulation in Mitosis

Although Myc and Egr1 appear to set the stage for DiM, what actually triggers apoptosis during a prolonged mitotic arrest is unclear. During the course of this work, we made two observations suggesting that Myc may modulate two recently identified mechanisms (Hayashi et al., 2012; Orth et al., 2012). First, we noted that ICAD, the inhibitor of CAD, was markedly reduced by Myc RNAi (Figure 3A). This was intriguing in light of the demonstration

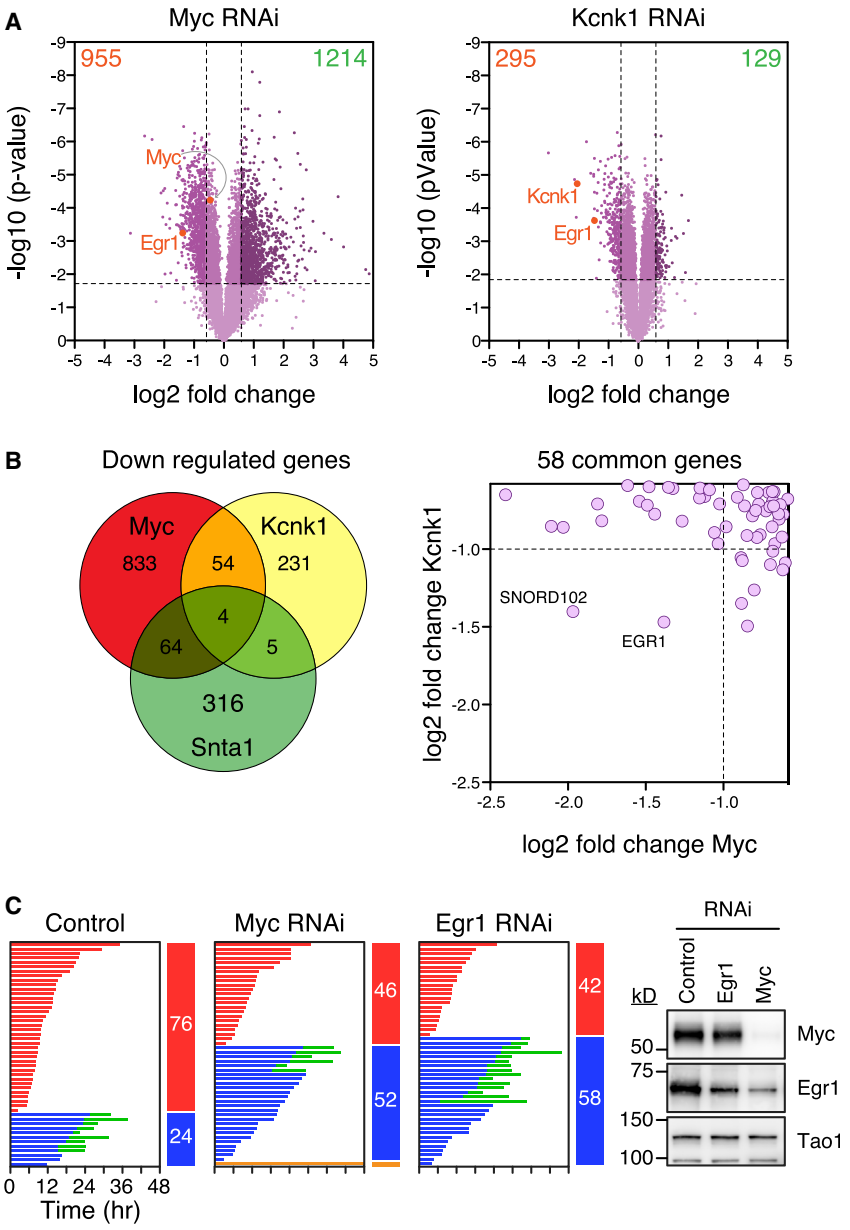

Figure 7. Egr1 Is a Regulator of Mitotic Cell Fate

(A) Volcano plots showing gene expression changes following Myc and Kcnk1 RNAi.

(B) Venn diagram and scatterplot showing common downregulated genes.

(C) Fate profiles of RKO cells exposed to 0.1 μM taxol following Egr1 RNAi and immunoblots showing reduced Egr1 following Myc RNAi.

See also Figure S6 and Table S7.

that CAD-dependent DNA damage incurred during mitosis activates p53 following slippage (Orth et al., 2012). In addition to being an inhibitor of CAD, ICAD is also a chaperone essential for CAD function (Nagase et al., 2003), and accordingly, inhibition of both ICAD and Myc reduced CAD (Figure S7A). Moreover, ICAD RNAi suppressed DiM (Figure 8A), suggesting that by stabilizing CAD, Myc promotes accumulation of DNA damage during mitosis thereby accelerating DiM. Consistently, γ-H2AX accumulation was less prevalent in taxol-treated Myc RNAi cells (Figure S7B).

We were also intrigued by the very rapid DiM in cells lacking Bcl-xL and Mcl1 (Figure S3F). In addition, we noticed that in the absence of taxol, Bcl-xL/Mcl1-deficient cells often died upon mitotic entry (Figure S7C). However, it seems unlikely that ICAD/CAD-dependent damage accumulates fast enough to trigger apoptosis during an unperturbed mitosis. Indeed, ICAD RNAi had little protective effect in cells co-depleted for Bcl-xL and Mcl1 (not shown). In contrast, telomere deprotection might cause a burst of DNA damage upon mitotic entry (Hayashi et al., 2012). Indeed, inhibiting Aurora B in Bcl-xL/Mcl1-deficient cells reduced DiM from 69% to 34% (Figure S7C) and suppressing telomere deprotection by overexpressing TRF2 also had a protective effect (Figures 8B and S7D). Inhibiting Myc in Bcl-xL/Mcl1-deficient cells had an even more penetrant effect, reducing DiM in the absence of taxol from 69% to 10% (Figure S7C). Although this could simply reflect Myc's role setting the balance between pro-survival and pro-death factors, these observations raise the possibility that Myc may also modulate the DNA damage-inducing pathways that trigger apoptosis during a prolonged mitotic arrest.

DISCUSSION

The success of the siRNA screen was predicated on the existence of genes essential for DiM. Consistent with the SAC being indirectly required for DiM (Taylor and McKeon, 1997), we identified all the known SAC components. Indeed, SAC genes frequently manifest in antimitotic RNAi screens, yet apoptotic regulators rarely do (Díaz-Martínez et al., 2014). This suggests that the two networks governing mitotic fate are rather different: while the SAC consists of essential genes, the DiM network involves redundant sub-networks. Myc drives expression of the apoptotic network required for DiM, providing a simple explanation for why it manifested in the screen. The different architectures of the two networks may reflect evolutionary origins and/or buffering capacities. The SAC, which is conserved from yeast to man, is an "all-or-nothing" mechanism that responds to a single input, unattached kinetochores, and is not buffered by transcription (Lara-Gonzalez et al., 2012). In contrast, apoptosis, a metazoan characteristic, responds to multiple inputs and can be "fine-tuned" by transcriptional buffering depending on developmental context and homeostatic pressures (Barkett and Gilmore, 1999). The differing architectures also support the notion that they are largely independent (Gascoigne and Taylor, 2008; Huang et al., 2010).

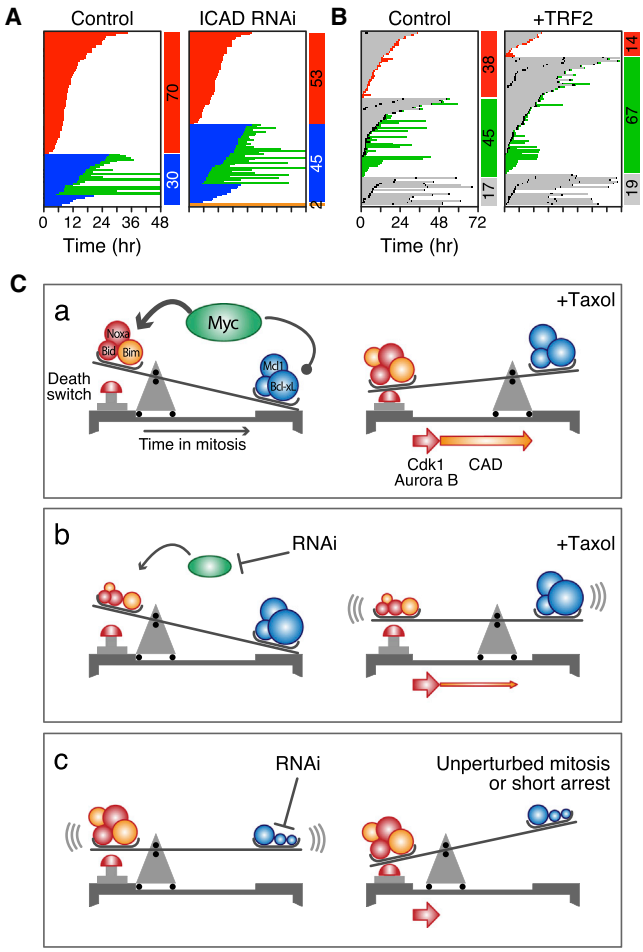

Figure 8. Inhibition of ICAD Enhances Slippage

(A) Fate profiles of RKO cells exposed to 0.1 μM taxol following ICAD RNAi.

(B) Fate profiles of RKO cells in the absence of taxol following RNAi-mediated co-repression Bcl-xL/Mcl1 plus tet-induced overexpression of TRF2. In (B), 0 hr represents when imaging started.

(C) Mechanistic model, see text for details.

See also Figure S7.

In addition to driving proliferation, Myc overexpression drives apoptosis via ARF-MDM2-p53 (McMahon, 2014). Because p53 is disengaged during mitosis, it is not clear how this mechanism could contribute to DiM, and indeed p53 is not required for Myc-dependent mitotic death. Moreover, Myc can upregulate Bim, Bid, and Noxa independently of p53 (Campone et al., 2011; Egle et al., 2004; Eischen et al., 2001; Hemann et al., 2005; Iaccarino et al., 2003; Muthalagu et al., 2014; Nikiforov et al., 2007). Recent evidence shows that Myc drives p53-independent apoptosis by cooperating with Egr1, itself a Myc target (Boone et al., 2011). Myc promotes *EGR1* expression via a non-canonical mechanism involving ARF and in turn, Myc and Egr1 are co-recruited to the promoters of *BIM* and *NOXA* (Boone et al., 2011; Wirth et al., 2014). It seems likely, therefore, that in interphase, Myc and Egr1 upregulate a cluster of redundant pro-apoptotic BH3-only proteins and suppress Bcl-xL, establishing the apoptotic network which can later induce DiM without the need for p53 engagement and de novo gene expression. Upon entry into mitosis, the apoptotic network is balanced so that a pro-survival environment is maintained (Figure 8C). However, in the presence of mitotic blockers, the balance slowly tips in favor of the pro-apoptotic BH3-only proteins, eventually triggering cell death. Several processes help tip the balance, including accumulation of DNA damage due to partial CAD activation and telomere deprotection (Hayashi et al., 2012; Orth et al., 2012). Also, slow degradation of Mcl1, possibly due to incomplete APC/C inhibition (Harley et al., 2010), weakens pro-survival function. When Myc is inhibited, the initial balance is more heavily weighted toward pro-survival, mitotic death is thus delayed providing more time for CyclinB1 degradation and slippage. Myc inhibition may also suppress DNA damage accumulation, weakening the apoptotic trigger. When Bcl-xL and Mcl1 are co-inhibited, the balance is so heavily weighted toward pro-death that cells cannot survive a short mitotic arrest, and even an unperturbed mitosis can induce apoptosis.

Myc is also required for efficient apoptosis in response to drugs that drive cells through an aberrant mitosis. Whether this is because these cells inherit an apoptotic balance tipped in favor of pro-survival or cannot initiate a robust post-mitotic response remains to be seen. Consistent with the latter, Myc also promotes cell cycle restraint following SAC override. One possibility to account for this is the ARF-MDM2-p53 pathway; by inducing ARF and thus suppressing MDM2, Myc may sensitize the p53-dependent mechanism that detects DNA damage incurred when chromosomes missegregate (Janssen et al., 2011). This may explain why ARF-deficient mouse embryonic fibroblasts tolerate aneuploidies (Silk et al., 2013). Alternatively, following chromosome missegregation induced by SAC override, Myc's ability to drive global gene expression might elevate the proteotoxic burden that arises in aneuploid daughter cells, thus enhancing cell cycle suppression (Tang and Amon, 2013). Interestingly, several mitotic regulators are synthetic lethal with Myc overexpression, including Cdk1, Survivin, Aurora B, and the SUMO-activating enzyme SAE-2 (den Hollander et al., 2010; Goga et al., 2007; Kessler et al., 2012; Yang et al., 2010). Whether this is due to deregulation of mitosis per se as opposed to deregulation of cellular responses to mitotic abnormalities is unclear. Consistent with the former, SAE-2 modulates a spindle assembly gene expression program (Kessler et al., 2012). Consistent with the latter, our observations show that Myc enhances both DiM and post-mitotic responses.

Antimitotic agents continue to be important frontline drugs, emphasized by the impressive effect of combining taxanes with targeted therapies in the treatment of breast cancer (Slamon et al., 2001). Whether taxanes inhibit tumor growth via antimitotic or other tubulin-dependent mechanisms remains unclear (Komlodi-Pasztor et al., 2012; Mitchison, 2012). Consistent with Myc enhancing antimitotic apoptosis, ovarian cancers treated with taxol and carboplatin responded better if Myc was more highly expressed (Iba et al., 2004). Consistently, Her2-negative breast cancers that responded to docetaxel and capecitabine had higher Myc levels. The correlation between Myc and cell cycle/SAC genes is especially striking because Her2-positive tumors do not show a similar pattern. This suggests that docetaxel-capecitabine responses require cell cycle progression and a robust SAC response. In contrast, anti-tumor effects mediated by trastuzumab-docetaxel-capecitabine are more likely dominated by

inhibition of Her2-dependent PI3K/Akt survival signaling (Berns et al., 2007), and therefore less dependent on mitotic entry and SAC activation. Taken together, these observations suggest that the Myc network may yield potential biomarkers. However, a recent study found that while triple-negative breast cancers exhibited elevated Myc expression, this did not predict responses to neoadjuvant chemotherapy (Horiuchi et al., 2012). Consistent with the mechanisms we describe here, this study did however observe that elevated Myc sensitized triple-negative cells to Cdk1 inhibition in a Bim-dependent, p53-independent manner. Thus, taking together our observations, the synthetic lethality relationships described above, and the provocative clinical observations, there is considerable merit in further exploring the links between the BH3-only/Bcl-xL pathway and mitotic regulators in the context of Myc-driven tumors. Interestingly, Myc inhibition had little effect on three cell lines we studied, suggesting that this avenue may provide insight into intrinsic resistance, while changes and/or heterogeneity in Myc expression may provide insight into acquired taxane resistance.

Myc suppresses Bcl-xL in various contexts (Eischen et al., 2001) and they inversely correlate in the breast cancer gene expression profiles we analyzed. Moreover, Bcl-xL overexpression potently blocks Myc-driven apoptosis (Pelengaris et al., 2002) and our observations reaffirm Bcl-xL as a potent mitotic survival factor. Although Mcl1 and Bcl-xL can partially compensate for each other during mitosis (Shi et al., 2011), degradation of Mcl1 during a mitotic arrest means that Bcl-xL becomes particularly critical following slippage. Because slippage is a clinically relevant phenotype (Zasadil et al., 2014), these observations make a compelling case for combining Bcl-xL inhibitors with antimitotic agents. Indeed, the Bcl2/Bcl-xL inhibitor navitoclax sensitizes ovarian cancer cell lines to taxol (Wong et al., 2012). Similar combination strategies may also help revive the prospects of targeted antimitotic agents that have thus far been disappointing in the clinic (Komlodi-Pasztor et al., 2012; Mitchison, 2012). Exploring Myc-dependent apoptotic pathways for predicative biomarkers may also facilitate better clinical evaluation of these agents. Finally, as a potent driver of tumorigenesis, Myc is itself an attractive anti-cancer target (McKeown and Bradner, 2014; Sodir and Evan, 2011). However, if superimposed on existing taxane chemotherapy regimens, targeting Myc may be counterproductive, weakening both the SAC and post-mitotic apoptosis, thereby fueling genomic instability. This should not detract from Myc as a target as long as mitigating strategies are also explored. Our observation that pharmacological inhibition of Bcl-xL potently restores apoptosis in Myc-deficient cells exposed to low-dose taxol further supports the case for exploring Bcl-xL inhibitors in the context of antimitotic agents.

EXPERIMENTAL PROCEDURES

siRNA Library Screen

RKO cells were synchronized for 16 hr using 2 mM thymidine, released then seeded in 96-well plates (Greiner Bio-One) containing Opti-MEM media (Life-Technologies), DharmaFECT 1 transfection reagent (Dharmacon), and siRNAs at a final concentration of 66 nM, after which 0.1 μM taxol and viability reagent (CellTiter 96 AQueousOne Solution Cell Proliferation Assay, Promega) were added after 24 and 68 hr, respectively, and the absorbance at 490 nm measured after 72 hr. For the tertiary screen, the mitotic index at 24 hr was determined using a BD Pathway (BD Biosciences). Cell lines and small molecule inhibitors are described in the Supplemental Experimental Procedures.

Functional Experiments

siRNAs and DharmaFECT 1 combined in Opti-MEM media were added to RKO cells plated at 10×10^4 cells/ml, yielding a final siRNA concentration of 66 nM. For siRNA sequences, see the Supplemental Experimental Procedures. Open reading frames described in the Supplemental Experimental Procedures were cloned into pcDNA5/FRT/TO based vectors and isogenic, tetracycline-inducible, stable cell lines generated by co-transfection with pOG44 (Invitrogen) into Flp-In T-REx RKO cells. Phase contrast imaging, cell proliferation, and apoptosis measurements were performed on an IncuCyte ZOOM (EssenBioScience) with CellPlayer Kinetic Caspase-3/7 Apoptosis Assay Kit (EssenBioSciences). Image sequences were analyzed manually and statistical analysis performed with GraphPad Prism. On fate profiles, 0 hr corresponds to mitotic entry unless stated otherwise in the legend. Immunoblotting was performed using antibodies described in the Supplemental Experimental Procedures.

Gene Expression Profiling

Cells transfected with siRNAs were synchronized, released for 5 hr, then RNA was prepared using Trizol (Life Technologies). One hundred nanograms of RNA was hybridized with custom nCounter Reporter and Capture probe sets (Nanostring Technologies) at 65°C overnight, unhybridized probes removed, complexes bound to the imaging surface, and images acquired using the nCounter Digital Analyzer. Transcript counts were normalized to housekeeping genes using nSolver Analysis Software. For global gene expression profiling, total RNA was processed using the Illumina TruSeq Stranded mRNA Sample Preparation Kit, then cDNA libraries sequenced on an Illumina HiSeq 2000 using single read, 50 cycle runs. Quality of sequencing reads was assessed using FastQC (Babraham Bioinformatics) and aligned to a reference genome (hg19, UCSC Genome Browser) using TopHat. Sequencing yielded on average 23.7 million unique reads per sample with a 60.7%–65.7% mapping rate. Cufflinks was used to generate transcript abundance as fragments per kilobase of transcript per million mapped reads (FPKM), and statistical analysis of FPKM values was calculated using R (Bioconductor).

Inactivation of Myc in the Mouse Intestine

Cre-mediated inactivation of *MYC* in the intestinal epithelium was induced via three intraperitoneal (i.p.) injections of 80 mg/kg β-naphthoflavone in 1 day. Four days later, 10 mg/kg taxol was administered via i.p. injection, tissue harvested after various time points, fixed in 4% formaldehyde, then stained for cleaved caspase 3 (R&D systems). All animal experiments were conducted under an appropriate animal project license approved by the UK home office and in accordance with the Animal Welfare and Experimental Ethics Committee at the University of Glasgow.

Statistical Methods

Statistical analysis was performed in GraphPad Prism 6 as follows: ANOVA plus Bonferroni (Figures 2C and 2F); linear regression (Figure 2D); correlation (Figures S1B and 5E); Paired t test (Figure 2G); Wilcoxon t test (Figure 4A); Mann-Whitney (Figures 4B, 5A, 5B, 5D, 6, S3A, S3I, and S5B); Kruskal-Wallis (Figure S1E). In figures, p values were $^*p < 0.05$, $^{**}p < 0.01$, $^{***}p < 0.001$, $^{****}p < 0.0001$. Scatterplots show mean and SD. Unless stated otherwise in the figure legend, box-and-whisker plots show median, interquartile ranges, plus min to max range. Figure S1D, mean ± SD; Figure S4B, mean ± SEM.

ACCESSION NUMBERS

The accession number for the global gene expression data reported in this paper is GEO: GSE68219.

SUPPLEMENTAL INFORMATION

Supplemental Information includes Supplemental Experimental Procedures, seven figures, and seven tables and can be found with this article online at http://dx.doi.org/10.1016/j.ccell.2015.06.001.

AUTHOR CONTRIBUTIONS

C.T. performed the RNAi screen, Nanostring analysis, and functional experiments. A.T., A.B., O.S., L.N., S.L., and C.S. contributed to the functional experiments. R.A.R., D.H., and O.J.S. contributed the mouse data. B.B. and D.J.P. synthesized the Cenp-E inhibitor. P.L., Y.S., and D.W.C. contributed the HiSeq analysis. S.S.T. conceived the study and wrote the manuscript. All authors read and commented on the manuscript.

ACKNOWLEDGMENTS

This work was supported by the Genomic Technologies and Bioimaging Core Facilities in the Faculty of Life Sciences. We thank Stefan Knapp (University of Oxford) and Bert Vogelstein (Johns Hopkins) for reagents; and Andy Hayes, Leo Zeef, Dave Spiller, Andy Sharrocks, Mike White, Gino Poulin, Donald Ogilvie, Dean Jackson, and William Weiss for useful discussions. Funding was provided by Cancer Research UK, the Medical Research Council, and the Wellcome Trust. S.S.T. is supported by a Cancer Research UK Senior Fellowship.

Received: October 10, 2014
Revised: March 4, 2015
Accepted: June 8, 2015
Published: July 13, 2015

REFERENCES

A'Hern, R.P., Jamal-Hanjani, M., Szász, A.M., Johnston, S.R., Reis-Filho, J.S., Roylance, R., and Swanton, C. (2013). Taxane benefit in breast cancer—a role for grade and chromosomal stability. Nat. Rev. Clin. Oncol. *10*, 357–364.

Bah, N., Maillet, L., Ryan, J., Dubreil, S., Gautier, F., Letai, A., Juin, P., and Barillé-Nion, S. (2014). Bcl-xL controls a switch between cell death modes during mitotic arrest. Cell Death Dis. *5*, e1291.

Barkett, M., and Gilmore, T.D. (1999). Control of apoptosis by Rel/NF-kappaB transcription factors. Oncogene *18*, 6910–6924.

Berns, K., Horlings, H.M., Hennessy, B.T., Madiredjo, M., Hijmans, E.M., Beelen, K., Linn, S.C., Gonzalez-Angulo, A.M., Stemke-Hale, K., Hauptmann, M., et al. (2007). A functional genetic approach identifies the PI3K pathway as a major determinant of trastuzumab resistance in breast cancer. Cancer Cell *12*, 395–402.

Boone, D.N., Qi, Y., Li, Z., and Hann, S.R. (2011). Egr1 mediates p53-independent c-Myc-induced apoptosis via a noncanonical ARF-dependent transcriptional mechanism. Proc. Natl. Acad. Sci. USA *108*, 632–637.

Brito, D.A., and Rieder, C.L. (2006). Mitotic checkpoint slippage in humans occurs via cyclin B destruction in the presence of an active checkpoint. Curr. Biol. *16*, 1194–1200.

Campone, M., Noël, B., Couriaud, C., Grau, M., Guillemin, Y., Gautier, F., Gouraud, W., Charbonnel, C., Campion, L., Jézéquel, P., et al. (2011). c-Myc dependent expression of pro-apoptotic Bim renders HER2-overexpressing breast cancer cells dependent on anti-apoptotic Mcl-1. Mol. Cancer *10*, 110.

Conacci-Sorrell, M., McFerrin, L., and Eisenman, R.N. (2014). An overview of MYC and its interactome. Cold Spring Harb Perspect Med *4*, a014357.

den Hollander, J., Rimpi, S., Doherty, J.R., Rudelius, M., Buck, A., Hoellein, A., Kremer, M., Graf, N., Scheerer, M., Hall, M.A., et al. (2010). Aurora kinases A and B are up-regulated by Myc and are essential for maintenance of the malignant state. Blood *116*, 1498–1505.

Díaz-Martínez, L.A., Karamysheva, Z.N., Warrington, R., Li, B., Wei, S., Xie, X.J., Roth, M.G., and Yu, H. (2014). Genome-wide siRNA screen reveals coupling between mitotic apoptosis and adaptation. EMBO J. *33*, 1960–1976.

Dumontet, C., and Jordan, M.A. (2010). Microtubule-binding agents: a dynamic field of cancer therapeutics. Nat. Rev. Drug Discov. *9*, 790–803.

Egle, A., Harris, A.W., Bouillet, P., and Cory, S. (2004). Bim is a suppressor of Myc-induced mouse B cell leukemia. Proc. Natl. Acad. Sci. USA *101*, 6164–6169.

Eichhorn, J.M., Alford, S.E., Sakurikar, N., and Chambers, T.C. (2014). Molecular analysis of functional redundancy among anti-apoptotic Bcl-2 proteins and its role in cancer cell survival. Exp. Cell Res. *322*, 415–424.

Eick, D., and Bornkamm, G.W. (1986). Transcriptional arrest within the first exon is a fast control mechanism in c-myc gene expression. Nucleic Acids Res. *14*, 8331–8346.

Eilers, M., and Eisenman, R.N. (2008). Myc's broad reach. Genes Dev. *22*, 2755–2766.

Eischen, C.M., Woo, D., Roussel, M.F., and Cleveland, J.L. (2001). Apoptosis triggered by Myc-induced suppression of Bcl-X(L) or Bcl-2 is bypassed during lymphomagenesis. Mol. Cell. Biol. *21*, 5063–5070.

Filippakopoulos, P., Qi, J., Picaud, S., Shen, Y., Smith, W.B., Fedorov, O., Morse, E.M., Keates, T., Hickman, T.T., Felletar, I., et al. (2010). Selective inhibition of BET bromodomains. Nature *468*, 1067–1073.

Garnett, M.J., Edelman, E.J., Heidorn, S.J., Greenman, C.D., Dastur, A., Lau, K.W., Greninger, P., Thompson, I.R., Luo, X., Soares, J., et al. (2012). Systematic identification of genomic markers of drug sensitivity in cancer cells. Nature *483*, 570–575.

Gascoigne, K.E., and Taylor, S.S. (2008). Cancer cells display profound intra- and interline variation following prolonged exposure to antimitotic drugs. Cancer Cell *14*, 111–122.

Gascoigne, K.E., and Taylor, S.S. (2009). How do anti-mitotic drugs kill cancer cells? J. Cell Sci. *122*, 2579–2585.

Glück, S., Ross, J.S., Royce, M., McKenna, E.F., Jr., Perou, C.M., Avisar, E., and Wu, L. (2012). TP53 genomics predict higher clinical and pathologic tumor response in operable early-stage breast cancer treated with docetaxel-capecitabine ± trastuzumab. Breast Cancer Res. Treat. *132*, 781–791.

Goga, A., Yang, D., Tward, A.D., Morgan, D.O., and Bishop, J.M. (2007). Inhibition of CDK1 as a potential therapy for tumors over-expressing MYC. Nat. Med. *13*, 820–827.

Hann, S.R. (2014). MYC cofactors: molecular switches controlling diverse biological outcomes. Cold Spring Harb Perspect Med *4*, a014399.

Harley, M.E., Allan, L.A., Sanderson, H.S., and Clarke, P.R. (2010). Phosphorylation of Mcl-1 by CDK1-cyclin B1 initiates its Cdc20-dependent destruction during mitotic arrest. EMBO J. *29*, 2407–2420.

Hayashi, M.T., Cesare, A.J., Fitzpatrick, J.A.J., Lazzerini-Denchi, E., and Karlseder, J. (2012). A telomere-dependent DNA damage checkpoint induced by prolonged mitotic arrest. Nat. Struct. Mol. Biol. *19*, 387–394.

Hemann, M.T., Bric, A., Teruya-Feldstein, J., Herbst, A., Nilsson, J.A., Cordon-Cardo, C., Cleveland, J.L., Tansey, W.P., and Lowe, S.W. (2005). Evasion of the p53 tumour surveillance network by tumour-derived MYC mutants. Nature *436*, 807–811.

Horiuchi, D., Kusdra, L., Huskey, N.E., Chandriani, S., Lenburg, M.E., Gonzalez-Angulo, A.M., Creasman, K.J., Bazarov, A.V., Smyth, J.W., Davis, S.E., et al. (2012). MYC pathway activation in triple-negative breast cancer is synthetic lethal with CDK inhibition. J. Exp. Med. *209*, 679–696.

Huang, H.C., Mitchison, T.J., and Shi, J. (2010). Stochastic competition between mechanistically independent slippage and death pathways determines cell fate during mitotic arrest. PLoS ONE *5*, e15724.

Iaccarino, I., Hancock, D., Evan, G., and Downward, J. (2003). c-Myc induces cytochrome c release in Rat1 fibroblasts by increasing outer mitochondrial membrane permeability in a Bid-dependent manner. Cell Death Differ. *10*, 599–608.

Iba, T., Kigawa, J., Kanamori, Y., Itamochi, H., Oishi, T., Simada, M., Uegaki, K., Naniwa, J., and Terakawa, N. (2004). Expression of the c-myc gene as a predictor of chemotherapy response and a prognostic factor in patients with ovarian cancer. Cancer Sci. *95*, 418–423.

Janssen, A., van der Burg, M., Szuhai, K., Kops, G.J., and Medema, R.H. (2011). Chromosome segregation errors as a cause of DNA damage and structural chromosome aberrations. Science *333*, 1895–1898.

Keen, N., and Taylor, S. (2009). Mitotic drivers—inhibitors of the Aurora B Kinase. Cancer Metastasis Rev. *28*, 185–195.

Kessler, J.D., Kahle, K.T., Sun, T., Meerbrey, K.L., Schlabach, M.R., Schmitt, E.M., Skinner, S.O., Xu, Q., Li, M.Z., Hartman, Z.C., et al. (2012). A

SUMOylation-dependent transcriptional subprogram is required for Myc-driven tumorigenesis. Science *335*, 348–353.

Komlodi-Pasztor, E., Sackett, D.L., and Fojo, A.T. (2012). Inhibitors targeting mitosis: tales of how great drugs against a promising target were brought down by a flawed rationale. Clin. Cancer Res. *18*, 51–63.

Lara-Gonzalez, P., Westhorpe, F.G., and Taylor, S.S. (2012). The spindle assembly checkpoint. Curr. Biol. *22*, R966–R980.

Lessene, G., Czabotar, P.E., Sleebs, B.E., Zobel, K., Lowes, K.N., Adams, J.M., Baell, J.B., Colman, P.M., Deshayes, K., Fairbrother, W.J., et al. (2013). Structure-guided design of a selective BCL-X(L) inhibitor. Nat. Chem. Biol. *9*, 390–397.

Li, Q., and Dang, C.V. (1999). c-Myc overexpression uncouples DNA replication from mitosis. Mol. Cell. Biol. *19*, 5339–5351.

Lowe, S.W., Cepero, E., and Evan, G. (2004). Intrinsic tumour suppression. Nature *432*, 307–315.

McKeown, M.R., and Bradner, J.E. (2014). Therapeutic strategies to inhibit MYC. Cold Spring Harb Perspect Med *4*, a014266.

McMahon, S.B. (2014). MYC and the control of apoptosis. Cold Spring Harb Perspect Med *4*, a014407.

Minn, A.J., Boise, L.H., and Thompson, C.B. (1996). Expression of Bcl-xL and loss of p53 can cooperate to overcome a cell cycle checkpoint induced by mitotic spindle damage. Genes Dev. *10*, 2621–2631.

Mitchison, T.J. (2012). The proliferation rate paradox in antimitotic chemotherapy. Mol. Biol. Cell *23*, 1–6.

Murray, S., Briasoulis, E., Linardou, H., Bafaloukos, D., and Papadimitriou, C. (2012). Taxane resistance in breast cancer: mechanisms, predictive biomarkers and circumvention strategies. Cancer Treat. Rev. *38*, 890–903.

Muthalagu, N., Junttila, M.R., Wiese, K.E., Wolf, E., Morton, J., Bauer, B., Evan, G.I., Eilers, M., and Murphy, D.J. (2014). BIM is the primary mediator of MYC-induced apoptosis in multiple solid tissues. Cell Rep. *8*, 1347–1353.

Nagase, H., Fukuyama, H., Tanaka, M., Kawane, K., and Nagata, S. (2003). Mutually regulated expression of caspase-activated DNase and its inhibitor for apoptotic DNA fragmentation. Cell Death Differ. *10*, 142–143.

Nikiforov, M.A., Riblett, M., Tang, W.H., Gratchouck, V., Zhuang, D., Fernandez, Y., Verhaegen, M., Varambally, S., Chinnaiyan, A.M., Jakubowiak, A.J., and Soengas, M.S. (2007). Tumor cell-selective regulation of NOXA by c-MYC in response to proteasome inhibition. Proc. Natl. Acad. Sci. USA *104*, 19488–19493.

Orth, J.D., Loewer, A., Lahav, G., and Mitchison, T.J. (2012). Prolonged mitotic arrest triggers partial activation of apoptosis, resulting in DNA damage and p53 induction. Mol. Biol. Cell *23*, 567–576.

Pelengaris, S., Khan, M., and Evan, G.I. (2002). Suppression of Myc-induced apoptosis in beta cells exposes multiple oncogenic properties of Myc and triggers carcinogenic progression. Cell *109*, 321–334.

Phesse, T.J., Myant, K.B., Cole, A.M., Ridgway, R.A., Pearson, H., Muncan, V., van den Brink, G.R., Vousden, K.H., Sears, R., Vassilev, L.T., et al. (2014). Endogenous c-Myc is essential for p53-induced apoptosis in response to DNA damage in vivo. Cell Death Differ. *21*, 956–966.

Radulescu, S., Ridgway, R.A., Appleton, P., Kroboth, K., Patel, S., Woodgett, J., Taylor, S., Nathke, I.S., and Sansom, O.J. (2010). Defining the role of APC in the mitotic spindle checkpoint in vivo: APC-deficient cells are resistant to Taxol. Oncogene *29*, 6418–6427.

Rieder, C.L., and Maiato, H. (2004). Stuck in division or passing through: what happens when cells cannot satisfy the spindle assembly checkpoint. Dev. Cell *7*, 637–651.

Shi, J., Zhou, Y., Huang, H.C., and Mitchison, T.J. (2011). Navitoclax (ABT-263) accelerates apoptosis during drug-induced mitotic arrest by antagonizing Bcl-xL. Cancer Res. *71*, 4518–4526.

Silk, A.D., Zasadil, L.M., Holland, A.J., Vitre, B., Cleveland, D.W., and Weaver, B.A. (2013). Chromosome missegregation rate predicts whether aneuploidy will promote or suppress tumors. Proc. Natl. Acad. Sci. USA *110*, E4134–E4141.

Slamon, D.J., Leyland-Jones, B., Shak, S., Fuchs, H., Paton, V., Bajamonde, A., Fleming, T., Eiermann, W., Wolter, J., Pegram, M., et al. (2001). Use of chemotherapy plus a monoclonal antibody against HER2 for metastatic breast cancer that overexpresses HER2. N. Engl. J. Med. *344*, 783–792.

Sodir, N.M., and Evan, G.I. (2011). Finding cancer's weakest link. Oncotarget *2*, 1307–1313.

Soucek, L., Jucker, R., Panacchia, L., Ricordy, R., Tatò, F., and Nasi, S. (2002). Omomyc, a potential Myc dominant negative, enhances Myc-induced apoptosis. Cancer Res. *62*, 3507–3510.

Tang, Y.C., and Amon, A. (2013). Gene copy-number alterations: a cost-benefit analysis. Cell *152*, 394–405.

Taylor, S.S., and McKeon, F. (1997). Kinetochore localization of murine Bub1 is required for normal mitotic timing and checkpoint response to spindle damage. Cell *89*, 727–735.

Thompson, S.L., and Compton, D.A. (2010). Proliferation of aneuploid human cells is limited by a p53-dependent mechanism. J. Cell Biol. *188*, 369–381.

Topham, C.H., and Taylor, S.S. (2013). Mitosis and apoptosis: how is the balance set? Curr. Opin. Cell Biol. *25*, 780–785.

Upreti, M., Galitovskaya, E.N., Chu, R., Tackett, A.J., Terrano, D.T., Granell, S., and Chambers, T.C. (2008). Identification of the major phosphorylation site in Bcl-xL induced by microtubule inhibitors and analysis of its functional significance. J. Biol. Chem. *283*, 35517–35525.

Weaver, B.A. (2014). How Taxol/paclitaxel kills cancer cells. Mol. Biol. Cell *25*, 2677–2681.

Wiese, K.E., Walz, S., von Eyss, B., Wolf, E., Athineos, D., Sansom, O., and Eilers, M. (2013). The role of MIZ-1 in MYC-dependent tumorigenesis. Cold Spring Harb Perspect Med *3*, a014290.

Wirth, M., Stojanovic, N., Christian, J., Paul, M.C., Stauber, R.H., Schmid, R.M., Häcker, G., Krämer, O.H., Saur, D., and Schneider, G. (2014). MYC and EGR1 synergize to trigger tumor cell death by controlling NOXA and BIM transcription upon treatment with the proteasome inhibitor bortezomib. Nucleic Acids Res. *42*, 10433–10447.

Wolf, E., Lin, C.Y., Eilers, M., and Levens, D.L. (2015). Taming of the beast: shaping Myc-dependent amplification. Trends Cell Biol. *25*, 241–248.

Wong, M., Tan, N., Zha, J., Peale, F.V., Yue, P., Fairbrother, W.J., and Belmont, L.D. (2012). Navitoclax (ABT-263) reduces Bcl-x(L)-mediated chemoresistance in ovarian cancer models. Mol. Cancer Ther. *11*, 1026–1035.

Yang, D., Liu, H., Goga, A., Kim, S., Yuneva, M., and Bishop, J.M. (2010). Therapeutic potential of a synthetic lethal interaction between the MYC proto-oncogene and inhibition of aurora-B kinase. Proc. Natl. Acad. Sci. USA *107*, 13836–13841.

Zasadil, L.M., Andersen, K.A., Yeum, D., Rocque, G.B., Wilke, L.G., Tevaarwerk, A.J., Raines, R.T., Burkard, M.E., and Weaver, B.A. (2014). Cytotoxicity of paclitaxel in breast cancer is due to chromosome missegregation on multipolar spindles. Sci. Transl. Med. *6*, 229–243.

8.3 Appendix 3

Bennett, A., Sloss, O., Topham, C., Nelson, L., Tighe, A., Taylor, S.S.
Inhibition of Bcl-xL sensitizes cells to mitotic blockers, but not mitotic drivers
2016, Open Biology

OPEN BIOLOGY

rsob.royalsocietypublishing.org

Research

Cite this article: Bennett A, Sloss O, Topham C, Nelson L, Tighe A, Taylor SS. 2016 Inhibition of Bcl-xL sensitizes cells to mitotic blockers, but not mitotic drivers. *Open Biol.* **6**: 160134. http://dx.doi.org/10.1098/rsob.160134

Received: 3 May 2016
Accepted: 8 July 2016

Subject Area:
cellular biology

Keywords:
apoptosis, spindle checkpoint, paclitaxel, taxol, WEHI-539

Author for correspondence:
Stephen S. Taylor
e-mail: stephen.taylor@manchester.ac.uk

†Present address: School of Environment and Life Sciences, University of Salford, Salford M5 4WT, UK.

Electronic supplementary material is available at http://dx.doi.org/10.1098/rsob.160134.

THE ROYAL SOCIETY PUBLISHING

Inhibition of Bcl-xL sensitizes cells to mitotic blockers, but not mitotic drivers

Ailsa Bennett, Olivia Sloss, Caroline Topham†, Louisa Nelson, Anthony Tighe and Stephen S. Taylor

Manchester Cancer Research Centre, University of Manchester, Wilmslow Road, Manchester M20 4QL, UK

SST, 0000-0003-4621-9326

Cell fate in response to an aberrant mitosis is governed by two competing networks: the spindle assembly checkpoint (SAC) and the intrinsic apoptosis pathway. The mechanistic interplay between these two networks is obscured by functional redundancy and the ability of cells to die either in mitosis or in the subsequent interphase. By coupling time-lapse microscopy with selective pharmacological agents, we systematically probe pro-survival Bcl-xL in response to various mitotic perturbations. Concentration matrices show that BH3-mimetic-mediated inhibition of Bcl-xL synergises with perturbations that induce an SAC-mediated mitotic block, including drugs that dampen microtubule dynamics, and inhibitors targeting kinesins and kinases required for spindle assembly. By contrast, Bcl-xL inhibition does not synergize with drugs which drive cells through an aberrant mitosis by overriding the SAC. This differential effect, which is explained by compensatory Mcl-1 function, provides opportunities for patient stratification and combination treatments in the context of cancer chemotherapy.

1. Introduction

Antimitotic agents including the taxanes and vinca alkaloids are used extensively to treat numerous malignancies, including ovarian and breast cancer as well as various leukaemias [1]. Patient responses are, however, unpredictable; some cancers are intrinsically resistant and others acquire resistance. In addition, toxicity to the peripheral nervous system can be problematic [2]. To address these limitations, a raft of second-generation antimitotic agents has been developed, including drugs targeting mitotic kinesins and mitotic kinases [3–7]. Effective clinical use of these novel agents will require the development of predictive biomarkers and patient stratification. This in turn will require an in-depth understanding of the molecular mechanisms by which these drugs kill cancer cells. At present, however, our understanding of the mechanisms by which mitotic dysfunction leads to cell death is still in its infancy.

Traditional antimitotic agents and many second-generation drugs are mitotic blockers [4]. By preventing spindle assembly, these drugs chronically activate the spindle assembly checkpoint leading to a prolonged mitotic arrest which eventually leads to cell death, either directly during mitosis or following slippage back into interphase [8]. Death in mitosis (DiM) and post-mitotic death (PMD) both result from activation of the intrinsic apoptotic machinery, which is regulated by pro-apoptotic and anti-apoptotic members of the Bcl-2 family [9–13]. On the pro-apoptotic side, the BH3-only proteins, Bim, Bid, Bad and Noxa, have been shown to contribute to death in mitosis [14–17]. On the anti-apoptotic side, Bcl-xL and Mcl-1 have been shown to be important mitotic survival factors [18–23]. However, the relative importance of any given Bcl-2 family member is complicated by two issues. First, there is considerable functional overlap among both the pro- and anti-apoptotic factors [12,24–26]. Second, whether these proteins act differently during DiM and PMD is often obscured by

population-based approaches that do not distinguish between death in mitosis or following slippage.

Understanding the relative contributions of the various Bcl-2 family members to mitotic cell fate is important from an antimitotic chemotherapy perspective because several pro-survival inhibitors are being evaluated as anti-cancer drugs [27,28]. For example, the BH3 mimetic compound class comprises several molecules that dock into a hydrophobic groove of pro-survival Bcl-2 family proteins, thereby preventing binding of their pro-apoptotic BH3-only partners [29]. Frontrunners in this class include ABT-737 and ABT-263/Navitoclax, related molecules that both inhibit three Bcl-2 family members, namely Bcl-2, Bcl-xL and Bcl-w. Notably, Navitoclax accelerates apoptosis during mitotic arrest induced by either taxol or inhibitors targeting the Eg5 kinesin [21]. In addition, exposing the slippage-prone MDA-MB-231 breast cancer cell line to ABT-737 induces death in mitosis [18]. In these cases, suppressing Bcl-xL using RNAi phenocopied the BH3 mimetic, indicating that Bcl-xL plays an important pro-survival role during a prolonged mitotic arrest.

More recently, novel BH3 mimetics have been developed with enhanced specificity for individual pro-survival Bcl-2 family members, including ABT-199 (which targets Bcl-2 itself) [30], A-1210477 (which targets Mcl-1) [31], and WEHI-539 [32] plus a related compound, A-1155643 [33], both of which target Bcl-xL. A-1155643 enhances the efficacy of docetaxel *in vitro* and in mouse xenograft models [31], further supporting the notion that Bcl-xL resists apoptosis during a prolonged mitotic arrest. However, we recently showed that WEHI-539 induces post-mitotic apoptosis when RKO cells are treated with a low concentration of taxol [12], indicating that Bcl-xL also supports survival following an abnormal mitosis. Therefore, to further explore the role of Bcl-xL in the context of mitotic perturbations, we set out to determine the relative contribution of Bcl-xL to survival following exposure to various antimitotic agents, including mitotic blockers and drivers [4,34]. Moreover, to determine Bcl-xL's role during a prolonged mitotic arrest, following slippage and following an abnormal mitosis, we used single-cell time-lapse imaging to directly correlate mitotic behavior with subsequent cell fate [8].

2. Results

2.1. Validation of WEHI-539 as an effective Bcl-xL inhibitor

WEHI-539 was recently described as a potent and selective Bcl-xL inhibitor [32]. As a BH3 mimetic, it docks into a hydrophobic groove of Bcl-xL, thereby blocking the binding of Bcl-xL's BH3-only partner proteins. To assess WEHI-539 as a research tool in our experimental systems, we first performed four validation experiments. For each we used RKO colon cancer cells in which there is substantial functional overlap between Bcl-xL and Mcl-1: while inhibition of either in isolation has little impact, inhibiting both is sufficient to induce apoptosis in the absence of cytotoxic insult [12] (see the electronic supplementary material, figure S1*a*). To measure apoptosis, we used time-lapse imaging and cell fate profiling in conjunction with a fluorescent caspase 3/7 reporter [8,12]. First, we reasoned that if WEHI-539 is selective for Bcl-xL over Mcl-1, then it should only induce apoptosis in RKO cells in the absence of Mcl-1. Indeed, while WEHI-539 alone was relatively benign up to concentrations of 5 μM (electronic supplementary material, figure S1*a*), following Mcl-1 RNAi, 100 nM was sufficient to induce extensive apoptosis (figure 1*a*; electronic supplementary material, figure S1*a*).

Bcl-xL sequesters multiple BH3-only proteins, including the apoptosis activator Bim which is involved in taxol sensitivity [12,35,36]. Secondly, therefore, we asked whether WEHI-539 exacerbated the ability of a tet-responsive Bim transgene to induce apoptosis (electronic supplementary material, figure S1*b*). Indeed, while induction of Bim with 30 ng ml^{-1} tetracycline only induced moderate apoptosis, 100 nM WEHI-539 substantially enhanced the effect (figure 1*b*). Note that Bim overexpressing cells exposed to WEHI-539 typically died very shortly after mitosis (electronic supplementary material, figure S1*b*), an issue we return to in the Discussion.

Thirdly, we asked whether WEHI-539 blocked the binding of Bcl-xL to its partner BH3-only proteins. Indeed, when we affinity-purified GFP-tagged Bcl-xL in the presence of 100 nM WEHI-539, levels of co-purifying Bim, Bad, Bax and Bak were all reduced (figure 1*c*; electronic supplementary material, figure S1*c*). And finally, because overexpression of a tet-responsive Bcl-xL transgene potently resists taxol-induced apoptosis [12], we asked whether WEHI-539 reversed this effect. Indeed, while induction of Myc-tagged Bcl-xL with 100 ng ml^{-1} tetracycline completely blocked taxol-induced apoptosis, this was reversed by 100 nM WEHI-539 (figure 1*d*; electronic supplementary material, figure S1*d*). Thus, these observations confirm that WEHI-539 behaves as one would expect for a potent and selective Bcl-xL inhibitor.

Because we previously showed that Bcl-xL overexpression resists apoptosis both in mitosis and following slippage [12], we were interested to determine whether the effect of WEHI-539 in the context of Bcl-xL overexpression was via restoration of DiM or PMD. Cell fate profiling showed that in the presence of taxol, 86% of RKO cells underwent DiM and only 14% slipped (figure 1*e*). Every cell that slipped then underwent PMD, with an average of 18.5 h between mitotic exit and death. Consistent with our prior observations [12], overexpression of Bcl-xL dramatically shifted the balance from DiM to slippage, with 94% undergoing slippage. Of these, only 6% underwent PMD, with an average onset time of 26 h. Interestingly, while 50 and 100 nM WEHI-539 only marginally reversed the balance back towards DiM, these concentrations had a major impact on PMD, increasing both the frequency and accelerating its onset (figure 1*e*). By contrast, 500 nM WEHI-539 completely shifted the balance back in favour of DiM. Thus, these observations confirm that Bcl-xL is a potent pro-survival factor both during a prolonged mitotic arrest and following slippage.

2.2. WEHI-539 sensitizes cells to microtubule-binding agents

Having validated WEHI-539 as a valuable research tool to probe Bcl-xL function in the context of mitotic cell fate, we set out to determine whether it sensitized cancer cells to various mitotic blockers, initially focusing on the microtubule-binding agents taxol and nocodazole. RKO cells were exposed to a matrix of increasing drug concentrations, then caspase 3/7

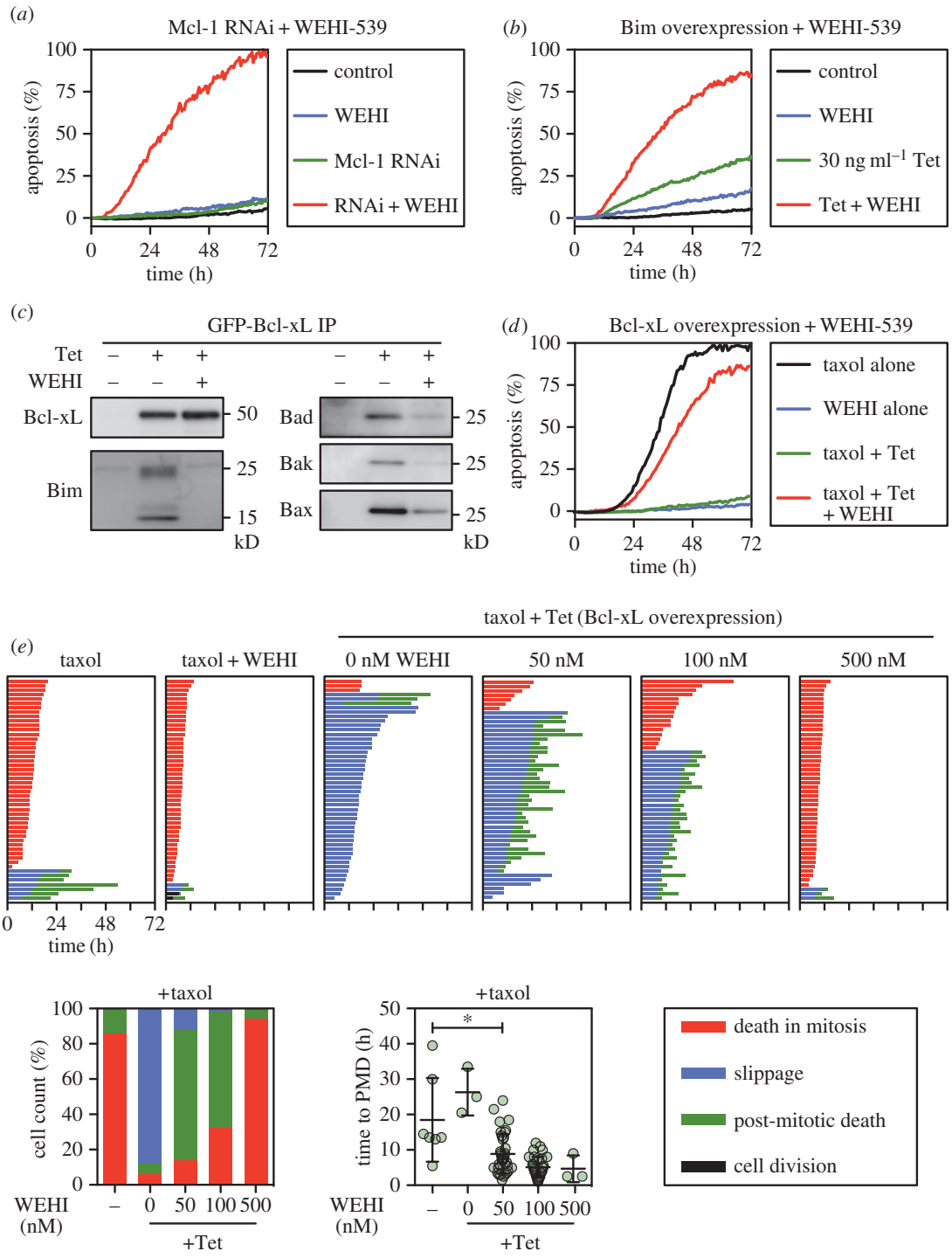

Figure 1. Validation of WEHI-539 as an effective Bcl-xL inhibitor. (*a*) Line graph showing apoptosis induction over a 72 h time course after RKO cells were transfected with siRNAs targeting Mcl-1 for 24 h before exposure to 100 nM WEHI-539. (*b*) Line graph showing apoptosis induction following expression of Bim with 30 ng ml^{-1} tetracycline (Tet) and exposure to 100 nM WEHI-539. (*c*) Immunoblots showing affinity purification of GFP-tagged Bcl-xL induced with 100 ng ml^{-1} tetracycline in the presence and absence of 100 nM WEHI-539, and detection of co-purifying Bim, Bad, Bak and Bax. Note that 100 nM WEHI-539 diminishes binding of pro-apoptotic proteins. (*d*) Line graph showing apoptosis induction by 100 nM taxol, suppression by the induction of Myc-tagged Bcl-xL, and restoration by 100 nM WEHI-539. (*e*) Cell fate profiles of RKO cells exposed to 100 nM taxol following induction of Myc-tagged Bcl-xL and exposure to increasing concentrations of WEHI-539. The number of cells undergoing death in mitosis (red), slippage (blue) and PMD (green) is quantitated in the bar graph. For the cells that undergo PMD, the scatter plot shows the time from mitotic exit to death. *$p < 0.05$. Zero hours on the fate profiles represents when cells entered mitosis.

activation measured by time-lapse imaging over a 72 h time course (figure 2*a*). As shown above, WEHI-539 alone was relatively benign but, as anticipated, taxol and nocodazole induced apoptosis in dose-dependent manners. Importantly, the matrix approach readily identified concentrations where the combination dramatically enhanced apoptosis. Specifically, while 10 nM taxol and 20 ng ml^{-1} nocodazole only induced apoptosis to 46% and 23% of the maximum, respectively, inclusion of 100 nM WEHI-539 induced near-maximal cell death (figure 2*b*). At these relatively low concentrations of antimitotic drug, while many RKO cells underwent DiM, rather than slipping the remainder eventually completed cell division (figure 2*c*). In taxol, some of the dividers underwent PMD but in nocodazole they all arrested in the next

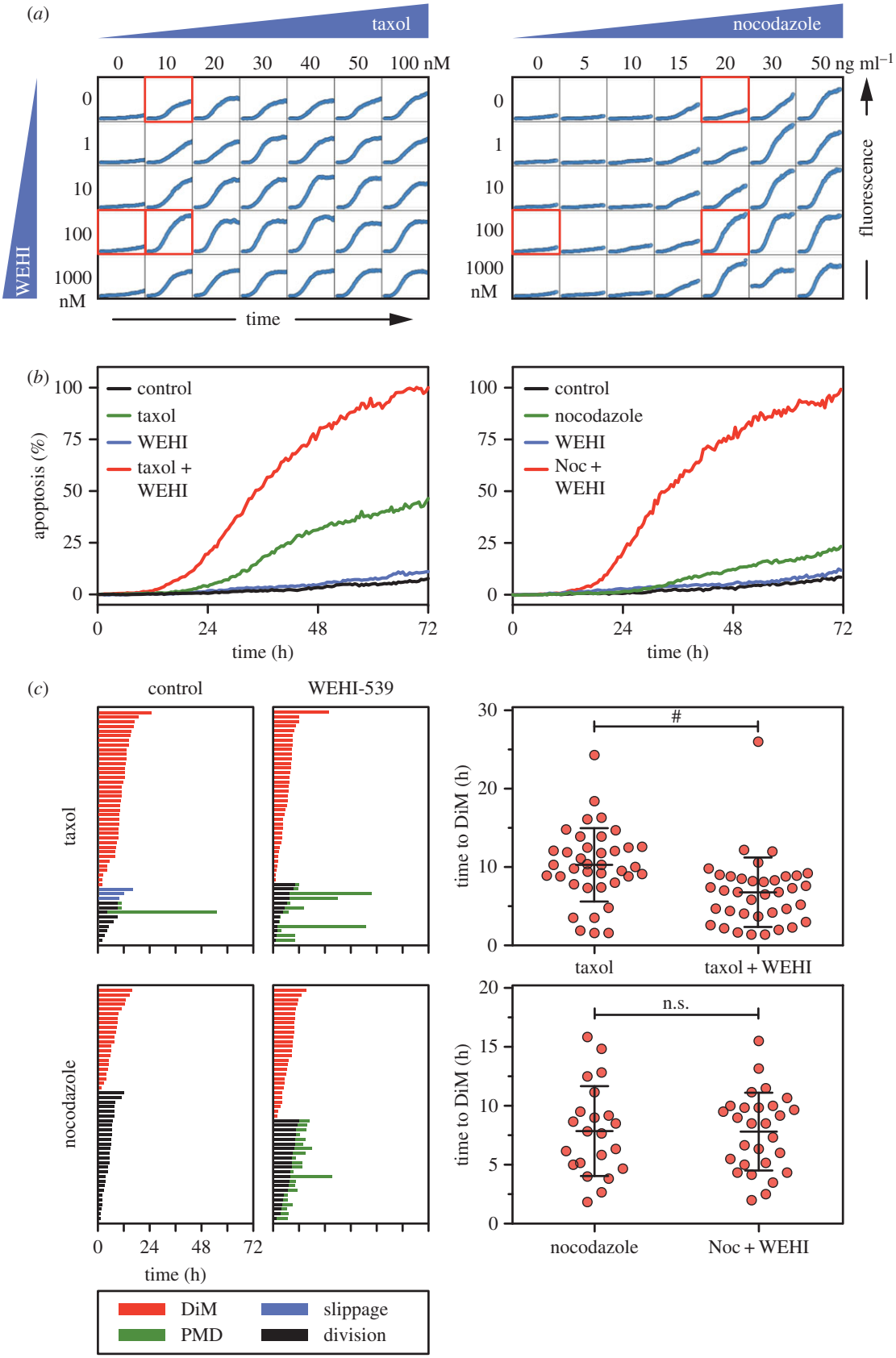

Figure 2. WEHI-539 sensitizes cells to microtubule-binding agents. (*a*) Concentration matrices showing apoptosis induction over a 72 h time course following exposure of RKO cells to either taxol or nocodazole and WEHI-539. (*b*) Line graphs showing apoptosis induction following exposure to 10 nM taxol or 20 ng ml^{-1} nocodazole (Noc) plus 100 nM WEHI-539. (*c*) Cell fate profiles of cells as treated in (*b*). For those cells undergoing death in mitosis, the scatter plots quantitate the time from mitotic entry to cell death. $^{\#}p < 0.0001$. Zero hours on the fate profiles represents when cells entered mitosis.

interphase. Interestingly, the mechanism by which WEHI-539 enhanced apoptosis differed between the two mitotic blockers. In taxol, WEHI-539 had two effects, accelerating DiM by approximately 3.5 h and increasing the frequency of PMD (figure 2*c*). By contrast, WEHI-539 did not accelerate DiM in nocodazole-treated cells but rather induced PMD in every cell that divided. Nevertheless, despite these differences, these observations build on prior reports [37], and

clearly demonstrate that pharmacological inhibition of Bcl-xL sensitizes cells to microtubule-binding agents.

2.3. WEHI-539 sensitizes cells to second-generation mitotic blockers

Like the microtubule-binding agents, several second-generation antimitotic drugs also block mitotic progression by disrupting spindle assembly [3,4]. These include inhibitors targeting mitotic kinesins, such as Eg5 and Cenp-E, and mitotic kinases such as Plk1. We therefore asked whether pharmacological inhibition of Bcl-xL also sensitized cells to agents targeting these mitotic regulators, focusing on the Eg5 inhibitor AZ138 [8], the Plk1 inhibitor BI 2536 [38] and the Cenp-E inhibitor GSK923295 [39]. As above, RKO cells were analysed following exposure to a matrix of increasing drug concentrations, which again readily identified combinatorial concentrations that enhanced apoptosis (electronic supplementary material, figure S2*a*). To define this phenomenon in more detail, we performed cell fate profiling at concentrations where the enhancement of apoptosis was particularly marked.

In the case of the Eg5 inhibitor, sensitivity to 200 nM AZ138 was enhanced by 100 nM WEHI-539 (figure 3*a*). Note however that 1 µM AZ138 is typically required to induce a potent mitotic block [8]. Indeed, at 200 nM, while 54% underwent DiM and 6% slipped, 40% eventually divided (figure 3*b*). As above with nocodazole, these dividers never entered another mitosis, suggesting cell cycle arrest. Notably, in the presence of 100 nM WEHI-549, 68% of the dividers underwent apoptosis (figure 3*b*). Thus, Bcl-xL inhibition sensitizes RKO cells to Eg5 inhibition by enhancing PMD rather than DiM. The ability of WEHI-539 to enhance apoptosis was particularly striking in the case of the Plk1 inhibitor BI 2536; whereas 50 nM alone only induced 21% apoptosis, 100 nM WEHI-539 increased this to 70% (figure 3*a*). As with nocodazole and the Eg5 inhibitor, WEHI-539 did not significantly accelerate the time to DiM but rather induced PMD following slippage or cell division (figure 3*b*,*c*). As above, at the relatively low concentration of 50 nM BI 2536, a substantial proportion of cells eventually divided (figure 3*b*). Therefore, we asked what happened at higher concentrations of BI 2536, which induced a potent cell division block. At 500 nM, the majority of cells underwent DiM or PMD after slippage (electronic supplementary material, figure S2*b*). Of those cells that slipped, 78% of cells underwent PMD after an average of 9.1 h (figure 3*d*). When 100 nM WEHI-539 was included, PMD was accelerated to 2.4 h (figure 3*d*; electronic supplementary material, figure S3*b*). Note that, paradoxically, at BI 2536 concentrations above 500 nM, apoptosis induction was reduced (electronic supplementary material, figure S2*a*), most probably due to suppression of mitotic entry [40]. Nevertheless, as with the Eg5 inhibitor, WEHI-539 sensitizes RKO cells to Plk1 inhibition largely by enhancing PMD. This phenomenon was strikingly apparent with the Cenp-E inhibitor. At 100 nM GSK923295, 66% of cells eventually divided, 21% of which then underwent PMD after an average of 12.6 h (figure 3*b*–*d*). Upon inclusion of 100 nM WEHI-539, 97% of the dividers underwent PMD after an average 3.6 h. Thus, together with the observations described above, these data demonstrate that inhibiting Bcl-xL can sensitize cells to second-generation mitotic blockers, largely by enhancing post-mitotic cell death.

2.4. WEHI-539 only has a minor impact when combined with mitotic drivers

In contrast to the microtubule-binding agents, several second-generation antimitotic drugs do not trigger a prolonged mitotic arrest, but rather drive cells through an abnormal division [4]. These include drugs targeting Aurora A, Aurora B and Mps1. To determine whether inhibiting Bcl-xL also sensitized cells to these drugs, we analysed WEHI-539 in combination with the Aurora A inhibitor MLN8054 [41], the Aurora B inhibitor ZM447439 [42] and the Mps1 inhibitor AZ3146 [43]. In isolation, all three drugs induced the expected phenotypes; MLN8054 induced a transient mitotic delay followed by cell division, ZM447439 induced a transient delay followed by cytokinesis failure and AZ3146 accelerated mitotic exit (figure 4*a*,*c*). While inhibiting Aurora A or Aurora B alone was not sufficient to induce apoptosis, at least during the 72 h time course, the Mps1 inhibitor induced PMD in 38% of cells (figure 4*c*). Interestingly, the concentration matrices failed to identify combinations where WEHI-539 significantly enhanced apoptosis (not shown). Even at relatively high concentrations of mitotic driver, WEHI-539 had little additional effect especially in the case of the two Aurora kinase inhibitors (figure 4*b*,*c*). WEHI-539 did have a minor effect when combined with Mps1 inhibitor, increasing PMD to 62% and accelerating its onset by 4 h, although this latter difference was not statistically significant (data not shown). Thus, while pharmacological inhibition of Bcl-xL convincingly sensitizes cells to mitotic blockers, it only has a minor effect when combined with mitotic drivers.

To explore this notion further, we used the concentration matrices to perform a Bliss independence analysis [44,45], and represented the data as heat maps with positive Bliss excess values coloured green and negative values red (electronic supplementary material, figure S3). The heat maps for the microtubule toxins AZ138, BI 2536 and GSK923295 are characterized by patches of green (i.e. positive Bliss excess scores). By contrast, the heat maps for MLN8054, ZM447439 and AZ3146 are dominated by negative values, further supporting the notion that inhibiting Bcl-xL has little impact in the context of a mitotic driver. Accordingly, the mitotic blockers all returned high Bliss sum values, while MLN8054 and ZM447439 returned negative Bliss sums (electronic supplementary material, figure S3*b*). AZ3146 gave a positive albeit low Bliss sum, consistent with the observation that it enhances PMD to some extent (figure 4*c*). Thus, this analysis confirms the notion that while pharmacological inhibition of Bcl-xL sensitizes cells to mitotic blockers, this effect is considerably less pronounced when combined with mitotic drivers.

2.5. Overexpression of Mcl-1 suppresses WEHI-539-induced post-mitotic death

To rationalize the differential effect Bcl-xL inhibition had on mitotic blockers versus mitotic drivers, we turned our attention to Mcl-1, a pro-survival factor that is degraded during a prolonged mitotic arrest [46–49] (see the electronic supplementary material, figure S4*b*). We reasoned that if both Mcl-1 and Bcl-xL promote post-mitotic survival, then degradation of Mcl-1 during a prolonged mitotic arrest could account for why cells treated with mitotic blockers become

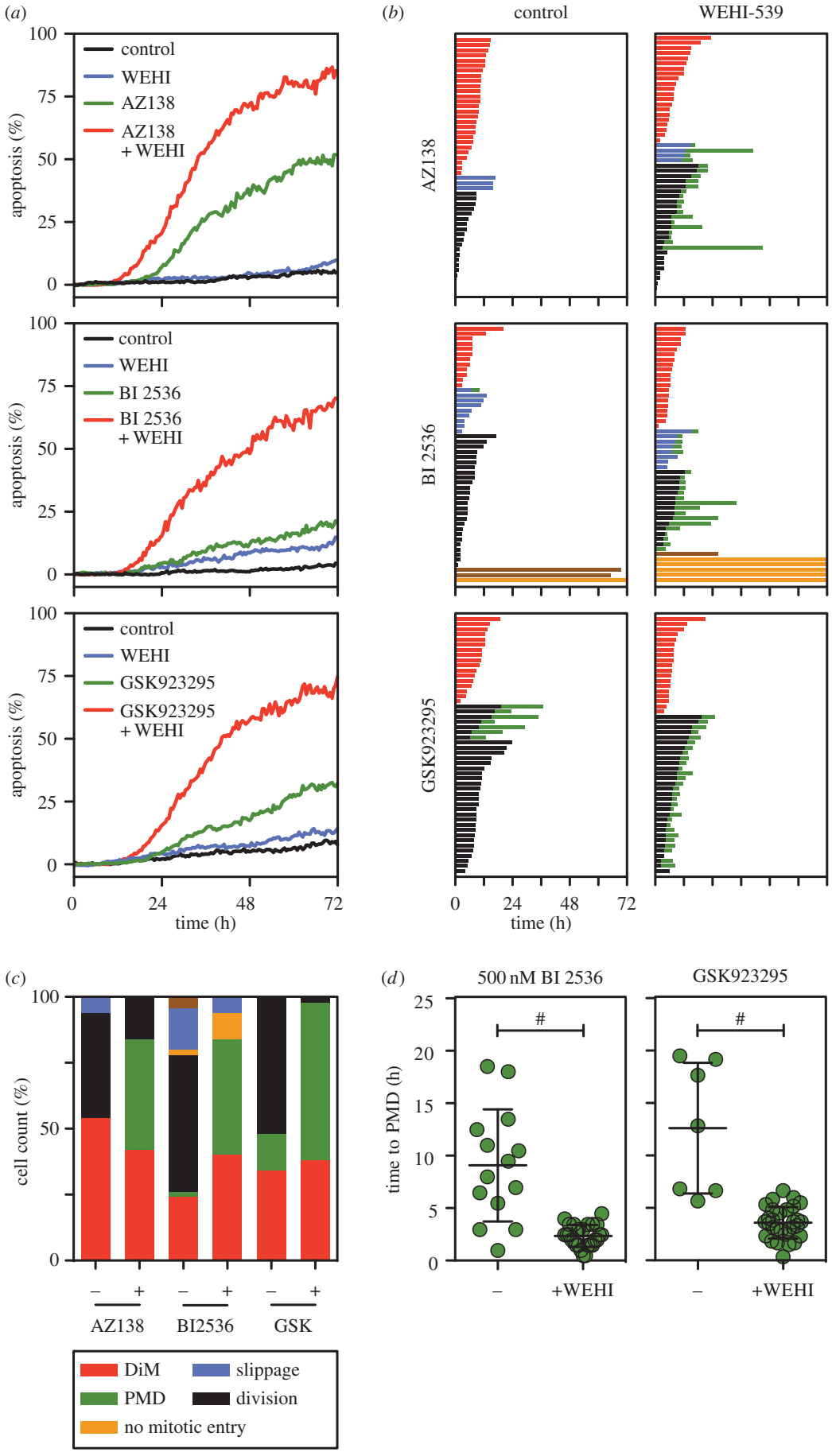

Figure 3. WEHI-539 sensitizes cells to second-generation mitotic blockers. (*a*) Line graphs showing apoptosis induction over a 72 h time course following exposure of RKO cells to 200 nM of the Eg5 inhibitor AZ138, 50 nM of the Plk1 inhibitor BI 2536, and 100 nM of the Cenp-E inhibitor GSK923295, plus 100 nM WEHI-539. (*b*) Cell fate profiles of cells treated as in (*a*). (*c*) Bar graph quantitation of (*b*) showing the number of cells undergoing each fate. (*d*) Scatter plot showing the time from mitotic exit to death for the cells that underwent PMD. Note that in the case of the Plk1 inhibitor, the data in panel (*d*) are derived from 500 nM BI 2536. $^{\#}p < 0.0001$. Zero hours on the fate profiles represents when cells entered mitosis.

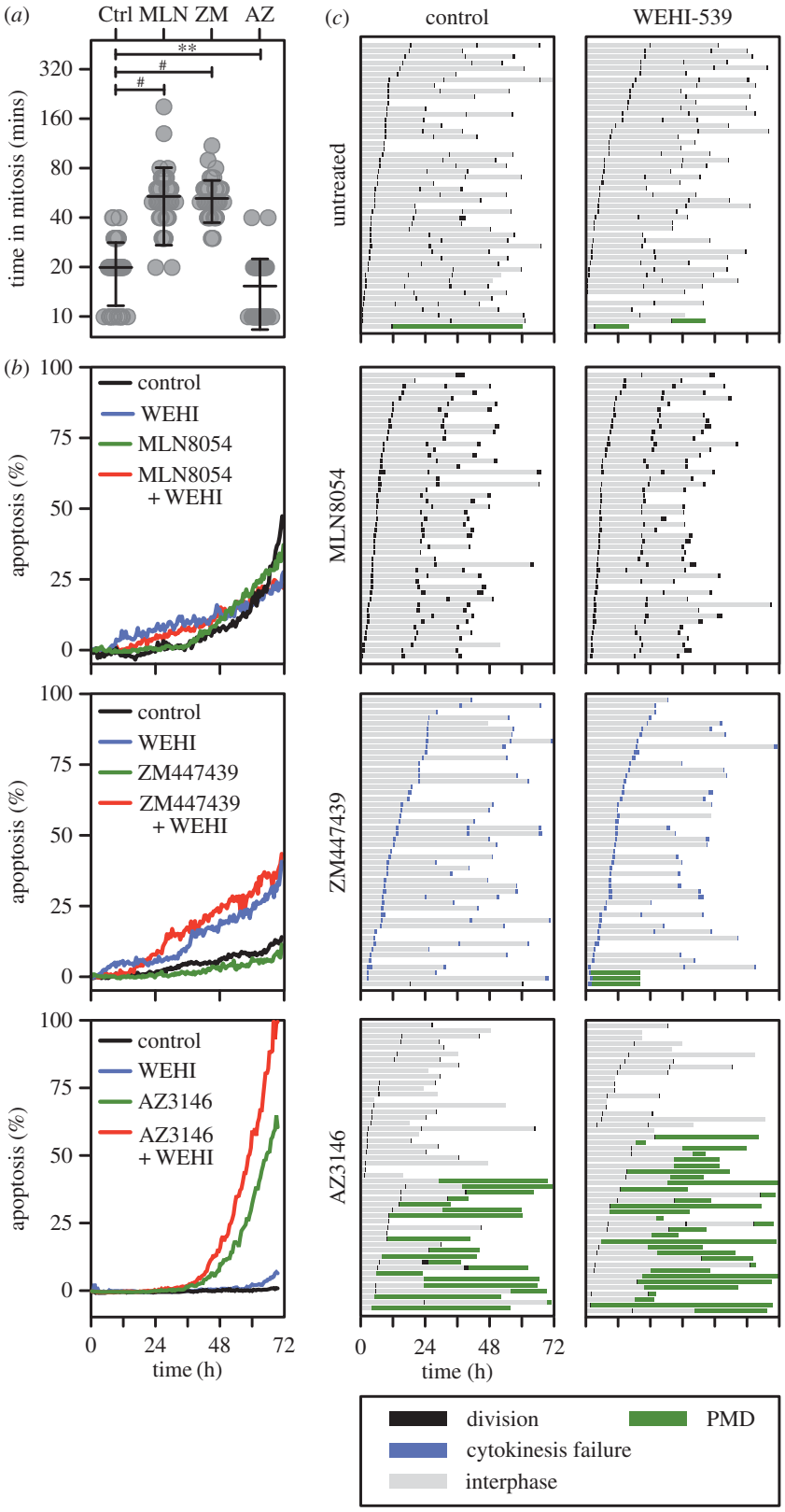

Figure 4. WEHI-539 only has a minor impact when combined with mitotic drivers. (*a*) Scatter plot quantitating the time RKO cells spent in mitosis following exposure to 250 nM of the Aurora A inhibitor MLN8054, 2 µM of the Aurora B inhibitor ZM447439 and 2 µM of the Mps1 inhibitor AZ3146. $^{**}p < 0.01$, $^{\#}p < 0.0001$. (*b*) Line graphs showing apoptosis induction following exposure to the drugs indicated in (*a*) plus 100 nM WEHI-539. (*c*) Cell fate profiles of cells treated as in (*b*). Zero hours on the fate profiles represents when imaging started.

critically dependent on Bcl-xL. Indeed, while Mcl-1 was largely depleted during a nocodazole arrest, its levels remained high in the presence of ZM447439 (electronic supplementary material, figure S4*b*). Therefore, to test this hypothesis further, we modulated Mcl-1 levels in RKO cells and asked whether this altered their sensitivity to combinations of antimitotic agents plus WEHI-539.

First, we generated an RKO cell line expressing a tet-inducible GFP-tagged Mcl-1 transgene in order to overexpress Mcl-1 (electronic supplementary material, figure S4*a*). When uninduced control cells were exposed to 20 ng ml^{-1} of nocodazole, the vast majority of cells arrested for an average of 4 h then divided (figure 5*a*). Of these, only 17% underwent PMD after an average of 32 h. Consistent with observations shown

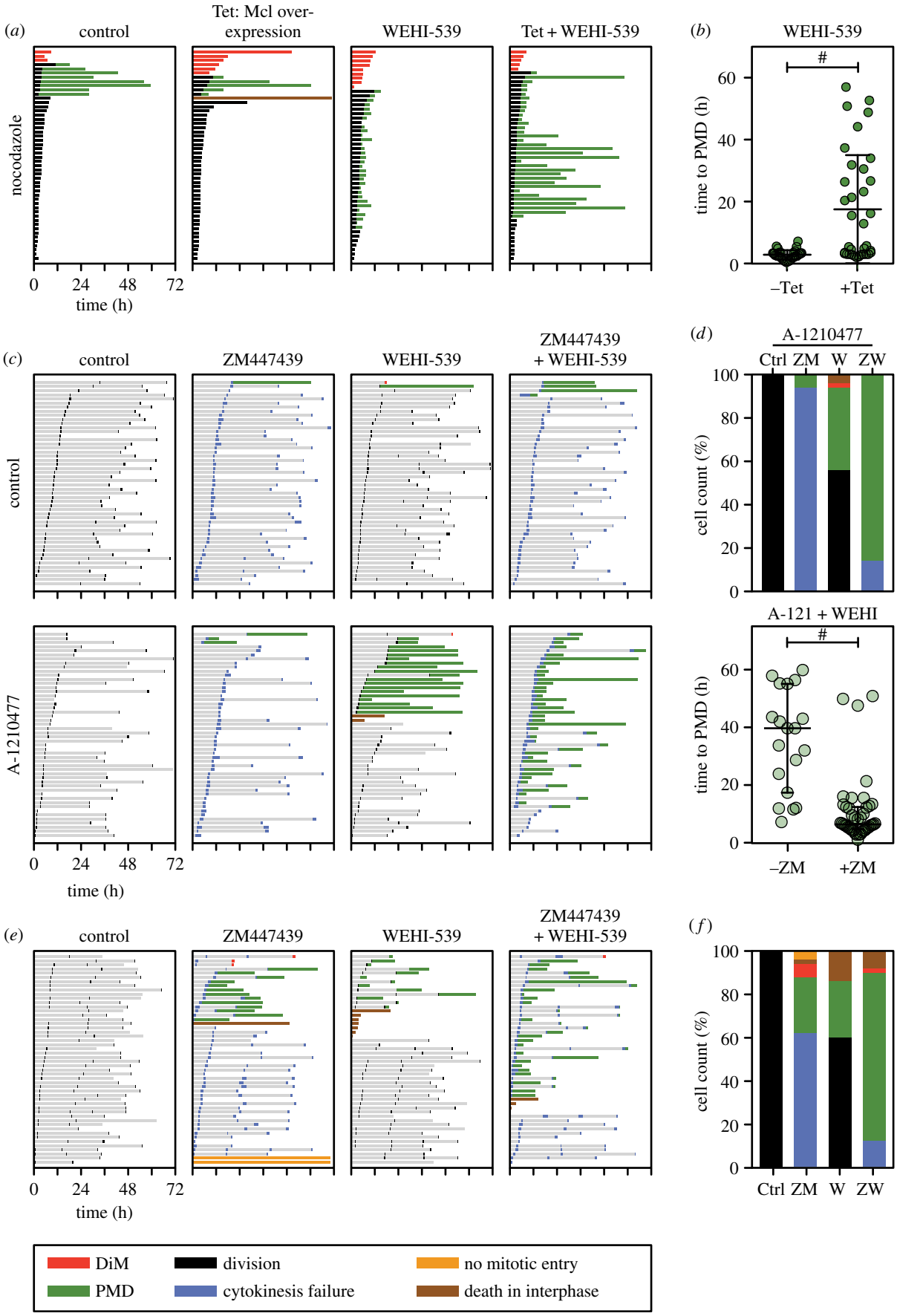

Figure 5. Inhibition of Mcl-1 sensitizes WEHI-539-treated cells to a mitotic driver. (*a*) Cell fate profiles of RKO cells treated with 20 ng ml^{-1} nocodazole and 100 nM WEHI-539 following induction of GFP-tagged Mcl-1 with 1 µg ml^{-1} tetracycline (Tet). (*b*) Scatter plot showing the time from mitotic exit to death for WEHI-539-treated cells in (*a*) that underwent PMD in the presence or the absence of overexpressed Mcl-1. $^{\#}p < 0.0001$. (*c*) Cell fate profiles of RKO cells exposed to 2 µM of the Aurora B inhibitor ZM447439, 100 nM WEHI-539 and 2 µM of the Mcl-1 inhibitor A-1210477. (*d*) Bar graph quantitation of (*c*) showing the number of cells undergoing each fate, and scatter plot quantitating the time from mitotic exit to death for the cells that underwent PMD. $^{\#}p < 0.0001$. (*e*) Cell fate profiles of DLD-1 cells exposed to 2 µM ZM447439 and 100 nM WEHI-539. (*f*) Bar graph quantitation of (*e*) showing the number of cells undergoing each fate. In panel (*a*), zero hours on the fate profiles represents when cells entered mitosis, while in panels (*c*) and (*e*) it corresponds to when imaging started.

in figure 2*c*, 100 nM WEHI-539 induced rapid PMD in the vast majority of dividers (figure 5*a*). Overexpression of Mcl-1 only had a minor impact in the absence of WEHI-539, prolonging time to death in the few cells that underwent DiM. However, Mcl-1 overexpression had a significant impact in the presence of WEHI-539, substantially prolonging the onset of PMD in a subset of the cells, extending the average time to PMD from 2.8 to 17.5 h (figure 5*b*). Thus, elevating Mcl-1 suppresses post-mitotic sensitivity to WEHI-539, consistent with the notion that a prolonged mitotic arrest sensitizes cells to Bcl-xL inhibitors by degrading Mcl-1.

2.6. Inhibition of Mcl-1 sensitizes cells to WEHI-539 plus an Aurora B inhibitor

Next, we suppressed Mcl-1 by RNAi and asked whether this sensitized Bcl-xL-inhibited cells to a mitotic driver. Consistent with the data in figure 4*c*, adding WEHI-539 to the Aurora B inhibitor ZM447439 had little effect. However, when Mcl-1 was suppressed by RNAi, apoptosis was induced in the majority of cells, either during mitosis or following cell division failure (electronic supplementary material, figure S4*c*). However, this experiment is complicated because co-inhibition of Mcl-1 and Bcl-xL in RKO cells is sufficient to induce apoptosis even in the absence of extrinsic insult [12] (see the electronic supplementary material, figure S1*a*). Indeed, despite reducing the concentration of siRNAs targeting Mcl-1 to 25 nM, when combined with 100 nM WEHI-539, the vast majority of cells died, either in mitosis or shortly thereafter (electronic supplementary material, figure S4*c*). In fact, the addition of the Aurora B inhibitor actually conferred protection, reducing the number of cells dying in mitosis and delaying PMD, possibly due to suppressing telomere deprotection [12,50] (see Discussion). Therefore, to enable better titration of Mcl-1 function, rather than RNAi we turned to the Mcl-1 inhibitor, A-1210477 [31]. Like WEHI-539, A-1210477 is a BH3-mimetic and inhibits Mcl-1 from binding its pro-apoptotic partners (electronic supplementary material, figure S4*d*). First, we analysed a concentration matrix to identify a combinatorial concentration of WEHI-539 and A-1210477 that induced minimal apoptosis (electronic supplementary material, figure S4*e*). When used in isolation, 100 nM WEHI-539 and 2 µM A-1210477 did not suppress proliferation or induce apoptosis, and in combination only had a minor effect (electronic supplementary material, figure S4*e*). Cell fate profiling confirmed that 2 µM A-1210477 in isolation or in combination with ZM447393 had little effect (figure 5*c*). When combined with WEHI-539, 2 µM A-1210477 induced apoptosis in 44% of cells. However, addition of ZM447439 greatly enhanced this, increasing the apoptotic fraction to 86% and accelerating the average time from mitotic exit to death from 35 h to 10 h (figure 5*c*,*d*). Thus, despite the technical difficulties inherent when suppressing both Mcl-1 and Bcl-xL, these observations show that Mcl-1 promotes post-mitotic survival when Bcl-xL-inhibited cells are driven through an abnormal division. In turn, this supports the hypothesis that RKO cells become dependent on Bcl-xL function after exiting a protracted mitosis due to degradation of Mcl-1 during the delay.

2.7. Mcl-1-deficient DLD-1 cells are sensitive to WEHI-539 when combined with ZM447439

If both Mcl-1 and Bcl-xL support post-mitotic survival when cells are exposed to mitotic drivers, then we reasoned that cell lines already deficient for Mcl-1 should be sensitive to the combination of a Bcl-xL inhibitor plus a mitotic driver. To test this, we turned to DLD-1 cells, another colon cancer cell line which, compared with RKO, has a relatively lower level of Mcl-1 [49]. In contrast to RKO, exposing DLD-1 cells to WEHI-539 and ZM447439 separately was sufficient to induce apoptosis in a fraction of cells (figure 5*e*,*f*), consistent with weakened Mcl-1 function. More importantly, however, combining WEHI-539 with ZM447439 induced PMD in 76% of cells. Thus, in a cell line lacking robust Mcl-1 function, post-mitotic survival in the presence of a mitotic driver is dependent on Bcl-xL function.

3. Discussion

Bcl-xL has previously been implicated as an important mitotic survival factor [12,18,20–22]. To further refine our understanding of Bcl-xL's role when mitosis is disrupted, we have taken advantage of WEHI-539, a BH3 mimetic that selectively and potently blocks binding of Bcl-xL to its BH3-only pro-apoptotic partner proteins [32]. Using concentration matrices to combine WEHI-539 with a panel of representative antimitotic agents, we have systematically analysed Bcl-xL's pro-survival potential in response to drugs that either block or accelerate mitotic progression. In addition, by using cell fate profiling we were able to differentiate death in mitosis from post-mitotic apoptosis. Our results demonstrate that Bcl-xL sustains survival following perturbations that induce a prolonged mitotic delay. By contrast, Bcl-xL function is less critical when cells are driven through an abnormal mitosis, most probably due to the compensatory action of Mcl-1.

3.1. Both Bcl-xL and Mcl-1 promote survival following an aberrant mitosis

During mitosis, transcription and translation are heavily suppressed. Indeed, the regulation of mitotic progression is governed largely by post-translational modifications, in particular protein phosphorylation and ubiquitin-mediated proteolysis [51–53]. Accordingly, the apoptotic proteome is also extensively modified during mitosis; for example, Caspase-9, Bid and Bcl-xL are phosphorylated by mitotic kinases [16,22,54–56]. Pro-apoptotic Bim is ubiquitinated by the anaphase-promoting complex (APC/C), the E3 ubiquitin ligase that also targets Cyclin B1 for degradation [15]. However, the net physiological effect these post-translational modifications have on the apoptotic threshold is unclear. Moreover, how these modifications change during a delayed or abnormal mitosis is also not clear. An exception is pro-survival Mcl-1, with several independent reports showing that it is slowly degraded during a checkpoint-mediated mitotic arrest [46,48,49]. Mcl-1 degradation is proteasome dependent and while several E3 ligases have been implicated, the exact mechanism remains to be delineated [49,57]. Nevertheless, several independent observations support the notion that Mcl-1 degradation serves as a mitotic 'death timer'

mechanism [14,58]. For example, we recently showed that when mitotic exit is blocked in RKO cells by expression of a non-degradable Cyclin B1 mutant, Mcl-1 RNAi accelerates DiM [49]. Conversely, overexpressing Mcl-1 delays taxol-induced DiM by over 5 h. Modulating Mcl-1 also influences post-mitotic survival. We recently showed that Mcl-1 RNAi in slippage-prone DLD-1 cells increases the frequency of apoptosis after slippage, while overexpressing it delays PMD [49]. Taken together with the functional overlap between Mcl-1 and Bcl-xL [12,24,25], these observations allowed us to formulate a simple hypothesis to account for why pharmacological inhibition of Bcl-xL sensitized cells to mitotic blockers but not mitotic drivers, namely that degradation of Mcl-1 during the prolonged delay induced by a blocker renders cells more dependent on Bcl-xL when they eventually exit mitosis. Our subsequent experiment showing that simultaneous inhibition of Bcl-xL and Mcl-1 accelerates PMD in response to an Aurora B inhibitor supports this hypothesis. In turn, this further supports the notion that both Bcl-xL and Mcl-1 contribute to survival following an aberrant mitosis.

3.2. In the absence of robust pro-survival activity, mitosis induces apoptosis

Consistent with their overlapping function, simultaneous inhibition of Bcl-xL and Mcl-1 can induce apoptosis even in the absence of cytotoxic insult. This has been shown previously by others [24], but we noted recently that co-repression of Bcl-xL and Mcl-1 by RNAi causes RKO cells to die either in mitosis or very shortly following mitotic exit [12]. Here, we made a similar observation: in the absence of any additional exogenous stress, Mcl-1 RNAi cells exposed to WEHI-539 died either in mitosis or very shortly after mitotic exit. This does not appear to be an RNAi-related phenomenon; when both Bcl-xL and Mcl-1 were inhibited pharmacologically, using WEHI-539 and A-1210477, apoptosis occurred frequently in mitosis or shortly thereafter (not shown). Moreover, when cells overexpressing Bim were exposed to WEHI-539, the vast majority of cells died shortly after completing mitosis. These observations indicate that in the absence of adequate pro-survival activity, mitosis itself is sufficiently stressful to cause apoptosis. One possible trigger for mitosis-specific stress is telomere deprotection, a phenomenon whereby mitotic Aurora B kinase activity displaces TRF2 from telomeres, giving rise to an exposed telomere that is recognized by DNA damage response pathways [50,59]. Consistent with this notion, we previously showed that overexpression of TRF2 or inhibition of Aurora B suppresses mitotic apoptosis in Bcl-xL/Mcl-1-deficient cells [12]. Here, we confirm this in that inhibition of Aurora B delayed apoptosis in Mcl-1RNAi cells exposed to WEHI-539. However, whether telomere deprotection is sufficient to account for apoptosis in cells with weakened pro-survival function remains to be seen. Indeed, this is a very intriguing phenomenon that warrants further investigation. Interestingly, a prolonged mitotic arrest results in mitophagy, reduction in ATP levels and activation of AMPK, and a metabolic switch from oxidative respiration to glycolysis [11]. One possibility therefore is that mitosis-dependent changes in metabolism and/or mitochondrial function could also contribute to mitotic stress that is sufficient to induce apoptosis in cells with weakened pro-survival function.

3.3. Identification of patients likely to benefit from antimitotic/Bcl-xL inhibitor combinations

The taxanes and other antimitotic agents are vitally important chemotherapy agents. Yet exactly how they yield patient benefit remains obscure. Recently, the Mps1 inhibitor NTRC 0066-0 was shown to potentiate the anti-tumour activity of docetaxel in a mouse model of triple-negative breast cancer [60]. Strikingly, however, the Mps1 inhibitor alone had little effect, strongly suggesting that docetaxel's anti-tumour activity is via a mitotic mechanism. Indeed, an analysis of breast cancer biopsies indicates that tumour responses correlate with abnormal mitoses observed shortly after taxol infusion [61]. Here, we show that Bcl-xL is a potent pro-survival factor in this context: over a range of clinically relevant taxol concentrations, WEHI-539 enhanced apoptosis by both accelerating death in mitosis and by elevating the frequency of apoptosis following an abnormal mitosis. These observations support and extend previous reports showing that Navitoclax enhances cell death in response to antimitotic agents [18,21,37,62,63]. Together, these observations make a compelling case for exploring Bcl-xL inhibitors in combination with taxanes in order to enhance antimitotic chemotherapy. However, such combinations will inevitably come with an increased toxicity profile. Indeed, Bcl-xL is a molecular clock in platelets, defining their lifespan [64,65]. Consequently, Bcl-xL inhibitors induce thrombocytopenia [66,67], and while this can be ameliorated clinically, judicious use will be required to open up a useful therapeutic window. Interestingly, ovarian cancers with relatively high Bcl-xL levels are less responsive to taxane-based therapy, and ovarian cancer cell lines with higher Bcl-xL/Mcl-1 ratios showed higher Bliss sum values when treated with Navitoclax and taxol [45]. Taken together with our observations, this suggests that patients whose tumours have high Bcl-xL/Mcl-1 ratios might be good candidates for Bcl-xL inhibitor trials in combination with antimitotic agents. Similarly, early-phase clinical trials evaluating novel mitotic blockers (e.g. those targeting Plk1 and Cenp-E) might also benefit by pre-selecting patients with high Bcl-xL/Mcl-1 ratios and exploring combinations with Bcl-xL inhibitors. Conversely, exploring Bcl-xL inhibitors may be less promising in the context of mitotic drivers unless patients whose tumours have low Mcl-1 levels can be identified.

4. Material and methods

4.1. Cell lines

Parental RKO and DLD-1 cells, plus RKO Flp-In T-Rex derivatives expressing Bim, Myc-tagged Bcl-xL and GFP-tagged Mcl-1, were as described [12,49,68]. All lines were cultured in DMEM plus 10% fetal calf serum (Life Technologies), 100 U ml^{-1} penicillin, 100 U ml^{-1} streptomycin and 2 mM glutamine (all from Sigma), then maintained at 37°C in a humidified 5% CO_2 atmosphere. A stable RKO line harbouring a tetracycline-inducible GFP-tagged Bcl-xL was generated as described [69]. In brief, a Bcl-xL cDNA [12]

was cloned into a pcDNA5/FRT/TO-based vector (Invitrogen) then co-transfected with pOG44 into Flp-In T-Rex RKO cells using Lipofectamine Plus (Thermofisher). Stable integrants were selected in 400 μg ml^{-1} hygromycin B (Roche) and 8 μg ml^{-1} blasticidin (Melford), colonies pooled and expanded to create an isogenic population. To synchronize cells in S-phase, cells were treated with 2 mM thymidine for 16 h.

4.2. Small molecule inhibitors

The following drugs were dissolved in DMSO and stored at −20°C: WEHI-539 [32] (Apexbio); taxol (Sigma); nocodazole (Sigma); AZ138 [8] (AstraZeneca)); AZ3146 [43] (AstraZeneca); BI 2536 [38] (Boehringer Ingelheim); GSK923295 [39,70]; MLN8054 [41] (Millennium Pharmaceuticals); ZM447439 [42] (Tocris); A-1210477 [31] (Medchemexpress). Tetracycline (Sigma) was dissolved in water, stored at −20°C, and used at concentrations indicated in the figure legends. Thymidine (Sigma) was dissolved in PBS at a concentration of 200 mM, and stored short-term at 4°C.

4.3. RNAi

For RNAi-mediated inhibition, cells were plated in μclear® 96-well plates (Greiner Bio-One) then transfected with a final concentration of 66 nM siRNA using DharmaFECT 1 transfection reagent (Dharmacon) in Opti-MEM media (Life Technologies). siRNAs were ON-TARGETplus SMARTpools (Dharmacon) as described [12] containing oligonucleotides with the following sequences: Bcl-xL (5′-GGACAGCAUAUCAGAGCUU-3′, 5′-GAAAUGACCAGACACUGAC-3′, 5′-CCUACAAGCUUUCCCAGAA-3′, 5′-UUAGUGAUGUGGAAGAGAA-3′), Mcl-1(5′ CGAAGGAAGUAUCGAAUUU-3′, 5′-GAUUAUCUCUCGGUACCUU-3′, 5′-GAAGGUGGCAUCAGGAAUG-3′, 5′-GGUUUGGCAUAUCUAAUAA-3′), non-targeting control (5′- UGGUUUACAUGUCGACUAA-3′, 5′-UGGUUUACAUGUUGUGUGA-3′, 5′-GGUUUACAUGUUUUCUGA-3′, 5′-UGGUUUACAUGUUUUCCUA-3′).

4.4. Proliferation and apoptosis assays

To measure apoptosis induction and proliferation and to perform cell fate profiling, 1×10^5 cells were seeded per well in μclear 96-well plates (Greiner Bio-One) and IncuCyte Kinetic Caspase-3/7 Apoptosis Assay Reagent (Essen BioScience) added. Note that this cell-permeable reagent consists of a caspase-3/7 recognition motif (DEVD) coupled to a DNA intercalating dye. Upon cleavage by activated caspase-3/7, the liberated dye binds nuclear DNA and emits green fluorescence [71]. Fluorescence values were then normalized to control wells on the same plate which exhibited maximum apoptosis yielding percentage apoptosis values which were plotted. Note also that to maximize fluorescence detection, DMEM was replaced with Leibovitz's L-15 (Sigma-Aldrich). Cells were then imaged using an IncuCyte ZOOM (Essen BioScience) equipped with a 20× objective and maintained at 37°C in a humidified 5% CO_2 atmosphere. Phase contrast and fluorescence images with two to four images per well were collected every 10–30 min and IncuCyte ZOOM software used in real-time to measure confluency, as a proxy for proliferation, and apoptosis, respectively. Image sequences were then exported in MPEG-4 format and analysed manually to generate cell fate profiles [8]. IncuCyte ZOOM data and timing data were imported into Prism 6 (GraphPad) for statistical analysis and presentation. Note that zero hours on the fate profiles represent either when cells entered mitosis or when imaging was started; see individual figure legends for details.

4.5. Immunoprecipitation

Flp-In T-Rex RKO cells harbouring an inducible GFP-tagged Bcl-xL transgene were seeded in 6-well plates and 100 ng ml^{-1} tetracycline added overnight. 10×10^5 cells were then harvested and lysed in 1 ml of buffer containing 0.1% Triton X-100, 100 mM NaCl, 10 mM Tris pH 7.4, 1 mM EDTA, 1 mM EGTA, 20 mM β-glycerophosphate, 10 mM NaF and protease/phosphatase inhibitors (Roche). The lysate was then clarified by centrifugation at 16 000*g* for 20 min at 4°C. To 1 ml of supernatant, 30 μg of a GST-GFP-nanotrap fusion protein was added [49,72] along with glutathione sepharose beads (Amintra). After incubation at 4°C with rotation for 2 h, beads were harvested by centrifugation and washed five times with lysis buffer. Bound proteins were eluted by boiling in sample buffer (0.35 M Tris pH 6.8, 0.1 g ml^{-1} sodium dodecyl sulfate, 93 mg ml^{-1} dithiothreitol, 30% glycerol, 50 μg ml^{-1} bromophenol blue) then resolved by SDS-PAGE.

4.6. Immunoblotting

Following SDS-PAGE, proteins were electroblotted onto Immobilon-P membranes. Following blocking in 5% dried skimmed milk (Marvel) dissolved in TBST (50 mM Tris pH 7.6, 150 mM NaCl, 0.1% Tween-20), membranes were incubated overnight at 4°C with the following primary antibodies diluted in TBST: 54H6 (Rabbit anti-Bcl-xL, 1 : 1000; Cell Signalling Technology), S-19 (Rabbit anti-Mcl-1, Santa Cruz Biotechnology), sheep anti-Tao1 (1 : 3000 [73]), rabbit anti-Bim (1 : 500; BD Biosciences), mouse anti-Bad (1 : 1000; Santa Cruz), rabbit anti-Bid (1 : 1000; Cell Signalling), mouse anti-Bax (1 : 1000; BD BioSciences), mouse anti-Bak (1 : 1000; Calbiochem), 4A6 (mouse anti-Myc tag; 1 : 1000; Millipore) and GFP (Rabbit anti-GFP; 1 : 1000; Cell Signalling). Membranes were then washed three times in TBST and incubated for at least 1 h with appropriate horseradish-peroxidase-conjugated secondary antibodies (Zymed). After washing in TBST, bound secondary antibodies were detected using either EZ-ECL Chemiluminescence Reagent (Biological Industries) or Luminata Forte Western HRP Substrate (Millipore) and a Biospectrum 500 imaging system (UVP).

4.7. Statistical methods and Bliss independence analysis

Prism v. 6 (GraphPad) was used for statistical analysis, with non-parametric Mann–Whitney *U*-tests for all figures, where $^*p < 0.05$, $^{**}p < 0.01$, $^{***}p < 0.001$, $^{\#}p < 0.0001$, n.s.: $p > 0.05$. Lines on scatterplots show mean and interquartile ranges. Combination synergy of WEHI-539 with antimitotic agents was determined by Bliss independence analyses [44,45]. A Bliss expectation for a combined response (C) was calculated by the equation: $C = (A + B) - (A \times B)$, where A and B are the percentage apoptosis induced by drug A and B at a given dose. The difference between the Bliss expectation and the extent of apoptosis observed is the

Bliss excess. Bliss excess scores were then summed across the dose matrix to generate a Bliss sum, where a value equal to zero indicates that the combination is additive, a value greater than zero indicates synergy, while a Bliss sum of less than zero indicates antagonism.

Data accessibility. Research materials are available upon request to S.S.T.

Authors' contributions. The project was conceived by S.S.T. and A.B. A.B. performed all the experiments with the exception of S4D which was performed by O.S. O.S., C.T., L.N. and A.T. contributed key reagents. A.B. and S.S.T. prepared the manuscript. All co-authors read and commented on the manuscript.

Competing interests. We declare we have no competing interests.

Funding. A.B. is funded by a studentship from Cancer Research UK and a University of Manchester Presidential Scholarship. O.S. and C.T. were supported by the Wellcome Trust and the Medical Research Council (MR/L006839/1), respectively. L.N., A.T. and S.S.T. are supported by Cancer Research UK.

Acknowledgements. We thank members of the Taylor lab for advice and comments on the manuscript.

References

1. Dumontet C, Jordan MA. 2010 Microtubule-binding agents: a dynamic field of cancer therapeutics. *Nat. Rev. Drug Discov*. **9**, 790–803. (doi:10.1038/nrd3253)
2. Rowinsky EK. 1993 Clinical pharmacology of Taxol. *J Natl Cancer Inst Monogr*. **15**, 25–37.
3. Jackson JR, Patrick DR, Dar MM, Huang PS. 2007 Targeted anti-mitotic therapies: can we improve on tubulin agents? *Nat. Rev. Cancer* **7**, 107–117. (doi:10.1038/nrc2049)
4. Keen N, Taylor S. 2009 Mitotic drivers—inhibitors of the Aurora B kinase. *Cancer Metastasis Rev*. **28**, 185–195. (doi:10.1007/s10555-009-9184-9)
5. Taylor S, Peters JM. 2008 Polo and Aurora kinases: lessons derived from chemical biology. *Curr. Opin. Cell Biol*. **20**, 77–84. (doi:10.1016/j.ceb.2007.11.008)
6. Lens SM, Voest EE, Medema RH. 2010 Shared and separate functions of polo-like kinases and aurora kinases in cancer. *Nat. Rev. Cancer* **10**, 825–841. (doi:10.1038/nrc2964)
7. Malumbres M. 2011 Physiological relevance of cell cycle kinases. *Physiol. Rev*. **91**, 973–1007. (doi:10.1152/physrev.00025.2010)
8. Gascoigne KE, Taylor SS. 2008 Cancer cells display profound intra- and interline variation following prolonged exposure to antimitotic drugs. *Cancer Cell*. **14**, 111–122. (doi:10.1016/j.ccr.2008.07.002)
9. Chipuk JE, Moldoveanu T, Llambi F, Parsons MJ, Green DR. 2010 The BCL-2 family reunion. *Mol. Cell*. **37**, 299–310. (doi:10.1016/j.molcel.2010.01.025)
10. Delbridge AR, Grabow S, Strasser A, Vaux DL. 2016 Thirty years of BCL-2: translating cell death discoveries into novel cancer therapies. *Nat. Rev. Cancer* **16**, 99–109. (doi:10.1038/nrc.2015.17)
11. Domenech E *et al.* 2015 AMPK and PFKFB3 mediate glycolysis and survival in response to mitophagy during mitotic arrest. *Nat. Cell Biol*. **17**, 1304–1316. (doi:10.1038/ncb3231)
12. Topham C *et al.* 2015 MYC is a major determinant of mitotic cell fate. *Cancer Cell* **28**, 129–140. (doi:10.1016/j.ccell.2015.06.001)
13. Topham CH, Taylor SS. 2013 Mitosis and apoptosis: how is the balance set? *Curr. Opin. Cell Biol*. **25**, 780–785. (doi:10.1016/j.ceb.2013.07.003)
14. Haschka MD, Soratroi C, Kirschnek S, Hacker G, Hilbe R, Geley S, Villunger A, Fava LL. 2015 The NOXA-MCL1-BIM axis defines lifespan on extended mitotic arrest. *Nat. Commun*. **6**, 6891. (doi:10.1038/ncomms7891)
15. Wan L *et al.* 2014 APC(Cdc20) suppresses apoptosis through targeting Bim for ubiquitination and destruction. *Dev. Cell* **29**, 377–391. (doi:10.1016/j.devcel.2014.04.022)
16. Wang P, Lindsay J, Owens TW, Mularczyk EJ, Warwood S, Foster F, Streuli CH, Brennan K, Gilmore AP. 2014 Phosphorylation of the proapoptotic BH3-only protein bid primes mitochondria for apoptosis during mitotic arrest. *Cell Rep*. **7**, 661–671. (doi:10.1016/j.celrep.2014.03.050)
17. Diaz-Martinez LA, Karamysheva ZN, Warrington R, Li B, Wei S, Xie XJ, Roth MG, Yu H. 2014 Genome-wide siRNA screen reveals coupling between mitotic apoptosis and adaptation. *EMBO J*. **33**, 1960–1976. (doi:10.15252/embj.201487826)
18. Bah N, Maillet L, Ryan J, Dubreil S, Gautier F, Letai A, Juin P, Barille-Nion S. 2014 Bcl-xL controls a switch between cell death modes during mitotic arrest. *Cell Death Dis*. **5**, e1291. (doi:10.1038/cddis.2014.251)
19. Chu R, Terrano DT, Chambers TC. 2012 Cdk1/cyclin B plays a key role in mitotic arrest-induced apoptosis by phosphorylation of Mcl-1, promoting its degradation and freeing Bak from sequestration. *Biochem. Pharmacol*. **83**, 199–206. (doi:10.1016/j.bcp.2011.10.008)
20. Minn AJ, Boise LH, Thompson CB. 1996 Expression of Bcl-xL and loss of p53 can cooperate to overcome a cell cycle checkpoint induced by mitotic spindle damage. *Genes Dev*. **10**, 2621–2631. (doi:10.1101/gad.10.20.2621)
21. Shi J, Zhou Y, Huang HC, Mitchison TJ. 2011 Navitoclax (ABT-263) accelerates apoptosis during drug-induced mitotic arrest by antagonizing Bcl-xL. *Cancer Res*. **71**, 4518–4526. (doi:10.1158/0008-5472.CAN-10-4336)
22. Upreti M, Galitovskaya EN, Chu R, Tackett AJ, Terrano DT, Granell S, Chambers TC. 2008 Identification of the major phosphorylation site in Bcl-xL induced by microtubule inhibitors and analysis of its functional significance. *J. Biol. Chem*. **283**, 35 517–35 525. (doi:10.1074/jbc.M805019200)
23. Kawabata T, Tanimura S, Asai K, Kawasaki R, Matsumaru Y, Kohno M. 2012 Up-regulation of pro-apoptotic protein Bim and down-regulation of anti-apoptotic protein Mcl-1 cooperatively mediate enhanced tumor cell death induced by the combination of ERK kinase (MEK) inhibitor and microtubule inhibitor. *J. Biol. Chem*. **287**, 10 289–10 300. (doi:10.1074/jbc.M111.319426)
24. Eichhorn JM, Alford SE, Sakurikar N, Chambers TC. 2014 Molecular analysis of functional redundancy among anti-apoptotic Bcl-2 proteins and its role in cancer cell survival. *Exp. Cell Res*. **322**, 415–424. (doi:10.1016/j.yexcr.2014.02.010)
25. Eno CO, Zhao G, Olberding KE, Li C. 2012 The Bcl-2 proteins Noxa and Bcl-xL co-ordinately regulate oxidative stress-induced apoptosis. *Biochem. J*. **444**, 69–78. (doi:10.1042/BJ20112023)
26. Wei MC *et al.* 2001 Proapoptotic BAX and BAK: a requisite gateway to mitochondrial dysfunction and death. *Science* **292**, 727–730. (doi:10.1126/science.1059108)
27. Delbridge AR, Strasser A. 2015 The BCL-2 protein family, BH3-mimetics and cancer therapy. *Cell Death Differ*. **22**, 1071–1080. (doi:10.1038/cdd.2015.50)
28. Leverson JD. 2016 Chemical parsing: dissecting cell dependencies with a toolkit of selective BCL-2 family inhibitors. *Mol. Cell Oncol*. **3**, e1050155. (doi:10.1080/23723556.2015.1050155)
29. Billard C. 2013 BH3 mimetics: status of the field and new developments. *Mol. Cancer Ther*. **12**, 1691–1700. (doi:10.1158/1535-7163.MCT-13-0058)
30. Souers AJ *et al.* 2013 ABT-199, a potent and selective BCL-2 inhibitor, achieves antitumor activity while sparing platelets. *Nat. Med*. **19**, 202–208. (doi:10.1038/nm.3048)
31. Leverson JD *et al.* 2015 Potent and selective small-molecule MCL-1 inhibitors demonstrate on-target cancer cell killing activity as single agents and in combination with ABT-263 (navitoclax). *Cell Death Dis*. **6**, e1590. (doi:10.1038/cddis.2014.561)
32. Lessene G *et al.* 2013 Structure-guided design of a selective BCL-X(L) inhibitor. *Nat. Chem. Biol*. **9**, 390–397. (doi:10.1038/nchembio.1246)
33. Tao ZF *et al.* 2014 Discovery of a potent and selective BCL-XL inhibitor with *in vivo* activity. *ACS Med. Chem. Lett*. **5**, 1088–1093. (doi:10.1021/ml5001867)
34. Manchado E, Guillamot M, Malumbres M. 2012 Killing cells by targeting mitosis. *Cell Death Differ*. **19**, 369–377. (doi:10.1038/cdd.2011.197)
35. Kutuk O, Letai A. 2010 Displacement of Bim by Bmf and Puma rather than increase in Bim level mediates paclitaxel-induced apoptosis in breast cancer cells. *Cell Death Differ*. **17**, 1624–1635. (doi:10.1038/cdd.2010.41)

36. Li R, Moudgil T, Ross HJ, Hu HM. 2005 Apoptosis of non-small-cell lung cancer cell lines after paclitaxel treatment involves the BH3-only proapoptotic protein Bim. *Cell Death Differ*. **12**, 292–303. (doi:10.1038/sj.cdd.4401554)
37. Leverson JD *et al.* 2015 Exploiting selective BCL-2 family inhibitors to dissect cell survival dependencies and define improved strategies for cancer therapy. *Sci. Transl. Med*. **7**, 279ra240. (doi:10.1126/scitranslmed.aaa4642)
38. Steegmaier M *et al.* 2007 BI 2536, a potent and selective inhibitor of polo-like kinase 1, inhibits tumor growth *in vivo*. *Curr. Biol*. **17**, 316–322. (doi:10.1016/j.cub.2006.12.037)
39. Wood KW *et al.* 2010 Antitumor activity of an allosteric inhibitor of centromere-associated protein-E. *Proc. Natl Acad. Sci. USA* **107**, 5839–5844. (doi:10.1073/pnas.0915068107)
40. 'Aspinall CF, Zheleva D, Tighe A, Taylor SS. 2015 Mitotic entry: non-genetic heterogeneity exposes the requirement for Plk1. *Oncotarget* **6**, 36 472–36 488. (doi:10.18632/oncotarget.5507)
41. Manfredi MG *et al.* 2007 Antitumor activity of MLN8054, an orally active small-molecule inhibitor of Aurora A kinase. *Proc. Natl Acad. Sci. USA* **104**, 4106–4111. (doi:10.1073/pnas.0608798104)
42. Ditchfield C, Johnson VL, Tighe A, Ellston R, Haworth C, Johnson T, Mortlock A, Keen N, Taylor SS. 2003 Aurora B couples chromosome alignment with anaphase by targeting BubR1, Mad2, and Cenp-E to kinetochores. *J. Cell Biol*. **161**, 267–280. (doi:10.1083/jcb.200208091)
43. Hewitt L, Tighe A, Santaguida S, White AM, Jones CD, Musacchio A, Green S, Taylor SS. 2010 Sustained Mps1 activity is required in mitosis to recruit O-Mad2 to the Mad1-C-Mad2 core complex. *J. Cell Biol*. **190**, 25–34. (doi:10.1083/jcb.201002133)
44. Lehar J *et al.* 2009 Synergistic drug combinations tend to improve therapeutically relevant selectivity. *Nat. Biotechnol*. **27**, 659–666. (doi:10.1038/nbt.1549)
45. Wong M, Tan N, Zha J, Peale FV, Yue P, Fairbrother WJ, Belmont LD. 2012 Navitoclax (ABT-263) reduces Bcl-x(L)-mediated chemoresistance in ovarian cancer models. *Mol. Cancer Ther*. **11**, 1026–1035. (doi:10.1158/1535-7163.MCT-11-0693)
46. Harley ME, Allan LA, Sanderson HS, Clarke PR. 2010 Phosphorylation of Mcl-1 by CDK1-cyclin B1 initiates its Cdc20-dependent destruction during mitotic arrest. *EMBO J*. **29**, 2407–2420. (doi:10.1038/emboj.2010.112)
47. Millman SE, Pagano M. 2011 MCL1 meets its end during mitotic arrest. *EMBO Rep*. **12**, 384–385. (doi:10.1038/embor.2011.62)
48. Wertz IE *et al.* 2011 Sensitivity to antitubulin chemotherapeutics is regulated by MCL1 and FBW7. *Nature* **471**, 110–114. (doi:10.1038/nature09779)
49. Sloss O, Topham C, Diez M, Taylor S. 2016 Mcl-1 dynamics influence mitotic slippage and death in mitosis. *Oncotarget* **7**, 5176–5192. (doi:10.18632/oncotarget.6894)
50. Hayashi MT, Cesare AJ, Fitzpatrick JA, Lazzerini-Denchi E, Karlseder J. 2012 A telomere-dependent DNA damage checkpoint induced by prolonged mitotic arrest. *Nat. Struct. Mol. Biol*. **19**, 387–394. (doi:10.1038/nsmb.2245)
51. Pines J. 2006 Mitosis: a matter of getting rid of the right protein at the right time. *Trends Cell Biol*. **16**, 55–63. (doi:10.1016/j.tcb.2005.11.006)
52. Nigg EA. 2001 Mitotic kinases as regulators of cell division and its checkpoints. *Nat. Rev. Mol. Cell Biol*. **2**, 21–32. (doi:10.1038/35048096)
53. Barr FA, Elliott PR, Gruneberg U. 2011 Protein phosphatases and the regulation of mitosis. *J. Cell Sci*. **124**, 2323–2334. (doi:10.1242/jcs.087106)
54. Allan LA, Clarke PR. 2007 Phosphorylation of caspase-9 by CDK1/cyclin B1 protects mitotic cells against apoptosis. *Mol. Cell*. **26**, 301–310. (doi:10.1016/j.molcel.2007.03.019)
55. Poruchynsky MS, Wang EE, Rudin CM, Blagosklonny MV, Fojo T. 1998 Bcl-xL is phosphorylated in malignant cells following microtubule disruption. *Cancer Res*. **58**, 3331–3338.
56. Sakurikar N, Eichhorn JM, Chambers TC. 2012 Cyclin-dependent kinase-1 (Cdk1)/cyclin B1 dictates cell fate after mitotic arrest via phosphoregulation of antiapoptotic Bcl-2 proteins. *J. Biol. Chem*. **287**, 39 193–39 204. (doi:10.1074/jbc.M112.391854)
57. Stewart DP, Koss B, Bathina M, Perciavalle RM, Bisanz K, Opferman JT. 2010 Ubiquitin-independent degradation of antiapoptotic MCL-1. *Mol. Cell Biol*. **30**, 3099–3110. (doi:10.1128/MCB.01266-09)
58. Tunquist BJ, Woessner RD, Walker DH. 2010 Mcl-1 stability determines mitotic cell fate of human multiple myeloma tumor cells treated with the kinesin spindle protein inhibitor ARRY-520. *Mol. Cancer Ther*. **9**, 2046–2056. (doi:10.1158/1535-7163.MCT-10-0033)
59. Colin DJ, Hain KO, Allan LA, Clarke PR. 2015 Cellular responses to a prolonged delay in mitosis are determined by a DNA damage response controlled by Bcl-2 family proteins. *Open Biol*. **5**, 140156. (doi:10.1098/rsob.140156)
60. Maia AR *et al.* 2015 Inhibition of the spindle assembly checkpoint kinase TTK enhances the efficacy of docetaxel in a triple-negative breast cancer model. *Ann. Oncol*. **26**, 2180–2192. (doi:10.1093/annonc/mdv293)
61. Zasadil LM, Andersen KA, Yeum D, Rocque GB, Wilke LG, Tevaarwerk AJ, Raines RT, Burkard ME, Weaver BA. 2014 Cytotoxicity of paclitaxel in breast cancer is due to chromosome missegregation on multipolar spindles. *Sci. Transl. Med*. **6**, 229ra243. (doi:10.1126/scitranslmed.3007965)
62. Tan N, Malek M, Zha J, Yue P, Kassees R, Berry L, Fairbrother WJ, Sampath D, Belmont LD. 2011 Navitoclax enhances the efficacy of taxanes in non-small cell lung cancer models. *Clin. Cancer Res*. **17**, 1394–1404. (doi:10.1158/1078-0432.CCR-10-2353)
63. Chen J *et al.* 2011 The Bcl-2/Bcl-X(L)/Bcl-w inhibitor, navitoclax, enhances the activity of chemotherapeutic agents *in vitro* and *in vivo*. *Mol. Cancer Ther*. **10**, 2340–2349. (doi:10.1158/1535-7163.MCT-11-0415)
64. Mason KD *et al.* 2007 Programmed anuclear cell death delimits platelet life span. *Cell* **128**, 1173–1186. (doi:10.1016/j.cell.2007.01.037)
65. Zhang H *et al.* 2007 Bcl-2 family proteins are essential for platelet survival. *Cell Death Differ*. **14**, 943–951. (doi:10.1038/sj.cdd.4402081)
66. Roberts AW *et al.* 2012 Substantial susceptibility of chronic lymphocytic leukemia to BCL2 inhibition: results of a phase I study of navitoclax in patients with relapsed or refractory disease. *J. Clin. Oncol*. **30**, 488–496. (doi:10.1200/JCO.2011.34.7898)
67. Tse C *et al.* 2008 ABT-263: a potent and orally bioavailable Bcl-2 family inhibitor. *Cancer Res*. **68**, 3421–3428. (doi:10.1158/0008-5472.CAN-07-5836)
68. Girdler F, Gascoigne KE, Eyers PA, Hartmuth S, Crafter C, Foote KM, Keen NJ, Taylor SS. 2006 Validating Aurora B as an anti-cancer drug target. *J. Cell Sci*. **119**, 3664–3675. (doi:10.1242/jcs.03145)
69. Tighe A, Johnson VL, Taylor SS. 2004 Truncating APC mutations have dominant effects on proliferation, spindle checkpoint control, survival and chromosome stability. *J. Cell Sci*. **117**, 6339–6353. (doi:10.1242/jcs.01556)
70. Bennett A, Bechi B, Tighe A, Thompson S, Procter DJ, Taylor SS. 2015 Cenp-E inhibitor GSK923295: novel synthetic route and use as a tool to generate aneuploidy. *Oncotarget* **6**, 20 921–20 932. (doi:10.18632/oncotarget.4879)
71. Cen H, Mao F, Aronchik I, Fuentes RJ, Firestone GL. 2008 DEVD-NucView488: a novel class of enzyme substrates for real-time detection of caspase-3 activity in live cells. *FASEB J*. **22**, 2243–2252. (doi:10.1096/fj.07-099234)
72. Rothbauer U, Zolghadr K, Muyldermans S, Schepers A, Cardoso MC, Leonhardt H. 2008 A versatile nanotrap for biochemical and functional studies with fluorescent fusion proteins. *Mol. Cell Proteomics* **7**, 282–289. (doi:10.1074/mcp.M700342-MCP200)
73. Westhorpe FG, Diez MA, Gurden MD, Tighe A, Taylor SS. 2010 Re-evaluating the role of Tao1 in the spindle checkpoint. *Chromosoma* **119**, 371–379. (doi:10.1007/s00412-010-0261-1)